

***Pop4*, a novel gene for diabetes mellitus
impacting beta cell function and survival in
mice**

Inaugural-Dissertation

zur Erlangung des Doktorgrades
an der Mathematisch-Naturwissenschaftlichen Fakultät
der Heinrich-Heine-Universität Düsseldorf

vorgelegt von

Jenny Minh An Khuong
aus Aalen

Düsseldorf, August 2024

aus dem Institut für Klinische Biochemie and Pathobiochemie
des Deutschen Diabetes Zentrum (DDZ),
Leibniz-Zentrum für Diabetesforschung an
der Heinrich-Heine Universität Düsseldorf

Gedruckt mit der Genehmigung der
Mathematisch-Naturwissenschaftlichen Fakultät der
Heinrich-Heine Universität Düsseldorf

Berichtersteller:

1. Prof. Dr. Hadi Al-Hasani
2. Dr. Bengt-Frederik Belgardt

Tag der mündlichen Prüfung: 13.12.2024

Abstract

Pancreatic beta cells play a key role in the pathogenesis of diabetes mellitus, as beta cell demise is a common process in both type 1 and type 2 diabetes mellitus. Previously, the *Pop4* gene emerged as a candidate gene underlying the peak region of *Nbg7p*, a quantitative trait locus on chromosome 7, associated with blood glucose and plasma insulin in a backcross of diabetes susceptible and resistant mice. Transcription of the *Pop4* gene was positively correlated with insulin gene expression in both an *in vitro* beta cell culture model and human pancreatic islets, suggesting a role for the gene in insulin production. POP4 is canonically described as a subunit of the ribonuclease P and MRP (RNaseP/MRP), which is involved in the maturation of tRNA and rRNA, in the regulation of histone variant 3.3 chromatin assembly and the homology-directed DNA damage response. To this end, the aim was to explore the beta cell autonomous role of *Pop4* in insulin synthesis function and investigate the effect on beta cell plasticity for the first time in an *in vivo* mouse model.

In this thesis, the novel generated beta cell-specific *Pop4* knockout mouse (*Pop4* β KO) with deletion of exons 4 and 5 was shown to develop diabetes mellitus in early adulthood due to insulin deficiency and a gradual loss of beta cell mass in a sex-independent manner. High-fat diet induced insulin resistance did not exacerbate beta-cell failure despite elevated circulating plasma insulin levels in female mice. Analysis of glucose-stimulated insulin secretion *in vivo* and *ex vivo* in isolated pancreatic islets revealed a defect in insulin secretion that preceded the onset of hyperglycemia and corroborating an early prediabetic state of *Pop4* β KO mice. Histological studies of prediabetic pancreatic islets revealed impaired insulin production and maturation accompanied by an increased abundance of phosphorylated histone H2A.X as a marker of DNA damage repair. The islet transcriptome in the prediabetic state suggests processes mediating beta-cell failure due to apoptosis and senescence through significantly increased gene expression of *p53* and *p21*. With respect to the described functional roles of POP4 in tRNA and rRNA processing, the protein synthesis appears to be unaffected in *Pop4* β KO mice, possibly by a compensation through overexpression of the RNase P/MRP subunits *Pop1* and *Rpp30*. Taken together, these data demonstrate, a critical role for POP4 in beta cell function and survival and in this context as a potential causal gene for diabetes mellitus.

Zusammenfassung

Pankreatische Betazellen spielen eine Schlüsselrolle bei der Entstehung von Diabetes mellitus, da ein Verlust an Betazellmasse sowohl bei Typ 1 als auch bei Typ 2 Diabetes auftreten kann. In früheren Studien wurde *Pop4* als Kandidatengen identifiziert, das in der Peak-Region von *Nbg7p*, einem quantitativen Locus auf dem Chromosom 7 in einem Rückkreuzungsmausmodell, der mit Blutglukose und Plasma Insulin assoziiert ist, unterliegt. Die Transkription von *Pop4* korrelierte positiv mit der Insulin-Genexpression sowohl in einem *in vitro* Betazellkulturmodell als auch in menschlichen pankreatischen Inseln, was auf eine Rolle des Gens bei der Insulinproduktion postuliert. POP4 wird kanonisch als Untereinheit der Ribonuklease P und MRP beschrieben, die unter anderem an der Reifung von tRNA und rRNA, an der Regulation der Histonvariante 3.3 im Chromatin und an der homologen Rekombination als DNA-Reparaturmechanismus beteiligt sein soll. Zu diesem Zweck sollte die autonome Rolle von *Pop4* in der Betazelle für die Insulinproduktion und darüber hinaus der Effekt auf die Betazellplastizität erstmals in einem *in vivo* Knock-out Mausmodell untersucht werden.

In dieser Thesis, zeigt die neue Betazell-spezifische *Pop4*-Knockout-Maus (*Pop4* β KO) mit einer Deletion der Exons 4 und 5 unabhängig vom Geschlecht die Entwicklung eines Diabetes mellitus im frühen Erwachsenenalter aufgrund eines Mangels an Insulin und einen graduellen Verlust der Betazellmasse. Eine fettreiche Diät, die eine Insulinresistenz hervorruft, konnte trotz einer stimulierten Erhöhung des zirkulierenden Plasmainsulinspiegels bei weiblichen Mäusen die oben genannten Effekte nicht verschlimmern. Die Analyse der Glukose stimulierten Insulinsekretion *in vivo* und *ex vivo* in isolierten Pankreasinseln zeigte einen Defekt, der dem Auftreten von Hyperglykämie vorausgeht und einen frühen prädiabetischen Zustand von *Pop4* β KO-Mäusen postuliert. Die histologische Untersuchung der Pankreasinseln zu diesem prädiabetischen Zeitpunkt zeigte eine Beeinträchtigung der Insulinproduktion und -reifung, begleitet von einem vermehrten Auftreten des phosphorylierten Histons H2A.X als Marker für die Reparatur von DNA-Schäden. Das Transkriptom der Inselzellen im prädiabetischen Stadium zeigte eine signifikant erhöhte p53 und p21 Genexpression was darauf hindeutet, dass der Verlust und das Versagen der Betazellen durch Apoptose und Seneszenz induziert sein könnte. Angesichts der beschriebenen funktionellen Rolle von POP4 in der tRNA und rRNA Prozessierung scheint die Proteinsynthese in den pankreatischen Betazellen nicht beeinträchtigt zu sein und das möglicherweise durch eine Kompensation von *Pop1* und *Rpp30*. Zusammengenommen deuten diese Daten auf eine neue, kritische Rolle von POP4 für die Funktion und das Überleben von Betazellen hin. In diesem Zusammenhang, stellt *Pop4* ein potentielles kausales Gen für Diabetes dar.

Table of Content

1	Introduction	1
1.1	Diabetes mellitus – heterogenous disorder with variety of therapies	1
1.2	Glucose homeostasis and pathophysiology of T1D and T2D	3
1.3	The key role of the pancreatic Islet of Langerhans	5
1.3.1	The mechanism of insulin synthesis, maturation and secretion	6
1.3.2	Beta cell failure in T1D and T2D	8
1.4	Genetic aspects of Diabetes mellitus	10
1.5	Diabetes mouse model C57BL6/J	12
1.6	Cre/LoxP system and the International Mouse Phenotyping Consortium (IMPC)	13
1.7	<i>Pop4</i> emergence as a candidate gene of a mouse QTL	14
1.8	Endoribonuclease subunit processing of precursor 4 (<i>Pop4</i>)	16
2	Aim	18
3	Material and Methods	19
3.1	Material	19
3.1.1	Mouse strains	19
3.1.2	Mouse diets	19
3.1.3	Expendables	20
3.1.4	Chemicals and solutions	21
3.1.5	Buffer and solutions	23
3.1.6	DNA ladder and polymerases	24
3.1.7	Primer sequences	24
3.1.8	Antibodies	25
3.1.9	Commercial kits	26
3.1.10	Equipment	27
3.1.11	Software	29
3.2	Methods	30
3.2.1	Animal experiments	30
3.2.2	Study design of metabolic characterization	32
3.2.3	Biochemical analyses	35
3.2.4	Molecular biology techniques	37
3.2.5	Histological techniques	45
3.3.2	Bioinformatical transcriptome analysis	51
3.3.3	Statistics	51
4	Results	52
4.1	Metabolic characterization of beta cell-specific <i>Pop4</i> knock-out mice	52
4.1.1	Genotyping of mice	52
4.1.2	Knock-out validation on DNA and mRNA levels	53
4.1.3	Gene expression of <i>Pop4</i> in other metabolic relevant tissues	55
4.1.4	Prediction of putative <i>Pop4</i> protein structure	56
4.1.5	Blood glucose development in male and female mice on a chow diet	58

4.1.6	Body weight and body composition development of male and female mice on chow diet	60
4.1.7	Fasting glucose and plasma insulin levels of male and female mice on chow diet	61
4.1.8	Blood glucose and body weight development of female mice on chow vs HFD	63
4.1.9	Body composition of females on chow vs HFD	64
4.1.10	Diabetes prevalence and HOMA-IR of female mice on chow vs HFD	64
4.1.11	<i>In vivo</i> intraperitoneal glucose tolerance test (ipGTT) of male mice	65
4.1.12	<i>Ex vivo</i> glucose stimulated insulin secretion (GSIS) of isolated islets of male mice	66
4.2	Histology of the Islets of Langerhans and pancreatic beta cell	67
4.2.1	Pancreas and pancreatic islet morphometrics	67
4.2.2	Impact of beta cell specific <i>Pop4</i> KO on pancreatic beta cell mass	71
4.2.3	Immunostaining of NKX6.1 beta cell identity and KI67 as proliferation marker	73
4.2.4	Immunostaining of γ H2A.X DNA damage repair marker	75
4.2.5	Electron microscopy of beta cells from isolated islets	77
4.3	Transcriptome analysis of isolated islets	80
4.3.1	Determination of Inter- and Intragroup variability	80
4.3.2	Analysis of differential expressed RNA transcripts	81
4.3.3	Gene ontology enrichment analysis	82
4.3.4	Pathway overrepresentation analysis with Consensus Pathway Database	84
4.3.5	Gene expression of islet hormones and alpha/beta cell marker	85
4.3.6	Gene expression of genes involved with functional aspects of POP4	87
4.3.7	Molecular pathways of apoptosis and senescence	91
5	Discussion	94
5.1	Beta cell specific knockout of <i>Pop4</i> leads to a diabetes phenotype	95
5.1.1	Validation of the Cre recombinase activity	95
5.1.2	The <i>Pop4</i> β KO model displays a deletion of exons 4 and 5	96
5.1.3	<i>Pop4</i> β KO mice develop an early adult onset of diabetes sex-independent	97
5.1.4	The diabetes in <i>Pop4</i> β KO mice develops due to a gradual loss of beta cell mass and reduced insulin secretion	98
5.1.5	The diabetic phenotypic traits remain consistent in female <i>Pop4</i> β KO mice despite of high fat diet induced insulin resistance	100
5.2	The prediabetic phase of <i>Pop4</i>βKO mice displays multiple signs of beta cell dysfunction	102
5.2.1	Prediabetic <i>Pop4</i> β KO mice exhibit glucose intolerance due to reduced insulin secretion	102
5.2.2	The prediabetic phase display a defect in insulin production and insulin maturation	102
5.2.3	The prediabetic phase indicates upregulation of apoptosis- and senescence-mediating genes	104
5.3	Implication of functional role of <i>Pop4</i> to <i>Pop4</i>βKO phenotype	107
5.3.1	<i>Pop4</i> 's role as a subunit of RNase P and RNase MRP	107
5.3.2	<i>Pop4</i> 's role in double stranded DNA repair	112
5.3.3	<i>Pop4</i> 's role in histone 3.3 chromatin assembly	116
5.4	Conclusion and outlook	118
6	Abbreviations	120
7	References	123
8	List of Tables	141
9	List of Figures	142
10	Acknowledgement	144
11	Eidesstaatliche Erklärung	146

1 Introduction

1.1 Diabetes mellitus – heterogenous disorder with variety of therapies

Diabetes mellitus is a group of metabolic disorders characterized by chronic elevated blood glucose levels (hyperglycemia) commonly resulting due to insulin deficiency or reduced insulin action (insulin resistance). In recent decades, the prevalence of type 2 diabetes has reached epidemic proportions, spreading from Western countries to all parts of the world (Roden and Shulman 2019). Projections for Germany alone indicate that there will be 10.7 million cases of type 2 diabetes by 2040, which represents one in eight individuals (Tonnie et al. 2019). Globally, the Diabetes Atlas reports an estimate of 537 million people with diabetes in 2021 and, alarmingly, almost as many adults at high risk of type 2 diabetes highlighting the growing public health challenge (Sun et al. 2022). A broad classification distinguishes the most common cases of diabetes mellitus into insulin-dependent type 1 (T1D) (Rodger 1991a) and non-insulin dependent type 2 (T2D) diabetes (Rodger 1991b), which have shared pathophysiological characteristics but are considered to be at extremes of the diabetes etiology (Harreiter and Roden 2023). Factors contributing to the development of diabetes mellitus are multifactorial and likely result from a complex interaction of genetics with evolving environmental factors. T1D is marked by absolute insulin deficiency due to T-cell mediated autoimmune destruction of insulin-producing pancreatic beta-cell. It may also emerge subsequently to a viral infection and most commonly associates to autoimmune thyroid diseases (Popoviciu et al. 2023; Martens, Gysemans, and Mathieu 2021). The majority of diagnosed diabetes cases (90%) constitute of T2D which is characterized by a combination of varying degrees of insulin resistance in the peripheral tissues and a relative insulin deficiency, unable to meet the insulin demand (Banday, Sameer, and Nissar 2020). The high incidence of new cases of T2D is strongly linked to the underlying obesity epidemic which promotes insulin resistance due to excess of body fat (Klein et al. 2022). Other risk factors for diabetes incidence can be attributed to metabolically unfavorable genetic mutations (Zhang et al. 2021) and epigenetic inheritance (Ling and Ronn 2019). Prolonged untreated hyperglycemia leads to polyuria, polydipsia and weight loss, among other symptoms. Several more serious complications can occur if prolonged hyperglycemia goes untreated. A life-threatening complication accounts to hyperglycemic emergency

referred to as diabetic ketoacidosis which results from a lack of insulin leading to the use of fatty acids and the production of acidic ketone bodies (Eledrisi and Elzouki 2020). Long-term complications of diabetes result from glycemic micro- and macrovascular damage, affecting the eye (retinopathy), kidney (nephropathy), peripheral and autonomous neurons (neuropathy), and the cardiovascular system (hypertension, heart disease) (Farmaki et al. 2020). Moreover, there are associations of diabetes mellitus to mental health issues such as schizophrenia, depression and anxiety which can, in turn, affect therapy adherence and overall health (Akhaury and Chaware 2022). The treatment of hyperglycemia employs various strategies to reduce glucose from the blood, depending on the underlying cause. The first-line medication metformin (IDF Clinical Guidelines, 2006) (Force 2006) reduces hepatic gluconeogenesis and enhances insulin-stimulated glucose disposal in peripheral tissues, with increasing evidence of impact on the gut microbiome among other beneficial effects (Rena, Hardie, and Pearson 2017; Cheng et al. 2024; Pavlo, Kamyshna, and Kamyshnyi 2023). SGLT-2 inhibitors prevent the kidneys from reabsorbing glucose, resulting in its excretion through urine (Saisho 2020). Thiazolidinediones, also known as glitazones, are insulin sensitizers that act by increasing glucose uptake in peripheral tissues while simultaneously decreasing glucose production (Lebovitz 2019). Other drugs, such as sulfonylureas and meglitinides, stimulate insulin secretion as insulin secretagogues (Lv et al. 2020). The novel class of drugs, the glucagon-like peptide-1 (GLP-1) receptor agonists, act as incretin mimetics. They slow gastric emptying, stimulate insulin production, and suppress appetite (Zhao et al. 2021). Recently, GLP-1 receptor agonists have been approved for the treatment of obesity, achieving weight loss of up to 15% (Singh, Krauthamer, and Bjalme-Evans 2022). In combination with other incretin mimetics, they demonstrate even a higher efficacy (Gutgesell et al. 2024). The use of dipeptidyl peptidase 4 (DPP-4) inhibitors enhances endogenous GLP-1 action by reducing its degradation. In cases of insulin deficiency, particularly in T1D, various injectable recombinant human insulin analogues with different acting efficacy and range are effectively used. However, the life-threatening risk of hypoglycemia should be considered when administering insulin injections. Furthermore, the utilization of devices such as the continuous glucose monitoring (CGM) technology and closed-loop insulin pump technology can facilitate enhanced diabetes monitoring and treatment (Gupta, Acharya, and Shukla 2022). Although therapy options and drug availability

have increased, glucose control in T2D has only marginally improved over the past decade, as demonstrated by an American cohort study (Fang et al. 2021). Efforts to stratify and subcluster prediabetic (Prystupa et al. 2023) and diabetic individuals (Zaharia et al. 2019; Ahlqvist et al. 2018) should aid in adjusting therapy to subgroups and improve therapy outcomes, paving the way to precision medicine. Current diabetes research is focused on the treatment of diabetes long-term complications with limited therapy options such as diabetic polyneuropathy (Dewanjee et al. 2018) and ultimately the pancreatic islet replacement therapy (de Koning and Carlotti 2021; Ramzy et al. 2021; Silva et al. 2022). However, exercise and healthy nutrition remains ultimate tools in prevention of T2D and weight loss may induce remission at a prediabetic stage (Birkenfeld and Mohan 2024). Basic research continues to uncover disease mechanisms for the development of therapies for diabetes mellitus. An understanding of the genetic basis of beta cell function and survival may especially be a crucial factor in restoring, improving, protecting or developing functional beta cells.

1.2 Glucose homeostasis and pathophysiology of T1D and T2D

Diabetes mellitus is defined by a disrupted glucose homeostasis resulting in a chronic hyperglycemic state. Glucose homeostasis refers to the tight regulation of blood glucose within a narrow physiological range to ensure vital functions of cells and organs. In humans, normoglycemic blood glucose homeostasis ranges from ~70-100 mg/dL (~4-6 mM) (Mathew et al., 2023). The regulation of blood glucose is controlled by a network of hormone peptides that interact with target tissues. Among these, the key players in blood glucose regulation constitute to the antagonistically acting hormones insulin and glucagon, which are produced by specialized endocrine cell types located in the pancreatic islets of Langerhans. After food intake (postprandial), blood glucose levels rise and are sensed by pancreatic beta cells inducing the production and secretion of insulin. From a physiological standpoint, insulin serves to reduce blood glucose levels returning them to glucose homeostasis by glucose uptake in mainly skeletal muscle, adipose tissue, liver and brain. Conversely, during fasting phases or exercise, blood glucose may decline initiating a counteracting action from glucagon, secreted by the pancreatic alpha cells, to release stored glucose into the bloodstream (Goke 2008). Glucose is stored primarily in form of glycogen in the liver (Paredes-Flores, Rahimi, and Mohiuddin 2025) and in the muscle (Chadt and Al-Hasani 2020), and to a lesser extent in the adipose tissue (Markan, Jurczak, and Brady

2010) through a process known as glycogenesis. However, in the adipose tissue, glucose is predominantly stored as triglycerides in lipid droplets (Santoro, McGraw, and Kahn 2021). In addition to promoting glucose uptake, insulin inhibits the release of stored glucose, referred as gluconeogenesis, by the liver. In turn, to increase blood glucose levels, glucagon activates gluconeogenesis and inhibits glycogenesis (Roder et al. 2016). Together, both hormones regulate the glucose homeostasis by facilitating glucose uptake or production in accordance to the metabolic demands. In diabetes mellitus, the glucose homeostasis is disrupted resulting in a hyperglycemic state in which fasting blood glucose remains over 126 mg/dl (7 mM) and postprandial glycemia reaches beyond 200 mg/dl (12 mM). This is clinically tested with an oral glucose tolerance test (OGTT), in which 75 g of glucose is consumed in a liquid form and blood glucose is measured after 2 h (EISayed et al. 2023). In T1D the pathogenesis is marked by presence of autoantibodies against insulin, glutamic acid decarboxylase (GADA), zinc transporter 8 (Znt8) and tyrosine phosphatase-like protein IA-2 (IA-2A) and appear mostly at a juvenile age. The pancreatic islets during the course of the disease are infiltrated by CD8+ and CD20+ T cells conferring to an aggressive insulinitis. However, recently the classification of the heterogeneity of T1D proposes a novel subtype which appears in adolescence or adulthood as a slowly progressive insulin-dependent diabetes mellitus or also termed latent autoimmune diabetes in adults (LADA). As the name suggests, the disease progression appears slower and at onset residual insulin containing pancreatic islets remain while less infiltrating immune cells are detectable with an absence of insulinitis (Redondo and Morgan 2023). In contrast to this subtype is the fulminant type 1 diabetes defined by a rapid process of beta cell destruction and appearance of ketoacidosis with little appearance of autoantibodies (Hanafusa and Imagawa 2007). As onset is rapid, glycosylated hemoglobin (HbA1c) which is a marker for long-term hyperglycemia, appears inconspicuous (You et al. 2019). This type 1 diabetes subtype is quite severe and life threatening therefore requires a prompt therapy. On the other spectrum of diabetes etiology is T2D which is characterized by insulin resistance combined with relative insulin shortage. Insulin resistance is a state in which insulin is present while glucose uptake is impaired in peripheral tissues (Li et al. 2022). Obesity, caused by overnutrition and lack of physical activity is a risk factor for T2D due to facilitating insulin resistance. In metabolic healthy but overweight individuals beta-cells proliferative capacity may be able to compensate and maintain glucose homeostasis. In the progression to obesity, insulin resistance is accompanied

by elevated levels of insulin termed hyperinsulinemia. This higher insulin state may overcome insulin resistance transiently however in late stages a reduced beta cell mass together with relative insulin deficiency can manifest in T2D (Cerf 2013).

1.3 The key role of the pancreatic Islet of Langerhans

In 1889, German physicians von Mering and Minkowski identified the pancreas as the primary organ involved in the development of diabetes mellitus (Dittrich 1989). This discovery led to the recognition of the Islets of Langerhans, first described by Paul Langerhans in 1869, as a group of endocrine microorgans embedded within the pancreatic parenchymal acinar tissue comprised of several cell types. The composition of the Islets of Langerhans constitutes of insulin secreting beta cells (making up ~50% in human and 80-90% in mice), glucagon secreting alpha cells (35-40% in human and 15-20% in mice), somatostatin secreting delta cells (10-15% in human and 5% in mice), pancreatic polypeptide secreting epsilon cells and ghrelin secreting gamma cells (Weir and Bonner-Weir 1990). Only a minor up to 1-5% of the pancreas volume are occupied by the pancreatic Islets of Langerhans and their location is scattered throughout the pancreas generally near blood vessels. Interestingly, different islet sizes are apparent which varies greatly from 50-500 μm in diameter with an average of 200-500 endocrine cells in human (Abdulreda and Berggren 2021). Generally, less than 10% of the islets constitute to 50% of the beta cell volume thereby revealing the proportion of smaller amounts of large to higher amounts of small islets (Rorsman and Ashcroft 2018). In humans, the islet architecture appears unstructured with intermingling of the endocrine cells and a higher amounts of alpha cells compared to mouse islets in which a clear core of beta cells is surrounded by a mantle of non-beta cells (Kim et al. 2009). Noteworthy is, that though pancreas size increases with body size dependent on the species, the islet size remains in the same size range (Steiner et al. 2010). In humans all endocrine cells including the pancreatic beta cell are formed during the embryonic day (E)12.5-15.5 transition. The endocrinogenesis has been shown to be initiated by the emerged expression of transcription factor neurogenin 3 (Ngn3) (Georgia et al. 2010). This islet progenitor cell marked by expression of *Ngn3* gives rise to all islet lineage cells (Gradwohl et al. 2000). Differentiation towards a beta cell fate require the expression of several transcription factors which include *Foxa2a*, *Pdx1*, *Nkx6.1*, *Neurod1*, *Nkx2.2* and *Isl1* (Salinno et al. 2019). These transcription factors are important to maintain beta cell identity. The final maturation of the beta cells occurs

postnatal. The expression of the secreted peptid Urocortin3 (Ucn3) marks an early phase of postnatal maturation as well as Synaptotagmin4 (Syt4) which reduces calcium sensitivity important for the exocytosis of insulin granules. The Maf family is important as there is a switch of the high MafB levels in embryonic beta cells replaced by MafA expression which is also distinguishing beta from alpha cell fate (Nishimura et al. 2006). During the course of functional maturation of the beta cell, glucose stimulated insulin secretion capacity is enhanced at the expense of proliferation capacity while metabolic switch from amino acid to fatty acid to glucose occurs (Salinno et al. 2019). The maturation process of beta cells seem to be highly dynamic state as indicated by the heterogeneity in terms of insulin release, transcription profile and protein expression and the reversibility in beta cell function from a senescence state and de-/transdifferentiated state (Salinno et al. 2019; Barsby and Otonkoski 2022). The beta-cell mass is controlled by a balance of proliferation/neogenesis and apoptosis of beta-cells. In pregnancy or obesity the beta-cell mass has been shown to expand to adapt to the insulin demand (Weir and Bonner-Weir 2013; Rieck and Kaestner 2010). Proliferation by self-duplication has been attributed mainly to the beta cell mass expansion (Dor et al. 2004) however recently neogenesis of pancreatic beta cells has also been recognized to occur in adulthood (Bonner-Weir 2021; Gribben et al. 2021). Interestingly, most beta cells are quiescent and reside in a non-mitotic G0 phase while another beta cell population retain proliferation capacity (Hesselson et al. 2009). However, proliferation capacity of beta cells decreases with age from neonatal 4% to about 0.2% in humans and from 10% to 1% in adult mouse beta cell proliferation capacity which explains the higher diabetes risk with increasing age (Spears et al. 2021).

1.3.1 The mechanism of insulin synthesis, maturation and secretion

The discovery of insulin in 1921 by Frederick Banting and Charles Best has marked a revolution for diabetes mellitus therapy (Banting and Best 1922). From 1922 when Leonard Thompson as the first person received insulin injection, insulin therapy has significantly changed the course of diabetes mellitus disease, increased life expectancy and quality of life for diabetics (Cantley and Eizirik 2021). The amino acid composition of the polypeptide hormone insulin consisting of 51 amino acids was first sequenced by Frederick Sanger in 1955, which earned him the Nobel prize for chemistry (Sanger and Thompson 1953). Since then, numerous studies have improved the knowledge about insulin synthesis and secretion mechanism.

The synthesis and formation of functional insulin has been found to undergo three major proteolytic steps by processing of a larger precursor. Insulin is initially synthesized as an immature pre-proinsulin precursor which is directly translated into the endoplasmic reticulum (ER). The first step is the proteolytic cleavage of the signal peptide resulting in the proinsulin molecule (Liu et al. 2015; Hou, Min, and Pessin 2009). The second step is mediated by the oxidative environment of the inner ER which facilitates the forming of three disulfide bonds, two between the A- and B-chain and one disulfide intrachain on the A-chain. The proinsulin is folded for exit from the ER with the assistance of chaperones (Omar-Hmeadi and Idevall-Hagren 2021). Following, intracellular trafficking of insulin through the Golgi apparatus the rising Zn^{2+} concentration in the lumen initiates hexamerization of the insulin molecules with two zinc ions facilitated by zinc transporter 8 (Znt8). Next, the proinsulin is concentrated into clathrin coated immature granules in which a pH change from 6.5 in the trans Golgi membrane to ~ 5 mediates the action of prohormone convertase PC1/3, PC2 and carboxypeptidase E (CPE) cleaving the C-peptide and finally forming the mature bioactive insulin. As the C-peptide is released in equimolar amounts to insulin and generally more stable, it is used in clinical settings to indirectly evaluate islet function. Insulin secretion is unique to pancreatic beta cell in the islets of Langerhans and is tightly regulated by nutrient availability. The mechanism by which glucose stimulates insulin secretion in the pancreatic beta cells are the sensing of glucose by glucose transporter (GLUT1 in human or GLUT2 in mouse) which facilitates the transport of glucose into the cell. Endogenous glucose is then phosphorylated by glucokinase to glucose-6-phosphate and catabolized through glycolysis into pyruvate. Thereafter, pyruvate fuels the citric acid cycle (TCA) and oxidative phosphorylation in the membrane on the mitochondria leads to the production of energetic ATP. The higher ATP/ADP ratio in the cytosol leads to the closure of the ATP sensitive potassium channel (K_{ATP}) and depolarization of the plasma membrane which in turn opens the voltage dependent Ca^{2+} channel (VDCC). The influx of calcium leads to the fusion and exocytosis of insulin cargo (Rorsman and Ashcroft 2018). In a postprandial state, nutrients besides glucose, fatty acids, amino acids act as insulin secretagogues (Oyadomari et al. 2002). Additionally, the gastrointestinal track releases the gut hormones the incretins glucagon-like peptide (GLP-1) and gastric inhibitory polypeptide (GIP) which potentiates insulin secretion. The secretion of insulin occurs in a biphasic manner. Different insulin granules pools dependent on the localization

initiate the two phases of insulin release. A rapid first phase release last for a few minutes through an insulin granule pool pre docked at the plasma membrane termed the ready releasable pool (RRP). The majority of insulin granules however retain within the cytoplasm and require cytoskeletal remodeling for mobilization to the plasma membrane. These insulin granules mediate a slow sustained second phase insulin release (Wang and Thurmond 2009). Beta cells can produce up to 1 million insulin molecules per minute and this is potentiated after glucose intake (Ikegami, Babaya, and Noso 2021).

1.3.2 Beta cell failure in T1D and T2D

Diabetes mellitus covers a heterogeneous disease spectrum in both T1D and T2D with one factor in common: beta cell fail to adapt to the insulin demand resulting in hyperglycemia. Insulin deficiency, found in both T1D and T2D, is a result of a reduced beta cell function (beta cell dysfunction) and/or loss of beta cell mass (beta cell demise). Despite different pathogenesis and etiology of the subtypes of diabetes, shared susceptibilities and underlying mechanism in beta cell failure have been suggested by a variety of studies (Ikegami, Babaya, and Noso 2021; Dooley et al. 2016). A hypothesis regarding the heterogenous pathogenesis of beta cell failure suggests that it is dependent on the intrinsic defense mechanism of the beta cells which can vary due to genetic factors. Adding extrinsic factors such as immune activation or lifestyle insulin resistance, which are powerful stressors, can lead to beta cell defeat (Ikegami, Babaya, and Noso 2021). Once beta cell mass is compromised by beta cell demise such as in T1D, the theory is that the remaining beta cells would have to compensate by increasing insulin production and secretion leading to an overwork and stress for each individual beta cell (Ikegami, Babaya, and Noso 2021). The same can be applied to the state of insulin resistance in T2D, in which the insulin signaling in the target tissues show impairment. In turn, glucose uptake is hindered due to lack of glucose transporters at the plasma membrane. Due to remaining high blood glucose, the feedback to the insulin producing beta cells is suspended therefore leading to additional insulin secretion which can result in a hyperinsulinemic state (Bich, Mossio, and Soto 2020). In most cases, the production of more insulin can overcome the insulin resistance however increasing insulin production causes stress for the cell as production, processing, folding and packaging of insulin is increased. One of the first stress response is caused by excessive glucose oxidation (glucotoxicity) leading to oxidative stress. Glucose turnover in glycolysis and oxidative

phosphorylation process in the mitochondrial respiratory chain not only produces energy rich ATP but is also a major source of reactive oxygen species (ROS). As byproducts of normal cellular metabolism, depending on the concentration, ROS can elicit beneficial or harmful effects. As ROS are extremely reactive, antioxidant enzymes such as superoxide dismutase (SOD) are there to convert reactive superoxide anion (O_2^-) to hydrogenperoxid (H_2O_2) and further is detoxified by catalase (Cat) and glutathione peroxidase (GPx) action to H_2O and O_2 (Kulkarni et al. 2022). However, since beta cell display a low abundance of these enzymes, they are extremely prone towards oxidative stress (Drews, Krippeit-Drews, and Dufer 2010; Lei and Vatamaniuk 2011; Dinic et al. 2022). Prolonged hyperglycemic state produces an excess of ROS that exceeds the antioxidant capacity which causes damage to DNA, lipids (lipid peroxidation) and proteins (protein oxidation). For example, H_2O_2 has been shown to repress *Pdx1* binding to the insulin promotor which inturn affects insulin gene expression (Kaneto et al. 2002). Likewise, H_2O_2 causes a translocation of transcription factor *MafA* to the cytoplasm (Guo et al. 2013). Other studies found H_2O_2 to decrease other beta cell identity markers such *Nkx6.1*, *Pax4*, *Pax6*, *NeuroD* and also *Glut1* expression in human beta cells (Leenders et al. 2021). These studies indicate that oxidative stress is able to alter important transcription factors of insulin and mediate a loss of beta cell identity promoting a trans-/dedifferentiation of the beta cell. Damage to DNA through oxidate stress can further lead to apoptosis or senescence (Dinic et al. 2022). The second stress response is caused by a high insulin demand. Since beta-cells main function is production and secretion of insulin, over 50% of total mRNA in the cell are dedicated for insulin synthesis and processing (Barrabi et al. 2023). Therefore, the function of the endoplasmic reticulum (ER) is especially important for the beta cell. Chronic hyperglycemia, insulin resistance or loss of beta cell mass causes a high demand of insulin protein production. This results in an accumulation of proteins exceeding the folding capacity of the ER leading to unfolded or misfolded proteins a state termed as ER stress. To alleviate further accumulation, the unfolded protein response (UPR) is activated to slow global protein synthesis. Under normal conditions the UPR sensors bind to the chaperone binding immunoglobulin protein (BiP). However, unfolded or misfolded proteins causes a conformation change and dislocation of the chaperone BiP from the three UPR which are sensors inositol requiring enzyme1 α (*IRE1 α*), PKR-like endoplasmic reticulum kinase (*PERK*) and activating transcription factor 6 (*ATF6*) to bind the misfolded protein for proteasomal

degradation. The three UPR sensors triggers mechanisms to relieve ER stress. PERK phosphorylation activates transcription factors translation initiation factor 2 subunit 1 (eIF2 α) which transiently inhibits translation of proteins and thereby also preproinsulin. *IRE1 α* generates transcription factor X-box binding protein 1 (XBP1) which promotes expression of chaperones and degradation of proteins associated to the ER likewise to cleaved ATF6 transcription factor. Prolonged ER stress induce pro-apoptotic signaling through CHOP and result in the apoptosis of the beta-cell. In addition, high glucose levels deplete the cell from Ca²⁺ which is essential for ER function. The third stressor depicts the autoimmune system. Not only in T1D does the immune system mediate a beta cell destruction but also the chronic inflammation in T2D activates a cell destructing immune response. Insulinitis is the term for the inflammatory infiltration of the Islets of Langerhans by immune cells including T- and B-lymphocytes, macrophages, dendritic cells which appears in T1D. Genetic variations associated to the autoimmune destruction in T1D are found in the major histocompatibility complex (MHC) also known as the human leukocyte antigen (HLA) region in human (Sticht, Alvaro-Benito, and Konigorski 2021). In T2D the number of inflammatory macrophages within the islet are increased. High glucose and FFA levels induce a signaling cascade through MyD88 activating NF- κ B mediating release of chemokines and IL-1 receptor signaling which recruits proinflammatory M1-like macrophages to the beta-cell. The proinflammatory cytokines release by M1-like macrophage among which IL-1 β leads to beta-cell dysfunction and ultimately apoptosis. Through these molecular mechanisms like oxidative stress, ER stress and inflammation the beta becomes dysfunctional losing function and identity. To avert apoptosis, the beta cell presumably derails and is able to dedifferentiate to endocrine progenitor, transdifferentiate to alpha cell or goes into senescence before apoptosis leads to beta-cell failure (Salinno et al. 2019).

1.4 Genetic aspects of Diabetes mellitus

Beside contribution of environmental factors as causes for diabetes, the genetic background facilitates the susceptibility to the disease progression. In T1D genetic studies were able to explain up to 80% of the heritability mostly accounting to the MHC (HLA) loci (Prasad and Groop 2015). In T2D, heritability studies uncovered that first-degree relatives appear to have a 3-fold higher chance to develop T2D in their lifetime compared to individuals without the genetic family background and heritability among

individuals between 35-60 years of age has been estimated to around 69% (Meigs, Cupples, and Wilson 2000; Suzuki et al. 2024). However, genetic variants discovered to be associated to T2D so far can only explain up to 20% of the heritability factor (Goyal et al. 2023). Rare alleles or large number of common variants with low additive effects are thought to explain the the “missing heritability” component in T2D (Prasad and Groop 2015). Genetic studies using linkage analysis, candidate gene studies, genome wide common association studies and genome wide rare association studies have identified a variety of monogenetic diabetes forms, common genetic variants and rare variants (Laakso and Fernandes Silva 2022; Goyal et al. 2023). In particular, autosomal dominant monogenetic genes were discovered which are grouped as maturity onset diabetes of the young (MODY) type. These genes mainly belong to transcription factors for insulin including the hepatic nuclear factor A1 (HNF1A), PDX1, NEUROD1 and PAX4. Other MODY type confer to mutation in the glucose sensor glucokinase (Gck) or glucose transporters Glut1/2 confer. Mutations in subunits of the ATP sensitive potassium channel KCNJ11 (Kir6.2) and ABCC8 (SUR) have shown to lead to a neonatal diabetes (Tosur and Philipson 2022). In type 2 diabetes though, many genes with moderate contribution appear to confer to the pathophysiology. Genetic variations were observed to occur in PPAR, *TCF7L2*, *SLC30A8*, *CDKAL1* and *FTO* among many other associated to diabetes (Laakso and Fernandes Silva 2022; Goyal et al. 2023). Additionally, mouse studies are applied as a complementary tool to identify diabetes and adiposity susceptibility genes like *Tbc1d1*, *Zfp69*, *Iff1202b* and candidate genes such as *Atp4a*, *Pop4*, *Kti12*, *Osbpl9*, *Ttc39a*, *Calr4*, *S100z*, *Kdelr3* (Chadt et al. 2008; Scherneck et al. 2010; Altenhofen et al. 2023; Vogel et al. 2012; Schallschmidt et al. 2018; Jonas et al. 2022; Aga et al. 2020). The majority of identified genetic factors affect insulin secretion rather insulin sensitivity (Thomsen and Gloyn 2014; Laakso and Fernandes Silva 2022). Interestingly, most identified SNPs are located in non-coding regions as opposed to coding gene highlighting gene transcription major role. The identification of diabetes susceptibility genes has enabled the development of the polygenic risk score to predict the lifetime genetic risk for diabetes disease (Goyal et al. 2023; Laakso and Fernandes Silva 2022).

1.5 Diabetes mouse model C57BL6/J

In diabetes research, laboratory mouse models have proven invaluable for studying pathophysiology, genetic contributions, environmental factors and aid in preclinical drug development studies (Dominguez-Oliva et al. 2023; Singh, Gholipourmalekabadi, and Shafikhani 2024). The establishment of large databases and a variety in well characterized mouse models further aid in the application of mouse models. An inbred mouse model often used in diabetes studies is the C57BL/6J (6J) mice (Daniels Gatward et al. 2021). This mouse model is characterized by a black fur color due to mutation in the agouti gene and in diabetes research represents a commonly used model for diet induced obesity (DIO) showing glucose intolerance and impaired glucose stimulated insulin secretion in response to high-fat diets (Surwit et al. 1988). A brief history: The C57BL/6 mice were first generated in 1921 by Dr. C.C. Little. In 1948, a subline was established and maintained at the Jackson Laboratory, henceforth named C57BL/6J. In 1951, a separate colony was raised at the National Institutes of Health (NIH) and became known as C57BL/6N (Mekada and Yoshiki 2021). The background strain is important to note as the most common mouse models for obesity and T2D the ob/ob mutation in the leptin gene and the db/db mutation in the leptin receptor produce only mild diabetes phenotype due to islets hypertrophy and hyperplasia on the C57BL6/J background but on a C57BLKS/J background, a substrain with 71% C57BL6/J background, the mice develop severe diabetes and islet atrophy (Suriano et al. 2021; Hummel, Dickie, and Coleman 1966; Muzzin et al. 1996). SNP panels offered by the Jackson Laboratories in Maine, USA (JAX) can distinguish specific SNPs between the 6J substrains. One of the known mutation that differs between both strains constitutes in the nicotinamide nucleotide transhydrogenase (Nnt) gene. 6J mice show carry a in-frame five exon deletion resulting in missing of exons 7-11 and absence of the coding protein (Fontaine and Davis 2016). NNT is an integral protein of the inner mitochondrial membrane and produces NADPH which is important for removal of reactive oxygen species (ROS). Transgenic expression of Nnt in C57BL/6J rescues the metabolic dysfunction highlighting the mutation in glucose metabolism and importance for beta cell function (Freeman, Hugill, et al. 2006; Freeman, Shimomura, et al. 2006).

1.6 Cre/LoxP system and the International Mouse Phenotyping Consortium (IMPC)

The Cre/LoxP technology is a useful tool in dissecting the genetic contribution of individual genes to the pathophysiology of diseases and additionally enable the investigation of their cell autonomous roles and temporal resolution (Kim et al. 2018). The Cre recombinase is a site specific DNA recombinase, first discovered in the bacteriophage P1 (Hamilton and Abremski 1984). The site specific recombination enzyme recognizes specific DNA fragments called loxP (locus of x-over P1) sites and mediates site specific recombination between two loxP sites (Sternberg and Hamilton 1981). LoxP sequence is a 34 bp consensus sequence consisting of 13 bp inverted palindromic repeats and 8 bp core sequence. The molecular mechanism of the recombination works by a single recombinase molecule binding to each palindromic half of a loxP site forming a tetramer bringing the two loxP sites together resulting in recombination of the spacer area leaving a postrecombinational loxP site (Nagy 2000). Dependent on the orientation of the loxP sites a deletion, insertions, inversion or translocation can be achieved. Tandem oriented loxP sites leads to deletion inbetween while inverted loxP sites orientation cause an inversion of the sequence (Kim et al. 2018; Nagy 2000). By implementing Cre into cell-specific drivers aka promoters the recombination can be controlled in a spatial resolution (Kim et al. 2018; Song and Palmiter 2018). For the beta cell, several promoter driven Cre lines were explored. The Cre under rat *Ins2* promoter termed RIP-Cre were among the first Cre driver line for the beta cell field. However, *Ins2* expression was shown in embryonic and adult brain leading to an unwanted deletion in the brain beside the beta cell specific targeting (Song et al. 2010; Wicksteed et al. 2010). As mouse and rat uniquely possess two insulin genes, *Ins1* arising from gene duplication, the *Ins1^{Cre}* was created with selective beta cell excision of the targeted gene and showed no effect on body weight and glucose metabolism (Thorens et al. 2015). The Cre/LoxP system is utilized, among other applications, by the International Knockout Mouse Consortium (IKMC) to produce transgenic knock-out (KO) mice. The IKMC is an international consortium founded in 2007 aiming at generating a knock out (KO) of every protein coding gene in mice (Rosen, Schick, and Wurst 2015). These include the Knockout Mouse Project (KOMP) of the USA, the European Conditional Mouse Mutagenesis Program (EUCOMM) and the North American Conditional Mouse Mutagenesis Project (NorCOMM). KOMP2 is the second phase launched in 2011 by the NIH initiative generating KO mouse model

using CRISPR/Cas9 system. The knockout mice are generated in different centers all over the world. Up until the latest update (Release 20.1 12.12.2023), the number of phenotyped genes in total accounts to 8.707 knockout mice successfully generated accounting for an achievement of ~40%. The KO mice are generated through different systems however predominantly the Cre/LoxP system was implemented for the IMPC. The first step is the genetic targeting of the gene of interest in embryonic stem cells from C57BL/6N mice as germline transmission is higher than with ES cells from C57BL/6J mice (Fontaine and Davis 2016). Therefore, to design conditional alleles, a computational tool to identify oligonucleotide sequences suitable for recombineering are used to insert selection cassette and loxP sites around the critical exon in bacterial artificial chromosomes (BAC). The critical exons of the gene described to be selected by mainly three criteria: 1. Commonality in all transcripts 2. Identified by ArrayOligoSelector 3. Selected for the 5' most critical exons that disrupts at least 50% of the protein coding sequence (Skarnes 2011). Several helping plasmids and the target exon fragment are electroporated into the BAC and the successful recombineering is genotyped by long-range PCR. For the selection of chimeras, the mutation in the agouti locus was further repaired which results in C57BL/6N ES with heterozygous functional agouti gene displaying brownish coat color. The ES cells are thereafter microinjected into the blastocyst which is implanted into a surrogate female. To achieve germline transmission these chimera mice are mated (Fontaine and Davis 2016). Following a pipeline, the mice are phenotyped according to a set schedule and the data can be found on the IMPC website (<https://www.mousephenotype.org/>).

1.7 *Pop4* emergence as a candidate gene of a mouse QTL

Previous studies of our group aimed at identifying novel obesity and type 2 diabetes genes using linkage analysis as part of the collective diabetes cross (Vogel et al. 2018). Therefore, mouse models that differ in phenotypic trait of interest, in our case T2D prevalence, were selected: the New Zealand Obese (NZO) and the C3HeB/FeJ mouse strain (Schallschmidt et al. 2018; Vogel et al. 2018). Male NZO mice show a high diabetes penetrance of ~50% (Leiter et al. 1998) while C3HeB/FeJ mice exhibit high glucose tolerance (Champy et al. 2008). A backcross population of these mice intended to uncover genetic determinants of the C3HeB/FeJ or NZO influencing glucose metabolism through a linkage analysis. The *in silico* linkage analysis combines information about the genetic variation with continuous phenotypic traits of these mice

to map quantitative trait loci (QTL) where the association is termed significant by the logarithm of odds (LOD score). The genetic variation was determined using single nucleotide polymorphism (SNP) markers distinguishing these mouse strains and the phenotypic data were obtained covering metabolic traits over a defined time period. A strong association to a locus on chromosome 7 was uncovered to several traits including blood glucose, plasma insulin levels and body weight in male mice (**Figure 1A**). Introgression of the QTL locus named NZO blood glucose on Chromosome 7 (*Nbg7*) from C3H into the NZO genome could generally reduce blood glucose levels through sustained insulin secretion compared to control which validated the *in-silico* analysis (Schallschmidt et al. 2018). *Pop4* emerged as an underlying candidate gene from the haplotype and gene expression analysis. It was shown to be significantly lower expressed in C3H allele carriers in pancreatic islets indicated by data from microarray and qPCR. Further, *in-vitro* studies in the insulinoma mouse cell line Min6 showed that diminishing ~81% of the *Pop4* expression reduced glucose stimulated insulin secretion and lead to a decrease in insulin expression (**Figure 1 B+C**) (Schallschmidt et al. 2018). Moreover, expression data from human pancreatic islets indicate a correlation of *Pop4* expression with insulin expression (**Figure 1D**) (Asplund et al. 2022). The whole body *Pop4* knock out mouse model generated for IMPC showed embryonic lethality in both males and females however a heterozygous knockout diminished circulating insulin levels in the male mice (<https://www.mousephenotype.org/data/genes/MGI:1913411>).

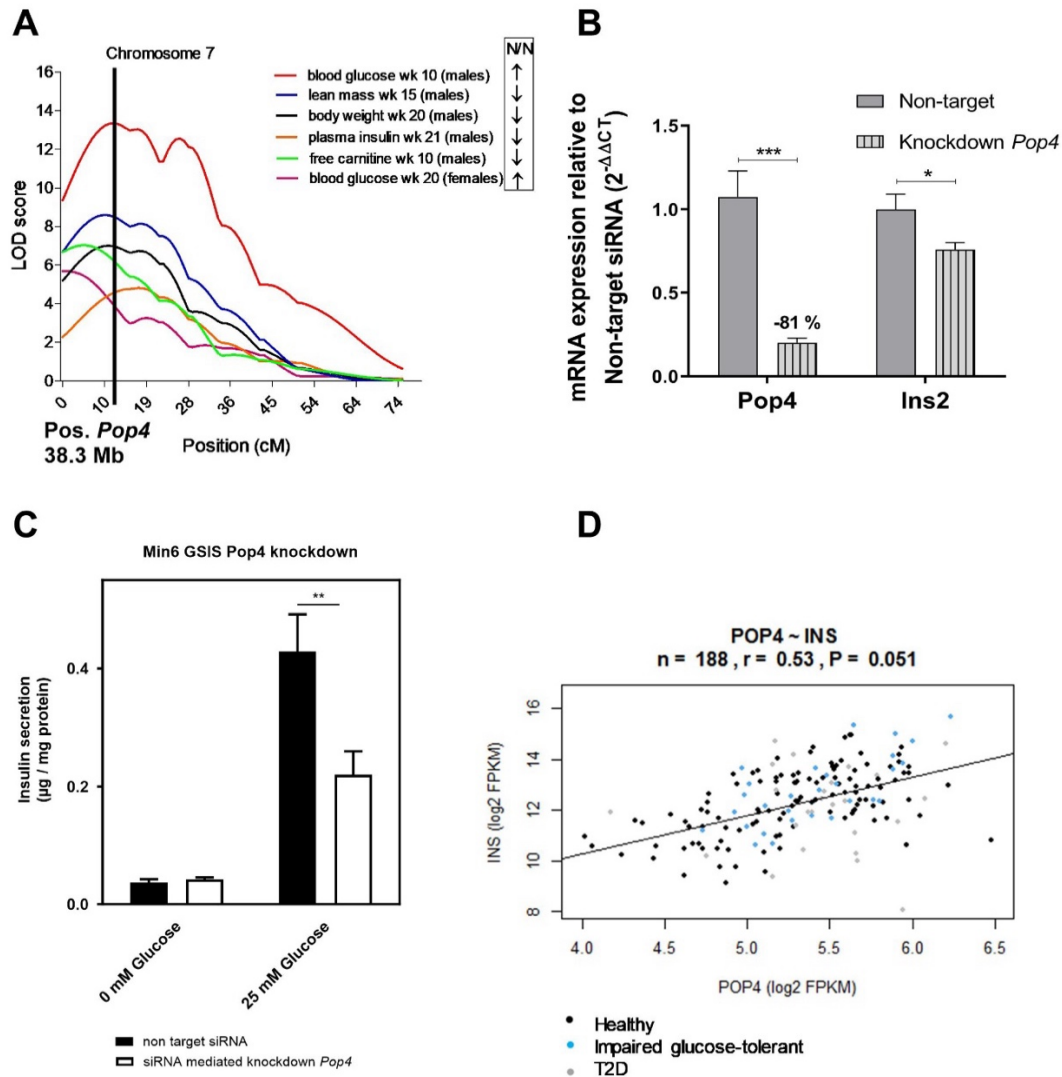


Figure 1: Previous data on *Pop4* relation to insulin secretion function.

(A) Quantitative trait loci on chromosome 7 from a backcross of NZO and C3H male mice depicting association to mainly blood glucose, body weight and lean mass, plasma insulin and free carnitine in males. *Pop4* position indicated directly in the peak of the QTL. (B) Validation of siRNA mediated knockdown of *Pop4* mRNA and *Ins2* expression level from a Min6 cells. (C) Glucose-stimulated insulin secretion assay without glucose and with 25 mM glucose stimulation of the insulinoma Min6 cell line. (D) Correlation of insulin (*INS*) expression and *Pop4* expression in human islets of health, impaired glucose tolerant and type 2 diabetics. (Schallschmidt et al. 2018; Asplund et al. 2022)

1.8 Endoribonuclease subunit processing of precursor 4 (*Pop4*)

POP4, alias ribonuclease P protein 29 (RPP29), encodes the ubiquitously expressed *Pop4/Rpp29* gene, which is described to play pivotal roles in essential processes. Canonically, it is described to be a subunit of the closely related ribonuclease (RNase) P and RNase mitochondrial RNA processing (MRP) complexes (Chu, Zengel, and Lindahl 1997). RNase P is highly conserved in the three domains of life from archaea, bacteria to eukaryotes (Kouzuma et al. 2003; Walker and Engelke 2006) while RNase MRP emerged as a gene duplication only in eukaryotes (Martin and Li 2007). The

endoribonuclease P and MRP are ribozymes that cleave RNA sequences via the non-coding RNA subunit (Guerrier-Takada et al. 1983). At least 10 protein subunits are shared between the related RNase P and RNase MRP complexes (Shaukat et al. 2021). Among them *Pop4* which was found 1997 in the yeast *Saccharomyces cerevisiae* and characterized as necessary for 5.8S rRNA and tRNA processing in immunoprecipitation studies together with other proteins it was renamed processing of precursor 4 (Chu, Zengel, and Lindahl 1997). Soon after, the human counterpart to yeast *Pop4*, termed h*Pop4*, was discovered and described to be localized to the nucleus and particularly in the nucleolus which is now known to be the site of ribosome biogenesis (van Eenennaam, Pruijn, and van Venrooij 1999; Jarrous, Wolenski, et al. 1999). In the same year, Jarrous et al. validated the existence of human *Rpp29* in HeLa cells however *Rpp29* only showed 23% sequence identity with yeast subunit *Pop4p* (Jarrous, Eder, et al. 1999; van Eenennaam, Pruijn, and van Venrooij 1999). In yeast, *Rpp29* interacts with other RNase P and MRP subunits but also interacts directly with the RNA subunit H1 (Jiang and Altman 2001; Jiang, Guerrier-Takada, and Altman 2001). Studies on Human RNase P have shown that the activity can be reconstituted by subunits H1, *Rpp21*, and *Rpp29* in the presence of $MgCl_2$ (Mann et al. 2003). Moreover, *Rpp29* functions in pairs with *Rpp21* and is the primary contact to the two helices of *Rpp21* (Amero et al. 2008). The gene harbors seven exons in human and eight in mouse, and to date, little is known about protein domains (<https://www.ncbi.nlm.nih.gov/gene/66161>). Studies on *Pop4* show that it interacts with the other subunits as the crystallographic structures of RNase P/MRP show that in human RNase P cryo EM structure of *Pop4* is in the wrist (Wu et al. 2018), which cleaves the 5' end of tRNA or cleaves the rRNA at the internal transcribed spacer (ITS) site in yeast (Lan et al. 2020) respectively. It is further described to play a role in double-stranded DNA repair together with *Rpp21* via binding to H1 RNA (Abu-Zhayia et al. 2017). Furthermore, it has been shown that knockdown of *Rpp29* represses histon 3.3 incorporation into chromatin structures, thus playing a role in gene transcription regulation (Newhart et al. 2016; Shastrula et al. 2018). Interestingly, predicted copy number variants of *Pop4* have been linked to ovarian cancer (Wrzeszczynski et al. 2011) while silencing of *Pop4* reduced cell viability in cancer cells (Natrajan et al. 2012) and upregulation of *Pop4* has been associated to osteosarcoma metastasis (Southeikal et al. 2023). To date, the relationship between *Pop4* and diabetes pathophysiology was not elucidated.

2 Aim

The aim of this thesis was to investigate the role of *Pop4* for pancreatic beta cell biology in an *in vivo* mouse model. Therefore, a knockout mouse model was generated via the Cre/LoxP technology specific for pancreatic beta cells to explore the cell autonomous role. Characterization of the knockout mouse model focused on the unique function of pancreatic beta cells in secreting insulin upon glucose stimulation. Morphological analyses aimed to elucidate beta cell plasticity, hormone availability at different metabolic timepoints of life. Further, initial analysis strive to explore the mechanisms that *Pop4* exerts in the pancreatic beta cells.

3 Material and Methods

3.1 Material

3.1.1 Mouse strains

Table 1: Mouse strains

Strain	Abbreviation	Origin
Flp deleter mouse/N	Flp	Dr. Thomas Wunderlich, Dr. Karina Schöfisch (MPI Cologne, Germany)
B6(Cg)-Ins1 ^{tm1.1(cre)Thor} /J	<i>Ins1</i> ^{Cre}	Jackson Laboratory (Bar Harbor, Maine, USA)
B6.Cg-Gt(ROSA)26Sor ^{tm9} (CAG-tdTomato)Hze/J	Rosa26 ^{tdTomato}	Jackson Laboratory (Bar Harbor, Maine, USA)
C57BL/6N-A ^{tm1Brd} Pop4 ^{tm1a} (EUCOMM)WtsiOulu	<i>Pop4</i> ^{fl/fl}	Infrafrontier, European Mouse mutant archive (EMMA, Oulu, Finland)
C57BL/6N-A ^{tm1Brd} Pop4 ^{tm1d} (EUCOMM)WtsiOulu	<i>Pop4</i> ^{βKO}	German Diabetes Center (Düsseldorf, Germany)

3.1.2 Mouse diets

Table 2: Mouse diets and dietary composition

Diet	Fat (cal %)	Protein (cal %)	Carbohydrate (cal %)	Total calorie content (kcal/g)
Chow (Ssniff Soest, Germany, V1126)	11	36	54	3.3
60% kcal from fat with blue dye (Research Diets, New Brunswick, USA, D12492)	60	20	20	5.2

3.1.3 Expendables

Table 3. List of expendable materials and supplier

Expendable material	Supplier
Combi tips advanced® (0.2 ml, 0.5 ml)	Eppendorf (Hamburg, Germany)
Contour Next Glucose strips	Bayer HealthCare (Leverkusen, Germany)
Copper grids H75 mesh	Veco GmbH (Marl, Germany)
CRYO tubes	Thermo Fisher Scientific (Waltham, Massachusetts, USA)
Disposable scalpels	B. Braun (Melsungen, Germany)
MaXtract high density tubes	Qiagen (Hilden, Germany)
MicroAmp® Fast Optical 96-well reaction plates	Applied Biosystems (Waltham, Massachusetts, USA)
MicroAmp® Optical adhesive film	Applied Biosystems (Waltham, Massachusetts, USA)
Microscope slide cassettes	Carl Roth (Karlsruhe, Germany)
Microscope slides	Paul Marienfeld (Lauda-Königshofen, Germany)
Microvette CB 300µl Lithium-Heparin	Applied Biosystems (Waltham, Massachusetts, USA)
PCR-foils (MicroAmp® Optical Adhesive Film)	Applied Biosystems (Waltham, Massachusetts, USA)
PCR-plates 4titude FrameStar® 384-Well	Azenta (Burlington, Massachusetts, USA)
QIAshredder	Qiagen (Hilden, Germany)
Safe-lock-tubes (0.5 ml, 1.5 ml, 2.0 ml)	Sarstedt (Nümbrecht, Germany)
Stainless beads (5 mm)	Qiagen (Hilden, Germany)
Sterican® needle G24x1" / ø 0,55 x 25 mm	B. Braun (Melsungen, Germany)
Sterican® needle G26x1" / ø 0,45 x 25 mm	B. Braun (Melsungen, Germany)
Syringe Omnifix® 1 ml	B. Braun (Melsungen, Germany)

3.1.4 Chemicals and solutions

Table 4: Chemicals and solutions with supplier information

Chemical/Solution	Supplier
6x DNA loading dye	Thermo Fisher Scientific (Waltham, Massachusetts, USA)
Bovine serum albumin (BSA) Fraction V, pH 7.0	Applichem (Darmstadt, Germany)
Chloroform	Applichem (Darmstadt, Germany)
Citric acid	Sigma-Aldrich (St. Louis, Missouri, United States)
CMRL medium without L-glutamine	Gibco by Life Technologies (Carlsbad, USA)
Complete protease inhibitor cocktail	Roche (Mannheim, Germany)
Deoxynucleotide triphosphate mix (dNTPs)	Promega (Madison, USA)
Diprotin A	Bachem (Bubendorf, Switzerland)
DMEM 1g/L D-Glucose, L-Glutamine, Pyruvate	Gibco by Life Technologies (Carlsbad, USA)
Formaldehyd solution 4%, pH 6.9	Sigma-Aldrich (Steinheim, Germany)
Glucose 20%	B. Braun (Meslungen, Germany)
GlycoBlue Coprecipitant	Thermo Fisher Scientific (Waltham, Massachusetts, USA)
Eosin yellowish	Merck (Darmstadt, Germany)
3,4-Epoxy cyclohexylmethyl-3,4-epoxy cyclohexylcarboxylate (ERL-4221 D)	Serva (Heidelberg, Germany)
Ethylenediaminetetraacetic acid (EDTA)	Roth (Karlsruhe, Germany)
Ethylene glycol tetraacetic acid (EGTA)	Roth (Karlsruhe, Germany)
Fetal Bovine Serum (FBS)	Gibco by Life Technologies (Carlsbad, USA)
Fluoroshield™ with DAPI	Sigma-Aldrich (Steinheim, Germany)
Random primer	Roche (Basel, Switzerland)
HD green DNA stain plus	Intas Science (Göttingen, Germany)

Chemical/Solution	Supplier
Hematoxylin	Merck (Darmstadt, Germany)
Hexanucleotide Primer	Roche (Basel, Switzerland)
Histopaque-1077	Sigma-Aldrich (St. Louis, Missouri, United States)
Liberase™ Research Grade (collagenase)	Roche (Basel, Switzerland)
Sodium chloride (NaCl)	Carl Roth (Karlsruhe, Germany)
Sodium bicarbonate (NaHCO ₃) solution (7,5%)	Gibco by Life Technologies (Carlsbad, USA)
Magnesium chloride (MgCl ₂)	Promega (Madison, Wisconsin, USA)
β-Mercaptoethanol	Merck (Darmstadt, Germany)
Penicillin/Streptomycin solution	Thermo Fisher Scientific (Waltham, Massachusetts, USA)
Dulbecco' Phosphate Buffered Saline with Magnesium and Calcium	Gibco by Life Technologies, Carlsbad, USA
PhosphoSTOP Phosphatase Inhibitor	Roche (Basel, Switzerland)
Proteinase K	Carl Roth (Karlsruhe, Germany)
Random primer	Roche (Basel, Switzerland)
Shandon EZ-Mount	Thermo Fisher Scientific (Waltham, Massachusetts, USA)
Sodium dodecyl sulfate (SDS)	Applichem (Darmstadt, Germany)
Tris(hydroxymethyl)-aminomethane (TRIS)	Carl Roth (Karlsruhe, Germany)
Triton X-100	Sigma-Aldrich (St. Louis, Missouri, United States)
Trypsin-EDTA	Sigma-Aldrich (St. Louis, Missouri, United States)
TRIzol® Reagent	Thermo Fisher Scientific (Waltham, Massachusetts, USA)
Xylene	AppliChem (Darmstadt, Germany)
Wax (Paraplast®PLUS)	Carl Roth (Karlsruhe, Germany)

3.1.5 Buffer and solutions

Table 5: Buffer or solution composition and application

Name	Ingredients	Application
Anticoagulant	25 mL 0.5 M EDTA, 92 mg aprotinin dissolved in 21 mL saline (0.15 M), 4 mL heparin (10.000 U/mL), 21.6 mg diprotin A	To avoid coagulation of the blood
Citric acid buffer	0.1 M Citrusacid in Aqua dest.	For the heat mediated antigen retrieval of pancreatic paraffin sections
DNA lysis buffer	0.1 M Tris-HCl (pH 8.0), 0.2 M NaCl, 5 mM EDTA, 0.4 % SDS	To isolate DNA for genotyping and validation of ablation of Exon 4 and 5 in sorted beta cells.
Eosin staining solution	0.1% Eosin G in 70% EtOH, 40 µl glacial acetic acid per 100 ml solution	For the Eosin staining step during HE staining
Protein Lysis buffer	20 mM Tris, 150 mM NaCl, 1 mM EDTA, 1 mM EGTA, 1% Triton X-100	To extract total protein from pancreatic islets
Krebs Ringer HEPES (KRH) buffer	15 mM HEPES, 5 mM KCl, 120 mM NaCl, 24 mM NaHCO ₃ , 1 mM MgCl ₂ , 2 mM CaCl ₂ , 1 mg/mL BSA	Media for the GSIS experiment
Pancreatic islet medium	15 % FBS, 0.1 % 50 mM β-Mercaptoethanol, 1 % penicillin/streptomycin, 0.5 % 1.11 M glucose, 2 % NaHCO ₃ solution (7.5 %) in CMRL medium without L-glutamine and HEPES	For the recovery of the pancreatic islets after overnight incubation
Phosphate-buffered saline (PBS)	137 mmol/L NaCl, 2.7 mmol/L KCl, 10 mmol/L Na ₂ HPO ₄ , 1.8 mmol/L KH ₂ PO ₄	As a washing buffer for immunostaining
PBS-T	0.2% Triton X-100 in 1xPBS	As a washing buffer and antibody diluent for immunostaining
Sodium citrate buffer	0.1 M sodiumcitrat in Aqua dest.	For the heat mediated antigenretrieval of pancreatic paraffin sections
TAE buffer	40 mM Tris acetate, 1 mM EDTA	To prepare the agarose gel and as a running buffer for the gel electrophoresis

3.1.6 DNA ladder and polymerases

Table 6: DNA ladder and supplier

DNA ladder	Supplier
50 bp	Thermo Fisher Scientific (Waltham, Massachusetts, USA)
100 bp	Thermo Fisher Scientific (Waltham, Massachusetts, USA)
1 kb	Thermo Fisher Scientific (Waltham, Massachusetts, USA)

Table 7: Polymerases for PCR and supplier

Polymerases	Supplier
DreamTaq DNA Polymerase	Thermo Fisher Scientific (Waltham, Massachusetts, USA)
Phusion™ High-Fidelity DNA Polymerase	Thermo Fisher Scientific (Waltham, Massachusetts, USA)

3.1.7 Primer sequences

For the genotyping of the mice, primer sequences were provided by JAX or EUCOMM for the respective mouse lines.

Table 8: Genotyping Primer sequences and the position in the genome

Target	Primersname	Sequence 5'→3'	Product length
Pop4	Pop4_196147_F	CCAAGGATCTGCCTCTCTGG	461 bp
	Pop4_196147_R	CCCCAACCTGCTACTCGAAC	
	CAS_R1_Term	TCGTGGTATCGTTATGCGCC	133 bp
Ins1Cre	Ins1-Cre Fwd (15832)	TGCGAACCTCATCACTCGT	300 bp
	Ins1-Cre Rev (19101)	TGGACTATAAAGCTGGTGGGCA T	
tdTomato	Tomato_WT_for (1)	AAGGGAGCTGCAGTGGAGTA	297 bp
	Tomato_WT_rev (2)	CCGAAAATCTGTGGGAAGTCAT	
	Tomato_TG_for (3)	GGC ATT AAA GCA GCG TAT CC	196 bp
	Tomato_TG_rev (4)	CTG TTC CTG TAC GGC ATG G	

For the validation of Exon 4 and 5 ablation on DNA and mRNA level to quantify mRNA level of Pop4 via RT-qPCR, primers were designed using NCBI Primer Blast online tool and produced by Eurogentec (Seraing, Belgium).

Table 9: Primer sequences to validate ablation of Exon 4 and 5

Target	Primername	Sequence 5' ->3'	Product length (KO/WT)
Pop4 Cas1+ Intron6	Cas1 F	AAGGCGCATAACGATACCAC	164/1179 bp
	Intron 6 R	ACTGATGGCGAGCTCAGACC	
Pop4 Exon 1+7	Pop4 TOPO1 F	GTCCGTGCACTTTGTTAATTGT	931/1079 bp
	Pop4 TOPO1 R	TCCTGGTGTGTTTCTGCTAGT	

Table 10: Primer sequences for RT-qPCR

Target	Primername	Sequence 5' ->3'	Product length
Pop4 Exon 4+5	Pop4 Exon4N F	ATACAGCCTGTTCCCTCCCTCT	323 bp
	Pop4 Exon5+6J R	GGCACTTGGATTTTCGTGACTG	
Beta actin	ActB F	CCACCATGTACCCAGGCATT	253 bp
	ActB R	AGGGTGTA AACGCAGCTCA	

3.1.8 Antibodies

Table 11: Antibodies with supplier information

Antibody	Host	Dilution	Product number	Supplier
Insulin, monoclonal	mouse	1:200	ICBTACLS	Thermo Fisher Scientific (Waltham, Massachusetts, USA)
Glucagon, monoclonal	rabbit	1:200	EP3070/ ab92517	Abcam (Cambridge United Kingdom)
Nkx6.1, monoclonal	rabbit	1:200	EPR20405/ ab221549	Abcam (Cambridge United Kingdom)
Ki-67, monoclonal	rat	1:750	SolA15	Thermo Fisher Scientific (Waltham, Massachusetts, USA)

Antibody	Host	Dilution	Product number	Supplier
γH2A.X (pS139), polyclonal	rabbit	1:500	ab11174	Abcam (Cambridge United Kingdom)
anti-Rat IgG (H+L) Alexa Fluor™ 647	goat	1:500	A21247	Invitrogen (Waltham, Massachusetts, USA)
anti-Rabbit IgG (H+L) Alexa Fluor™ 568	donkey	1:500	A10042	Invitrogen (Waltham, Massachusetts, USA)

3.1.9 Commercial kits

Table 12: Kits, their application and supplier

Kit	Application	Supplier
Glucagon ELISA (Mouse)	Glucagon concentration from GSIS of isolated pancreatic islets	Mercodia (Uppsala, Sweden)
GoScript® Reverse Transcription System	cDNA synthesis	Promega (Madison, Wisconsin, USA)
GoTaq® qPCR Master Mix	RT-qPCR	Promega (Madison, Wisconsin, USA)
Insulin ELISA (Mouse)	Insulin concentration from GSIS of isolated pancreatic islets	DRG (Marburg, Germany)
Proinsulin ELISA (Mouse)	Proinsulin from glucose stimulated insulin secretion of isolated pancreatic islets	Mercodia (Uppsala, Sweden)
Ultrasensitive Insulin ELISA (Mouse)	Plasma Insulin	DRG (Marburg, Germany)

Kit	Application	Supplier
RNase-free DNase set	To remove genomic DNA during RNA isolation	Qiagen (Hilden, Germany)
RNeasy Mini Kit	RNA isolation	Qiagen (Hilden, Germany)
Pierce™ BCA Protein Assay kit	Protein concentration	Thermo Fisher Scientific (Waltham, Massachusetts, USA)

3.1.10 Equipment

Table 13: Devices and supplier

Device/Instrument	Supplier
2100 Retriever	Aptum Biologics (South Hampton, UK)
ChemiDoc XRS+	Bio-Rad Laboratories (Hercules, California, USA)
Cooling table centrifuge 5425 R	Eppendorf (Hamburg, Germany)
Contour Next Glucometer	Bayer Healthcare (Leverkusen, Germany)
CytoFLEX SRT	Beckman Coulter (Brea, California, USA)
Electronic precision scale	Sartorius (Göttingen, Germany)
Feedtime	TSE-Systems (Berlin, Germany)
HERAcell 240i CO2 Incubator	Thermo Fisher Scientific (Waltham, Massachusetts, USA)
Histoembedder	Leica Microsystems (Wetzlar, Germany)
iMark Microplate reader	Bio-Rad Laboratories (Hercules, California, USA)
DMBRE Light microscope	Leica Microsystems (Wetzlar, Germany)
Mastercycler	Eppendorf (Hamburg, Germany)
Mini Centrifuge	Laboratory & Medical Supplies (Brigachtal, Germany)

Device/Instrument	Supplier
Multipipette®E3	Eppendorf (Hamburg, Germany)
NanoDrop 2000	Thermo Fisher Scientific (Waltham, Massachusetts, USA)
NMR, Whole body composition analyzer	Echo MRI (Houston Texas, USA)
PCR plate spinner	VWR International (Radnor, USA)
QuantStudio 7 Flex	Applied Biosystems (Foster City, USA)
Rotary microtome HM360	Thermo Fisher Scientific (Waltham, Massachusetts, USA)
StepOne Plus™ System	Applied Biosystems, Foster City, USA
Shandon™Excelsior™ Tissue Processor	Thermo Fisher Scientific (Waltham, Massachusetts, USA)
Shaking waterbath	Köttermann (Uetze, Germany)
Tecan Infinite 200 reader	Tecan Austria GmbH (Grödig, Austria)
TEM 910	Zeiss (Oberkochen, Germany)
Thermomixer Comfort	Eppendorf (Hamburg, Germany)
TissueLyser II	Qiagen (Hilden, Germany)
Uniprep-Gyrator	UniEquip (Planegg, Germany)
Vortex-Genie 2	Scientific Industries (New York, USA)
VS200 Slidescanner	Olympus Corporation (Tokyo, Japan)
Water transfer unit	Thermo Fisher Scientific (Waltham, Massachusetts, USA)
ZOE Fluorescent Cell Imager	Bio-Rad (Munich, Germany)

3.1.11 Software

Table 14: Computer software or online tools, manufacturer and application

Computer software	Manufacturer	Application
ConsensusPath Database and tools	Max Planck Institut for Molecular Genetics, Berlin, Germany (Kamburov et al. 2009)	Pathway analysis
Excel 2010 and 2018	Microsoft	Data management and analysis
Fiji	(Schindelin et al. 2012)	TEM analysis and Scale bar
Prism 9 and 10	Graph Pad	Statistical analysis and figure generation
Image Lab	Bio-Rad Laboratories, Munich, Germany	Imaging of Agarose Gel separation of DNA products
NCBI Primer Blast		Design DNA and cDNA primer pairs
PANTHER Database 18.0	Thomas lab at the University of Southern California (Mi, Muruganujan, and Thomas 2013; Thomas et al. 2022)	Gene ontology analysis
Quantstudio Real-Time PCR-Software	Applied Biosystems, Foster City, USA	qPCR analysis
QuPath0.4.4	(Bankhead et al. 2017)	Analysis of islet size, fluorescence quantification
Slidescanner Software	Olympus	Islet imaging

3.2 Methods

3.2.1 Animal experiments

3.2.1.1 Experimental animals

All animal experiments were approved by the ethics committee of the German Diabetes Center and of the State Ministry of Agriculture, Nutrition and Forestry (LANUV State of North Rhine-Westfalia, Germany, Reference 91_2019.A329). Animals were housed gender specific with maximal 6 littermate animals in acclimatized rooms (22°C) under 12 h light-cycle from 6 am to 6 pm in Macrolon type III Cages (EBECO, Castrop-Rauxel, Germany). The animals had *ad libitum* access to food as well as water supply unless otherwise stated. Mice were weaned between 19-21 days and earnotched to distinguish the animals.

3.2.1.2 Generation of knock-out mice by KOMP breeding strategy

Generation of a beta cell-specific conditional KO of *Pop4* was followed according to the IMPC knockout first allele design (<https://www.mousephenotype.org/>). Therefore, the mouse line C57BL/6N-A^{tm1Brd}Pop4^{tm1a(EUCOMM)Wtsi/WtsiOulu} generated for the EMMA project from the Wellcome Trust Sanger institute (Wtsi) in the University of Oulu Finland was commercially obtained. This line was generated by insertion of the L1L2 Bact_P cassette in the intronic region at position 37965074 of Chromosome 7 upstream of exon 4 of *Pop4* gene according to GRCm38. The vector comprised of an FRT site followed by lacZ and loxP sequences, a neomycin resistance cassette, and a second FRT and loxP site. Downstream of the exon 5, a third loxP site was inserted at position 37966113 to flank exons 4 and 5 of *Pop4*. Following the IMPC strategy, this line was crossed with flp deleter mice to ablate the sequence from the lacZ to the neomycin cassette, generating the tm1c line (**Figure 2**). To acquire a higher C57BL/6J background, this line was additionally crossed twice with C57BL/6J wildtype mice. For beta cell specific ablation, this line was crossed with the B6(Cg)-*Ins1*^{tm1.1(cre)Thor}Gt(ROSA)26Sor^{tm9(CAG-tdTomato)Hze/J} gifted from Dr. Bengt-Frederik Belgardt from the German Diabetes Center, in which the Cre gene replaced exon 2 of the beta-cell specific *Ins1* gene and the loxP flanked stop codon upstream of the tandem dimer Tomato (*tdTomato*) reporter gene was inserted into the Rosa26 locus.

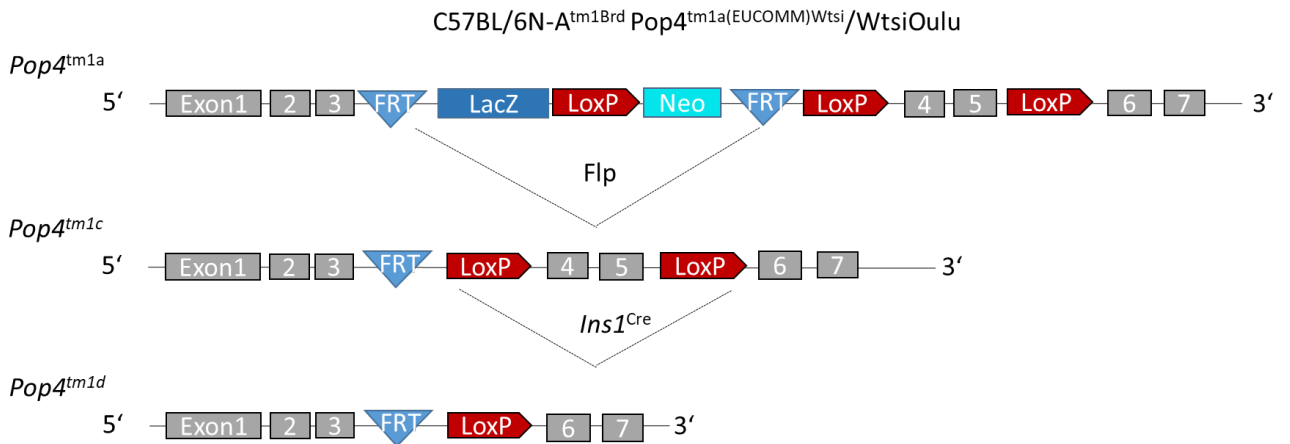


Figure 2. Schematic representation of the genomic sequence for the mouse crosses to generate the beta cell specific ablation in the *Pop4* gene.

The acquired tm1a line with the insertion of LacZ, Neomycin resistance flanked by FRT in the Intron 3 and loxP sites flanking Exon 4 and 5 of the *Pop4* gene. Upon crossing the mice with the flp deleter mice, the sequence in between the FRT sites is ablated generating the tm1c line. by crossing with *Ins1^{Cre}* mice the final ablation of Exon 4 and 5 of *Pop4* is achieved.

Further to generate littermate control mice, heterozygous *Pop4* floxed mice carrying the wildtype *Ins1* (*Ins1^{+/+}*) was crossed with heterozygous *Pop4* floxed mice with a transgenic *Ins1^{Cre/+}* to generate mice with wildtype (WT) control, *Ins1^{Cre/+}*, *Pop4^{fl/fl}* and *Pop4 β KO* genotype. Therefore, in theory each control group or *Pop4 β KO* should be obtained with approximately 12,5% chance of the aforementioned offsprings, whereas 50% of the generated offsprings will generate a parental genotype and were further used for breeding purposes (**Figure 3**).

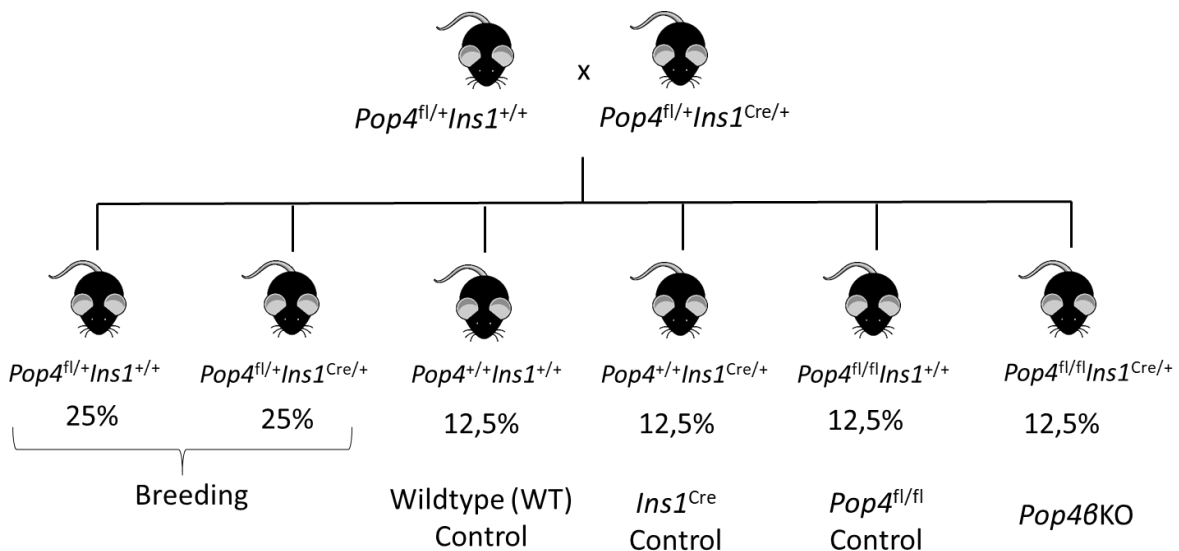


Figure 3. Breeding scheme to obtain littermate control and *Pop4 β KO* mice.

Heterozygous floxed *Pop4* are crossed with wildtype *Ins1* or Cre carrying *Ins1* to generate wildtype, *Ins1^{Cre/+}*, *Pop4^{fl/fl}* and *Pop4 β KO* besides heterozygous mice for further breeding.

3.2.2 Study design of metabolic characterization

After weaning, the mice were either subjected to a chow diet or 60% kcal from fat diet (**Figure 4**). Blood glucose and body weight were measured weekly and body composition of fat and lean mass were assessed every three weeks via nuclear magnetic resonance (NMR) spectroscopy. At 3, 8 and 11 weeks of age, the mice were fasted for 6 h and subsequently blood glucose was measured and tail blood was collected to obtain plasma. Male mice were phenotyped until week 15 and female mice until week 18. In addition, an *in-vivo* intraperitoneal glucose tolerance test (ipGTT) and *ex vivo* glucose-stimulated insulin secretion (GSIS) assay of isolated islets were performed at 8 weeks of age in male mice. At the final age, trunk blood after 6h fasting and metabolically relevant tissues were collected for further analyses.

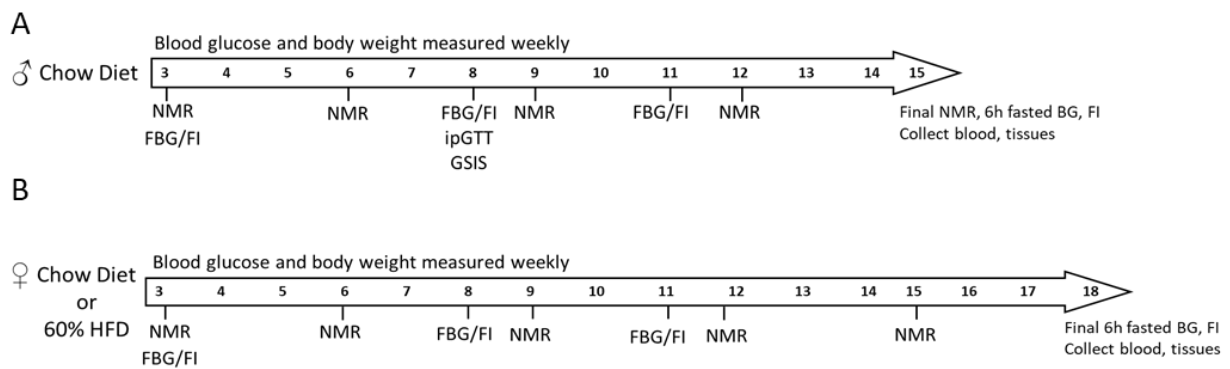


Figure 4. Phenotyping timeline for *Pop4*βKO animals and controls.

(A) Male timeline on Chow diet and (B) Timeline for female either on Chow or 60% high fat diet (HFD). NMR=nuclear magnetic resonance spectroscopy; FBG=6h fasting blood glucose; FI= 6h fasting plasma insulin; ipGTT= intraperitoneal glucose tolerance test; GSIS= glucose stimulated insulin secretion; BG=blood glucose.

3.2.2.1 Body weight and body composition measurement

Body weight was determined weekly using electronic scale. Body composition was measured by nuclear magnetic resonance (NMR) spectroscopy.

3.2.2.2 Blood glucose measurement

Random blood glucose was measured weekly in the morning between 8 am to 10 am using the Contour XT glucometer. Thereby, one drop of blood was collected by pricking the mouse tail vein. If the measurement was indicated as “high” the maximum value of the system of 600 mg/dL was noted.

3.2.2.3 Fasting blood glucose, body weight and plasma insulin

At 3, 8 and 11 weeks animals were fasted for 6 h and subsequently blood glucose, body weight and plasma was collected for plasma insulin measurements. The fasting was done overnight from 2.30-8.30 am using the feedtime device, a system which removes the food at a set time. The blood was collected into Lithium-Heparin coated microtubes and centrifuged at around 9000 x g for 5 minutes at 4°C. Plasma was collected and stored at -80°C until respective analysis.

3.2.2.4 *In vivo* intraperitoneal glucose tolerance test (ipGTT)

For the ipGTT, animals were fasted for 6 h, from 2 am to 8 am. Body weight and basal blood glucose was thereafter measured from cutting of the tail tip. Furthermore, blood was collected in Lithium-Heparin coated micro tube for plasma insulin measurements. Next, mice received an intraperitoneal injection of a sterile 20 % glucose bolus according to the body weight (1 g/kg body weight). At 15, 30, 60, 120 and 240 min after glucose injection, blood glucose was assessed, and blood was collected into Lithium-Heparin coated micro tubes. Subsequently, the collected blood was centrifuged at 9000 x g for 5 min at 4°C and plasma was collected and stored at -80°C until respective analysis.

3.2.2.5 Isolation of mouse pancreatic Islets of Langerhans and organ collection

For the pancreatic islet isolation, animals were fasted for 6 h and decapitated. Trunk blood was collected in anti-coagulant coated tubes and subsequently centrifuged for 10 min at around 9000 x g. The animal was dissected by skin incision around the abdominal area to expose the pancreas and the area around it. To isolate the pancreatic islets the ampulla, where the common bile duct meets the duodenum to carry the bile to the duodenum, was foremost clamped to block the flow. With a syringe mounted with a 20 g needle, 3 ml of the collagenase solution was slowly injected into the common bile duct to distend the pancreas. The pancreas was then removed, placed into a 50 ml falcon tube and temporarily stored on ice. Next, the tube was placed in a shaking 37°C water bath for 18 min. To stop the collagenase (Liberase TL), 50 ml of DMEM with the addition of 10 % fetal bovine serum (FBS) was added and shaken to disrupt the pancreas until the suspension turns homogenous. The solution was

centrifuged gently at 300 x g for 3 min at RT. The supernatant was discarded, and the pellet resuspended in 10 ml of fresh DMEM. The solution was poured over a 100 µm cell strainer. To ensure no tissue was adhering to the tube, the tube was washed with additional 15 ml DMEM and poured again over the cell strainer. The suspension was centrifuged for 3 min at 300 x g and the supernatant was discarded. Next, the cell pellet was resuspended in histopaque 1077 (density of 1,077 g/ml) and 13 ml of DMEM was gently layered on top of the histopaque ensuring minimal mixing of the solutions. The tube was then centrifuged for 25 min at 1200 x g without a brake to constitute a density gradient. Following the supernatant was poured into another falcon tube and centrifuged for 3 min at 300 x g. The final pellet was resuspended in islet medium and transferred into a petri dish. The isolated islets were hand-picked under a microscope and transferred into a petri dish with fresh islet media and incubated at 37°C with 5 % CO₂. Additionally, several organs including the brain, liver, quadriceps, gonadal white adipose tissue were dissected and immediately snapped frozen in liquid nitrogen and stored at -80°C.

3.2.2.6 *Ex vivo* glucose stimulated insulin secretion (GSIS) assay

The glucose-stimulated insulin secretion assay was carried out after overnight incubation of the isolated pancreatic islets of Langerhans. First groups of 8 islets were selected as technical duplicates per sample and collected in 20 µl of islet medium and put into a 96 well plate with rounded bottom wells. To equilibrate the insulin secretion, the islets were incubated in a basal glucose condition by addition of 80 µl of 2 mM Glucose in Krebs Ringer HEPES (KRH) buffer for 1 h. Thereafter the solution was replaced by the basal condition of 2 mM Glucose in KRH buffer for another 1h after which 80 µl of supernatant was collected and switched with the high glucose condition of 25 mM of Glucose in KRH buffer. The collected supernatant was centrifuged for 10 min at 15871 x g at 4°C and 60 µl is collected for measurements. After 1 h 80 µl of the supernatant of the high glucose condition was collected and centrifuged to collect 60 µl for further measurements.

3.2.2.7 Fluorescence activated cell sorting (FACS) of pancreatic islet cells

To analyse the DNA and mRNA Pop4 sequence from pancreatic beta cells, the pancreatic islets were picked after overnight incubation in islet medium and washed twice with 900 µl phosphate buffered saline (PBS) thereafter trypsinized in 200 µl pre-

warmed Trypsin-EDTA solution for 15 min into single cells (dissociating the cells every 5 min by pipetting up and down carefully). The dissociation was stopped using 500 μ l islet medium. Subsequently, cell suspension was processed for fluorescence activated cell sorting, sorting for tdTomato fluorescence (tdTomato⁺) and no fluorescence cells (tdTomato⁻). The sorting for the analysis of DNA structure was processed by Dr. Nadine Teichweyde from the Leibniz Institute of Environmental medical research. Further sorting for the mRNA analysis the FACS was processed by Celina Uhlemeyer from the Institute of vascular- and islet biology at the DDZ.

3.2.3 Biochemical analyses

3.2.3.1 Mouse Ultrasensitive Insulin and Insulin enzyme immunosorbent linked assay (ELISA)

To measure insulin concentration in plasma of the mice (Ultrasensitiv Insulin ELISA) and supernatant as well as lysate of the pancreatic islets (Insulin ELISA), commercial ELISA kits for mouse insulin were applied. These ELISAs are based on a direct sandwich technique in which two monoclonal antibodies are directed against separated antigenic determinants, one is bound to the microtiter plate and the other is coupled to peroxidase. When the sample is added the insulin will be 'sandwiched' between the two antibodies. First, the reagents were brought to RT and the standard calibrators and samples were added to the coated plate as a single (plasma samples) with volume of 25 μ l or 10 μ l in duplicates (supernatant and lysate of isolated pancreatic islets). Thereafter, 100 μ l of the enzyme conjugate containing the antibody was freshly diluted with the enzyme conjugate buffer and incubated on a plate shaker for 2 h at RT according to manufacturer's direction. After a washing step to remove excess antibody with provided wash buffer, 200 μ l of the light sensitive substrate 3,3',5,5'-tetramethylbenzidine (TMB) was added for 15 min at RT in the dark which reacts with the peroxidase to form a blue reaction product. The reaction was stopped by adding 50 μ l acidic 0.5 M H₄SO₄ stop solution which led to a color change. The yellow product can be spectrophotometrically measured at 450 nm. As a reference for the concentration calibrators are provided with known insulin concentration. The working range for the insulin ELISA was between 0.2 μ g/L to 6.12 μ g/L and for the ultrasensitive Insulin ELISA from 0.3 μ g/L to 1.5 μ g/L. Samples below the indicated range were put as 0 μ g/L.

3.2.3.2 Mouse Glucagon ELISA

For the quantification of glucagon concentration in the lysate of the pancreatic islets, a commercial ELISA kit for mouse glucagon was used (Glucagon ELISA, Mercodia). This kit is based on the same sandwich principle and was used according to manufacturer description. Briefly, the lyophilized calibrator standards were reconstituted with millipore water, 25 µl of the calibrator standards and the plasma samples were pipetted in duplicates. Subsequently, 200 µl of assay buffer was added. The plate was sealed and incubated on a plate shaker at 700-900 rpm overnight for 18-22 h at 4°C. The next day the assay buffer was removed, and plate washed with wash buffer by addition of 350 µl of wash buffer and discarding the buffer by inverting the plate over a sink. This procedure was repeated 6 times. Then 200 µl of enzyme conjugate was added and incubated for 1 h on a plate shaker (700-900 rpm) at RT. The enzyme conjugate was removed by washing step as described before. TMB substrate (200 µl) was added, and the plate incubated for 30 min at RT. To stop the reaction 50 µl of the acidic stop solution was added before measurement of optical density at 450 nm. The working range of the standard calibrators was from 1.54 pmol/L – 135 pmol/L.

3.2.3.3 Mouse Proinsulin ELISA

The proinsulin concentration was measured from the lysate of the isolated pancreatic islets after GSIS assay. The ELISA is based on the same principle of a sandwich ELISA as already described (3.2.3.1). Briefly, 25 µl of calibrators and samples were added in duplicates to the plate followed by 50 µl of freshly mixed enzyme conjugate before the plate was sealed and incubated for 2 h on a plate shaker at 700-900 rpm at RT. Plate was washed 6 times with 350 µl washing buffer and 200 µl of TMB substrate was added and incubated for 30 min at RT in the dark. To stop the reaction 50 µl of stop solution was added and optical density was measured at 450 nm within 30 min. The working range was from 3.74-188 pmol/L.

3.2.3.4 Bicinchonic acid assay (BCA)

To normalize the insulin content of the supernatant to the total protein content, a BCA assay was conducted with the lysate of the pancreatic islets according to manufacturer's instruction. The BCA is a colorimetric assay for the quantification of total protein content. In principle, the alkaline BCA stock solution contains bicinchonic acid combined with copper II sulfate pentahydrate solution that leads to peptide bonds

reducing Cu^{2+} ions to Cu^{1+} (biuret reaction) and the cuprous ion is chelated by two bicinchonic acid forming a purple-colored complex which is facilitated by temperature. The purple reaction product has a strong absorbance at 560 nm that is nearly linear with increasing protein concentrations. The BCA method is not a true end-point method, so the color continues to develop as time goes by. As a reference standard bovine serum albumin (BSA) was used to determine the standard curve. The working range was determined from 20-2000 $\mu\text{g/ml}$ protein concentration.

3.2.4 Molecular biology techniques

3.2.4.1 Genomic DNA extraction

To distinguish the animals genotype into wild type (WT), Cre recombinase (*Ins1^{Cre}*), homozygous floxed (*Pop4^{fl/fl}*) or *Pop4 β KO* ear notch skin was used to isolate genomic DNA. Genomic DNA was extracted by lysis of the skin biopsy in 200 μl DNA lysis buffer with addition of 10 μl Proteinase K o/n or 1-2 h at 60°C on a Thermomixer shaking at 1200 rpm. To remove hairs, the sample was centrifuged for 1 min at 15.800 x g, supernatant was collected to a new tube and isopropanol was added to precipitate the gDNA by vortexing the sample. Thereafter, samples were centrifuged for 10 min at 15.800 x g and gDNA pellet was washed with 70 % Ethanol twice. Genomic DNA was dried for 10 min at 60°C before elution in nuclease-free water. The DNA concentration was measured photometrically at 260 nm with the NanoDrop 2000.

3.2.4.2 Polymerase chain reaction (PCR)

The genomic DNA from skin biopsies collected during the ear notching was used as template for PCR of floxed sequence, Cre recombinase sequence and *Pop4* sequence. To distinguish wild-type *Pop4* from a transgenic *Pop4* sequence, a primer pair was designed with forward and reverse primer binding in intron 3 of the wild-type sequence. The detection of the transgenic *Pop4* product, utilizes the same forward primer and a separate reverse primer created in the transgene *Cas1* element. Furthermore, to detect the Cre recombinase sequence that replaced exon 2 at the initiation codon in the *Ins1* gene of the transgenic mice, the primer was designed with forward primer binding in exon 1 and reverse primer binding in the Cre sequence, resulting in a PCR product of ~300 bp in the mice carrying the transgenic element. Finally, the tdTomato element, which was collectively inserted with the loxP-flanked stop codon and the WPRE sequence into the *Rosa26* locus, was detected using two

separate primer pairs. The first primer pair was designed to detect the wild type *Rosa26* sequence of 297 bp, whereas the second primer pair binds to tdTomato and the WPRE sequence showing the PCR product. The general steps were the hot start to initiate the polymerase activity followed by denaturation of the double-stranded DNA in to single DNA strand allowing the annealing of the primer, elongation and amplification. These steps were repeated until desired DNA amount was achieved. The following reaction setup and programs were used respectively.

Table 15: Reaction setup for the *Pop4* PCR reaction

Compound	Volume (µl)	Stock concentration
MQ H ₂ O	5.8	
5xHF Puffer	4	
dNTPs	2	8 mM
Pop4 for	2	10 nM
Pop4 rev	1	10 nM
CAS rev	1	10 nM
Phusion-Taq	0.2	2 U/µl
DNA	4	10 ng/µl

Table 16: PCR reaction program to amplify *Pop4* sequence

Step	Temperature	Time	Repeats
Hot start	98° C	30 sec	-
Denaturation	98° C	30 sec	34x
Annealing	63° C	30 sec	
Elongation	72° C	45 sec	
	72° C	5 min	-
Storage	4° C	∞	-

Table 17: Reaction setup for the *Ins1^{Cre}* PCR reaction

Compound	Volume (µl)	Stock concentration
MQ H ₂ O	8.8	
10x Buffer (Green)	4	
dNTPs	2	8 mM
Ins1-Cre fwd	0.5	10 nM
Ins1-Cre rev	0.5	10 nM
Dream Taq Green	0.2	2 U/µl
DNA	4	10 ng/µl

Table 18: PCR reaction program to amplify *Ins1^{Cre}* sequence

Step	Temperature	Time	Repeats
Hot start	95° C	2 min	-
Denaturation	95° C	30 sec	34x
Annealing	62° C	30 sec	
Elongation	72° C	30 sec	
	72° C	5 min	-
Storage	4° C	∞	-

Table 19: Reaction setup for the *tdTomato* PCR reaction

Compound	Volume (µl)	Stock concentration
MQ H ₂ O	6.5	
10x Buffer (Green)	4	
dNTPs	3	8 mM
DMSO	1.3	
Tomato_WT_for (1)	0.5	10 nM
Tomato_WT_rev (2)	0.5	10 nM
Tomato_TG_for (3)	0.5	10 nM
Tomato_TG_rev (4)	0.5	10 nM
Dream Taq Green	0.2	2 U/µl
DNA	4	10 ng/µl

Table 20: PCR reaction program to amplify *tdTomato* sequence

Step	Temperature	Time	Repeats
Hot start	95° C	30 sec	-
Denaturation	95° C	15 sec	10x Decrease 0.5°C per cycle
Annealing	65-60° C	30 sec	
Elongation	72° C	60 sec	
Denaturation	95° C	15 sec	28x
Annealing	60° C	30 sec	
Elongation	72° C	60 sec	
	72° C	5 min	-
Storage	4° C	∞	-

Table 21: Reaction setup for the validation of the deletion of Exons 4+5

Compound	Volume (µl)	Stock concentration
MQ H ₂ O	9	
5x Phusion HF buffer	5	
dNTPs	2.5	8 mM
Cas1 F	2,5	10 nM
Intron 6 R	2,5	10 nM
Phusion Polymerase	0.5	2 U/µl
DNA	3	10 ng/µl

Table 22: PCR reaction program to amplify Exon4+5 of *Pop4* sequence

Step	Temperature	Time	Repeats
Hot start	95° C	30 sec	-
Denaturation	95° C	15 sec	34x
Annealing	63° C	30 sec	
Elongation	72° C	90 sec	
	72° C	5 min	-
Storage	4° C	∞	-

3.2.4.3 Agarose gel electrophoresis

To determine the PCR product size, gel electrophoresis was done in 1% or 2% agarose gel dependent on the expected DNA product. Agarose gel was prepared with 1x Tris-

Acetat-EDTA (TAE) buffer, boiled until the agarose was solubilized and HD greenDNA stain was added for the visualization of DNA bands. After polymerization of the agarose gel, the 20 µl of PCR product and 10 µl of the DNA ladder was loaded into individual gel pockets and electrophoresis was performed at constant 120 V for in electrophoretic chamber with 1x TAE buffer. The DNA bands were visualized with UV light (254 nm) using the ChemiDoc XRS+ system and Image Lab software was used for the documentation of the image.

3.2.4.4 Total RNA isolation of pancreatic islets

The RNA isolation from islets was performed using the Trizol Chlorofom method and the RNA extraction RNeasy-Mini Kit. Using the referred kit, around 80-100 islets were selected after overnight regeneration and washed with PBS (without Ca⁺² and Mg⁺²). Thereafter, 0.5 mL QIAzol was added and mixed to disrupt the tissue. After 5 min incubation at room temperature (RT) the lysate was transferred to a QIAshredder spin column and centrifuged at 18000 x g for 2 minutes at 4 °C. The flow-through was collected in a pre-centrifuged MAXtract High Density tube. In addition, 140 µl of chloroform was added and the phases were homogenized by inversion of the tubes for 15 sec and thereafter was incubated at RT for 5 min, before centrifugation at 12000 x g for 15 minutes at 4 °C. The separated aqueous phase containing the RNA was then collected to a new tube. 1.5x amount of the isopropanol was added to precipitate the RNA and 1 µl of Glycobluue was added to stain the RNA pellet. Furthermore, the mixed solution was transferred to the RNeasy-Mini columns containing a membrane that retains the RNA. To avoid genomic DNA contamination a DNase digestion step using the RNase-free DNase set was added to the membrane. After, the RNA was washed once with 500 µl of RWT buffer and twice with 350 µl of RPE buffer provided by the manufacture, the RNeasy-Mini columns were dried by centrifugation and the RNA was then eluted with Nuclease-free water in a new RNase free tube for storage at -80°C.

3.2.4.5 Total RNA extraction of organ tissues with Trizol-Chloroform

Total RNA was extracted from frozen (-80°C) gonadal white adipose tissue, liver, quadriceps, brain and kidney. Therefore, tissues were manually disrupted by grinding the tissue with a mortar that was cooled down with liquid nitrogen to avoid defrosting the respective tissue. Depending on the amount of tissues 500-1000 µl of Trizol Lysis reagent was added to the lysated tissue. Additionally, one metal bead per sample was

added to disrupt the tissue for 5 min at 25 Hz in the TissueLyser. After an incubation step of 5 min at room temperature (RT), 100-200 μ l of Chloroform was added and the tube was mixed by continuous inverting the tube for 15 seconds. The samples were incubated for another 3 min at RT before they were centrifuged for 15 min at 12.000 x g (4°C). After the centrifugation step, a clear aqueous phase was collected containing the RNA. The upper clear phase was carefully transferred to a new tube avoiding touching the interphase and 500 μ l of Isopropanol was added and homogenized to precipitate the RNA. Additionally, the solution was incubated for 10 min at -20°C and centrifuged for 15 min at 4°C and 12.000 x g. The supernatant was then discarded and the pellet was washed twice with 1 mL 75 % Ethanol by shortly vortexing the tube to lift the pellet from the bottom of the tube. The washing liquid was then discarded and to accelerate the evaporation of the remaining Ethanol, the tube was heated for 5 min at 55°C spinning 300 rpm. Finally, the RNA was eluted in 50-100 μ l of RNase free water and incubated for 5 min at 300 rpm (55°C) in the Thermomixer before the concentration was accessed by photometric measurement using the Nanodrop. If samples were not further proceeded, the RNA was stored at -80°C.

3.2.4.6 Quality and quantity of RNA via Nanodrop

To determine the purity and the quantity of the isolated RNA, a spectro-photometric analysis was conducted using the Nanodrop. Therefore, 1 μ l of the isolated RNA sample was placed to the pedestal. The Nanodrop measured the absorbance at 230 nm, 260 nm and 280 nm and calculated the 260/230 ratio and 260/280 ratio which determined the purity of the RNA sample. Nucleic acids absorb UV light at 260 nm while proteins and phenolic compounds have an absorbance at 280 nm, organic compounds such as Trizol absorb light at 230 nm. Depending on the ratio ranging from 0,0 to 2,0 for RNA the contamination can be estimated. Pure RNA sample have a 260/230 and 260/280 ratio of 2.0. All samples above a 260/280 ratio of 1.5 were used.

3.2.4.7 Complementary DNA (cDNA) synthesis

The reverse transcription converts the RNA template into the complementary DNA (cDNA). For the synthesis of the cDNA 500 ng to 2 μ g of RNA was used depending on the concentration of RNA that was achieved during RNA isolation. The amount was diluted to have a total of 10 μ l in volume. Together with dNTPs and Hexanucleotide primers the RNA was pre-incubated for 5 min at 65°C to remove secondary RNA

structures. Thereafter, the sample was incubated 1 min on ice and briefly centrifuged to collect the liquid down. To start the cDNA synthesis, GoScript reverse transcriptase with reaction buffer and MgCl₂ were added. The annealing of the primers was achieved with 25°C, synthesis at 42°C and inactivation of the reverse transcriptase polymerase at 70°C. Before proceeding with the real-time PCR, the cDNA was diluted accordingly: 500 ng diluted 1:10, 1 µg diluted 1:20 and 2 µg diluted 1:40 with Nuclease-free water. The cDNA was stored at -20°C until proceeding with the qPCR.

Table 23: Reaction setup for cDNA synthesis

Step 1 –Preincubation	
Compound	Volume (µl)
RNA	10
dNTPs (0.25 mM)	1
Hexanucleotidprimer (0.1 µg/µl)	2
Total volume	13
Step 2 –cDNA synthesis	
Step	Volume (µl)
RNA mixture	13
GoScript 5x reaction buffer	4
MgCl ₂	2
GoScript Reverse Transcriptase	1
Total volume	20

Table 24: cDNA synthesis programm

Step 1 –Preincubation		
Step	Temperature	Duration
Preincubation	65°C	5 min
Storage	4°C	∞
Step 2 –cDNA synthesis		
Step	Temperature	Duration
Annealing	25°C	5 min
cDNA synthesis	42°C	60 min
<i>RT</i> -inactivation	70°C	15 min
Hold	4°C	∞

3.2.4.8 Real-time quantitative polymerase chain reaction (*RT*-qPCR)

The real-time quantitative polymerase chain reaction (*RT*-qPCR) method allows for monitoring the amplification of a target gene during the whole course of the process, hence the term 'real-time'. Essentially the method is based on the same principals as the conventional polymerase chain reaction (PCR). However, due to the use of a fluorescent dye that intercalates between the double-stranded DNA (dsDNA), the amplification can be monitored throughout the amplification cycles. Thereby, the carboxy-X-rhodamin (CXR) reference dye was used, as it provided brighter dsDNA-dependant green fluorescence than the conventionally used SYBR®-Green dye and therefore allowed an earlier detection of the amplification product. The analysis is based on the correlation of the accumulated emitted fluorescence signal with the amount of amplification product. A 384-well plate was used for the reaction setup. For the *RT*-qPCR reaction a mastermix for each primer was prepared using following components. The respective cDNA was added to each well in advance.

Table 25: Composition for one well of qPCR sample

Component	Volume
2x GoTaq® qPCR Master Mix	5 µl
Forward primer (dilution in Nuclease-free-H ₂ O)	0,5 µl

Reverse primer (dilution in Nuclease-free-H ₂ O)	0,5 µl
cDNA (2.5 ng/µl)	4 µl
In total per well	10 µl

Beforehand, 20 µl of the CXR was added to the 1ml 2x GoTaq® qPCR Master Mix. After pipetting all components together, the 384-well plate was sealed with an optical clear film and shortly centrifuged so all components were located to the bottom of each well. The *RT*-qPCR was executed by QuantStudio 7 Flex according to following protocol:

Table 26: qPCR settings in QuantStudio 7 Flex

Step	Temperature	Duration	Cycles
Hot start	95°C	2 min	1x
Denaturation	95°C	15 sec	40x
Annealing/Extension	60°C	60 sec	
Dissociation (melting curve analysis)	60°C-95°C	75 sec	1x

3.2.5 Histological techniques

3.2.5.1 Fixation of the pancreatic tissue

To preserve the original tissue morphology of the pancreas, the pancreas was immediately transferred into 4 % formaldehyde solution in PBS buffer (pH 6.9) after dissection. The pancreatic tissue was fixated for at least 24 h before proceeding with embedding.

3.2.5.2 Embedding of the pancreatic tissue

The pancreatic tissues were embedded in paraffin using the Shandon Excelsior Tissue Processor. In the tissue processor, the pancreas was first dehydrated using an ethanol dilution series (Step 1-6). As Xylene is soluble in both alcohol and paraffin, it was then used as an intermedium to allow the liquefied paraffin (Wax) to permeate the tissue, replacing the xylene. To lastly obtain the tissue blocks, the wax had to harden within

the embedding cassettes. The blocks were removed from the embedding cassettes and placed in molds and further replenished with liquefied paraffin on the embedding station.

Table 27: Embedding protocol of the Shandon Excelsior Tissue processor

Steps	Solution	Temperature	Time
1.	Ethanol 70 %	RT	1h
2.	Ethanol 70 %	RT	1h
3.	Ethanol 96 %	RT	1h
4.	Ethanol 96 %	RT	1h
5.	Ethanol 100 %	RT	1h
6.	Ethanol 100 %	RT	2h
7.	Xylene	RT	1h
8.	Xylene	RT	1h
9.	Xylene	RT	1h
10.	Wax	60 °C	1h
11.	Wax	60 °C	1h
12.	Wax	60 °C	1h

3.2.5.3 Microtome sectioning

The embedded tissue blocks were sectioned in parallel to the long axis of the gland at 5 μm thickness with a rotary microtome. The pancreatic tissue blocks were first trimmed until reaching a proper representative profile of the pancreatic tissue. A series of 10-15 consecutive sections of 5 μm at sampling intervals of 50-75 μm linear scan through the tissue, were chosen. After each level 50-75 μm was discarded. The sections were further transferred to a water bath at 40-45°C, which allowed stretching of the sections before collection onto a microscope slide. The sections were dried overnight at room temperature before proceeding with the staining.

3.2.5.4 Hematoxylin- and Eosin (HE) staining

Within each level that was obtained, one section was chosen for standard hematoxylin and eosin (HE) staining of the pancreatic tissue. In-between each of the analyzed section, the distance resembles about 100-150 μm within the original pancreatic tissue. Using xylene solution as an intermedium, the paraffin was removed and an ethanol dilution series of 100%-70% dehydrated the tissue (deparaffinization). Mayer's Hematoxylin solution was used to stain basophil structures such as the nuclei and ribosomes in blue while eosin mediated reddish staining in all acidophil structures including cell plasma, mitochondria and the endoplasmic reticulum. Addition of tap water was used to induce a pH change in the tissue, mediating a purple stain of the acidic nuclei. The stained tissue was mounted with a xylene containing medium (Shandon EZ-mount) for long-term preservation. The sections were then sealed with coverslips and dried overnight at room temperature. Due to toxicity and flammability of xylene, all the steps were performed under the fume hood.

Table 28: HE Staining protocol

Steps	Solution	Incubation time
1.	Xylene	5 min
2.	Xylene	5 min
3.	Ethanol 100%	5 min
4.	Ethanol 100%	5 min
5.	Ethanol 96%	5 min
6.	Ethanol 96%	5 min
7.	Ethanol 70%	5 min
8.	Ethanol 70%	5 min
9.	Mayer's Hematoxylin	2 min
10.	Aqua bidest	Short wash
11.	Tap water	10 min
12.	Ethanol 70%	2 min
13.	Eosin 0,1% solution	30 sec
14.	Ethanol 96%	Short wash
15.	Ethanol 96%	5 min
16.	Ethanol 100%	2 min
17.	Ethanol 100%	2 min

Steps	Solution	Incubation time
18.	Xylene	5 min
19.	Xylene	5 min

3.3.1.1 Immunohistochemical staining

For the immunohistological assessment of the pancreatic islets, specimen sections were deparaffinized by xylene twice in 5 min steps and rehydrated by a declining alcohol series. Thereafter, the sections were rinsed with phosphate-buffered saline (PBS) and PBS-T for 5 min each. A heat-mediated antigen retrieval was achieved by boiling the sections for 20 min in citrate buffer using the 2100 Retriever. After the sections cooled down, PBS-T with addition of 5% BSA was used to block unspecific epitopes for 1 hour at RT. Subsequently, sections were incubated depending on the setup with a combination of primary antibody against Insulin (dilution 1:200) and Glucagon (dilution 1:200), Insulin, Nkx6.1 (dilution 1:200) and Ki67 (1:750) and a combination of Insulin and γ H2A.X (1:500) overnight in an humidified chamber at 4°C. To avoid drainage, the incubated sections were covered with a piece of parafilm. The next day, the sections were washed with PBS thrice and in PBS-T once before incubation with the fluorophore coupled secondary antibody directed against the respective primary antibody in a humidified chamber for 1 hour at room temperature covered with parafilm. The secondary antibodies were diluted 1:500 in PBS-T with addition of 5% BSA. The antibody solution was decanted thereafter and the sections were washed with PBS thrice for 10 min each. Finally, the fluids were carefully removed from surrounding of the section and fluoroshield with DAPI was distributed to mount the section with coverslips. The slides were dried for 1-2 h at room temperature in the dark or overnight at 4°C. Before scanning the slides, excess fluoroshield were removed with 70% EtOH to clean the slides.

Table 29: Immunostaining protocol

Step	Process	Solution	Temperature	Incubation Time
1.	Deparaffinization	Xylene	RT	5 min
2.		Xylene	RT	5 min
3.	Rehydration	100% EtOH	RT	5 min

Step	Process	Solution	Temperature	Incubation Time
4.		100% EtOH	RT	5 min
5.		96% EtOH	RT	5 min
6.		96% EtOH	RT	5 min
7.		70% EtOH	RT	5 min
8.		70% EtOH	RT	5 min
9.	Wash	PBS	RT	5 min
10.		PBS-T	RT	5 min
11.	Block	PBS-T+5% BSA	RT	1h
	Heat-mediated antigenretrieval	Citrate buffer	RT	20 min boiling in 2100 Retriever, cool down about 1h.
12.	Primary Antibody	See Antibody list	4°C	overnight
13.	Wash	PBS	RT	5 min
		PBS-T	RT	5 min
14.	Secondary Antibody	See Antibody list	RT	30 min
15.	Wash	PBS	RT	5 min
16.	Mount	Fluoroshield+DAPI	o/n 4°C	One day

3.3.1.2 Transmission electron microscopy (TEM)

The processing and TEM selection of images of the pancreatic islets were conducted by Kay Jeruschke and Carmen Weidlich from Histology Unit at the DDZ. Three to four pancreatic islets were selected per sample for the analysis excluding pancreatic islets with signs of necrosis (dark core under brightlight and absent tdTomato fluorescence). For the basal condition, the pancreatic islets were selected after overnight regeneration while for the stimulated condition the islets were incubated with high glucose of 25 mM for 5 min at 37 °C, 5% CO₂. Thereafter, pancreatic islets were washed with BSA-free KRH buffer and fixed in 2,5% gluteraldehyde in KRH buffer for 1 hour at room temperature. Pancreatic islets were additionally postfixed in 2% osmium tetroxide in

0.19 M sodium cacodylate buffer at pH 7.4 for 30 min and subsequently stained with 2% uranyl acetate in maleate buffer at pH 4.7. An increasing alcohol series was used to dehydrate the specimen and before embedding in epoxy resin. Ultrathin sections were prepared onto Formvarcarbon-coated grids and stained with lead citrate to be viewed under transmission electron microscope.

3.3.1.3 Histological morphometric analysis

3.3.1.3.1 Analysis of the HE stained pancreatic section

The HE stained pancreatic section were imaged at 40x magnification using the Slidescanner. To quantitate the pancreas area, the threshold tool of Fiji was used. Thereby, cell structures like fat tissue or blood vessels were blanked to achieve a greater estimation. The pancreatic islet structures were visually detected as they appear in a lighter purple coloring and manually encircled to quantitate the area. The analysis was done a blinded manner to avoid bias detection. The analysis was done by two independent observers.

3.3.1.3.2 Fiji Analysis of TEM Images

From the processed pancreatic islet samples, 10-15 images were selected based on the intactness of the cell structure done by Kay Jeruschke and Carmen Weidlich. Thereafter, images were analyzed with Fiji Software. To obtain the two dimensional area of the cell, the outer membrane was manually encircled. Thereafter, visible nucleus area as well as mitochondrial structures were additionally encircled. The immature and mature granules were manually counted. To reduce bias the analysis was done by two independent observers and in a blinded manner.

3.3.1.3.3 Histological immunofluorescence Analysis

The immunostained pancreatic sections were imaged at 40x magnification using the Slidescanner. Thereafter, QuPath software was used to detect and quantify the fluorescenced stained areas. For insulin and glucagon areas custom trained pixel classifier was used together with a macro (Uhlemeyer et al. 2023) to detect insulin stained or glucagon-stained area in a semi-automated way. The detection was validated by manually adjusting the detected areas. For the detection of Nkx6.1 and Ki67 positive stained nuclei, the positive cell detection analysis tool was used by

indicating DAPI stained areas as nuclei and providing a threshold for the respective channel. Subsequently, automatic detection was controlled to avoid false positive detection and was manually corrected. Same positive cell detection mode was used for the detection of γ H2A.X positive nuclei.

3.3.2 Bioinformatical transcriptome analysis

After total RNA isolation of pancreatic islets from *Pop4* β KO and *Pop4*^{fl/fl} mice, RNA quality control analysis and subsequent sequencing were performed at the Sequencing Core Unit of Heinrich-Heine University Düsseldorf (Genomics & Transcriptomics Laboratory, BMFZ) using Illumina Nextseq 2000 sequencing technique at 30 million single-read per sample. Data quality control, alignment and differential expression (DE) analysis of sequenced data were processed by Dr. Stephan Majda, DDZ. Briefly, quality control was performed with MultiQC (Version 1.13) tool (Ewels et al. 2016) and pseudo alignment was done with Kallisto tool (Bray et al. 2016) mapped to cDNA of GRCm39. Read counts and transcript per million reads (TPMs) were calculated with txim port R package version 1.10.0 and lengthScaledTPM method (Soneson, Love, and Robinson 2015). For the differential expression (DE) analysis between the two genotypes *Pop4* β KO vs *Pop4*^{fl/fl}, the 3D RNA-seq tool (Guo et al. 2021) was used that integrates the voom pipeline of limma R package (Version 3.52.2) (Ritchie et al. 2015). The log₂-fold change (L2FC) of transcript expression were calculated based on the condition *Pop4* β KO to *Pop4*^{fl/fl}. Statistics were applied using t-test and adjusted for multiple testing with Benjamini-Hochberg to control false discovery rate (Benjamini and Yekutieli, 2001). Normalized data was used for principle component analysis (PCA) to investigate inter- and intra sample variability. Gene Ontology Enrichment Analysis was done using the Panther Overrepresentation tool (Released 20230705). Overrepresentation analysis of canonical pathways was done using Consensus Pathway Database (Herwig et al. 2016) (Release 35 05.06.2021). Further, visualization of pathways was achieved with Kyoto encyclopedia of genes and genomes (KEGG) mapper tool (Kanehisa and Sato 2020; Kanehisa, Sato, and Kawashima 2022).

3.3.3 Statistics

Generated data were subjected to statistical testing by two-way ANOVA or Student's t-test with Bonferroni posthoc test as indicated using GraphPad Prism 9/10 software. Data are reported as mean \pm standard error of the mean (SEM) with biological replicates stated in the respective figure legend.

4 Results

In the following results section, the role of *Pop4* in pancreatic beta cell function and plasticity were explored in three consecutive steps. First, a beta cell-specific knock-out mouse model was generated and metabolically characterized with a particular focus on functional insulin secretion ability. Next, a histological assessment of pancreatic islets and beta cells was performed to investigate both morphology and pathology. Finally, a transcriptome analysis of pancreatic islets was conducted to elucidate the mechanism that *Pop4* elicits on pancreatic beta cell function.

4.1 Metabolic characterization of beta cell-specific *Pop4* knock-out mice

4.1.1 Genotyping of mice

In order to select the mice with the accurate genotype, genotyping was conducted based on PCR amplification of genomic DNA and subsequent gel electrophoresis. All mice used for the experiments were selected based on the genotype distinguishing the wildtype sequence from transgenic elements that was incorporated into the genomic DNA of *Pop4*, *Ins1* and *Rosa26* DNA sequence (3.2.1.2).

To distinguish wild-type *Pop4* from a transgenic *Pop4* sequence, a primer pair was designed with forward and reverse primer binding in intron 3 of the wild-type sequence, resulting in a 461 bp DNA product. To detect the transgenic *Pop4* sequence, a reverse primer was created in the transgene Cas1 element to obtain a 133 bp PCR product, whereas heterogeneous mice displayed both products (**Figure 5A**). Furthermore, to detect the Cre recombinase sequence that replaced exon 2 at the initiation codon in the *Ins1* gene of the transgenic mice, the primer was designed with forward primer binding in exon 1 and reverse primer binding in the Cre sequence, resulting in a PCR product of ~300 bp in the mice carrying the transgenic element (**Figure 5B**). Finally, the *tdTomato* element, which was collectively inserted with the loxP-flanked stop codon and the WPRE sequence into the *Rosa26* locus, was detected using two separate primer pairs. The first primer pair was designed to detect the wild type *Rosa26* sequence of 297 bp, whereas the second primer pair binds to *tdTomato* and the WPRE

sequence showing the PCR product at 196 bp. Appearance of both bands displayed a heterogeneous genotype (Figure 5C).

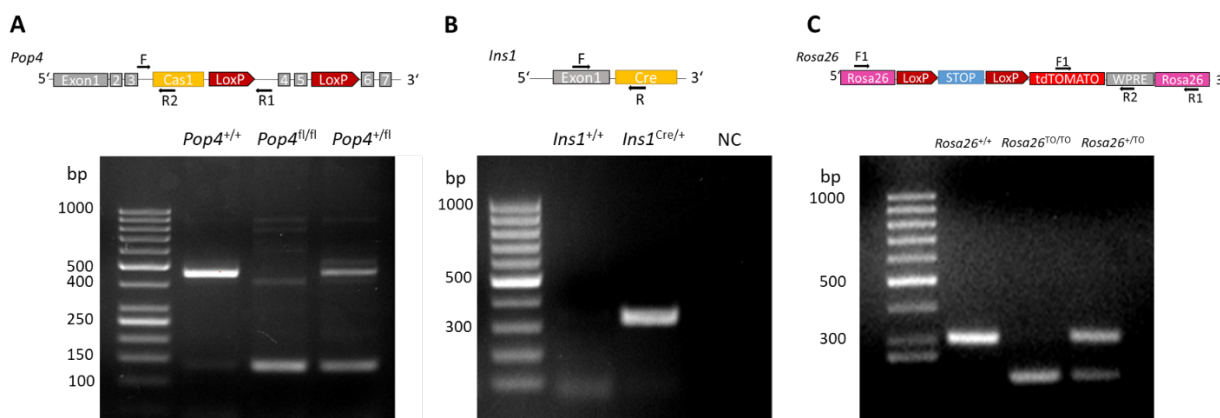


Figure 5. Genotyping of the mice by PCR and gel electrophoresis. Scheme of gDNA with transgenic element and indication of primer binding sites illustrated above the gel electrophoresis images of the respective PCR. (A) *Pop4* homozygous wildtype (*Pop4*^{+/+}) can be distinguished by a PCR product of 461bp from *Pop4* homozygous floxed (*Pop4*^{fl/fl}) with a PCR product of 133bp and the heterogenous displaying both bands (*Pop4*^{+/fl}). (B) *Ins1* homozygous wildtype (*Ins1*^{+/+}) and negative control (NC) display no PCR product versus the *Ins1* gene harboring Cre recombinase with a PCR product of ~300 bp (*Ins1*^{Cre/+}). (C) *Rosa26* wildtype (*Rosa26*^{+/+}) shows a PCR product of 297 bp and homozygous flanked *tdTOMATO* (*Rosa26*^{TO/TO}) with a PCR product of 196 bp and the heterozygous presenting both bands (*Rosa26*^{+/TO}). The respective DNA ladder with base pair (bp) indication of the ladder are shown on the outer left lane.

4.1.2 Knock-out validation on DNA and mRNA levels

In order to detect the ablation of exons 4 and 5, pancreatic islets were isolated from *Pop4*^{fl/fl} mice carrying Cre recombinase in the *Ins1* gene and *tdTomato* in the *Rosa26* locus which is termed the *Pop4* β KO genotype. To validate the Cre activity, the *tdTomato* fluorescence was observed after isolation of the islets (Figure 6 upper row). Here, the beta cell core of pancreatic islets appears in bright red fluorescence of *tdTomato*, showing the beta cell-specific activity of Cre recombinase. Because ablation occurs solely in beta cells, the pancreatic islets were dispersed into single cells via trypsinization and sorted via fluorescence-activated cell sorting (FACS). Figure 6 shows the dispersion into single cells and the overlap of the brightfield and red channels shows that most cells are *tdTomato*-positive beta cells and a minor number of cells show no fluorescence. The remaining non-fluorescent cells likely display pancreatic endocrine cells including alpha, delta, epsilon and gamma cells.

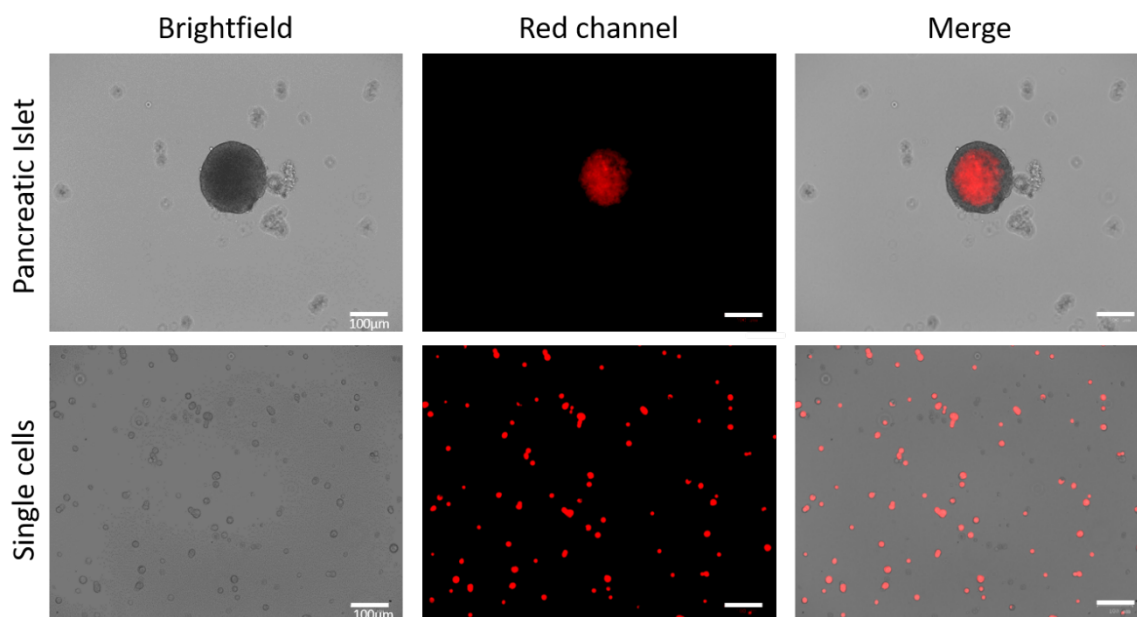


Figure 6. Validation of Cre activity by tdTomato fluorescence in pancreatic islet and single endocrine cells. Representative images of a pancreatic islet and single cells after trypsinization. The cell structures are shown under brightfield, under the red channel and in merged form. Scale bar represents 100 μm .

After FACS analysis the cells were collected as tdTOMATO positive (tdTOM⁺) and tdTOMATO negative (tdTOM⁻) cell fractions. Genomic DNA was isolated from the cells, and primers were designed in the Cas1 sequence and downstream of the LoxP sequence to verify the ablation at DNA level. Figure 7A shows that tdTOM⁺ beta cells depict a band of 164 bp validating the deletion of exons 4 and 5 of *Pop4* while the tdTOM⁻ cells (remainder endocrine cells) show a band at 1179 bp representing the wildtype sequence of *Pop4*.

For mRNA levels, the setup was repeated and additionally the *Ins1*^{Cre/+} mouse was used as a negative control. Subsequently, the isolated mRNA was transcribed to complementary DNA (cDNA), and primers in exons 1 and 7 were designed to detect excision of exons 4 and 5. Figure 7B depicts that in control *Ins1*^{Cre/+} the wildtype *Pop4* sequence in both tdTOM⁺ and tdTOM⁻ appears at 1071 bp while in *Pop4* β KO tdTOM⁺

the cDNA product shows a band at 931 bp, validating the excision of exons 4 and 5 also at the mRNA level.

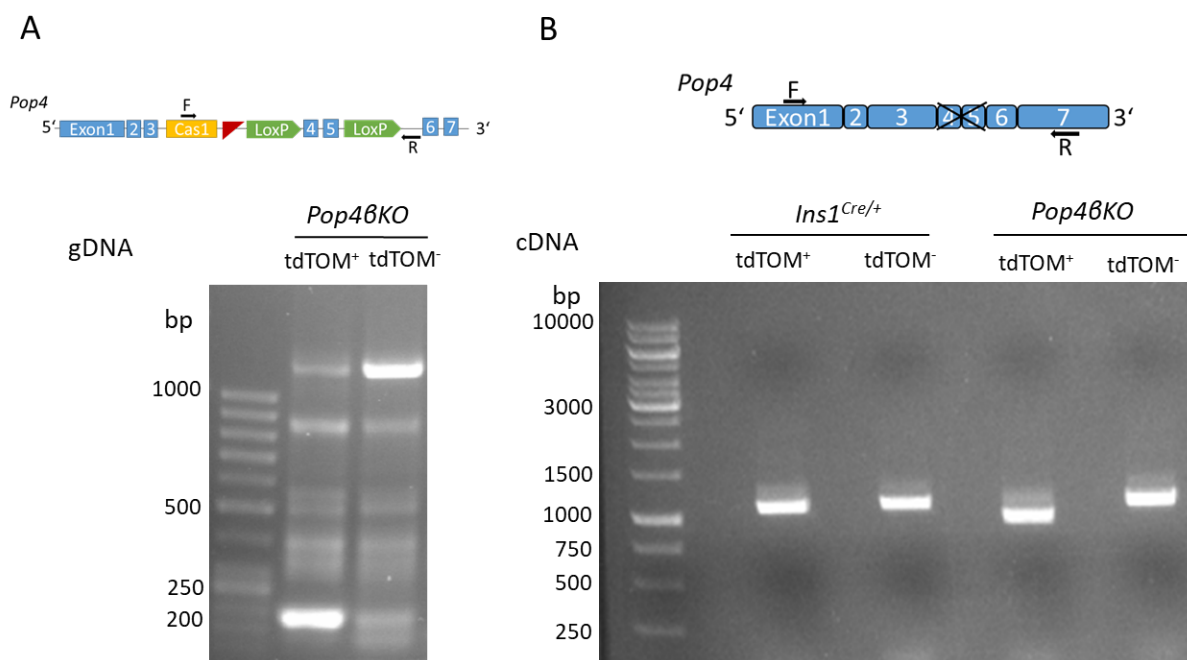


Figure 7. Validation of ablation of exons 4 and 5 of *Pop4* gene in beta-cells on gDNA and mRNA level. Scheme of (A) gDNA and (B) mRNA structures with transgenic elements in *Pop4* to indicate primer binding sites illustrated above the gel electrophoresis images of the respective PCR. (A) Primers were designed for Cas1 and downstream of loxP to detect the ablation of exons 4 and 5 on gDNA level. (B) Primers were designed in exon 1 and exon 7 for the cDNA of *Pop4* to detect the excision of exon 4 and 5. The tdTomato⁺ (tdTOM⁺) represent the beta cells from a *Pop4* β KO mice while the tdTomato⁻ (tdTOM⁻) show the remainder of islet endocrine cells.

4.1.3 Gene expression of *Pop4* in other metabolic relevant tissues

In order to confirm the tissue-specific ablation solely in beta cells of the wildtype *Pop4* mRNA sequence in other metabolically relevant tissues using quantitative real-time PCR (qPCR). For this purpose, primers were designed to bind to exon 4 and exon junction of exons 5 and 6, which should be only present in wildtype *Pop4* but not in excised in *Pop4* β KO genotype. In general, *Pop4* ubiquitous expression was present in all analyzed tissues. The quadriceps, kidney, and gonadal white adipose tissue showed quite high variation in the expression of *Pop4* compared to liver and brain in which expression appeared more homogenous for the animals. As the pancreatic islets were used as a proxy for the pancreatic beta cells an expression of *Pop4* is detectable. However, *Pop4* β KO depicts a tendency for lower expression compared to the control *Pop4*^{fl/fl} (Figure 8).

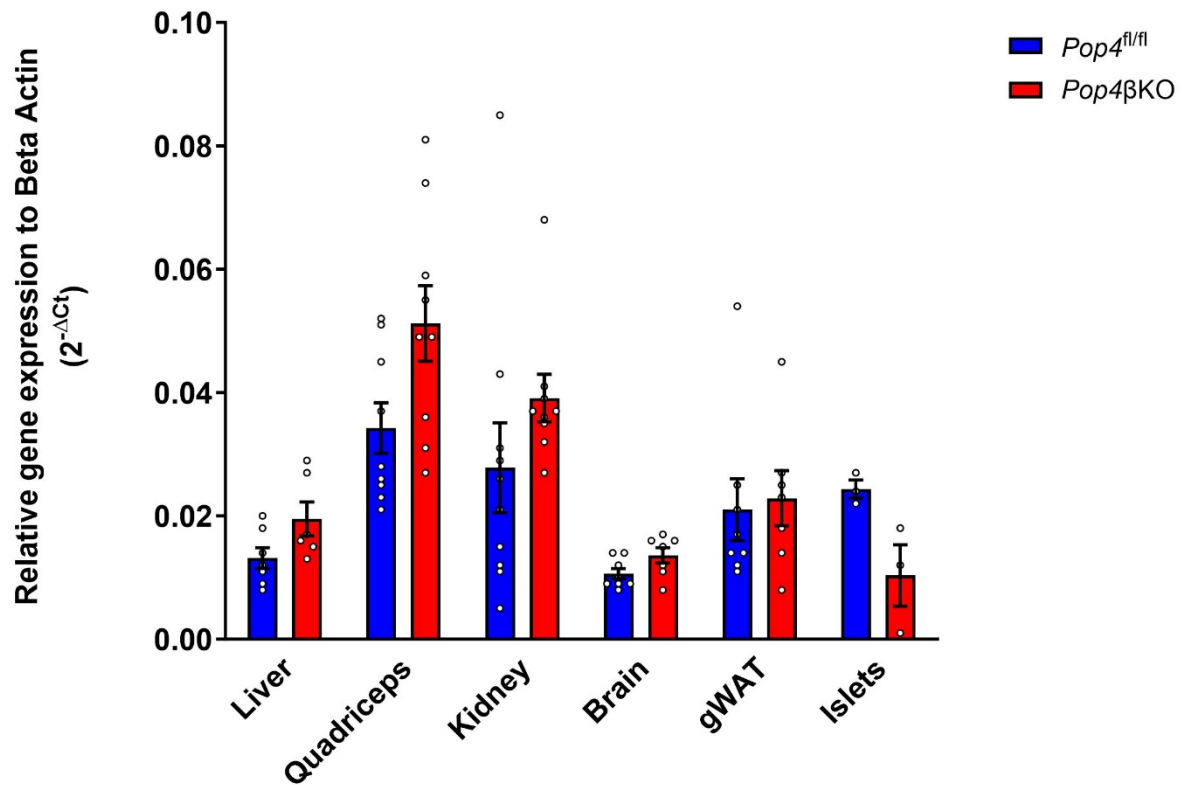


Figure 8. Quantitative gene expression of exon 4 to exon junction 5-6 of *Pop4* in different tissues. Relative gene expression of *Pop4* was normalized to housekeeper beta actin for liver, quadriceps, kidney, gonadal white adipose, brain and pancreatic islets tissues. Data are shown as mean ± SEM from 3-9 animals. Student's t-test was performed between *Pop4*^{βKO} and *Pop4*^{fl/fl}.

4.1.4 Prediction of putative *Pop4* protein structure

To evaluate the resulting protein structure of *Pop4*, the mRNA sequence with deletion of exons 4 and 5 were translated into the respective amino acid sequence. Thereafter,

the putative amino acid sequence of the *Pop4*βKO was aligned to the wildtype sequence (Figure 9).

```

Pop4 WT      1  MKAAIYHAFSHKEAKDHDVQELGSQRAEAFVRAFLKQSI PHMSQEDCESH 50
                |||
Pop4βKO      1  MKAAIYHAFSHKEAKDHDVQELGSQRAEAFVRAFLKQSI PHMSQEDCESH 50

Pop4 WT      51  LQRKAVILEYFTRLKPRPRPKKSKGLSAKQRRDMRLFDIKPEQQRYSLF 100
                |||
Pop4βKO      51  LQRKAVILEYFTRLKPRPRPKKSKGLSAKQRRDMRLFDIKPEQQSHEIQ 100

Pop4 WT      101 LPLHELWKQYIRDLCNGLK-PDTQPQMIQAKLLKADLHGAIISVTKSKCP 149
                :||
Pop4βKO      101 VPL-----LCGSYRNPSAGDQTCL----- 119

Pop4 WT      150 SYVGVGTGILLQETKHVFKIITREDHLKVIPKLNCFVTFIEIDDFISYIYGS 199
Pop4βKO      120 ----- 119

Pop4 WT      200 KFQLRASERSAKKFKAKGSIDL      221
Pop4βKO      120 ----- 119

```

Figure 9: Amino acid sequence alignment of the wildtype (WT) POP4 and the putative POP4 with deletion of exon 4 and 5 (*Pop4*βKO). The respective upper panel shows the wildtype sequence and the lower panel the amino acid sequence of the putative *Pop4*βKO. Matching alignment (green) is achieved in 45,5% and indicated by a pairing line while non-alignment with dots. The deletion of exons 4 and 5 causes a frameshift and a shortened amino acid sequence of 119 compared to 221 of the wildtype. Alignment was done with the EMBOSS Needle tool.

The translated amino acid sequence of exons 4 and 5 deleted *Pop4* show a frameshift leading to premature stop codon after position 119. While the 95 amino acid remains as the wildtype sequence the following 24 amino acid sequence are markedly changed. A predicted mouse protein structure shows that the residual *Pop4*βKO structure likely misses the C-terminal protein structure (Figure 10).

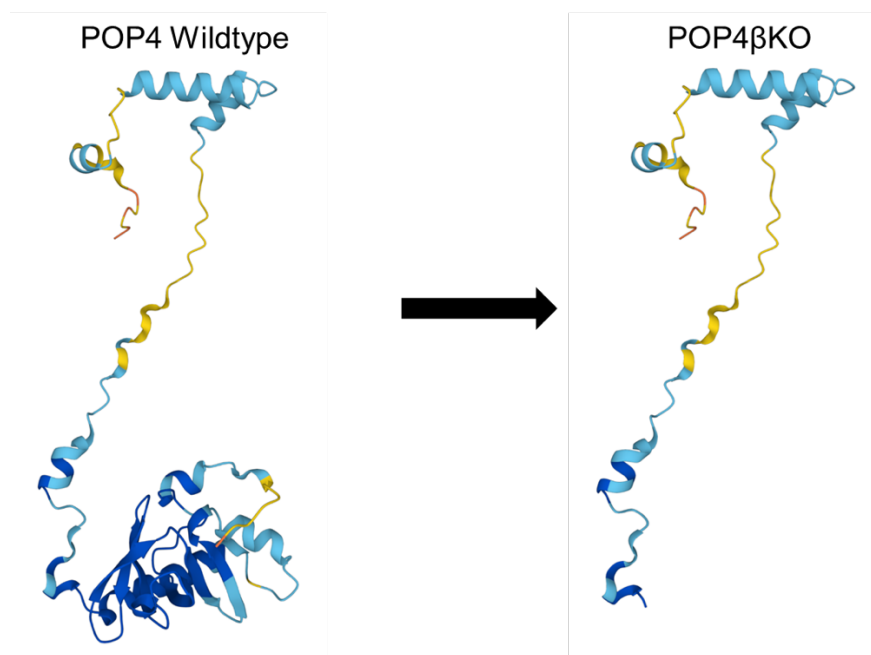


Figure 10: Predicted mouse protein structure of POP4 and the putative POP4 with deletion of exons 4 and 5. The tertiary structure of the putative protein structure with very high prediction confidence indicated in dark blue, high confidence in light blue and low in yellow. Prediction done by Alphafold tool (Uniprot Q9CR08).

4.1.5 Blood glucose development in male and female mice on a chow diet

Blood glucose levels were measured weekly after weaning of the mice at 3 weeks of age until 15 weeks of age in males and until 18 weeks of age in females mice. To exclude effects exerted by transgenic Cre recombinase (*Ins1^{Cre/+}*), loxP sites flanking exons 4 and 5 of *Pop4* (*Pop4^{fl/fl}*) and wildtype B6 background (WT) these mice were characterized as littermate controls compared to *Pop4βKO* mice.

In Figure 11A, the presented random blood glucose levels from 3 to 15 weeks of age in male mice from WT, *Ins1^{Cre/+}* and *Pop4^{fl/fl}* controls depict euglycemic blood glucose levels on average between 130 mg/dL to 180 mg/dL. In comparison, male *Pop4βKO* mice gradually developed hyperglycemia significantly starting at week 8 (mean: 227 mg/dL \pm SD 49 mg/dL) compared to age-matched *Pop4^{fl/fl}* mice (mean: 168 mg/dL \pm SD 20 mg/dL), at 9 weeks (mean: 232 mg/dL \pm SD 54 mg/dL) compared to age-matched *Ins1^{Cre/+}* mice (mean: 170 mg/dL \pm SD 33 mg/dL) and manifesting at week 10 to all age-matched controls (mean: 266 mg/dL vs control 179 mg/dL). At 11 weeks of age, majority of the male *Pop4βKO* animals crossed the hyperglycemia threshold of >300 mg/dL. Two out of 9 *Pop4βKO* mice show delayed hyperglycemia starting at

week 13. At the final 15 weeks of age, 7 out of 9 male *Pop4* β KO mice exhibited random blood glucose levels of at least 600 mg/dL.

Female *Pop4* β KO mice exhibited similar hyperglycemic outcomes (Figure 11B). However, female *Pop4* β KO showed a delayed onset of hyperglycemia compared to male *Pop4* β KO starting at week 13 compared to age-matched controls (mean: 242 mg/dL vs mean: controls 145 mg/dL). At 18 weeks of age, 7 out of 10 female *Pop4* β KO mice exhibited random blood glucose levels of >600 mg/dL. The diabetes prevalence depicted more clearly, that male *Pop4* β KO diabetes prevalence starts at 10 weeks of age and at 12 weeks of age all males cross the diabetes threshold of 300 mg/dL accounting for the diabetes prevalence (Figure 11C). Female mice diabetes prevalence starts at 13 weeks of age however only at 18 weeks all animals cross the diabetes threshold (Figure 11D).

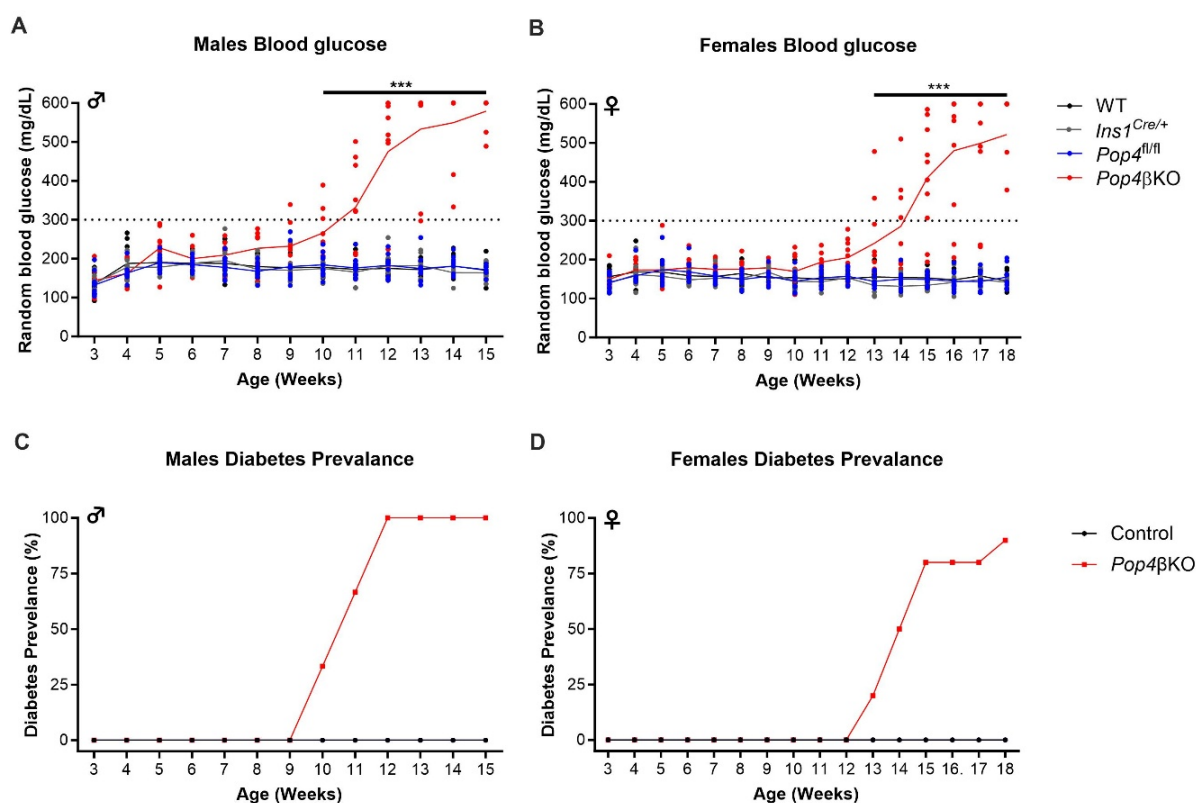


Figure 11. Blood glucose development and diabetes prevalence of male and female mice on standard chow diet. Blood glucose depicted in mg/dL were measured weekly in the morning for males (A) and females (B) of wild type (black), *Ins1*^{Cre/+} (grey), *Pop4*^{fl/fl} (blue) and *Pop4* β KO (red) mice. (C) and (D) show gender specific diabetes prevalence according to hyperglycemia threshold of ≥ 300 mg/dL. Dots represent individual animals and line represent mean from 7-10 animals per genotype. Statistical testing was done with Two-way ANOVA followed by Bonferroni post-hoc test, ***= $p < 0.001$.

4.1.6 Body weight and body composition development of male and female mice on chow diet

In terms of body weight development depicted in Figure 12, both male and female mice on a chow diet exhibited no significant changes in body weight between the genotypes from 3 to 13 eg. 17 weeks of life. At the final stages, for males at 14 and 15 weeks of age *Pop4* β KO experienced a loss of body weight and females at 18 weeks between the *Pop4* β KO to all age-matched controls. Moreover, body weight gain was comparable between the different genotypes showing no effect of Cre recombinase or LoxP sequence on body weight development.

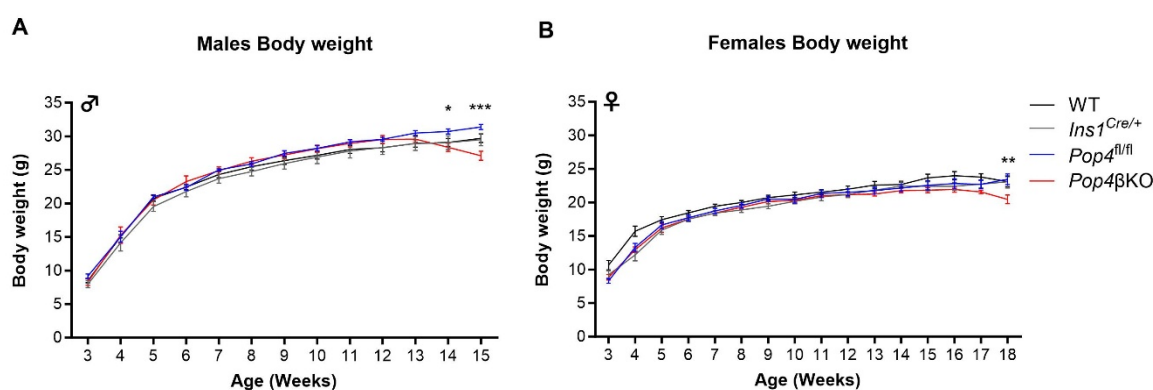


Figure 12: Body weight development of male and female mice on chow diet. Body weight was measured weekly in gram for males (A) and females (B) of Wildtype (black), *Ins1*^{Cre/+} (grey), *Pop4*^{fl/fl} (blue) and *Pop4* β KO (red) mice. Data are shown as mean \pm SEM from 7-10 animals per genotype. Statistical testing was done with Two-way ANOVA followed by Bonferroni post-hoc test, *= $p < 0.05$; **= $p < 0.01$; ***= $p < 0.001$.

As body weight didn't exhibit differences during the animal course of life, the body composition of lean and fat mass in the males and females *Pop4* β KO likewise show no significant differences to the age-matched controls (WT, *Ins1*^{Cre/+}, *Pop4*^{fl/fl}). However, the *Pop4* β KO males show a tendency of decreased lean mass from 12 to 15 weeks of age (Figure 13A). In terms of fat mass *Pop4* β KO males show minor gain from 12 to 15 weeks compared to the controls (Figure 13B). In *Pop4* β KO males and females, there is a tendency that fat mass appears to be lower in all measured weeks compared to controls (Figure 13C+D).

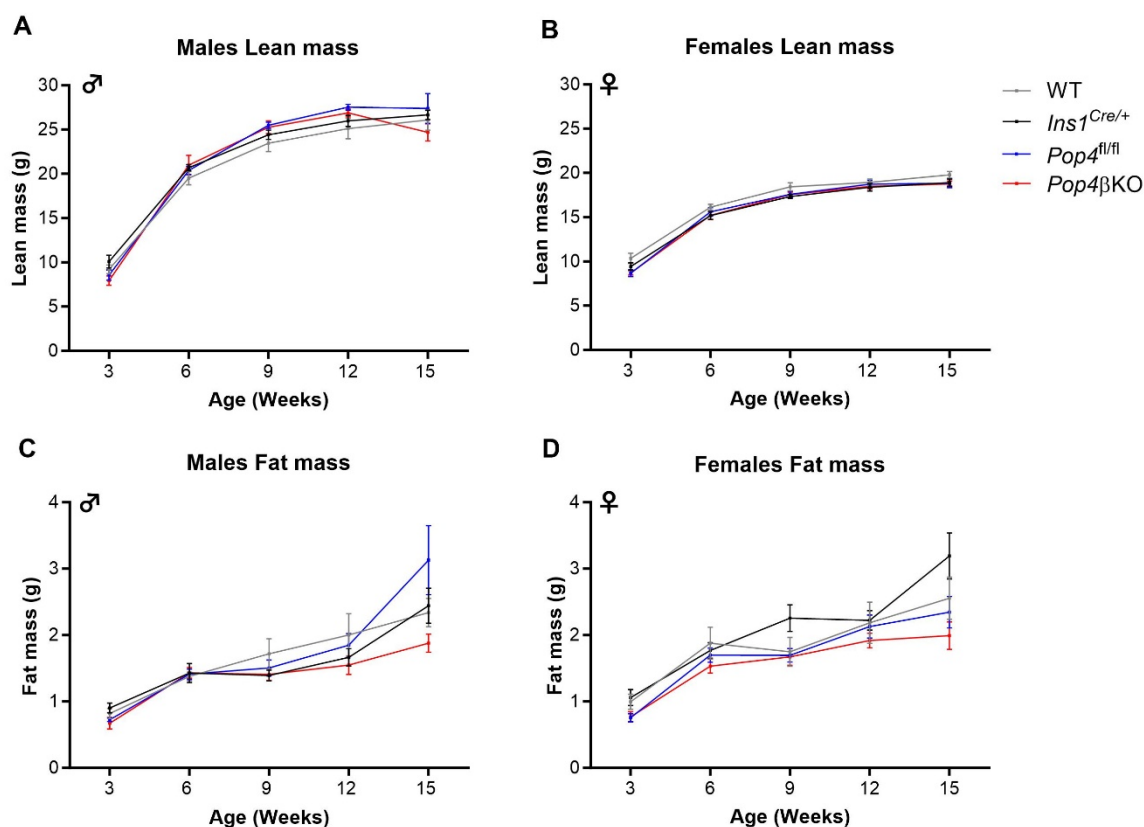


Figure 13. Body composition of lean and fat mass of males and females mice. Body composition of lean and fat mass were measured in gram every 3 weeks in (A+C) males and (B+D) females mice. Wildtype are shown in black, *Ins1^{Cre/+}* in grey, *Pop4^{fl/fl}* in blue and *Pop4 β KO* in red. Data are shown as mean \pm SEM from 7-10 animals per genotype. Statistical testing was done with Two-way ANOVA followed by Bonferroni post-hoc test.

4.1.7 Fasting glucose and plasma insulin levels of male and female mice on chow diet

To prevent influence of variability in food intake on basal blood glucose concentrations, the animals were fasted for 6 hours to obtain fasted blood glucose and fasted plasma insulin levels at defined time points. Four time points were chosen: 3 weeks as the earliest time point, 8 weeks before the onset of hyperglycemia, 11 weeks when the majority of *Pop4 β KO*s exhibited hyperglycemia, and the last time point 15 weeks for males and 18 weeks for females at severe hyperglycemic state. In the male mice, there were no significant changes in 6 hours fasted blood glucose levels at 3, 8 and 11 weeks of age between *Pop4 β KO* and controls. At 15 weeks of age, male *Pop4 β KO* mice show severe hyperglycemia with 7 out of 9 animals reaching a fasted blood glucose level of at least 600 mg/dl, which was significantly higher than that of all the controls (mean 148 mg/dl) (Figure 14A). Female *Pop4 β KO* already show higher fasted blood glucose levels at 8 weeks of age compared to age-matched *Ins1^{Cre/+}* control (mean 154

mg/dl vs 128 mg/dl). At 11 weeks of age *Pop4* β KO females (mean 171 mg/dl) showed higher fasting blood glucose levels than age-matched *Pop4*^{fl/fl} (mean 128mg/dl) and age-matched *Ins1*^{Cre/+} mice (mean 112mg/dl). At the final stages at 18 weeks of age higher blood glucose has manifested in *Pop4* β KO compared to all age-matched controls in the female mice (**Figure 14B**). Individual differences between the animals in fasting plasma insulin levels is shown in Figure 14C+D. In males the plasma insulin levels varied between animals but no significant differences were observed at 3 and 8 weeks of age. *Pop4* β KO show reduced plasma insulin levels compared to age-matched WT at 11 weeks of age. At 15 weeks of age, *Pop4* β KO mice showed significantly lower fasted plasma insulin levels than all age-matched controls. For females, the fasted plasma insulin levels presented matching results to the males and only at 18 weeks the reduced plasma insulin levels of *Pop4* β KO could be detected compared to age-matched controls (**Figure 14D**).

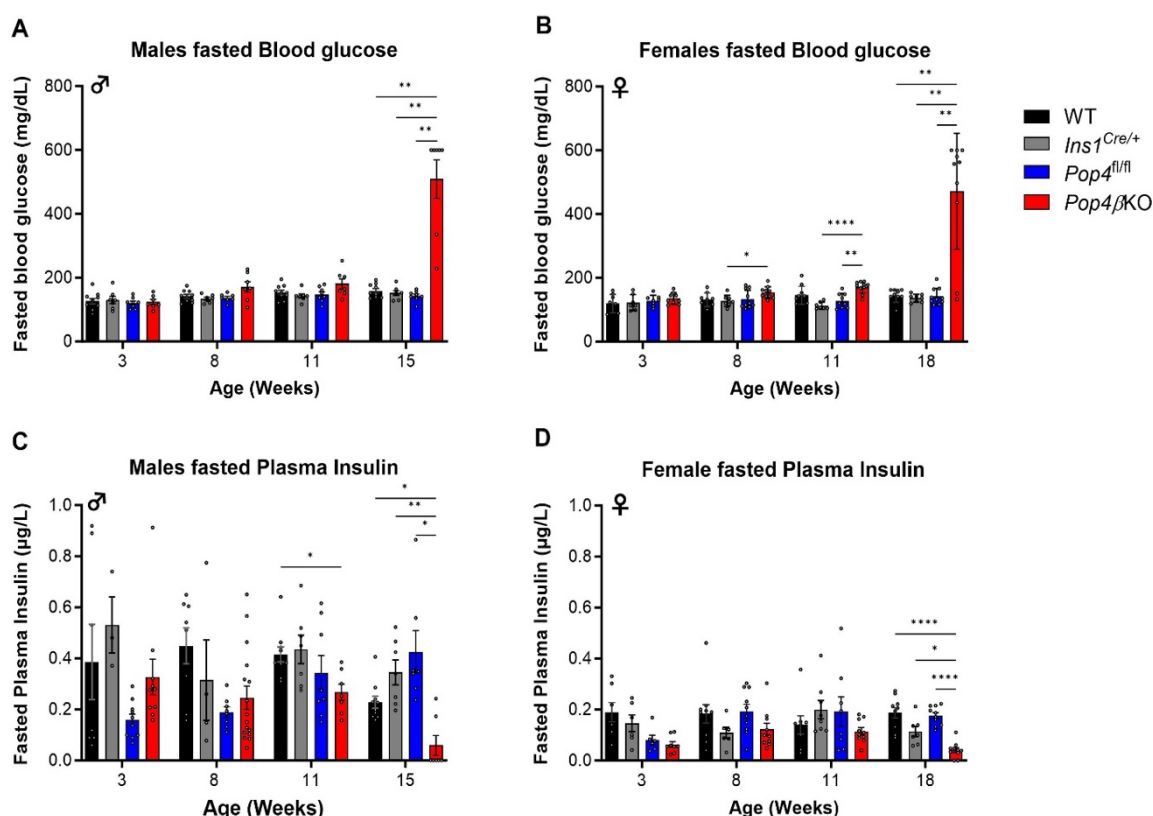


Figure 14: Fasted blood glucose and plasma insulin levels of males and females on a chow diet.

Animals were fasted for 6 h and blood were collected to measure blood glucose and plasma insulin levels. Wildtype controls shown in black, *Ins1*^{Cre/+} in grey, *Pop4*^{fl/fl} in blue and *Pop4* β KO in red. Data shown as bars showing mean \pm SEM, dots represent individual animals. Statistical testing was done with Two-way ANOVA followed by Bonferroni post-hoc test, * $p < 0.05$; ** $p < 0.01$; **** $p < 0.0001$.

4.1.8 Blood glucose and body weight development of female mice on chow vs HFD

In order to evaluate, if an obesity-promoting diet would further accelerate the onset of hyperglycemia and diabetes in the animal, female mice were investigated on a high fat diet with 60% calories from fat. Since female control animals on the chow diet did not exhibit changes in metabolic traits of interest, the metabolic phenotyping of HFD proceeded with *Pop4^{fl/fl}* as the only control.

In concordance with the chow diet, female *Pop4 β KO* animals fed a 60% HFD showed onset of hyperglycemia starting significantly at week 13 compared to age-matched *Pop4^{fl/fl}* control (Figure 15A). Furthermore, at 18 weeks of age body weight dropped and was lower compared to *Pop4^{fl/fl}* control (Figure 15B). The data of the 6h fasted blood glucose levels at the different time points of life indicate that female mice on HFD already show elevated blood glucose starting at week 8, whereas the chow diet animals hyperglycemia started at week 11 (Figure 15C). Accompanying fasted insulin levels depict elevated levels at 11 weeks of age between HFD and chow *Pop4 β KO* animals before the loss of insulin for both at week 18 (Figure 15D).

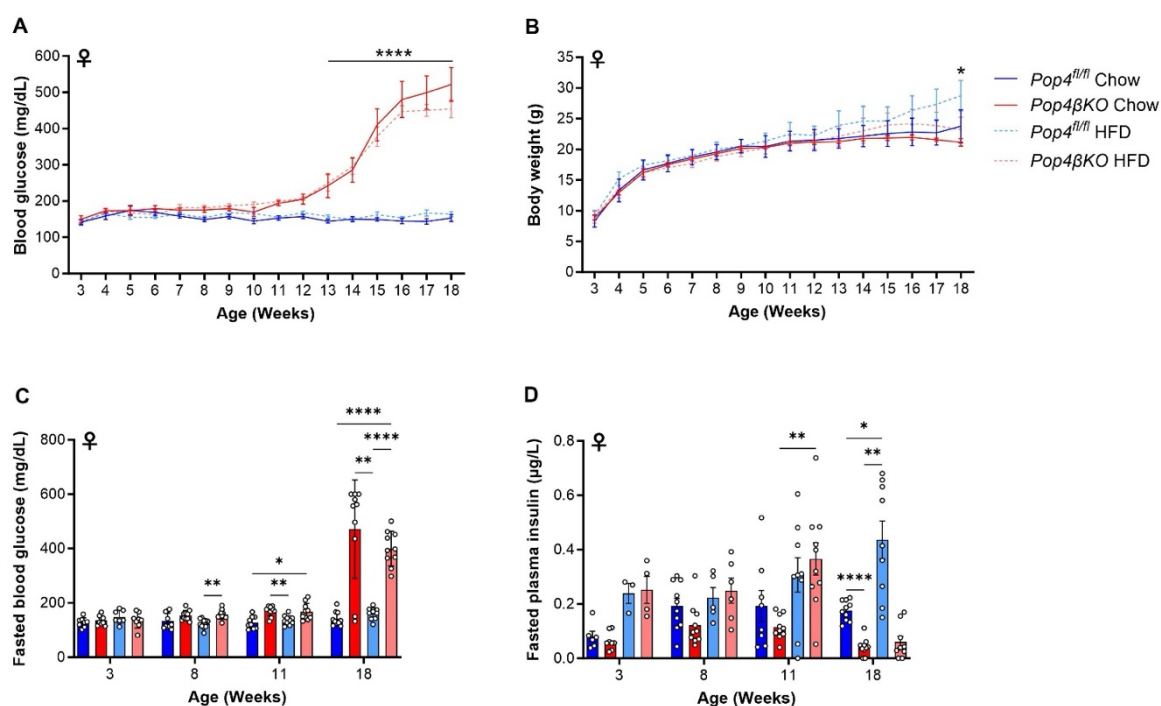


Figure 15. Comparison of metabolic traits on 60% high fact diet vs chow diet in female mice. (A) Blood glucose levels, (B) body weight, (C) 6 h fasted plasma glucose and (D) plasma insulin levels were compared. Data are shown as mean \pm SEM and dots represent values of individual animals (C+D) from 5-10 animals per genotype. *Pop4^{fl/fl}* on Chow diet shown in blue, *Pop4 β KO* on chow in red, *Pop4^{fl/fl}* on HFD in light blue and *Pop4 β KO* on HFD in lighter red. Statistical testing was done with Two-way ANOVA followed by Bonferroni post-hoc test, *= $p < 0.05$; **= $p < 0.01$; ****= $p < 0.0001$.

4.1.9 Body composition of females on chow vs HFD

Body composition was assessed using nuclear magnetic resonance imaging to distinguish lean and fat mass. Lean mass was comparable between the genotypes *Pop4^{fl/fl}* and *Pop4 β KO* with both chow and high-fat diet (Figure 16A). However, compared to chow diet, *Pop4 β KO* and *Pop4^{fl/fl}* female animals on the high-fat diet showed significantly higher fat mass at 15 weeks of age compared to chow fed animals (Figure 16B).

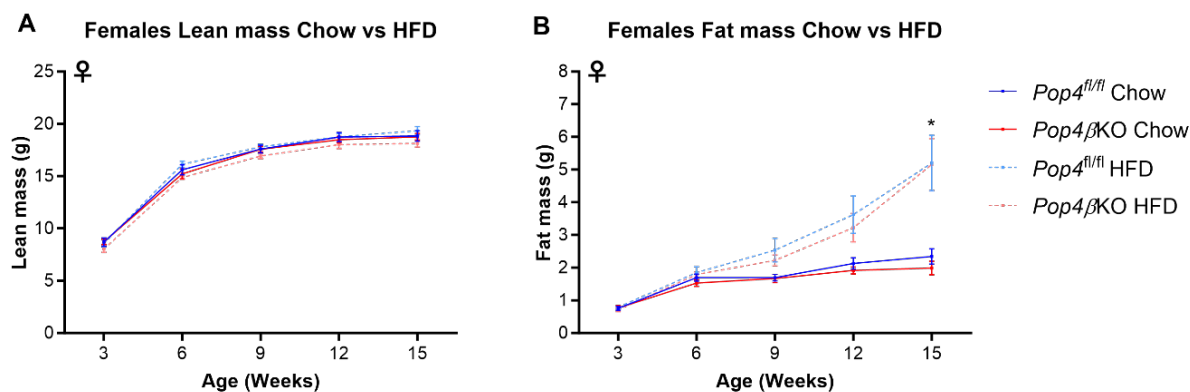


Figure 16. Body composition of lean and fat mass of females mice on chow and high fat diet (HFD). Body composition of (A) lean and (B) fat mass are shown in gram. *Pop4^{fl/fl}* on chow diet shown in blue, *Pop4 β KO* on chow in red, *Pop4^{fl/fl}* on HFD in light blue and *Pop4 β KO* on HFD in lighter red. Data are shown as mean \pm SEM from 8-10 animals per genotype. Statistical testing was done with Two-way ANOVA followed by Bonferroni post-hoc test. $p < 0.05$.

4.1.10 Diabetes prevalence and HOMA-IR of female mice on chow vs HFD

In terms of diabetes prevalence, even though hyperglycemic onset occurs at a matching timepoint for chow and high-fat diet (HFD) fed animals, the high-fat fed animals show higher diabetes prevalence at an earlier timepoint compared to chow fed female mice (Figure 17A).

To validate the high fat diet challenge on the metabolic condition of the mice, the homeostatic model assessment of insulin resistance (HOMA-IR) was calculated based on the fasted blood glucose and plasma insulin levels depicted in Figure 15. The HOMA Index at 3 and 8 weeks of age show no significant difference between the genotypes *Pop4 β KO* to *Pop4^{fl/fl}* with chow or high-fat diet. At 11 weeks of age HFD *Pop4 β KO* females show a significant higher insulin resistance compared to both *Pop4 β KO* and *Pop4^{fl/fl}* on chow diet according to HOMA-IR values (Figure 17B). As at 18 weeks of age, *Pop4 β KO* female mice presented a loss of insulin, the HOMA-IR value was not calculated.

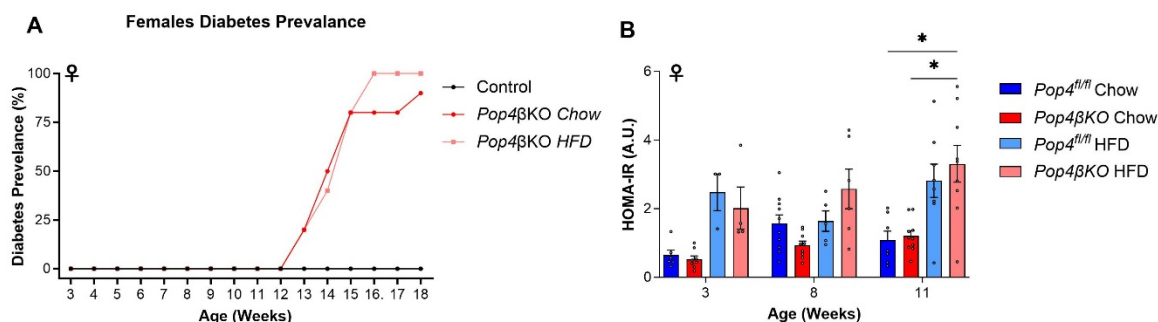


Figure 17. Diabetes prevalence and HOMA-IR at 3, 8 and 11 weeks of age for the female mice on chow compared to HFD. Diabetes prevalence is calculated based on number of animals crossing the hyperglycemia threshold of 300 mg/dL indicated in percentage of total animals. HOMA-IR was calculated by multiplying the fasted glucose levels with the fasted insulin levels and divide by 405. Data are presented as mean \pm SEM with individual values as dots from 4-10 animals. *Pop4^{fl/fl}* on chow diet shown in blue, *Pop4βKO* on chow in red, *Pop4^{fl/fl}* on HFD in light blue and *Pop4βKO* on HFD in lighter red. Statistical testing was done with Two-way ANOVA followed by Bonferroni post-hoc test. * $p < 0.05$.

4.1.11 *In vivo* intraperitoneal glucose tolerance test (ipGTT) of male mice

To investigate if the mice exhibit changes in glucose metabolism before the hyperglycemia occurs, the male mice were challenged with an intraperitoneal glucose tolerance test at 8 weeks of age to examine glucose tolerance and insulin secretion *in vivo*. Since WT, *Ins1^{Cre/+}* and *Pop4^{fl/fl}* control showed no significant changes in blood glucose and plasma insulin levels at 8 weeks of age, this experiment was proceeded with all genotypes as one control group.

During the ipGTT shown in Figure 18A both control and *Pop4βKO* show steep increase in blood glucose till 30 min after injection. At 60 min after injection control mice could lower blood glucose levels while the high blood glucose levels of *Pop4βKO* persevered (490 mg/dL \pm SD 94 vs 294 mg/dL \pm SD 974 mg/dL) and only started reducing after 120 min. At 240 min after injection both genotypes returned to normoglycemic levels. The total rise in glucose level during the glucose challenge, indicated by the area under the curve (AUC), for the blood glucose curves corroborate with the decrease glucose tolerance result of the *Pop4βKO* (Figure 18C).

The plasma insulin levels during the course of the ipGTT show that *Pop4βKO* mice secreted lower amounts of insulin compared to control (Figure 18B). At 30 min control mice show twice as much plasma insulin levels compared to *Pop4βKO* mice. Overall, the total plasma insulin levels of *Pop4βKO* depict a lower secretion capacity also indicated by the area under the curve for plasma insulin (Figure 18D).

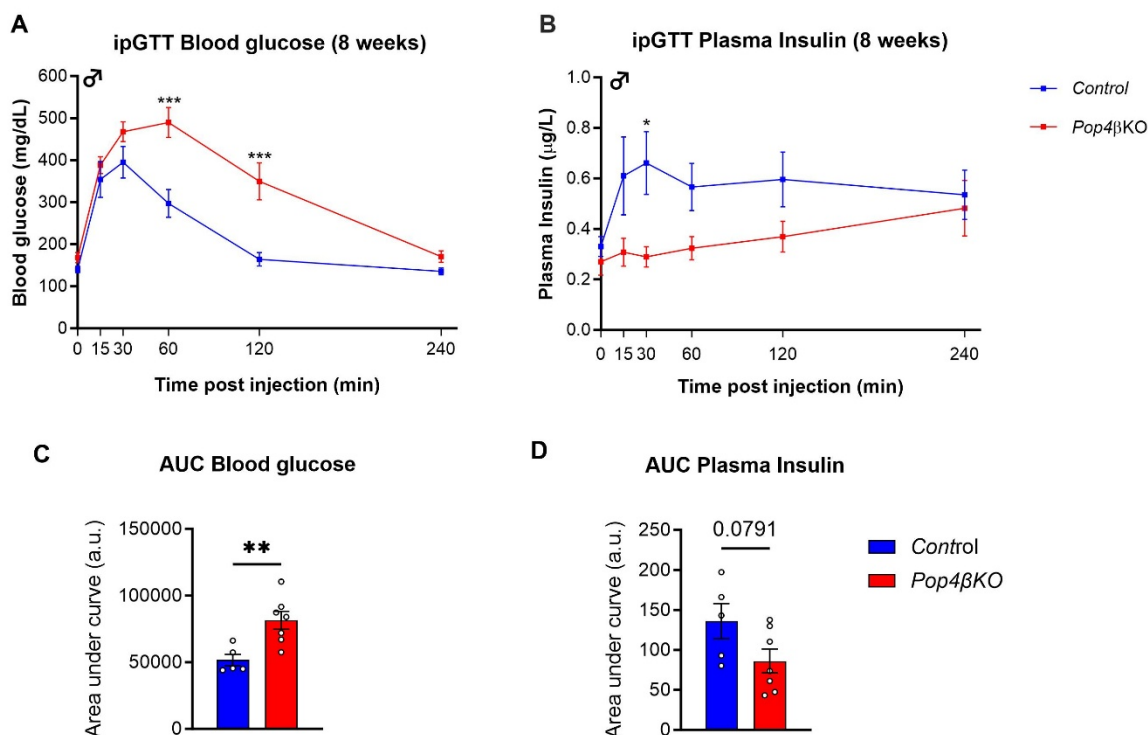


Figure 18: Intraperitoneal glucose tolerance test at 8 weeks of age in male mice. (A) Blood glucose levels and (B) Plasma insulin levels were measured after 6 hours fasting which represents timepoint 0. After glucose bolus of 1g/kg animal weight blood glucose and plasma insulin was assessed from timepoint 15, 30, 60, 120 and 240 minutes post injection. Control mice shown in blue and *Pop4 β KO* mice shown in red. Data are shown as mean \pm SEM from 5-7 animals per genotype. Statistical testing was done with Two-way ANOVA followed by Bonferroni post-hoc test or unpaired Student's t-test, *= $p < 0.05$, ***= $p < 0.001$. Data collection for this experiment was done with help from Dr. Delsi Altenhofen.

4.1.12 *Ex vivo* glucose stimulated insulin secretion (GSIS) of isolated islets of male mice

To observe the insulin secretion function, a glucose stimulated insulin secretion assay of isolated islets was conducted at 8 weeks of age from male mice. The results show that there was no significant difference in insulin secretion capacity in the islets of the *Pop4 β KO* compared to control with low glucose stimulation of 2 mM glucose but with high glucose stimulation with 25 mM glucose the *Pop4 β KO* depict tendency for reduced insulin secretion (Figure 19A).

Additionally, the insulin, proinsulin and glucagon content were assessed in the lysate of the isolated islets post GSIS. No significant differences were found in mature insulin content and glucagon content however proinsulin content was significantly reduced in the *Pop4 β KO* islets (Figure 19B). All values were normalized to pancreatic islets endogenous protein content which were comparable between the genotypes (Figure 19C).

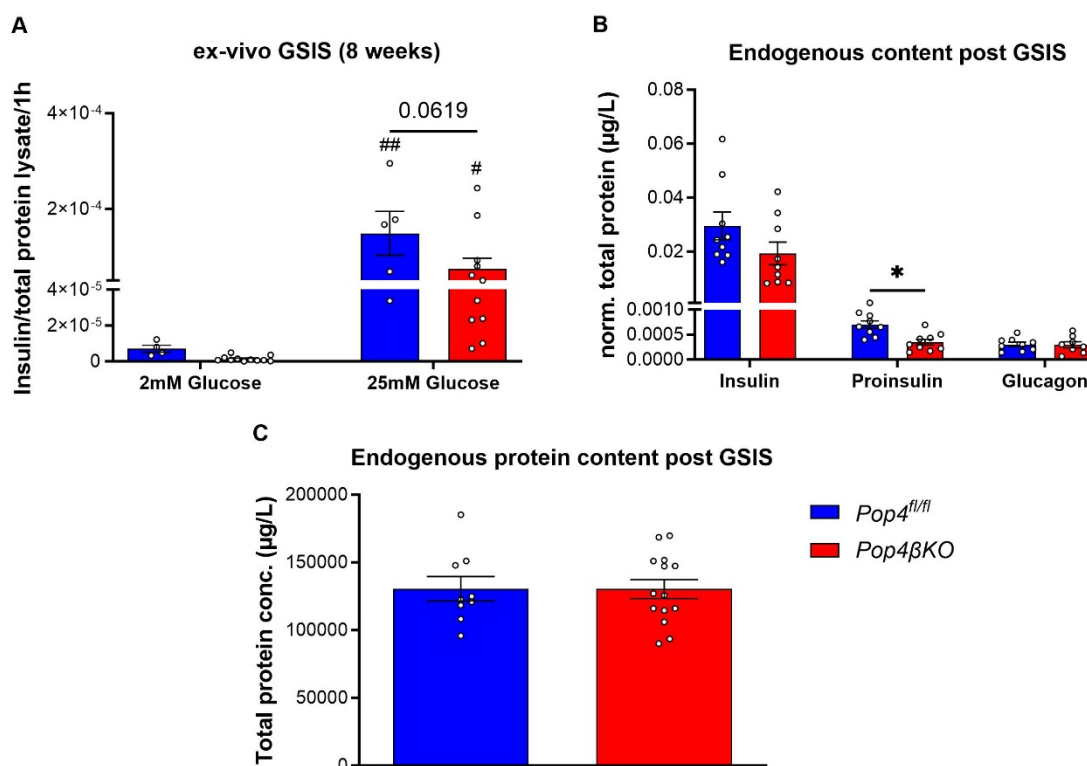


Figure 19. Insulin secretion assay and protein content in isolated pancreatic islets. (A) Secreted insulin content is depicted from a glucose stimulated insulin secretion (GSIS) assay of isolated pancreatic islets of *Pop4 β KO* compared to control. Selected pancreatic islets were stimulated with 2 mM glucose and thereafter 25 mM glucose for 1 hour each. Insulin concentration in the media was measured with a dedicated ELISA and the insulin concentration was normalized to protein concentration of these islets. (B) The mean Insulin, Proinsulin, Glucagon and (C) protein content of the islets is shown which depict the endogenous level post GSIS assay. Data from 5-11 animals indicated as a dot are shown. For each animal, the mean level of protein of 8 islets are depicted from duplicate measurement. Control mice shown in blue and *Pop4 β KO* mice are shown in red. Data are shown as mean \pm SEM per genotype. Statistical testing was done with Two-way ANOVA followed by Bonferroni post-hoc test or unpaired Student's t-test, *= p <0.05.

4.2 Histology of the Islets of Langerhans and pancreatic beta cell

In order to gain further insights into islet morphology and beta cell structure, several histological approaches were employed at different timepoints to examine the pathology in the *Pop4 β KO* pancreatic islet tissue of male mice.

4.2.1 Pancreas and pancreatic islet morphometrics

To analyze the endocrine multicellular micro organelle the Islets of Langerhans, selected sections from consecutive cut levels of the PFA fixed paraffin embedded pancreas were stained with Hematoxylin Eosin (HE) to visualize the morphology of the tissue. Six sections with a distance of 100-150 μ m were chosen to estimate islet size and islet number for the respective pancreata.

The selected timepoints were 3, 9 and 15 weeks. The timepoint 3 weeks was selected to observe the pancreatic islets at an early timepoint. The timepoint 9 weeks was select

to depict the status right before the onset of hyperglycemia and 15 weeks was chosen as the last time point in which overt hyperglycemia has manifested.

Figure 20 depict representative images of the pancreatic islet of each time point for both *Pop4* β KO and control *Pop4*^{fl/fl}. The morphology at 3 and 9 weeks of age did not show distinct differences in the islet cell structure or nucleus. At 15 weeks though the islet morphology was distinctively different. The cells within the pancreatic islets showed a reduced cell size evident by higher visible density of the dark stained nuclei (**Figure 20**).

The morphometric analysis showed overall that the measured mean pancreas area depicted a gradual increase in size with age, significantly from 3 to 15 weeks of age however no differences in area when comparing the *Pop4* β KO to *Pop4*^{fl/fl} control within the respective timepoints (**Figure 21A**). The *Pop4* β KO depicted a tendency in increased pancreas area from 3 to 9 weeks but a significant decrease from 9 to 15 weeks of age. In terms of islet size presented as islet diameter, the average islet diameter ranges from ~50-85 μ m. At 3 and 9 weeks of age the islet diameter didn't show differences between genotypes and only show significant smaller islet diameter at 15 weeks of age (**Figure 21B**). Additionally, the percentage of islet to pancreas area again show solely a decrease at 15 weeks of age in islet area (**Figure 21C**). The estimated number of islets depicted as islet density, in general show highest density at 3 weeks of age for both genotypes. Especially islet density in *Pop4* β KO exhibit significant decrease from 3 to 9 and to 15 weeks of age while *Pop4*^{fl/fl} display reduced islet density from 3 to 9 weeks of age (**Figure 21D**). As pancreatic islet ranges in size additional clustering of islet sizes were appointed to gather additional information at the three timepoints. According to the aforementioned mean pancreatic islet size, islets with diameter size under 50 μ m were assigned as small islets, between 50 to 100 μ m in diameter size as medium sized islets and over 100 μ m were designated as big islets. It appears that the majority of the measured pancreatic islet size cluster for small and medium sized islets. At 3 weeks of age, both genotypes show that around half of the measured pancreatic islets were of smaller islet size, followed by medium sized islets and bigger islets making the smallest contribution. At 9 weeks of age, smaller sized islets and medium sized islets were evenly distributed and bigger islets were more apparent than at 3 weeks of age. At the final 15 weeks of age, significantly less of the smaller sized islets was detected especially in the *Pop4* β KO genotype whereas more medium sized islets were

recognized especially in the *Pop4* β KO. Bigger sized islets at 15 weeks of age showed no difference between the genotype (Figure 21E).

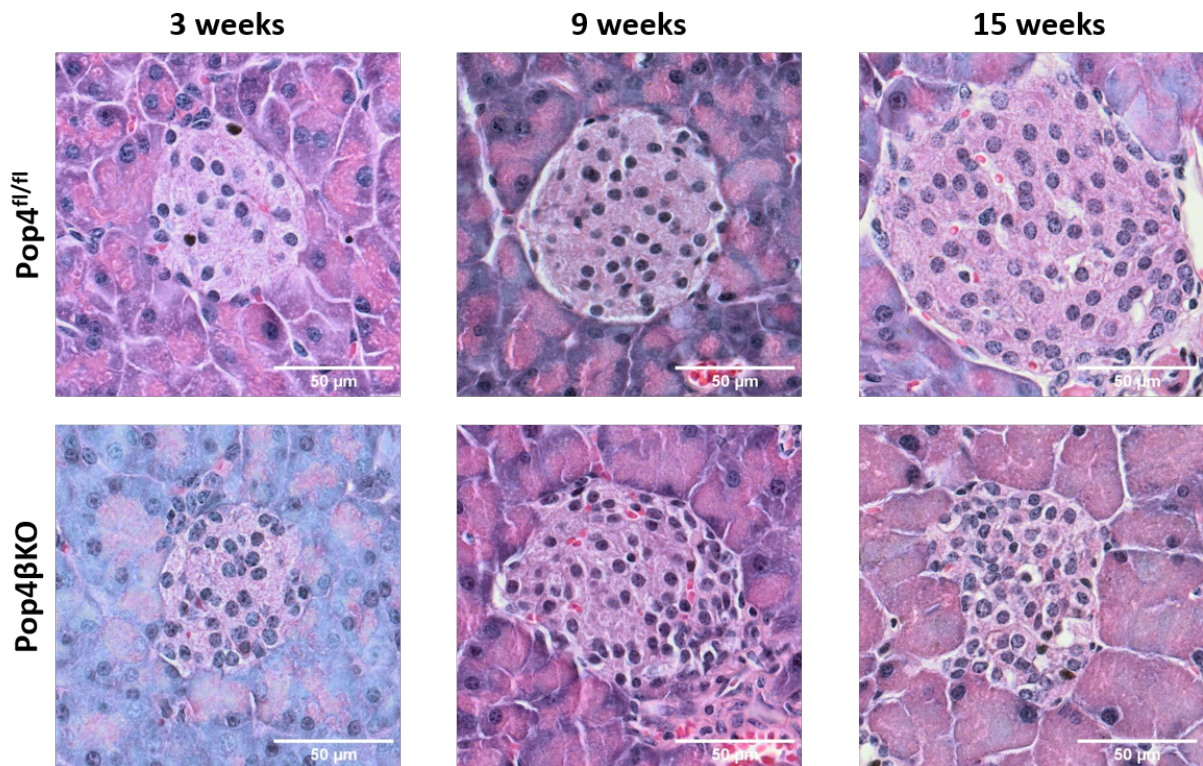


Figure 20. Representative images of HE stained pancreatic islet. Hematoxylin stained pancreatic section of *Pop4* β KO compared to *Pop4*^{fl/fl} during the timepoints 3, 9 and 15 weeks of age. Scale bar represents 50 μ m.

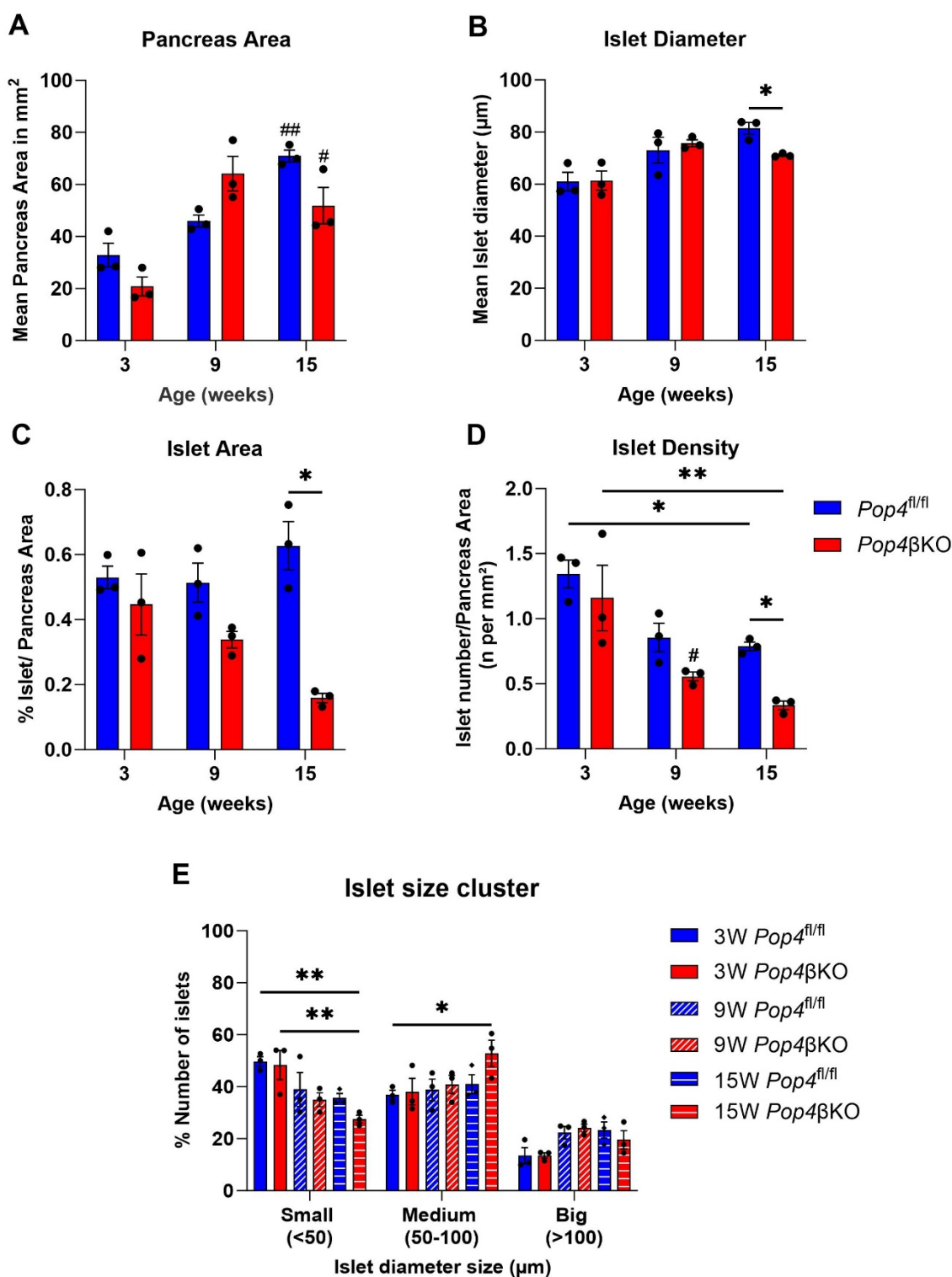


Figure 21. Morphometrics of pancreatic sections and respective pancreatic islet areas. (A) Mean pancreas area, (B) islet diameter, (C) Ratio of Islet to pancreas area in %, (D) islet density as number per mm² pancreas area and (E) islet size cluster are presented. Data are shown as mean \pm SEM and individual values as dots from 3 animals per genotype. *Pop4^{fl/fl}* control mice shown in blue and *Pop4^{βKO}* mice shown in red. Statistical testing was done with Two-way ANOVA followed by Bonferroni post-hoc test, * $p < 0.05$, ** $p < 0.01$ *Pop4^{fl/fl}* vs *Pop4^{βKO}* or # $p < 0.05$; ## $p < 0.01$ respective genotype timepoint to timepoint before.

4.2.2 Impact of beta cell specific *Pop4* KO on pancreatic beta cell mass

Immunostaining of the endogenous insulin and glucagon content on subcellular resolution in pancreatic tissue section were performed in order to understand the temporal changes of the pancreatic islets cell composition (Figure 22).

Thereby, overall the insulin positive area makes up ~70-90% of the islet area whereas the glucagon area makes up to 10-15% in the control (Figure 23A). The pancreatic islets at 3 weeks of age show no difference in insulin and glucagon positive area between *Pop4 β KO* compared to *Pop4^{fl/fl}*. This changes at timepoint 9 weeks of age, in which the islets of *Pop4 β KO* show lower insulin positive area and a tendency for higher glucagon positive area compared to *Pop4^{fl/fl}*. At 15 weeks of age, the pancreatic islets appear to loose insulin positive area and instead show a significant higher glucagon area (Figure 23B). Whereas observing these parameters for the islet clusters, all islet cluster show equal reduction of insulin area and increased glucagon area at 15 weeks of age (Figure 23C+D).

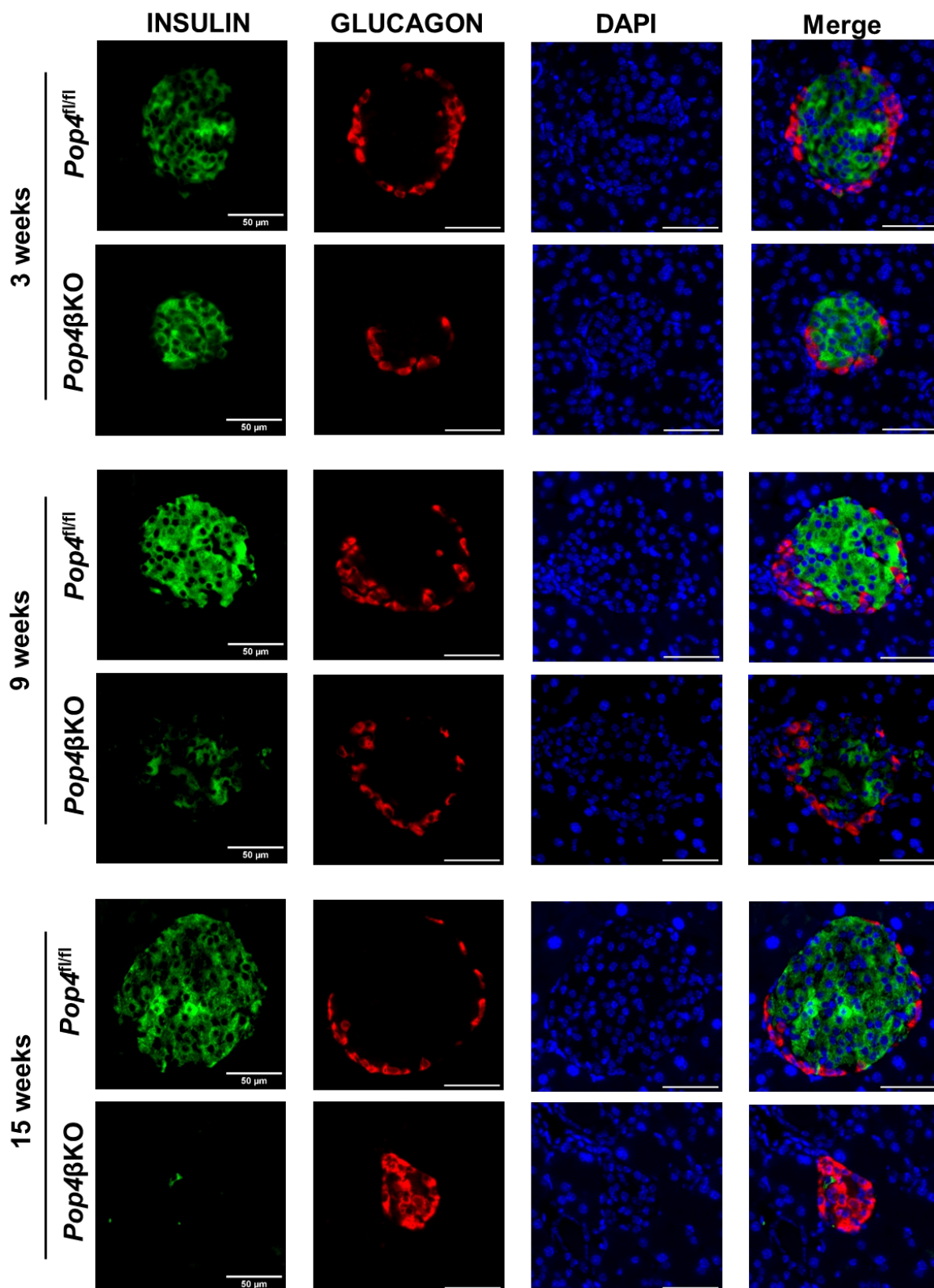


Figure 22. Representative images of immunostainings detection of Insulin and Glucagon in pancreatic tissue sections to visualize beta cell and alpha cell area. Immunofluorescence staining targeting insulin in green (first column), glucagon in red (second column), DAPI in blue (third column) and the merged images (fourth column). The first two rows show 3 weeks, third and fourth row 9 weeks and fifth and sixth row show 15 weeks pancreatic section of *Pop4 β KO* compared to *Pop4^{fl/fl}*. Scale bar represents 50 μ m.

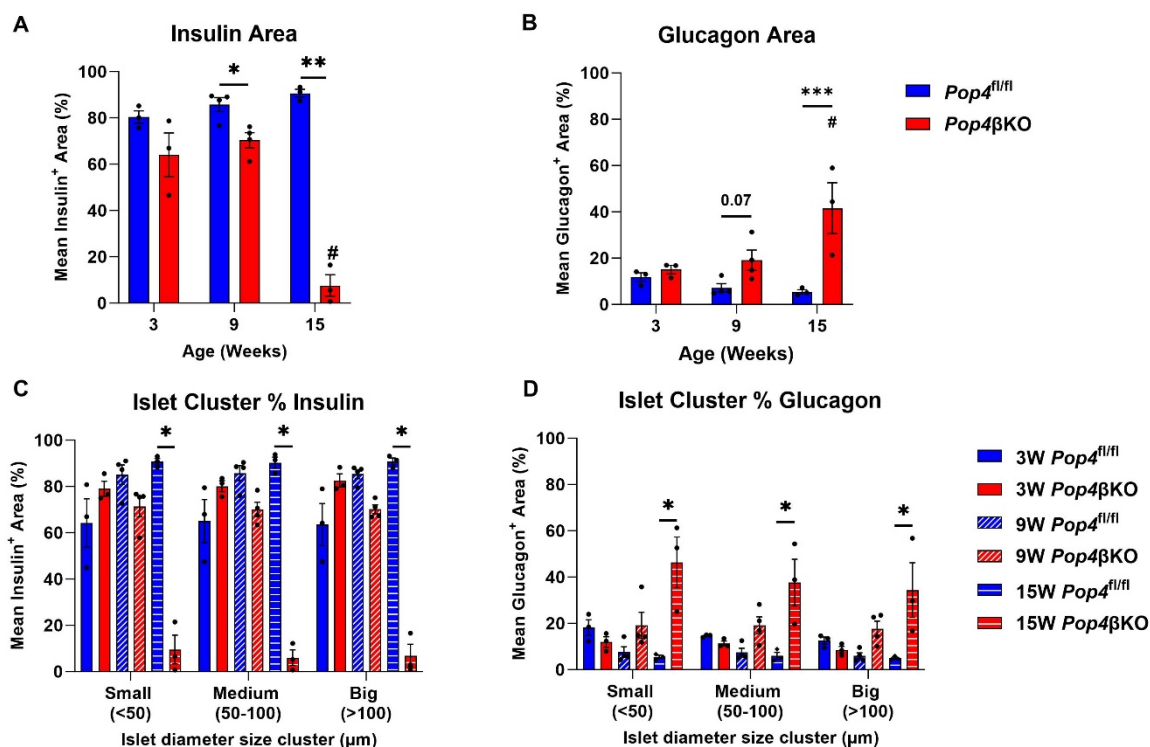


Figure 23. Quantification of immunostained insulin positive and glucagon positive area. (A) Mean Insulin⁺ area and (B) mean glucagon⁺ area (C+D) Insulin and glucagon area depicted in islet size cluster small (<50 μ m), medium (50-100 μ m) and big islets (>100 μ m). Data are shown as mean \pm SEM and individual values as dots from 3 animals per genotype. *Pop4^{fl/fl}* control mice shown in blue and *Pop4 β KO* mice shown in red. In C and D 9 weeks are indicated in diagonally striped bars and 15 weeks as horizontally striped bars. Statistical testing was done with Two-way ANOVA followed by Bonferroni post-hoc test, *= p <0.05; **= p <0.01; ***= p <0.001 *Pop4^{fl/fl}* vs *Pop4 β KO* or #= p <0.05 respective genotype timepoint to timepoint before.

4.2.3 Immunostaining of NKX6.1 beta cell identity and KI67 as proliferation marker

In order to address the changes in insulin and glucagon content that appear in the pancreatic islets, the beta cell identity and proliferation capacity were further assessed by immunofluorescence staining. Therefore, the nuclear transcription factor NKX6.1 a beta cell identity marker and the nuclear KI67 proliferation marker expressed during all active cell cycle phases was immunostained and quantitated (Figure 24). In general, ~70-85% of the nuclei within the insulin⁺ area show expression of NKX6.1 marker at 3 and 9 weeks of age with no changes between genotypes. However, at 15 weeks NKX6.1 signal appear significantly reduced in *Pop4 β KO* (Figure 25A). In terms of proliferation marker KI67, interestingly at 3 weeks of age *Pop4 β KO* show significant higher appearance of proliferation marker compared to *Pop4^{fl/fl}*. Altogether, KI67⁺ nuclei show tendency of decrease with age in both genotypes which is diminished at

15 weeks of age in *Pop4* β KO (Figure 25B). Next, to evaluate indirectly if more beta cells are apparent, the proportion of NKX6.1 nuclear beta cell marker to the insulin⁺ area was calculated. This analysis displayed a reduction in ratio of beta cells to insulin area for *Pop4* β KO at 15 weeks of age (Figure 25C).

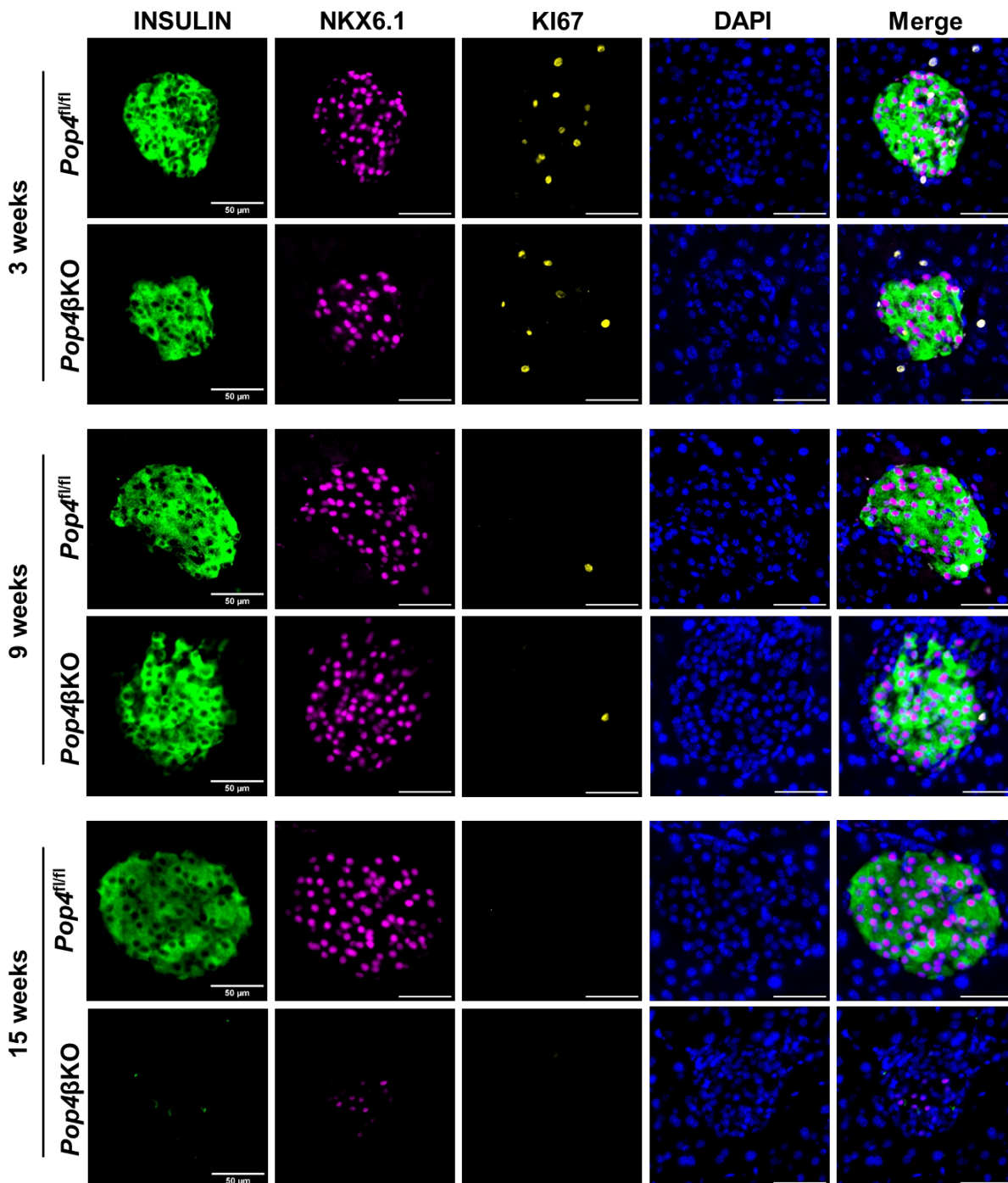


Figure 24. Representative images of immunostainings detection in pancreatic tissue sections to visualize beta cell identity and proliferation. Immunofluorescence staining targeting insulin in green (first column), NKX6.1 in magenta (second column), KI67 in yellow (third column), DAPI in blue (fourth column) and the merged images (fifth column). The first two rows show 3 weeks, third and fourth row 9 weeks and fifth and sixth row show 15 weeks pancreatic section of *Pop4* β KO compared to *Pop4*^{fl/fl}. Scale bar represents 50 μ m.

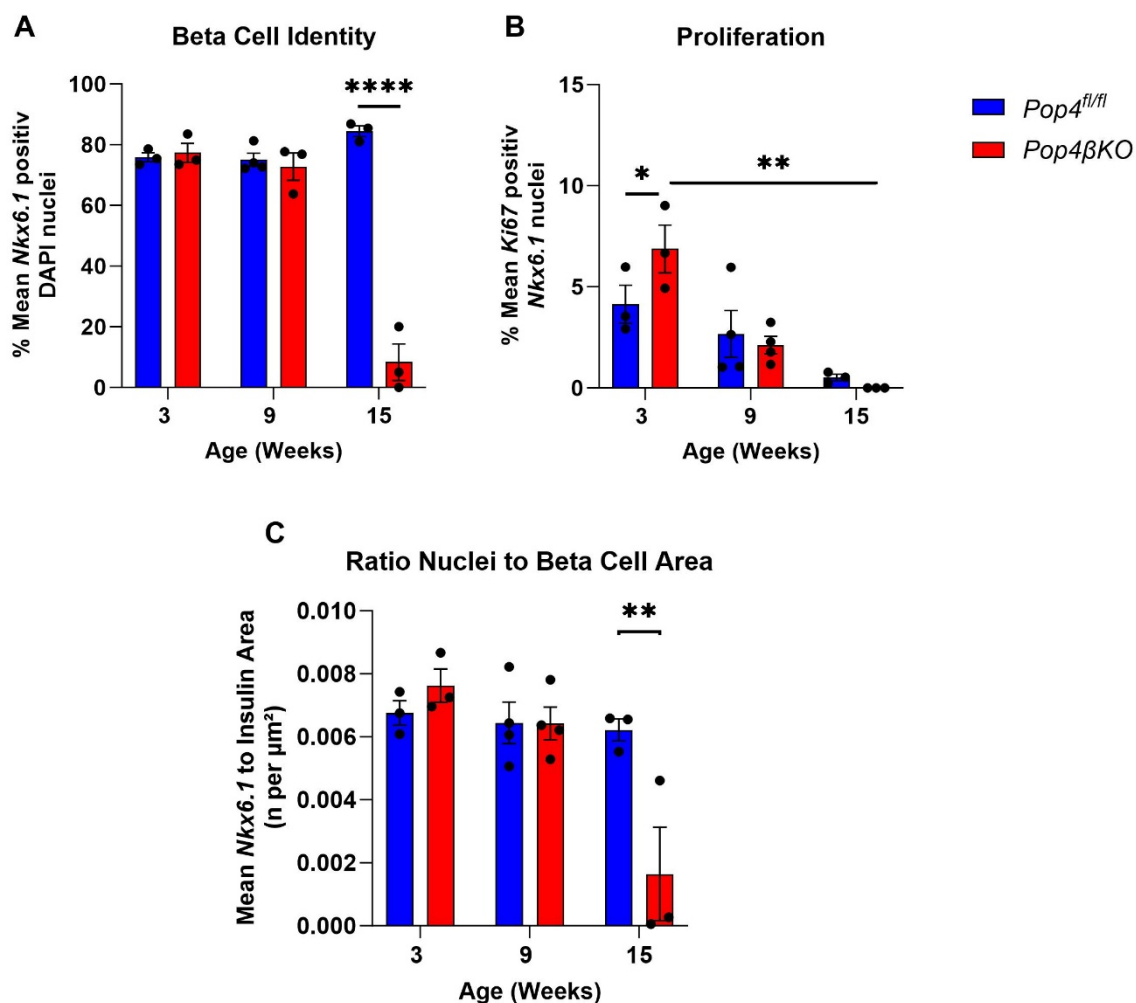


Figure 25. Quantification of immunostained beta cell identity marker NKX6.1 and proliferation marker KI67. (A) Mean percentage of NKX6.1⁺ DAPI stained nuclei, (B) mean percentage of KI67 positive NKX6.1 nuclei and mean NKX6.1 ratio to insulin area within pancreatic islet are depicted for 3, 9 and 15 weeks pancreata. Data are shown as mean SEM of 3-4 animals. Each dot represents an animal. Statistical testing was done with Two-way ANOVA followed by Bonferroni post-hoc test, *= $p < 0.05$; **= $p < 0.01$; ****= $p < 0.0001$ *Pop4 β KO* vs *Pop4^{fl/fl}*.

4.2.4 Immunostaining of γ H2A.X DNA damage repair marker

POP4 is described to play a role in DNA damage repair of double stranded DNA breaks through homologous recombination. Therefore, to access if the ablation of *Pop4* in the beta cells accelerated the DNA damage appearance, the detection of the phosphorylated Histon 2A.X (γ H2A.X) which marks DNA damage repair was immunohistochemically conducted.

The immunostaining was processed for 9 weeks of age, at the timepoint before hyperglycemia onset to evaluate if this could be one of the causes for loss of insulin content and beta cell mass. Figure 26 shows representative images of Insulin to visualize the beta cell area, DAPI to visualize the nuclei and the γ H2A.X DNA damage marker that is expressed in the nuclei. The quantification and image shows that γ H2A.X

could be detected in *Pop4* β KO beta cells when compared to *Pop4*^{fl/fl}. About 5% the islets of the *Pop4* β KO expressed colocalized γ H2A.X positive nuclei (Figure 27). Additionally, db/db pancreatic sections were used as a positive control to evaluate the staining since DNA damage is known to be present in db/db beta cells at 16 weeks of age.

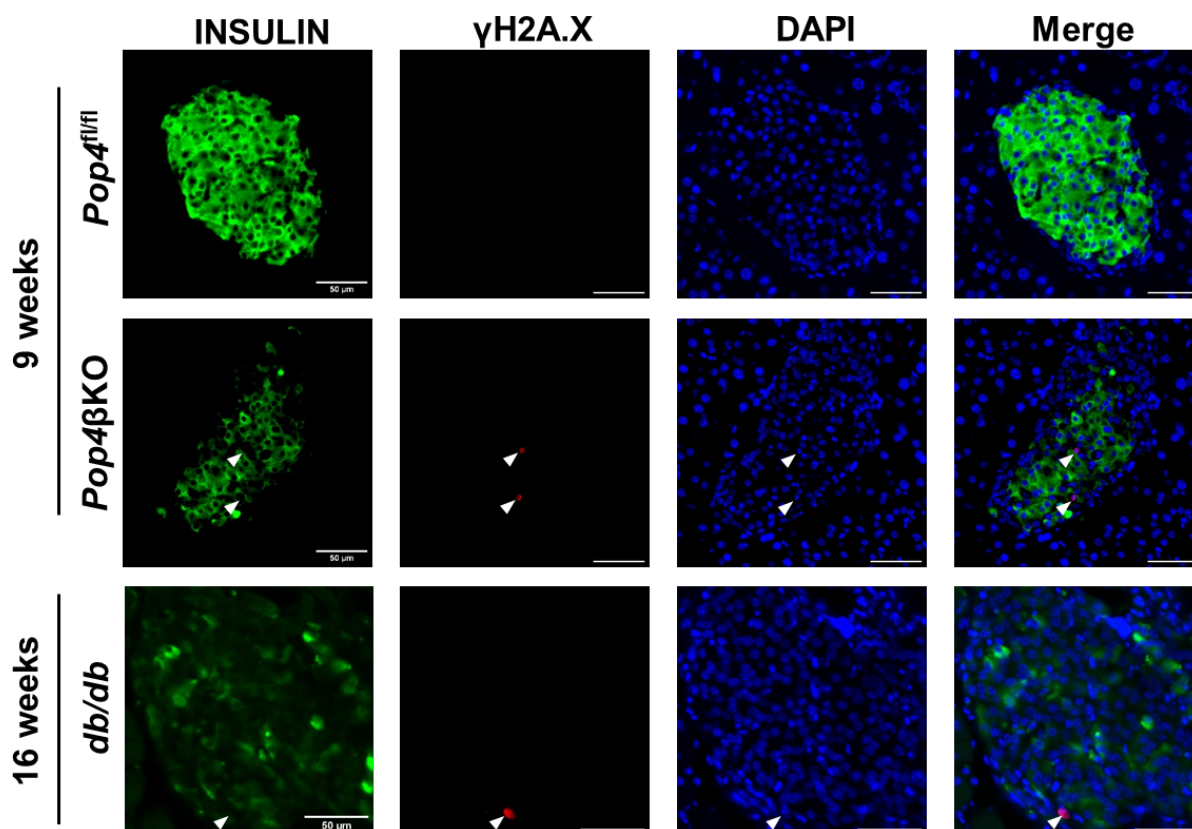


Figure 26. Representative immunostaining images to investigate DNA damage marker γ H2A.X in beta cell area. Immunofluorescence staining in pancreatic sections targeting Insulin (green), γ H2A.X (red) and DAPI (blue). First row shows the indicated staining for *Pop4*^{fl/fl} and second row for *Pop4* β KO both at 9 weeks of age. To verify the staining detection, db/db pancreatic section of 16 weeks old animals was immunostained acting as a positive control. White arrow indicate the location of γ H2A.X stained nuclei. Scale bar represent 50 μ m.

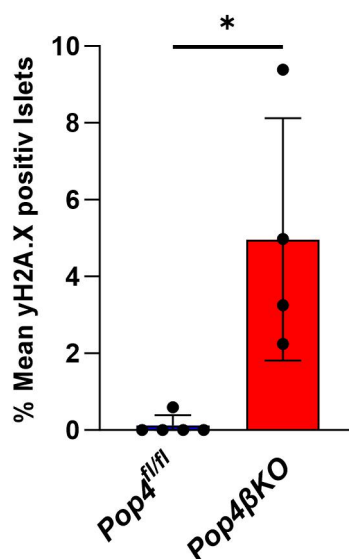


Figure 27. Quantification of γ H2A.X positive stained nuclei. Immunostained pancreatic sections for Insulin and γ H2A.X at 9 weeks of age from *Pop4 β KO* and *Pop4^{fl/fl}* Control. Statistical testing was done with Student's T-test, *= $p < 0.05$.

4.2.5 Electron microscopy of beta cells from isolated islets

Considering the changes in proinsulin levels within the islets noticed from the glucose stimulated insulin secretion of isolated islets of *Pop4 β KO* mice, the insulin vesicles maturation dynamics were of interest. Therefore, to observe a snapshot of insulin vesicles dynamics and beta cellular ultrastructure, pancreatic islets were processed for transmission electron microscopy (TEM). To exclude artefacts from the islet isolation procedure beta cell images were selected for intactness of the cell structure.

Figure 28 shows representative images of beta cell ultrastructure obtained by TEM. Thereby, an individual cell can be distinguished by cell gaps around the outer cell membrane. Noticeably, the beta cells in particular present a multitude of granules which ascribed as insulin granules. Different status of insulin maturation can be observed by granules with a lighter gray core defined as immature while mature granules show a crystalline core with a surrounding halo. Moreover, the nucleus appears as a large circular-like structure within the cytoplasm and mitochondrial structures emerge as dark grey tubular structures dispersed within the cell cytoplasm (Figure 28).

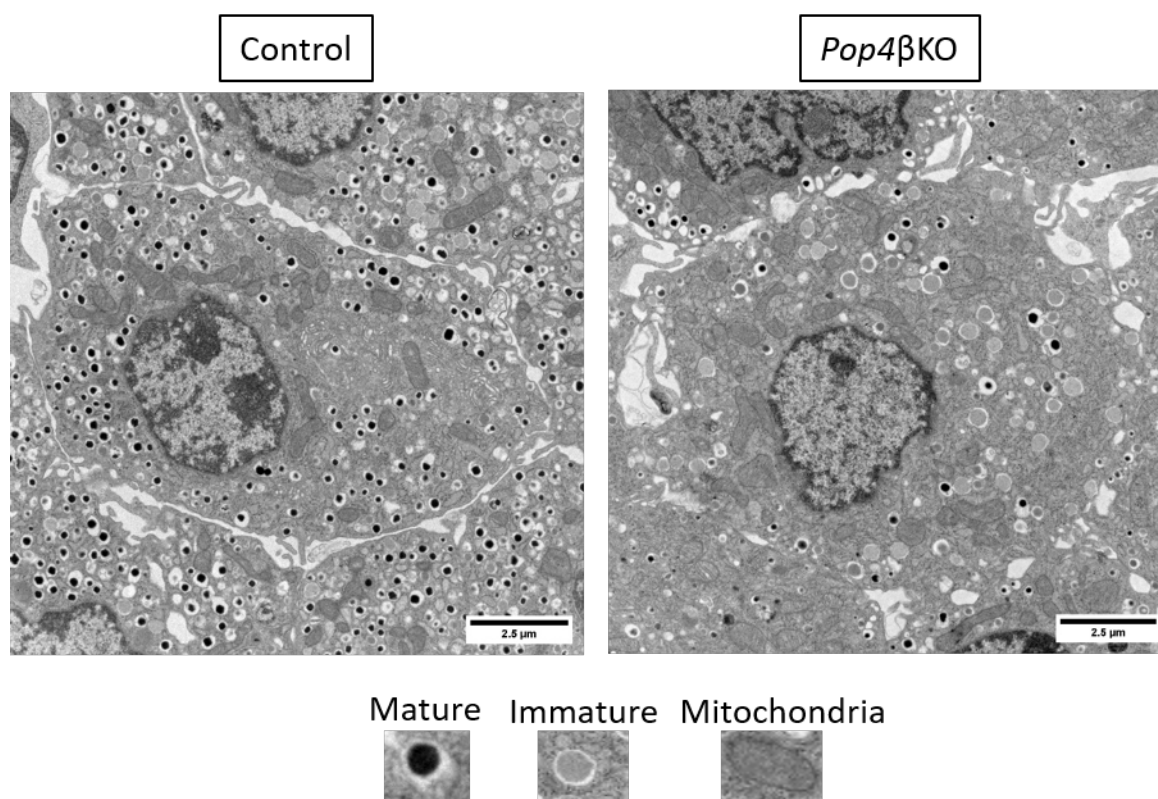


Figure 28. Beta Cell ultrastructure obtained by transmission electron microscopy of isolated islets at 8 weeks of age. Representative image of Control and (B) *Pop4βKO* beta cell and examples of mature/immature insulin granule as well as a mitochondrial area are shown. Scale bar represents 2,5 μm.

To first observe the beta cell and its cell structures, quantitative data were assessed by measuring the beta cell, the nucleus and mitochondrial area as a sum of the individual visible mitochondria areas. Between control islets and *Pop4βKO* the beta cell, nucleus and mitochondrial area (**Figure 29**) does not show significant differences. The beta cell areas range from $\sim 90 \mu\text{m}^2$ to $\sim 140 \mu\text{m}^2$ from which $\sim 20\text{-}30\%$ account for the nucleus and $\sim 4\text{-}9\%$ for the mitochondrial area. Morphologically, no discern changes was observed with the structures in the beta cell ultrastructural snapshot (**Figure 29**).

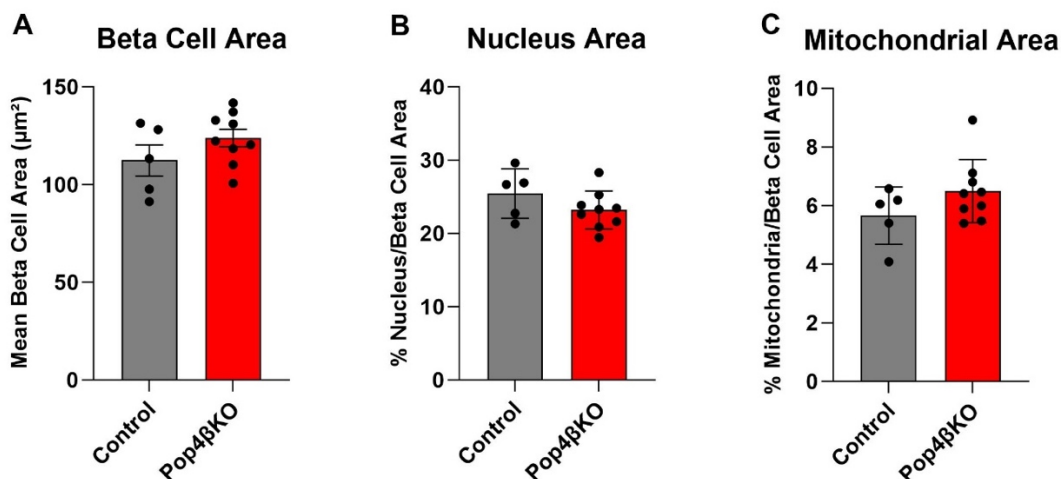


Figure 29: Morphometric of nucleus and mitochondrial Area. (A) Nucleus Area was measured by encircling the structures in electron microscopy images of the beta cell. (B) Mitochondrial area was defined by encircling visible mitochondria and sum up the area. Control islets were *Ins1^{Cre}/+* and *Pop4^{fl/fl}* genotype and shown in grey. *Pop4βKO* is shown in red. Data are shown as mean \pm SEM from 5-9 Islets of 3 animals indicated as dots. 10-19 beta cells were analyzed per islet. Statistics were done by Student's T-test.

In terms of the insulin granules, the mean number of counted insulin granules displayed a tendency for lower number insulin granules in the *Pop4βKO*. From the total insulin vesicles the control islets presented ~95% as mature insulin vesicles while only ~5% as immature granules whereas the *Pop4βKO* present a significant higher percentage of immature insulin granules of ~18% and mature granules of ~82% in comparison (Figure 30).

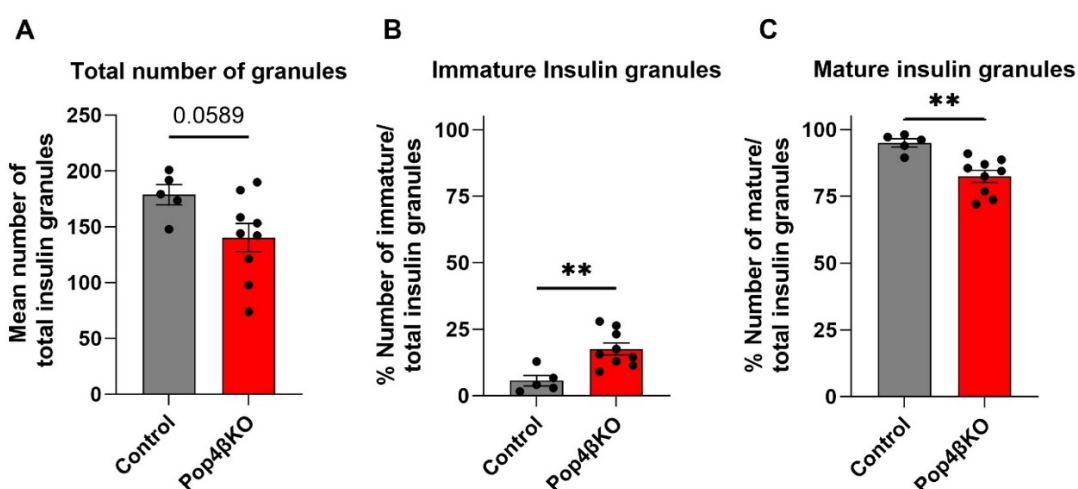


Figure 30: Morphometrics of beta cells and insulin vesicles. Islets of Control mice and *Pop4βKO* mice were isolated at 8 weeks of age and analyzed under electron microscopy to obtain images of beta cells. (A) Beta cell area was measured by manual encircling and insulin vesicles were counted distinguishing immature from mature insulin vesicles. Control were pooled from *Ins1^{Cre}/+* and *Pop4^{fl/fl}* genotype and shown in grey. *Pop4βKO* is shown in red. Data are shown as mean \pm SEM from 5-9 islets from 69-109 beta cells of 3 animals. Statistical analyses with Student's t-test, **= $p < 0.01$ Control vs *Pop4βKO*.

Further investigation of the insulin vesicle dynamics of isolated islets was done by stimulating the beta cells with a high glucose amount (25mM Glucose for 5 min) in comparison to unstimulated state. Interestingly, the beta cell area depict a tendency of an increase in size especially in the glucose stimulated state (Figure 31A). In terms of immature insulin vesicles, the glucose stimulus exacerbate the immature insulin granules abundance (Figure 31B).

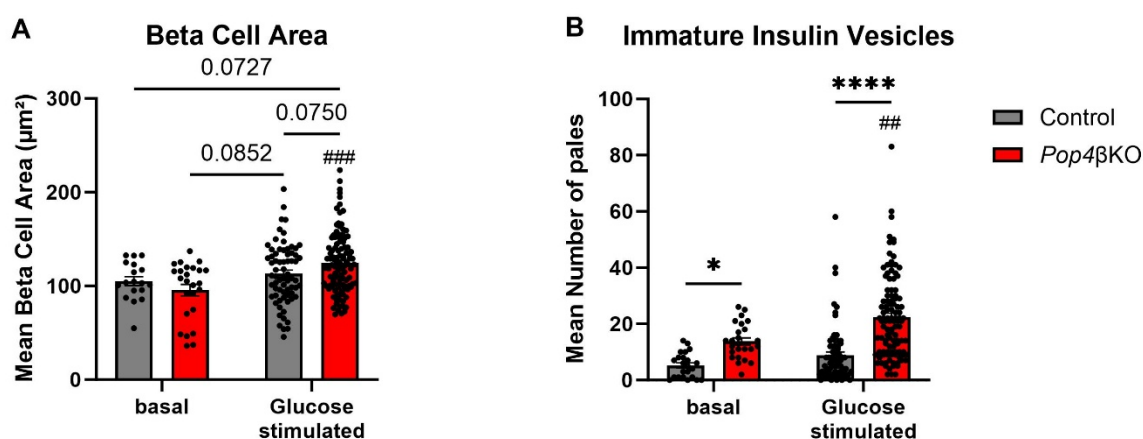


Figure 31: Comparison of beta cells under basal and glucose stimulated condition. (A) Depict mean number of immature Insulin vesicles and the beta cell Area of Control vs *Pop4βKO* beta cells. Control were pooled *Ins1^{Cre/+}* and *Pop4^{fl/fl}* genotype and shown in grey. *Pop4βKO* is shown in red. Data are shown as mean \pm SEM from 25-109 beta cells per genotype of 3 animals. Statistical testing was done with Two-way ANOVA followed by Bonferroni post-hoc test, $*=p<0.05$, $****=p<0.001$ control vs *Pop4βKO* or $###=p<0.001$; $##=p<0.01$ basal vs glucose stimulated.

4.3 Transcriptome analysis of isolated islets

To assess the primary defects before the impairment of beta cell function on mRNA levels, a transcriptome analysis from pancreatic islets of 8 weeks old animals was conducted. The whole pancreatic islet organ was selected to obtain sufficient material and to address the islet composition changes as indicated by the immunofluorescence stainings. Single-end poly-A enriched RNA-sequencing and Kallisto pseudo alignment was processed.

4.3.1 Determination of Inter- and Intragroup variability

In order to visualize the sample variability within the experimental groups of *Pop4βKO* to the *Pop4^{fl/fl}* control, a principal component analysis (PCA) and a Spearman correlation was performed. Thereby, the PCA compresses the large gene dataset into a minimal set of dimensions or principle components which gives information about the variation of the dataset. Figure 32A shows the PCA plot visualizing the principal components PC1 and PC2. PC1 represents 31.58% of the variability and PC2 represents 12.76%. Thus, in total this graph represents 44.34% of the variability in the

dataset. The samples from the *Pop4^{fl/fl}* control exhibit a greater degree of similarity indicated by their proximity to one another compared to *Pop4 β KO* samples. The variation of the *Pop4 β KO* samples indicate a higher biological variability within the group (Figure 32A).

According to ENCODE guidelines for bulk-RNAseq correlation coefficient (r) of >0.9 is recommended for the sample in datasets. Therefore, Figure 32B shows the Spearman correlation of the normalized transcript data and the color gradient indicates the Spearman correlation score. The sample in the datasets show high correlation of >0.9 with each other, therefore validating the conformity of the dataset (Figure 32B).

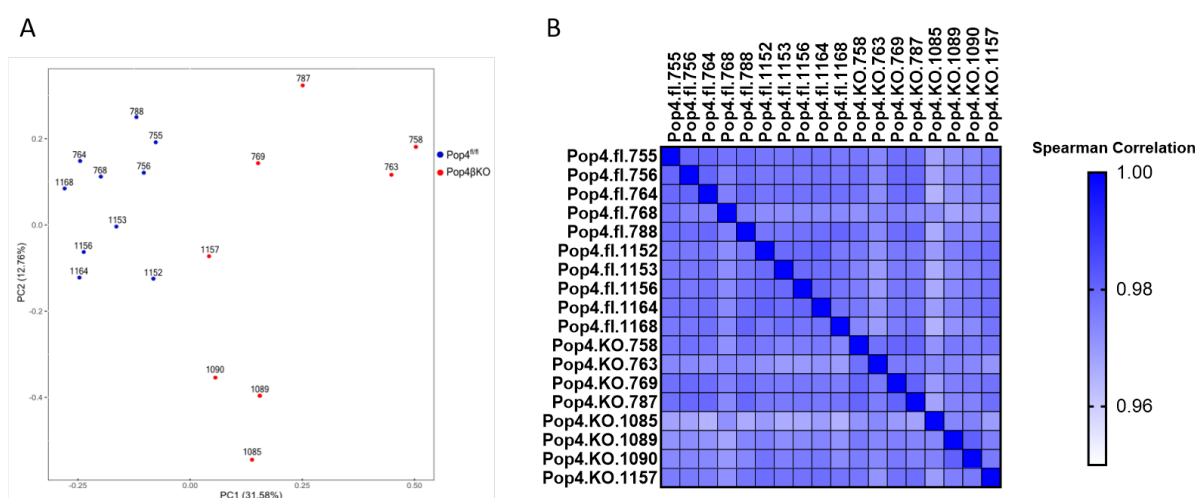


Figure 32. Assessment inter- and intra-variability of samples. (A) Principal component analysis plot displays the two primary principle components PC1 and PC2. PCA was applied to normalized counts (Transcript per million). Each dot represents a sample with the animal ID indicated above. (B) Spearman correlation visualizes the correlation (r) between samples. Genotype and animal ID are indicated in labels. $Pop4.fl = Pop4^{fl/fl}$, $Pop4.KO = Pop4\beta KO$.

4.3.2 Analysis of differential expressed RNA transcripts

Next, the differentially expressed genes were assessed. In total, transcripts of 21430 genes were identified in the samples from which 3904 (18,22%) are significantly differentially expressed genes ($p < 0.05$) (Figure 33A). From those genes, 1988 (51%) show downregulation and 1916 (49%) upregulation (Figure 33B). Figure 33C shows the Top 10 up- and downregulated genes.

Processing of precursor 1 (*Pop1*) as a partner subunit of *Pop4* in the RNase P/MRP emerged as the upregulated gene with the lowest adjusted p-value followed by Cyclin dependent kinase inhibitor 1A (*Cdkn1a*) alias p21, Amphiregulin (*Areg*), *Thumpd1*, *Map10*, *Stbd1*, *Sun2*, *Zfand2a*, *Hdgfl3* and *Lrrc8b*. Top downregulated by p-value genes are Insulin 1 (*Ins1*), *Emid1*, *Adh1*, *Gne*, *Kcnab3*, *Mlph*, *Cyb5b*, *Bhlha15*, ATPase H+/K+ transporting subunit alpha (*Atp4a*) and *Nell1*.

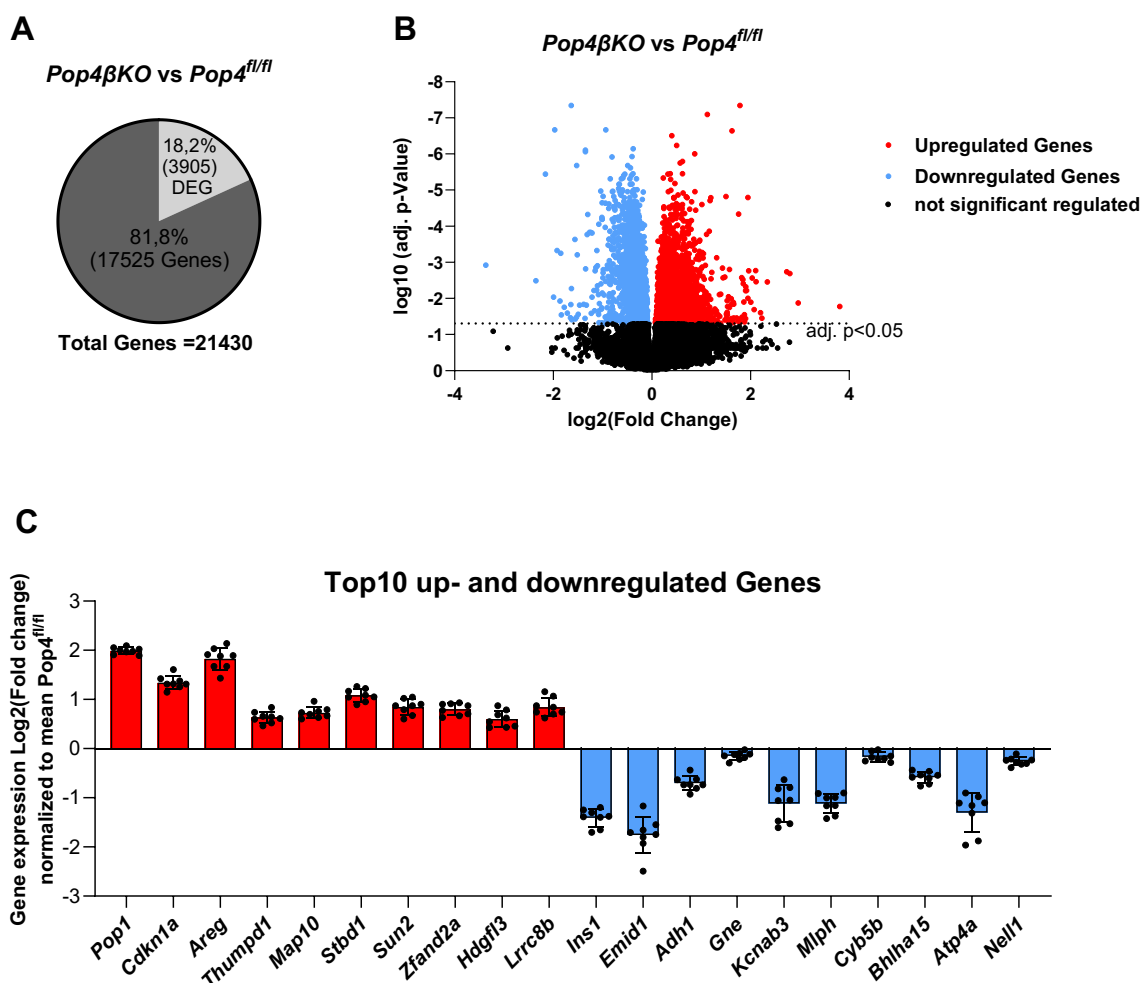


Figure 33. Differential gene expression analysis. (A) Pie chart shows the percentage of differential regulated genes compared to identified genes. (B) Volcano plot showing all genes categorized into significant up- (green) or downregulated (red) and non-differentially (black) regulated genes indicated by the log₂ fold change. (C) Top 10 up- or downregulated genes are depicted normalized to the mean of *Pop4^{fl/fl}* control. Data are presented as mean \pm SEM from islets of 8-10 animals.

4.3.3 Gene ontology enrichment analysis

To further investigate the biological context of the differentially regulated genes, a gene ontology enrichment analysis was conducted. The Gene Ontology Resource is a consortium that offer a comprehensive, computational model of biological systems for multiple species with information on functions of genes. Since different tools exist for the GO Enrichment analysis, the selection of the Panther tool was based on the tool using the most updated release of the GO terms.

The enrichment analysis unveils information about how many of the input genes are involved in a biological process, exceed a molecular function or are abundant in a cellular component quantitated as „enriched“. The results of the Biological Processes showed that the significant regulated genes are enriched in 903 biological processes. Figure 34 highlights the most relevant ones indicated by the fold-enrichment. Among

those biological processes, insulin processing and insulin secretion (or peptide hormone processing) as well as ER-nucleus, ER to Golgi signaling, ER unfolded protein response, regulation of response to endoplasmic reticulum stress and response to oxidative stress and calcium-ion regulated exocytosis stood out. The second group of processes concern processes of cellular dysfunction including intrinsic apoptotic signaling pathway by p53, response to DNA damage, regulation of DNA damage response and G1/S transition of mitotic cell cycle. Other processes involved rRNA processing such as maturation of 5.8 rRNA or ribosomal large subunit biogenesis. For molecular function insulin receptor binding, SMAD binding, SNARE binding, protein kinase binding and small GTPase binding appear among the 84 GO terms. In cellular component, 155 terms were revealed, highlighting COPI vesicle coat, preribosome large subunit precursor, Golgi-associated and endoplasmic reticulum related terms (Figure 34).

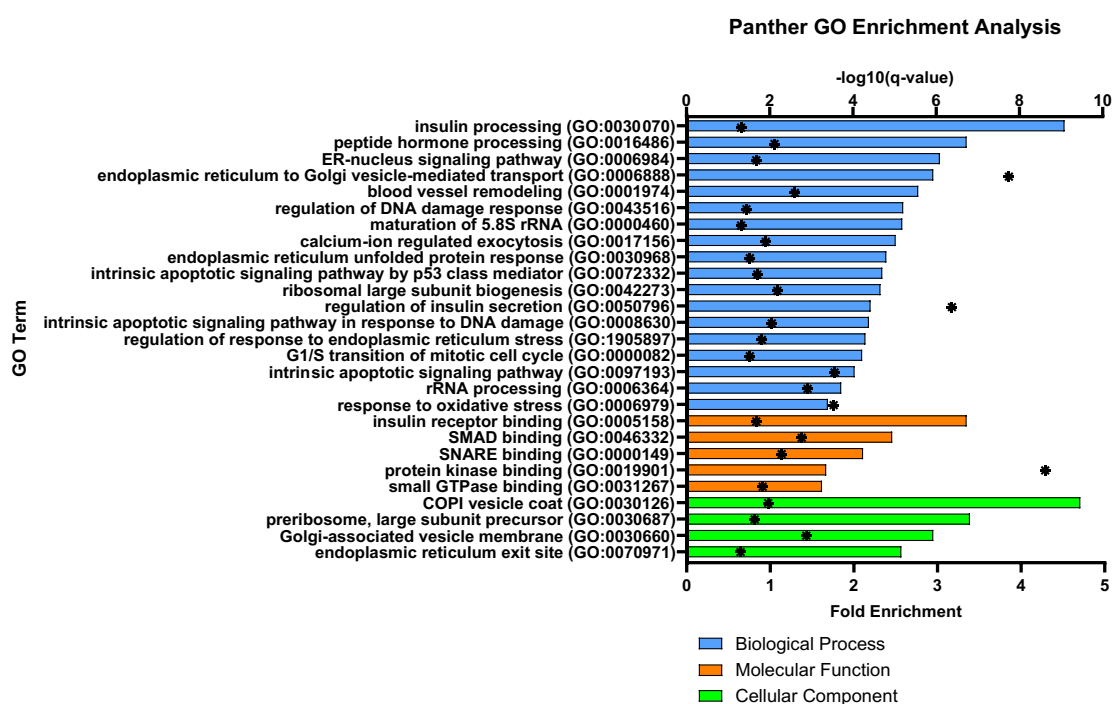


Figure 34. Gene ontology analysis of differentially regulated genes using Panther tool. Differentially regulated genes were used as input for the GO overrepresentation analysis. The results of the enrichment of GO Terms for Biological processes are visualized in blue, molecular function in orange and cellular component in green. The respective fold enrichment value is visualized as bars by the lower x-axis and the significance is presented as $-\text{Log}_{10}(\text{q-value})$ and (*) asterisk indicated by the upper x-Axis.

4.3.4 Pathway overrepresentation analysis with Consensus Pathway Database

Additionally, a cross database analysis was conducted with dataset of significantly regulated genes in order to obtain information about pathways they are entailed with. Therefore, the Consensus Pathway Database (CPDB) offers an overrepresentation analysis for gene sets using mouse Kyoto encyclopedia of genes and genomes (KEGG) and Reactome pathway databases. The input genes resulted in similar pathways comparable to GO Biological Processes Terms such as Membrane Trafficking, ER to Golgi Transport, Vesicle mediated Transport and protein processing in endoplasmic reticulum. The downregulated genes are over-represented in pathways of insulin secretion and insulin processing and involve metabolic processes such as metabolism of lipids, carbohydrates and amino acid and derivatives. Additionally, glycolysis, TCA cycle and oxidative phosphorylation associated-genes show significant downregulation (**Figure 35A**).

The upregulated genes are involved in extracellular matrix organization, apoptosis, ferroptosis and immune system pathways. More specific pathways are p53 signaling pathway, Extra-nuclear estrogen signaling, sphingolipid signaling, Metabolism of non-coding RNA and cellular senescence (**Figure 35B**).

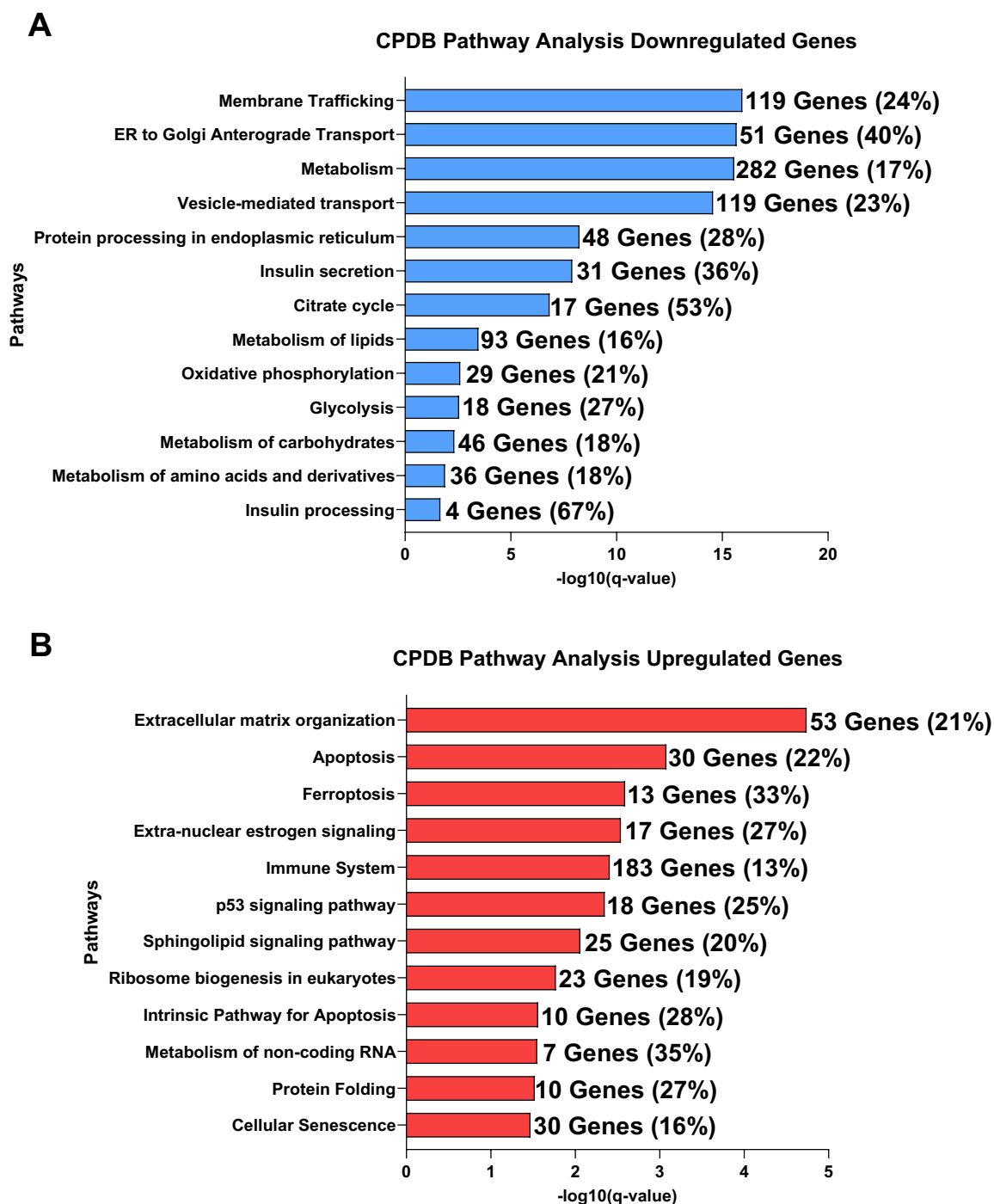


Figure 35. Consensus Pathway DB over-representation analysis of differentially down- and upregulated genes.(A) Analysis of significant overrepresented pathways for downregulated genes and (B) upregulated genes shown as $-\log_{10}(q\text{-value})$ and thereafter the number of differentially expressed genes and the constitutive percentage of genes for the pathway.

4.3.5 Gene expression of islet hormones and alpha/beta cell marker

Since whole pancreatic islets were processed for the bulk RNAseq, validating pancreatic islet composition was estimated by the expression of pancreatic islet

hormones. Thereby, Insulin 1 (*Ins1*) and Insulin 2 (*Ins2*) are the highest expressed hormone genes followed by Glucagon (*Gcg*), Somastostatin (*Sst*), Pancreatic polypeptide (*Ppy*) and Ghrelin (*Ghrl*) reflecting the cell composition of the islet of Langerhans. Noticeably, *Pop4* β KO show significantly lower expression of *Ins1* and *Ins2* but higher expression of *Gcg* (Figure 36A).

To follow up this result beta and alpha cell markers are displayed as a heatmap in Figure 33B. Beside *Ins1* and *Ins2*, Islet amyloid polypeptide (*Iapp*), *Hopx*, *Pdx1*, *MafA*, *Pcsk1*, *Gjd2*, *Ucn3*, *Slc2a2* and *G6pc2* are beta cell markers that are significantly downregulated. Alpha cell markers such as *Arx*, *MafB*, *Irx*, *Fev*, *Gls* and *Ptger3* show significant upregulation. Some beta and alpha cell markers depict a heterogenous regulation such as *Pfkfb2*, *Abcc8*, *Nkx2-2*, *Pax6*, *Sh3gl2*, *Pcsk2*, *Foxa2* for beta cells and *Isl1*, *Dpp4*, *Chga* for alpha cells (Figure 36B).

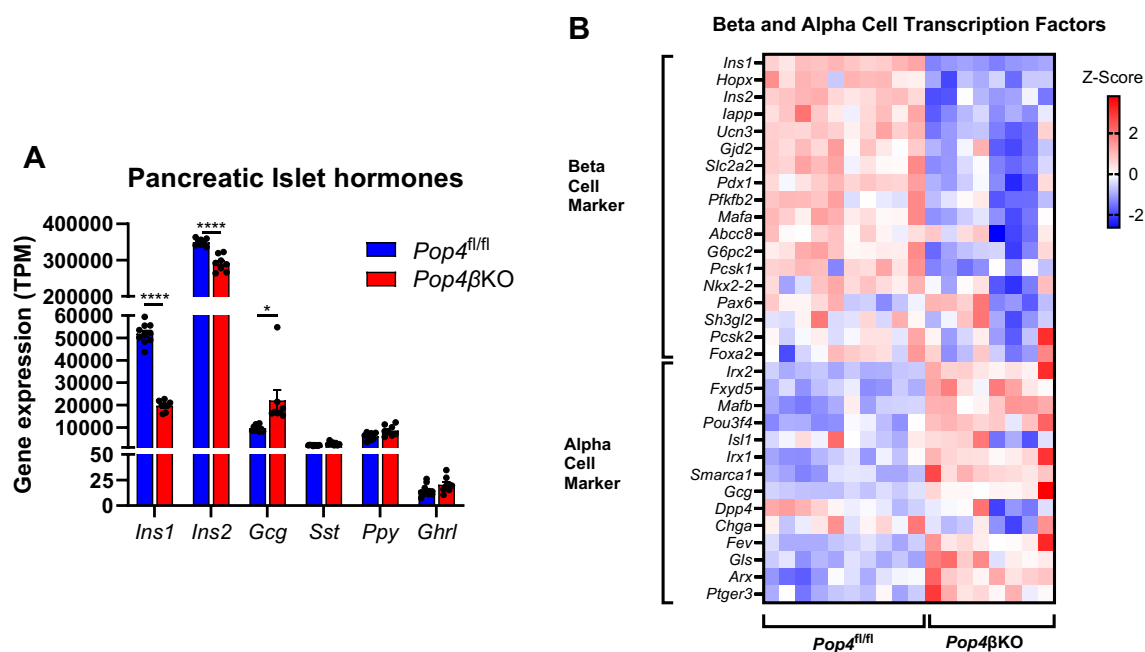


Figure 36. Gene expression of pancreatic islet hormones and cell markers. (A) Differentially expressed pancreatic islet hormone genes between Islets of *Pop4* β KO and *Pop4^{fl/fl}* control. Data are shown as mean \pm SEM and each dot represents an individual animal and statistical test was corrected for multiple testing, adjusted p-value $*=p<0.05$; $****=p<0.0001$. (B) Heatmap of significantly regulated pancreatic beta- and alpha cell marker of individual animals of *Pop4* β KO and *Pop4^{fl/fl}* control. Each column represents the gene expression pattern of one animal indicated as Z-score color scale. Red hues represents Z-score <0 thereby downregulation while blue hues represents $Z>0$ showing upregulation against control and no regulation presented in white.

In the pathway of insulin secretion annotated by KEGG (Figure 37) genes which play a role in the process of glucose stimulated exocytosis of insulin granules are mainly

showed significant upregulation in *Pop4* β KO compared to control. Interestingly, *Pop4* is expressed in the *Pop4* β KO. Moreover, the distinct RNA component of RNase P (*Rpph1*) and RNase MRP (*Rmrp*) showed no difference in gene expression (**Figure 38A**).

In terms of RNase P canonical function in cleaving the 5' end of the pre-tRNA, tRNA function rely on tRNA synthetases which charges the tRNA with their cognate amino acid. Therefore, several tRNA synthetases could show a differentially regulation in *Pop4* β KO compared to *Pop4*^{fl/fl} including isoleucine synthetase (*Iars*), tryptophanyl tRNA synthetase (*Wars*), seryl-aminoacyl tRNA synthetase 2 (*Sars2*) and mitochondrial alanyl-tRNA synthetase 2 (*Aars2*), mitochondrial cysteinyl-tRNA synthetase 2 (*Cars2*), mitochondrial tryptophanyl tRNA synthetase 2 (*Wars2*) which present significant upregulation (**Figure 38B**).

Additionally, tRNA posttranscriptional modification are known to impact proper function of tRNA and has been linked to beta cell function (Arroyo et al. 2021). Especially *Trmt2b*, *Trmt10a*, *Trmt61a* and *Trmt6* were upregulated significantly in the *Pop4* β KO islets at 8 weeks of age (**Figure 38C**).

RNase MRP implication in rRNA processing and the GO terms ribosome large subunit biogenesis and 5.8S rRNA maturation pointed to altered process of ribosome biogenesis. Genes mediating ribosome biogenesis of production and assembly of all four ribosomal RNA (rRNA) and a majority of protein coding genes present significant upregulation. Figure 35 presents the significant regulated genes which obtain a role in proper ribosome biogenesis such as genes involved in rRNA modifications such as *Nob1*, *Nob56*, *Gar1*, *Nhp2* and pre-rRNA processing like *Ffar1*, *Utp14a/b*, *Bmx1*, *Rcl1* and also *Pop5* and *Rpp30* of the RNase MRP complex. Other factors aid in the maturation of the 40S and 60S subunit such as *Gtpbp4*, *Nob1*, *Nmd3*, *Riok2* and *Eif6* show significant upregulation (**Figure 38D**).

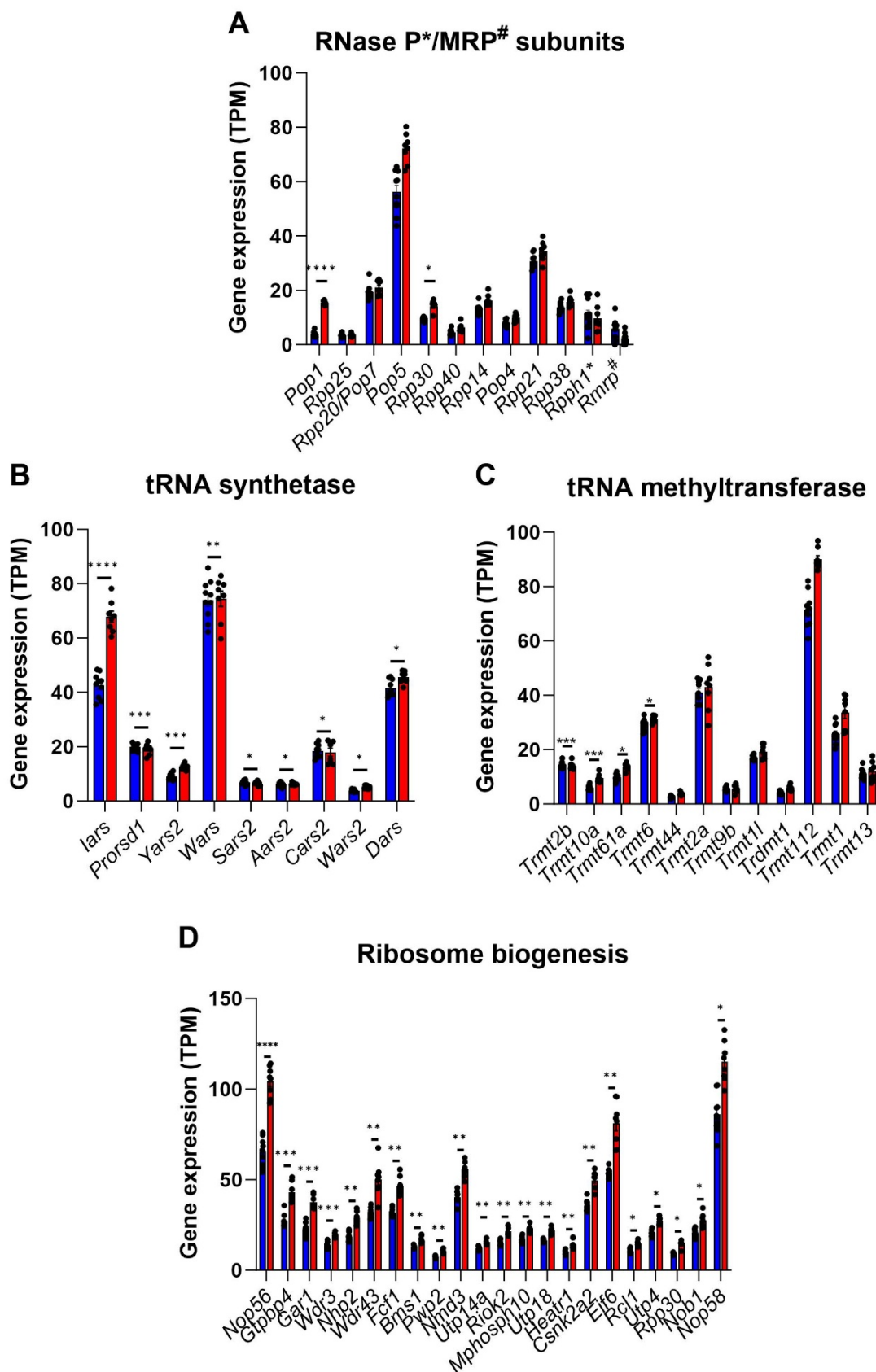


Figure 38. Genes involved in canonical function of POP4. (A) RNase P and MRP subunits genes are shown representing canonical implications described for POP4. The specific RNA component is indicated as * for RNase P and # for RNase MRP. (B) Genes of the categories of tRNA synthetase and

(C) tRNA methyltransferase are shown. (D) Genes involved in ribosome biogenesis obtained from the KEGG pathway mapper are depicted. Genes are normalized as transcript per million. Statistical testing was corrected for multiple testing. Adjusted p-value, *= $p < 0.05$; **= $p < 0.01$; ***= $p < 0.001$; ****= $p < 0.0001$.

Further non-canonical function of POP4 in DNA damage repair through homologous recombination were assessed by selecting genes involved within double stranded DNA repair processes. Both *Parp1* and *Atm* were significantly downregulated. PARP1 (*Parp1*) recruits DNA damage checkpoint protein ATM (*Atm*) and activates the signaling cascade of DDR response. The MRN complex in turn regulates ATM activation which is composed of *Mre11*, *Rad50* and *Nbs1* (*Nbn*). *Atm* gene encode for the initiator kinase which activates the DDR response by phosphorylation of their targets such as CHEK1 (*Chk1*), CHEK2 (*Chk2*), P53 (*Trp53*), BRCA1/2 (*Brca1/2*) and H2A.X (*H2a.x*) in which *Trp53* showed significant upregulation in *Pop4* β KO islet cells (Figure 39).

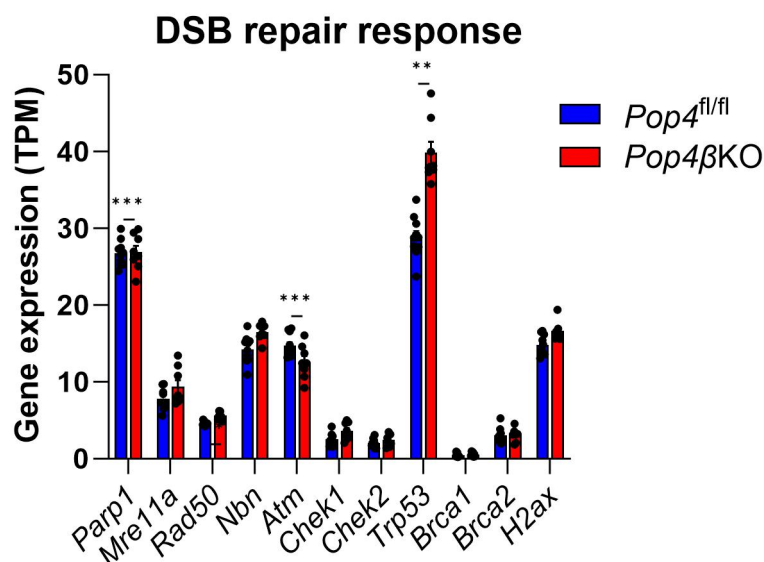


Figure 39. Genes of double stranded (DSB) DNA repair response. Genes are normalized as transcript per million. Statistical testing is corrected for multiple testing. Adjusted p-value, **= $p < 0.01$; ***= $p < 0.001$.

4.3.7 Molecular pathways of apoptosis and senescence

Further examining the intricate pathways of apoptosis and cellular senescence which can mediate loss of beta cells both are substantially regulated by the beta cell specific KO of *Pop4*. In the apoptosis pathway, genes of the extrinsic apoptotic pathway including FAS (*Fas*), TRAIL and TNF receptor and ligand are upregulated though downstream factors such as FADD, TRADD, DAXX showed no or down regulation. However, apoptosis triggering intrinsic pathway through the mitochondria appear to show greater regulation. *Atf4* (ATF4) and downstream factor *Ddit3* (CHOP) shows upregulation targeting *Bcl2* (BCL2). Though pro survival *Bcl2* show upregulation together with *Bax* (BAX), *Bak1* (BAK) and *Bid* (BID). Interestingly *Cytc* (Cytochrome C) and *Apaf1* (APAF1) show upregulation although downstream effector Caspase 9 (*Casp9*) is not regulated. Gene encoding for *Diabolo* (DIABOLO) known as Smac also show significant upregulation which depict inhibition of XIAP an endogenous inhibitor of caspase 9. XIAP in turn decreases inhibition of the effector caspases 3 which show markedly upregulation. Upregulation of *Trp53* regulates the transcription of several as fore mentioned pro apoptotic genes in addition to *Bbc3* (PUMA) and *Pmaip1* (NOXA) (Figure 40).

5 Discussion

This study investigated the beta cell autonomous role of *Pop4* on beta cell function and beta cell mass for the first time in an *in-vivo* mouse model. Previous data indicated that the gene expression of *Pop4* highly correlated to insulin gene expression postulating a role of *Pop4* in insulin production. Thus, a metabolic characterization of the beta-cell specific mouse model focused on blood glucose development and insulin secretion function. The deletion of exons 4 and 5 of the *Pop4* gene using Cre recombinase under the beta cell specific *Ins1* promoter showed that absence of wildtype *Pop4* leads to spontaneous adult-onset diabetes in mice of C57BL/6N and C57BL/6J mixed background. To further challenge the metabolism of these mice, a diet-induced insulin resistance was investigated which did not exacerbate aforementioned effects in female mice. Before hyperglycemia occurs, the mice exhibit reduced glucose tolerance due to reduced insulin secretion capacity measured both *in vivo* as well as *ex vivo* from isolated pancreatic islets. At this stage the pancreatic islets are morphometrically inconspicuous though reduced endogenous insulin levels indicate impairment in beta cell function accompanied by defect in insulin maturation and appearance of DNA repair marker γ H2A.X. Importantly, at the time of overt hyperglycemia, a significant loss of plasma insulin has been determined due to a substantial loss of beta cell mass. An observation of the transcriptome was conducted of pancreatic islets to disclose the mechanism of a missing *Pop4* function for the pancreatic beta cell. Results indicate gene expression changes in beta and alpha cell marker and genes coding for important proteins in insulin synthesis and secretion. Further bioinformatical tools, highlights downregulated genes affecting general metabolism, vesicle/membrane trafficking while simultaneously genes in apoptosis and senescence pathway particularly p53/p21 signalling upregulated. Moreover, functional aspects of POP4 especially in tRNA and rRNA processing involved genes and double stranded DNA response were observed. In the following, these aspects will be discussed in further detail.

5.1 Beta cell specific knockout of *Pop4* leads to a diabetes phenotype

5.1.1 Validation of the Cre recombinase activity

Before characterizing the mouse model, the initial study focused on the validation of the system to induce the ablation of exons 4 and 5 in the *Pop4* gene sequence. As aforementioned the Cre/LoxP system is an established system which is based on recombination of specific sites used for genetically engineered mouse study of human diseases (Kim et al. 2018). Tissue-specific promoters enable spatial control of the recombination and combined with reporter strains allow genetic lineage tracing (Taylor et al. 2019). First, the functional activity of the Cre recombinase was observed with the help of the reporter tdTomato. The tdTomato protein emits a bright red fluorescence and the gene was inserted as a transgene together with a loxP flanked Stop codon in the ROSA26 locus of the mouse strain (Madisen et al. 2010). Fluorescence imaging of isolated pancreatic islets of mice carrying an *Ins1^{Cre}* revealed a red fluorescence core within the pancreatic islets. From literature, it is known that the architecture of mouse pancreatic islets displays beta cells located to the core of the pancreatic islets (Adams and Blum 2022). The red fluorescence visible solely in the core of the pancreatic islets validates that the Cre recombinase expressed under a beta cell specific promoter of *Ins1* gene successfully ablated transgene stop codon and lead to expression of the fluorescence reporter tdTomato in the pancreatic beta cells. Moreover, the islet transcriptome of Cre carrying mice highlights a reduction of over 50% of the *Ins1* expression. This result is partially contributed by the design of the *Ins1^{Cre}* line (Thorens et al. 2015). As the insertion of Cre recombinase was constructed to replace exon 2 of the *Ins1* gene, one functional copy of the *Ins1* remains and therefore the gene dosage decreases by half (Skovso et al. 2022). Importantly to note is that the gene dosage of *Ins1* through mutants or knockout models has been shown to have no influence on insulin content when *Ins2* gene is present which was observed in the NOD or 129/SV background strain (Leroux et al. 2001; Babaya et al. 2006). One copy of the insulin gene has been shown to suffice for the production of insulin as it can be upregulated by metabolic feedback control to maintain homeostasis (Chentoufi and Polychronakos 2002). Actually, on the contrary, a lower gene dosage of *Ins1* was shown to be beneficial as this protects NOD mice from T1D progression (Skovso et al. 2022) alluding proinsulin 1 as a key player for autoimmunity (Moriyama et al. 2003). Interestingly, this study suggests a protective effect of Cre recombinase itself on the

diabetes rate of female NOD mice (Skovso et al. 2022). This highlights the possible beta cell autonomous role of the Cre itself similar to off-target effect seen in other cell types such as fibroblasts (Loonstra et al. 2001) or cardiomyocytes (Pugach et al. 2015; Rashbrook, Brash, and Ruhrberg 2022). Postulation on this considers mammalian genome to harbor many pseudo loxP sites which could act as recognition sites for the Cre recombinase (Thyagarajan et al. 2000; Pugach et al. 2015). Additionally, by using hemizygous mice with one copy of Cre, as this has been shown to suffice for intended recombination, the toxicity effect is further minimized (Baba et al. 2005; Rashbrook, Brash, and Ruhrberg 2022). As for this study the *Ins1^{Cre}* control did not elicit noticeable effect on relevant metabolic traits however off-target effects may not be fully excluded.

5.1.2 The *Pop4* β KO model displays a deletion of exons 4 and 5

The deletion of exons 4 and 5 in the *Pop4* gene sequence by the Cre recombinase action was further validated at DNA and mRNA level in isolated beta cells, successfully demonstrating ablation by a shorter sequence structure. Quantitative analysis of the expression of *Pop4* gene sequence from exon 4 to exon 5 in other metabolically important tissues further confirmed the ablation in pancreatic islets. However, this result also emphasizes that the expression of *Pop4* is not islet-specific but rather ubiquitous, highlighting a higher expression in quadriceps muscle and kidney tissue. The ablation of both exons proposes a frameshift mutation, but the gene expression level of *Pop4* remained unchanged as shown by the islet transcriptome. Therefore, the deletion of exons 4 and 5 might not affect the mRNA decay. Since the specificity of several commercially available antibodies against the POP4 protein could not be validated (results not shown), a protein prediction tool was used to gain an understanding of the effect of deletion of exons 4 and 5 on the protein structure. This revealed that the frameshift appears to lead to changes of the amino acid composition. The murine protein sequence of POP4 with exons 4 and 5 deleted aligns with the wildtype POP4 from first amino acid until lysine at position 95 (Q95), followed by 24 amino acid changes and a premature stop codon. The resulting truncated protein sequence consists of 119 amino acids compared to wildtype POP4 protein sequence of 221 amino acid, of which 45,5% account of the wildtype amino acid composition. Prediction for protein structure using the Alphafold tool was used to speculate on the protein structure. The predicted tertiary mouse protein shows unstructured regions in the N-terminus followed by alpha helices structure while the C-terminus displays beta sheet and alpha helix structures which the latter structures are likely missing in the

putative truncated POP4 protein structure. Overall, the prediction for the putative protein structure of the deletion variant lead to a frameshift and a premature stop codon that significantly alters the protein structure by disruption of approximately 50% of the protein sequence, most likely rendering the resulting truncated protein dysfunctional or loose function.

5.1.3 *Pop4* β KO mice develop an early adult onset of diabetes sex-independent

The beta cell-specific knockout of exons 4 and 5 of the *Pop4* gene results in hyperglycemia onset being observed between 10-12 weeks or 2-3 months of age in male mice while in female mice onset occurred from 13-18 weeks or 3-4 months of age with 100% diabetes prevalence in all mice. The observed weight loss is likely secondary to the onset of overt diabetes. Sexual maturity, which occurs between 5 and 8 weeks of age in most mouse models is commonly used to define the adult stage of life (Jackson et al. 2017). However, the observation of mouse lifespan based on the C57BL/6 cohort considers 3-6 months as the mature adult stage, which is equivalent to 20-30 years in humans (K. Flurkey 2007). Some attempts to compare a mouse lifespan with a human lifespan note several differences, mainly the shorter lifespan of the mouse, the maturation rates (K. Flurkey 2007) and the differences in developmental stages (Dutta and Sengupta 2016), thus showing the difficulty of an exact relation. Moreover, human's beta cell development occurs in parallel to fetal development while in mice fetal beta cells remain immature and gain functional maturity only at a postnatal stage (Basile, Kulkarni, and Morgan 2019). Considering this, the *Pop4* β KO demonstrate a relatively early onset of diabetes during a mature adult age with biological variations among the animals that may explain the observed range of hyperglycemia onset. The timing of the onset of hyperglycemia in early adulthood also suggests that the defect is degenerative rather than developmental in nature, as postnatal pancreatic endocrinogenesis should be completed by this time.

The delayed onset of hyperglycemia in female mice suggests that females possess a higher tolerance or coping mechanism which mediates the delay in hyperglycemic onset. Indeed, glucose homeostasis and metabolic dysfunction have been observed to have a sex-specific component (Mauvais-Jarvis 2015). Several studies indicate that females have a higher glucose tolerance even under insulin resistant conditions in mice (Jo et al. 2023) and humans (Mauvais-Jarvis 2015; Li et al. 2022). The female hormone

estrogen, especially estradiol, has been shown to contribute to this protective effect (Riant et al. 2009; Vogel et al. 2013; De Paoli, Zakharia, and Werstuck 2021; Merino and Garcia-Arevalo 2021). In addition to affecting insulin sensitivity through actions in skeletal muscle, liver, and adipose tissue (Mauvais-Jarvis 2015), estrogen protects pancreatic beta cells from apoptosis by maintaining mitochondrial function, suppressing ER stress and increasing beta cell resilience to metabolic stressors such as insulin resistance (Zhou et al. 2018; Brownrigg et al. 2023; Jo et al. 2023). The diabetes penetrance highlights that the underlying cause of the diabetes phenotype in these mice forces a severe mechanism, as diabetes occurs with full penetrance, affecting all mice regardless of sex.

5.1.4 The diabetes in *Pop4 β* KO mice develops due to a gradual loss of beta cell mass and reduced insulin secretion

At the overt hyperglycemic state at the last measured timepoint of *Pop4 β* KO mice, the circulating plasma insulin level measured after a 6 hours fast showed that this mouse model display a significant loss of basal plasma insulin levels also termed insulinopenia compared to all age matched controls on both sexes. The histological assessment of the pancreatic islets concerning morphology, insulin content and beta cell identity marker Nkx6.1 at this overt diabetic stage in male mice revealed that there is a substantial loss of beta cell mass with majority of pancreatic islets displayed nearly a complete loss in beta cell mass reflected in the significant smaller pancreatic islet size and very low insulin content and beta cell identities. This severe beta cell demise especially at the overt hyperglycemic stage is marking this mouse model an insulin-deficient diabetes type. Therefore, elucidating similarities and differences to established insulin deficiency diabetes model may aid in the identification of the mechanism. The classic insulin-deficient type 1 diabetes mouse model, the non-obese diabetic (NOD) mouse, develops diabetes at 10-14 weeks of age foremost in female mice and delayed in male mice (Makino et al. 1980; Chen et al. 2020). This appears quite similar to the timepoint of hyperglycemia onset of the *Pop4 β* KO mouse model however the sex-specific differences of the NOD mouse model appear reversed. It is known that insulinitis is the driver in the diabetes pathogenesis of NOD mice (Anderson and Bluestone 2005). The inflammation of the pancreatic islets of Langerhans through infiltration of immune cells especially CD4⁺ and CD8⁺ T cells appear way ahead of the hyperglycemia already at a prediabetic 5-6 weeks of age. This stands in contrast to the

Pop4 β KO model in which insulinitis did not seem to appear throughout the morphological assessment of the pancreatic islets of the male mice. Further, the diabetes prevalence or incidence of the NOD mice varies from 60-80% in females and 20-30% in male which imply that the defect is less severe and quite variable compared to the *Pop4 β KO* model. Interestingly, the incidence of diabetes in the NOD model seems highly dependent on the environmental housing conditions whereby germfree environment promotes diabetes incidence (Anderson and Bluestone 2005) which does not appear to be a factor for the diabetes incidence in the *Pop4 β KO* model. It seems that autoimmune beta cell destruction apparent in NOD mice may not be the primary defect causing insulin-deficient diabetes in *Pop4 β KO* mice. While insulinitis was not observed at the indicated timepoints, the involvement of the immune system cannot be completely ruled out.

Another mouse model for monogenetic diabetes resulting in insulin deficiency accounts to the Akita mouse which has a heterozygous missense mutation (Cyt96Tyr) in the *Ins2* gene. The mutation on C57BL/6 background has been shown to lead to conformation change of proinsulin and aberrant proinsulin folding resulting in ER stress and apoptosis induced beta cell destruction (Yoshioka et al. 1997; Kayo and Koizumi 1998; Oyadomari et al. 2002). Hyperglycemia onset already starts at 3-4 weeks of age in this model and more severely in males than females. The *Pop4 β KO* model appear to demonstrate less severe phenotype as the hyperglycemia occurs at a later age. The defect occurs however due to a beta cell destruction as disruption of apoptosis factor *Chop* was able to delay diabetes in Akita mice (Oyadomari et al. 2002). Compared to the Akita phenotype, the *Pop4 β KO* phenotype dissimilarity indicate that the defect likely does not directly affect the proinsulin structure.

Two compounds which chemically induce insulin deficiency constitute to alloxan and streptozotocin (STZ) (Van Belle, Taylor, and von Herrath 2009). Alloxan is a urea derivate which chemically induces a selective necrosis of beta cells leading to a complete absence of insulin. As it is a glucose analogue it enters the pancreatic beta cells via the GLUT2 transporter and inhibits the action of glucokinase, therefore impairing glucose stimulated insulin secretion. Moreover, alloxan generates reactive oxygen species (ROS) especially hydroxyl radicals leading to oxidative stress and beta cell death (Lenzen 2008). Likewise, streptozotocin (STZ) produced by the bacteria streptomyces achromogenes, is analogue of N-acetylglucosamine and has been found likewise to selectively destroy beta cells. As STZ is an antibiotic, it inhibits synthesis of

DNA by alkylation and crosslinking the DNA. This leads to DNA damage by DNA fragmentation and cell destruction. Depending on the dose of STZ, beta cell ablation occurs via different mechanism and timeline. A single high dose of STZ (>150 mg/kg) was shown to be cytotoxic and leads to necrosis while multiple low doses show a more gradual loss of beta cell mass and delayed hyperglycemia onset. A high dose of STZ leads to ablation in 24-48h while multiple injections show a gradual loss of insulin appearing within 20 days (Lenzen 2008). Necrosis of beta cells as shown with both compounds might not apply to *Pop4* β KO as the fast ablation of beta cells within 1-2 days were not observed. However, the low STZ condition show similarity to *Pop4* β KO in the aspect of gradual loss of beta cell mass.

5.1.5 The diabetic phenotypic traits remain consistent in female *Pop4* β KO mice despite of high fat diet induced insulin resistance

As *Pop4* was identified in a polygenic type 2 diabetes mouse model, the New Zealand Obese mice, it was initially believed that the phenotype of the KO model reflects a type 2 diabetes. Therefore, a diet containing higher fat amounts (60% calories from fat diet) was fed to induce insulin resistance challenging a higher insulin secretion and exacerbating stress for the beta cell. Due to a higher fat content, the composition of the high fat diet (HFD) consisted of a lower carbohydrate and lower protein content compared to the composition of the chow diet. Therefore, the HFD promotes a diet induced obesity challenging the metabolism of the mice. As the background strain is a mix of the C57BL6/N and C57BL6/J due to the generation of these mice (Fontaine and Davis 2016), this might contribute to the observed phenotype as seen with background strains in *ob/ob* and *db/db* mouse models (Siersbaek et al. 2020). As mentioned C57BL6/N are derived from C57BL6/J but through generations of separation yield several differences in the genetics and phenotypic expression (Mekada and Yoshiki 2021). The most prominent genetic difference known is the loss of function through an inframe mutation (missense and multi-exon deletion) in the nicotinamide nucleotide transhydrogenase (*Nnt*) in C57BL6/J mice in liver and pancreatic islets (Toye et al. 2005) which is not present in C57BL6/N (Hull et al. 2017). *Nnt* functions in the mitochondria and reduces ROS therefore the C57BL6/J display a lower insulin secretion capacity compared to the C57BL6/N. As the background strain was not characterized to identify the proportion of the mixed background strains, it is assumed

that the *Pop4* β KO might be susceptible to glucose intolerance and lower insulin secretion. The HFD challenge indeed led to a diet-induced insulin resistance in female *Pop4* β KO mice reflected in the HOMA-IR value as body weight especially fat mass increased significantly compared to the chow-fed animals and higher amounts of basal circulating plasma insulin levels were detected especially at diabetic stage of life. However, the onset of hyperglycemia remains consistent at 13 weeks of age. This stands in contrast to a type 2 diabetes susceptibility gene which similarly to *Pop4* relates to tRNA function. Variations in the gene Cdk5 regulatory associated protein 1-like 1 (CDKAL1) was found to be associated to type 2 diabetes across different genome wide association studies (Steinthorsdottir et al. 2007; Scott et al. 2007; Zeggini et al. 2007). The mouse model with beta cell-specific knock out reveals that CDKAL1 functions as a methylthiotransferase in tRNA^{Lys}, which is crucial for the precise codon translation of amino acid lysine (Lys). Defects in this function has been revealed to result in misfolded proinsulin, likely due to misreading of lysine at the cleavage site of the C-peptide. This has been shown to lead to ER stress response and beta cell destruction through apoptosis. Additionally, the pancreatic islet size of these mice depict hypertrophy with 45% kcal from fat diet. Beta cell CDKAL1 KO mice exhibit reduced glucose tolerance at 5 weeks of age, and a high-fat diet exacerbates hyperglycemia, causing glucose intolerance to appear after 3 weeks on HFD (Wei et al. 2011b). Moreover, random blood glucose of animals after 3 weeks on HFD depict hyperglycemia compared to animals on a low fat diet (Wei et al. 2011a). Despite having a higher body weight and higher fat mass, female *Pop4* β KO on high fat diet did not exhibit an exacerbated blood glucose levels compared to the chow diet. Actually, on the contrary the high fat diet showed a tendency for attenuated random blood glucose levels from 16 to 18 weeks of age in the female mice which likely reflects the lower carbohydrate content of the high fat diet composition. However, diabetes penetrance was achieved before the chow-fed animals indicating that the HFD exhibits an effect. As no histological assessment of the pancreatic islets was carried out, the sufficient insulin secretion is postulated to be a result from increased insulin secretion capacity or a higher beta cell mass. However, in most cases a high fat diet stimulates hyperplasia more than hypertrophy of the beta cells (Hull et al. 2005; Ahren, Ahren, and Wierup 2010). Therefore, assumption might be that the HFD triggered hyperplasia of the pancreatic beta cells compensate for the insulin demand by the diet induced insulin resistance. The dissimilarity of this model in terms of the high-fat diet challenge

hints that the mechanism of misfolded proinsulin resulting endoplasmic stress are unlikely the causal driver mediating the beta cell demise in *Pop4 β KO* mouse model.

5.2 The prediabetic phase of *Pop4 β KO* mice displays multiple signs of beta cell dysfunction

5.2.1 Prediabetic *Pop4 β KO* mice exhibit glucose intolerance due to reduced insulin secretion

Even though basal plasma insulin levels before the onset of hyperglycemia of the *Pop4 β KO* mice did not exhibit differences compared to all age matched controls, the *in vivo* glucose tolerance test and the *ex vivo* glucose stimulated insulin secretion assay of isolated pancreatic islets showed an impairment in insulin release at this stage. The occurrence of the phenotype in both sexes presumably underlies the same mechanism therefore, further analyses were focused on the male *Pop4 β KO* mice. The idea that beta cell function is impaired right before the onset of hyperglycemia is known from several human studies (Tabak et al. 2009; Ohn et al. 2016). The glucose tolerance test at the prediabetic age in male *Pop4 β KO* mice shows that lower amounts of insulin are secreted remarkably after 30 min of glucose injection where the highest insulin secretion capacity is expected (Phillips et al. 1994). This result is in line with several human studies which describe a reduced glucose-induced first phase insulin release to predict diabetes onset and were found in both T1D and T2D (Weir and Bonner-Weir 2021; Del Prato 2003). The first phase of insulin release is mediated by a ready releasable pool of insulin granules which indicates that this granule pool appear to be depleted in the islets of *Pop4 β KO* mice (Omar-Hmeadi and Idevall-Hagren 2021; Hou, Min, and Pessin 2009). Moreover, the measurement of the endogenous proinsulin levels post GSIS reveal a deficiency supporting an impairment in insulin production.

5.2.2 The prediabetic phase display a defect in insulin production and insulin maturation

The final loss in plasma insulin content and beta cell mass led to the investigation in the causality by observing the beta cell morphology and mass before the onset of hyperglycemia. The male *Pop4 β KO* mice exhibit no discern differences in plasma insulin levels, islet morphology and insulin content at 3 weeks of age confirming the proper postnatal functional maturation of pancreatic beta cells. As indicated by the

results of the assessment of insulin secretion function in the prediabetic phase at 9 weeks of age, the histology validates the insulin deficiency before the hyperglycemia onset. Moreover, the reduced levels of insulin protein detected by the immunohistology might appear to be due to significant reduced insulin gene expression of the two insulin genes *Ins1* and *Ins2* as indicated by islet transcriptome. The morphometric analysis of the pancreatic islets at the prediabetic age at 9 weeks of age further points out that mean islet size shows no significant difference in overall islet area which might imply that there was no significant loss in pancreatic beta cell mass at that stage. Moreover, the beta cell identity marker specifies similar amounts of existing beta cells within the pancreatic islets at the prediabetic phase. This may indicate that a beta cell dysfunction due to reduced insulin gene expression occurs before the destruction of beta cells at the prediabetic stage. It has been shown in human studies though that in the prediabetic phase of T1D the onset of hyperglycemia is caused by a combination of reduced beta cell mass and beta cell dysfunction (Chen et al. 2017).

Further, the assessment of insulin granules from ultrastructural images of the pancreatic beta cell at the prediabetic phase suggests that less insulin granules were assembled shown by a tendency for lower amounts of insulin granules detected which appears in line with lower gene expression of insulin as aforementioned. Interestingly, the maturation of immature granules to mature insulin granules appears defective as higher amounts of immature insulin granules and concomitantly lower amounts mature insulin granules were detected. This is supported by the results of lower expression of *Pcsk1* and *Pcsk2* genes in the transcriptome of the pancreatic islets which enzyme activity is important for proinsulin to functional insulin maturation. As the endoplasmic reticulum is heavily involved in the maturation of preproinsulin to proinsulin, the islet transcriptome analysis which showed the downregulation of genes involved in ER protein processing further indicate that less insulin is processed due to a lower insulin production.

Dedifferentiation of pancreatic beta cells occurs as a pivotal process during beta cell failure likely as a protective mechanism against cell death (Son and Accili 2023). The dedifferentiation of beta cells is characterized by reduced expression of beta cell identity markers. Interestingly, the islet transcriptome at the prediabetic phase reveal downregulation of several important beta cell markers in particular *MafA*, *Pdx1*, *Foxa2*, *Ucn3* and *Nkx2.2*. *Pdx1* is an important transcription factor maintaining beta cell identity and deletion have shown to induce physiological features of alpha cells (Gao

et al. 2014). However, as aforementioned the detection of the *Nkx6.1* beta cell identity marker did not show differences to the control at the prediabetic age. Transdifferentiation of beta cells into alpha-like glucagon expressing cells has been shown in various mouse models under hyperglycemic conditions (Moin and Butler 2019). The detection of a higher glucagon positive area at both the prediabetic and overt diabetic stage were initially suggestive of a transdifferentiation process of pancreatic beta cells to an alpha cell like identity which was reflected likewise by the upregulated alpha cell identity markers of the pancreatic islets transcriptome. The beta cell transdifferentiation, as a consequence of metabolic stress, into an alpha-cell like characteristic was shown in mouse models lacking *Nkx2.2* (Gutierrez et al. 2017) or *Pdx1* (Gao et al. 2014). These studies have shown an overlap expression of insulin and glucagon with immunohistological stainings. However, the immunostaining of *Pop4β*KO islets at the prediabetic timepoint did not appear to show a high overlap of insulin and glucagon-stained areas. The islet transcriptome data indicate a downregulation of important beta cell markers and upregulation of alpha cell markers however in contrast the histology of the pancreatic islets likely does not suggest a dedifferentiation and transdifferentiation of the pancreatic beta cells at the prediabetic timepoint. Further, it appears likely that the detection of higher glucagon positive area appears due to the loss of beta cell mass indicated by the observed insulin area and thereby the two-dimensional assessment of the three-dimensional pancreatic islets produces the technical artefact. Overall, the prediabetic phase present impairment in insulin synthesis and maturation which leads to beta cell dysfunction as a process to diabetes onset.

5.2.3 The prediabetic phase indicates upregulation of apoptosis- and senescence-mediating genes

As the histology of the pancreatic islets clearly shows a beta cell demise from the prediabetic phase to the overt diabetic phase in the *Pop4β*KO, the question arose which mechanism mediates the decrease in beta cell mass. In the majority of cases, apoptosis of beta cells is the primary cause of beta cell death mediating hyperglycemia and diabetes (Cnop et al. 2005). Apoptosis as a programmed cell death mechanism in beta cells occurs as a stress response in both T1D and T2D. The controlled cell death can be initiated through an intrinsic or extrinsic pathway (Thomas et al. 2009). Gene ontology analysis and Consensus Pathway Database

overrepresentation analysis of the islets transcriptome indicates regulation of genes involved in intrinsic apoptotic signaling pathway. Visualization of the apoptosis pathway using the KEGG Mapper tool shows however both intrinsic and extrinsic factors participating in the regulation of apoptosis signaling. The extrinsic pathway is a death receptor-induced pathway. Indeed, the cell death receptor tumour necrosis factor (TNF), tumour necrosis factor related apoptosis receptor (TRAIL-R) and *Fas* were significantly upregulated in the islet transcriptome data at the prediabetic age. The cell death receptor FAS is normally not constitutively expressed in beta cells but only upregulated by cytokine triggers such interleukin-1 (IL-1) (Thomas et al. 2009). In line, *Fas* ligand and interleukin 1 (*Il-1*) showed significant upregulation further indicating an active extrinsic apoptosis signaling. On the other hand, the intrinsic apoptosis signaling pathway involves the mitochondria therefore also called mitochondrial apoptosis. Several stimuli activate the intrinsic apoptosis pathway among them DNA damage and ER stress (Wanner, Thoppil, and Riabowol 2020). In line the higher expression of activating transcription factor 4 (*Atf4*) as a transcriptional regulator of the unfolded protein response induces the transcription of C/EBP homologous protein (*Chop*) which is likewise significantly upregulated which mediates apoptosis factors. A key role is appointed to tumor suppressor gene *p53* (in rodents *Trp53*) also called the guardian of the genome. The upregulation of *p53* which acts as a transcription factor, mediates the expression of target genes of the BH3 domain only proteins including BIM, BID, PUMA and NOXA which suppresses cell survival B-cell lymphoma-2 (BCL-2) proteins (Aubrey et al. 2018). In concordance, *Trp53* and target genes *Bbc3* (PUMA) as well as *Bid* were significantly upregulated and *Pmaip1* (NOXA) showed a tendency for higher expression in *Pop4*βKO islets transcriptome data. Further, BH3 domain only proteins activate the proapoptotic BCL-2 proteins BAX and BAK which oligomerization forms pores in the mitochondrial membrane and allows the release of cytochrome c (CycC) and SMAC/DIABOLO into the cytosol (Westphal, Kluck, and Dewson 2014). The cytosolic cytochrome c can bind to apoptotic protease activating factor 1 (APAF1) to form apoptosomes which recruits and activates initiator caspase pro-caspase 9 (Wanner, Thoppil, and Riabowol 2020). Moreover, the released SMAC/DIABOLO protein inhibits the family of apoptosis inhibitory proteins which potentiates the apoptosis process (Adrain, Creagh, and Martin 2001). The encoding genes *Bax*, *Bak*, *CycC* and *Diabolo* also presented significant upregulation in the islet transcriptome. Finally, both the extrinsic and intrinsic signaling culminates in the activation of the

caspase cascade by activating initiator caspases 8 and 9 which in turn mediates the executive caspases 3, 6 and 7 degrading cellular components (Tomita 2016). Interestingly, the gene expression of caspase 3 (*Casp3*) was highly overexpressed in the islets transcriptome of *Pop4 β KO*, which activity is considered most important among the caspases and facilitates degradation of the DNA and cytoskeleton disintegrating the cell into apoptotic bodies (Elmore 2007).

Besides indicators for cell death by apoptotic signals, the islet transcriptome suggested the process of senescence occurring in the islet cells of *Pop4 β KO* mice. Senescence is a hallmark of aging and characterized by cell cycle arrest and secretion of cytokines (Huang et al. 2022). One of the top upregulated genes from the islet transcriptome at the prediabetic phase was the gene *Cdkn1a* coding for p21 which is another target of p53. The protein p21 is a cyclin-dependent kinase inhibitor and its binding to different cyclin complexes inhibits the cell cycle progression at the G0/1 or S phase which initiates cell cycle arrest (Al Bitar and Gali-Muhtasib 2019). Cell cycle progression is controlled by binding of cyclin dependent kinases to cyclins to induce cell cycle progression followed by phosphorylation of Rb and inhibition of E2F transcription factor which activation mediates cell cycle arrest (Varghese and Dhawan 2023). Interestingly, genes coding for the Cyclin D and E as well as RB were significantly downregulated therefore indicating that the upregulation of *p21* in combination with downregulation of the cyclins and RB might initiate a process mediating a cell cycle arrest. Moreover, the activity of p21 has been indicated as an early marker of senescence and the senescence state is maintained by the activity of p16 (Huang et al. 2022). However, *Cdkn2a* encoding for p16 showed no significant regulation in the transcriptome data of *Pop4 β KO* islets which may indicate that the cells of the islets at the prediabetic stage present an early senescence rather than prolonged senescence state. Further, the activation of p21 aids in the prevention of apoptosis partially by the regulation of anti-apoptotic BCL-2 protein family (Wanner, Thoppil, and Riabowol 2020). In concordance, the upregulated *Bcl2* gene, which mediates a pro-survival signal, further suggest that the islet transcriptome indicates a senescence signal besides of an apoptotic signal. Senescent beta cell transcriptome has been characterized by distinctive downregulation of markers for beta cell identity in addition to genes involved in the glucose-stimulated insulin secretion function (Aguayo-Mazzucato 2020). The transcriptome of the *Pop4 β KO* islets display similar results especially in downregulation of genes involved in glycolysis, cellular deposition, incretin pathway

receptors and enzymes involved in insulin granule maturation. Moreover, senescent cells can develop a particular phenotype termed the senescence associated secretory phenotype (SASP) (Kumari and Jat 2021; Varghese and Dhawan 2023). Mouse beta cells displaying this phenotype have shown hypersecretion of proinflammatory cytokines such as Igfbp3, Interleukin 6 (IL-6), Cxcl10, Serpine 1 and metalloproteins (Thompson et al. 2019). These cytokines mediate paracrine senescence which impacts surrounding environment by degrading extracellular matrix and promoting lymphocytic infiltration (Varghese and Dhawan 2023; Brawerman, Pipella, and Thompson 2022). In line, the CPDB pathway analysis indicate 21% of genes concerning extracellular matrix organization to be significantly upregulated. Among them, the islet transcriptome of *Pop4* β KO mice exhibited overexpression of *Tgf β* and several metalloproteins such as *Mmp2*, *Mmp3*, *Mmp10*, *Mmp12*, *Mmp13*. Further, *Il-6* and *Il-1alpha* shown a tendency to be upregulated. Senescence triggered by the p53/p21 pathway in response to DNA damage caused by varying factors like oxidative stress. The triggered cell cycle arrest, enables the repair of the damaged DNA, however, a prolonged senescence state may induce other effects. As mentioned double stranded DNA breaks together with senescence were detected in beta cells of type 1 diabetes (Thompson et al. 2019). Interestingly, removing the senescent cells within the islets attenuated the type 1 diabetes progression (Thompson et al. 2019). Senescent cells also occur in pancreatic islets in the context of type 2 diabetes implicating its role and contribution in a general beta cell dysfunction. The implication of both apoptosis and senescence signals in the islet transcriptome of the *Pop4* β KO mice propose beta cells either undergoing apoptotic or senescence fate. Indeed, mouse models such as the NOD mice and T2D mouse models display islets where most beta cells undergo apoptosis while a minority of beta cells develop senescence (Cha, Aguayo-Mazzucato, and Thompson 2023). Overall, the *Pop4* β KO islet transcriptome highlights a mixed signal pointing to upregulation of apoptosis and senescence factors possible in different beta cell subpopulations which in turn mediate different mechanism of beta cell failure.

5.3 Implication of functional role of *Pop4* to *Pop4* β KO phenotype

5.3.1 *Pop4*'s role as a subunit of RNase P and RNase MRP

POP4 alias RPP29 is foremost canonically described as a subunit of the closely related RNase P and RNase MRP holoenzymes both eliciting essential functions as their

activity is in particular important for proper tRNA maturation and rRNA subunit maturation (Chu, Zengel, and Lindahl 1997). Both ribozymes consists of several protein cofactors and a catalytic non-coding RNA subunit that mediates the cleavage activity (Jarrous 2002). Interestingly, RNase P and ribosomes are the only ribozymes in all domains of life and the special catalytic active RNA subunit has been postulated to be a relic from the pre-biotic RNA world in which RNA acted as both enzyme and genetic information (Walker and Engelke 2006). The catalytic center of both RNase complexes is almost identical in conformation with a distinct RNA component termed *Rpph1* or H1 for RNase P and *Rmrp* for RNase MRP in human (Lan et al. 2020). Most of the protein subunits of RNase P and MRP are shared between both ribozymes including POP1, POP4/RPP29, POP5, RPP20, RPP25, RPP29, RPP30 and RPP38 (Shaukat et al. 2021). Further, distinct protein cofactors of RNase MRP are SNME1 and RMP1 in yeast while RNase P uniquely possess RPP21 protein subunit (Zhou et al. 2024). Among the protein subunits, POP4 has been described as a core component of the RNase P (Mann et al. 2003) and highly conserved as one of the most ancient eukaryal proteins (Reiner et al. 2011). *In vitro* studies have shown that POP4 together with RPP21 and the RNA subunit H1 were sufficient to reconstitute the RNase P activity (Mann et al. 2003). Structurally, POP4 has evolved from the archaeal ancestor RPP29 with a new N-terminal motif (Lan et al. 2020). The C-terminal domain is conserved and directly interacts with the catalytic domain of the RNA subunit in the RNase P complex (Sharin et al. 2005) which leads to the postulation that the missing of the C-terminal of POP4 in the *Pop4 β KO* might be limiting the RNase P activity. Moreover, among these protein cofactors which are shared between RNase P and RNase MRP, *Pop1* and *Rpp30* were significantly higher expressed in the pancreatic islets of *Pop4 β KO* in the islet transcriptome dataset. POP1 is the largest protein subunit in both RNase P/MRP and emerged uniquely in eukaryotes (Lygerou et al. 1994). The unique emerging of *Pop1* in eukaryote has been suggested due to POP1 role of a scaffold to stabilize RNase P RNA as a substitute for the loss of RNA stabilization through RNA interaction occurring in bacteria (Fagerlund et al. 2015). Interestingly, in yeast RNase MRP has a *Pop1-Pop4-Rmp1* motif which has a binding surface to the internal transcribed spacer (ITS_{A3}) site, which indicates that POP4 also actively contributes to maturation of rRNA (Lan et al. 2020). Further, POP1 has been linked to breast cancer as silencing of *Pop1* has been shown to induce cell cycle arrest while overexpression promoted cell progression which mechanistically was shown due

to interaction with telomerase complex stabilizing and protecting the telomeres (Zhu et al. 2023). On the other hand, RPP30 has been shown to interact with POP4/RPP29 via the C-terminal tail in the human RNase P structure (Wu et al. 2018). Moreover, RPP30 has also been proposed as a marker for gastric cancer (Kan et al. 2022). In *Drosophila melanogaster*, mutation of *Rpp30* induced sterile females displaying replication stress in the atrophied ovaries however with normal levels of mature tRNAs and high levels of unprocessed pre-tRNAs (Molla-Herman et al. 2015). What appears common to POP1 and RPP30 however is the described interaction with the RNA subunit in the RNase complexes and the interaction with POP4 (Wu et al. 2018; Reiner et al. 2011). Therefore, the unexpected increased expression of partner subunits *Pop1* and *Rpp30* in the pancreatic islets might indicate that the deletion of exons 4 and 5 impact on the POP4 protein structure destabilizes the RNase P and MRP protein complexes by the missing RNA interaction and therefore triggering a compensatory effect by overexpression of the *Pop1* and *Rpp30* subunit to stabilize the RNA subunit ensuring RNase P and MRP function as a hypothesis.

RNase P catalyzes the hydrolysis of a specific phosphodiester bond in all pre-tRNAs resulting in the cleavage of the 5'-end sequence contributing to the maturation of tRNAs in the nucleus (Xiao et al. 2005). Besides that, a RNA free protein only variant exists in eukaryotes termed proteinaceous RNase P (PRORP) which localizes to the mitochondria to process mitochondrial tRNAs (Rossmannith, Giege, and Hartmann 2024; Sridhara 2024). The inhibition of only one protein subunit of RNase P holoenzymes has been shown to affect expression of RNase P structure and function therefore all proteins subunits are considered essential (Cohen, Reiner, and Jarrous 2003; Wu et al. 2018). Therefore, to indirectly evaluate if the *Pop4*βKO would impair proper tRNA function, genes coding for the family of aminoacyl tRNA synthetase (aaRSs) which charges the tRNAs with the matching amino acid were observed from the islet transcriptome data at the prediabetic stage. Among these, only two nuclear aaRSs the isoleucine synthetase (*Iars*) and tryptophanyl tRNA synthetase (*Wars*) and of the mitochondrial four aaRSs namingly the seryl-aminoacyl tRNA synthetase 2 (*Sars2*), alanyl-tRNA synthetase 2 (*Aars2*), cysteinyl-tRNA synthetase 2 (*Cars2*), tryptophanyl tRNA synthetase 2 (*Wars2*) were significantly differential regulated. Beside cleavage of 5'- and 3'-end in pre-tRNA, tRNAs undergo extensive number of posttranscriptional modifications which are important for the correct folding, stability and function of tRNAs. Two posttranscriptional modifications of tRNA have been linked

to cause diabetes in human. As aforementioned, CDKAL1 acts as a methylthiotransferase of the tRNA^{Lys} and has been shown to cause the development of type 2 diabetes due to aberrant proinsulin processing (Ghosh et al. 2022). The tRNA methyltransferase TRMT10A has been linked to young onset type 2 diabetes and encephaly. A nonsense mutation in the TRMT10A gene was identified by linkage analysis and whole exome sequencing in a family leading to a premature stop codon and absence of mRNA and protein structure (Mundlos et al. 2013). TRMT10A is described to catalyze the methylation of guanine 9 in several tRNAs such as tRNA^{Gln} and tRNA^{iMeth} (Cosentino et al. 2018). As TRMT10A is ubiquitously expressed but especially high in pancreatic islets and the brain, the absence of TRMT10A in pancreatic beta cells was shown to lead to hypomethylation inducing oxidative stress and apoptosis due to 5'-tRNA^{Gln} fragments which mediates the beta cell death (Cosentino, Cnop, and Igoillo-Estève 2019). The islet transcriptome revealed that among 12 detected tRNA methyltransferases (TRMT) 4 were significantly regulated however *Trmt10a* contrary to the expectation was significantly upregulated. Moreover, knockdown of protein cofactors or the H1 RNA subunit of RNase P was shown to lead to inhibition of transcription of other small non-coding RNA genes such as 5S rRNA, 7SL RNA and U6 snRNA probably by binding to genetic loci of transcriptionally active tRNA and 5S rRNA genes in a cell cycle dependent manner which highlights the diverse substrates of RNase P (Jarrous and Liu 2023). Interestingly, human RNase P has been shown to cleave a tRNA like segment of the 3' end of the metastasis-associated lung adenocarcinoma transcript 1 (MALAT1), which has been linked as marker for human cancer and diabetes related complications (Esakova and Krasilnikov 2010; Abdulle et al. 2019). Notably, a tRNA modopathy, a mitochondrial disease, confers to mitochondrial diabetes in which mitochondrial tRNA point mutations have been linked to a beta cell defect in insulin secretion in humans (Takano, Ogawa, and Hayakawa 2023; Maassen et al. 2004). Further, the TRMT10A example highlights tRNA fragmentation as a deleterious stress response (Magee and Rigoutsos 2020). Though there was no observation of an impaired tRNA function due to an indirect observation of the gene expression affecting proper tRNA function, the implication of tRNA defects to diabetes pathophysiology is of relevance as indicated by several examples however the role of tRNA in *Pop4*βKO observed phenotype remains unclear. RNase MRP was first described to generate RNA primers for DNA replication in the mitochondria however the high amount localizing in the nucleolus uncovered that the

activity catalyzes the cleavage of the internal transcribed spacer (ITS) site for ribosomal RNA maturation and therefore plays a role in ribosomal biogenesis (Woodhams et al. 2007; Lan et al. 2020). Additionally, in yeast RNase MRP has various substrates such as 5' UTR of cyclin B2 and CTS1 mRNA thereby participates in cell cycle regulation (Zhou et al. 2024). Moreover the only human disorder described with RNase MRP thus far confers to mutations in the RNA subunit of RNase MRP which showed a cartilage-hair hypoplasia, a recessive inherited disorder (Martin and Li 2007). Intriguingly, the bioinformatical analysis of the islet transcriptome points to differentially regulated genes playing a role in rRNA processing, maturation of 5.8S rRNA and upregulation of 19% of genes in the ribosome biogenesis pathway. Indeed, the results showed upregulation of genes involved in rRNA modifications, pre-rRNA processing and in the maturation of the 40S and 60S ribosomal subunits. Interestingly, increased ribosome biogenesis was shown to induce pancreatic beta cell failure in db/db mice (Asahara et al. 2009). Further, other indications for ribosome implications for diabetes have been shown by ribosomal RNA methyltransferase transcription factor B1 mitochondrial (TFB1M) (Sharoyko et al. 2014) and dimethyladenosine transferase 1 homolog (DIMT1) (Verma et al. 2022). A common variant of TFB1M was identified to be associated with reduced insulin secretion and T2D risk (Koeck et al. 2011). A beta cell specific loss of TFB1M which methylates adenine of 12S ribosomal RNA in the mitochondria has been shown to result in defect in mitochondrial protein translation causing dysfunction and apoptosis as well as necrosis of the pancreatic islets (Sharoyko et al. 2014). Interestingly, the beta cell specific KO mice of TFB1M developed an insulinopenic diabetes similar to *Pop4 β KO* however the hyperglycemia onset appear only at 4 month of age which appeared due to mitochondrial dysfunction further displaying an alternate mitochondrial structure which has not been apparent in the *Pop4 β KO* mice (Sharoyko et al. 2014). A homolog of TFB1M is DIMT1 which was shown to be positively correlated to insulin expression in human from T2D donors. Impaired DIMT1 function in *in vitro* cell culture models for pancreatic islets revealed the impact on mitochondrial function which perturbed insulin secretion and attenuated protein synthesis ascribed to defects in rRNA processing as reduced interaction of Nob1 and PES-1 were detected (Verma et al. 2022). These examples of perturbed rRNA synthesis further incline defects in proper rRNA biosynthesis to influence protein synthesis. However, co-immunoprecipitation and co-sedimentation studies suggest that human Pop4 may not to be required for RNase MRP function (Welting et al. 2006).

As both tRNA and rRNA are essential for protein translation machinery, an altered function of RNase P and MRP might affect overall protein levels. The presented data however indicate no gross defects in protein synthesis although no experiment was particularly designed to study that matter. Firstly, no difference in protein concentration within the islets were detected post GSIS. The observation of the insulin vesicles in the basal and stimulated state from the ultrastructural images of the pancreatic beta cells displayed elevated number of insulin vesicles which further suspend a defect in protein synthesis. Moreover, the female mice which underwent HFD induced insulin resistance showed that insulin levels could be elevated by diet stimuli which points out that protein synthesis might not be affected in a significant matter. The role of rRNA biosynthesis defects through the role of POP4 in RNase MRP revealed in contrary to the expectation of an upregulated pathway which may be apparent due to negative feedback in rRNA synthesis however this could not be elucidated and the contribution to the observed phenotype likewise remains debatable.

5.3.2 *Pop4*'s role in double stranded DNA repair

Since a described function of *Pop4* is the participation in double stranded DNA repair of homology directed repair mechanism (Abu-Zhayia et al. 2017), the hypothesis was that failure in double stranded DNA repair or repair response could explain the beta cell dysfunction and death leading to the onset of hyperglycemia. Indeed, beta cell death in T1D (Horwitz et al. 2018) and T2D (Mukherjee et al. 2021) were described to be associated with DNA damage or DNA damage response. Defect in DNA damage response detected in beta cells was shown to promote islet inflammation in early type 1 diabetes patients, a rat model and STZ treated mice (Tay et al. 2019; Horwitz et al. 2018). Moreover, the diabetic db/db mouse at the chronic hyperglycemic state at 16 weeks of age display an increase in DNA repair markers indicating DNA damage (Tay et al. 2019). Also, T2D and congenital hyperinsulinism which have been shown to be caused by glucokinase mutation led to apoptosis associated DNA damage (Tornovsky-Babeay et al. 2014). Coupled to these indications, the islets transcriptome data suggested that genes participating in the regulation of DNA damage response are differentially expressed in *Pop4* β KO mice. DNA damage occurs due to varying factors, from naturally spontaneously occurring due endogenous processes of metabolism or environmental factors such as radiation. Therefore, functional DNA repair processes are crucial for genome integrity and to avoid deleterious mutagenesis processes.

Double stranded DNA breaks thereby is the most deleterious lesion of DNA damage for the cell as one lesion can cause cell death (Borges, Linden, and Wang 2008). Therefore, two repair processes exist which utilizes different strategies for DNA repairment depending on the cell cycle phase and chromatin context (Ray Chaudhuri and Nussenzweig 2017). The non-homologous end joining repair utilizes the ligation of broken DNA ends by small modifications which creates deletions or insertions. This process can be utilized during the whole cell cycle however it is error prone and can result in loss of DNA information. The homology-directed repair (HDR) can be utilized only when a homologous DNA strand is present, mostly during G2/S phase of the cell cycle and achieves DNA damage repair through homologous recombination. The DNA damage response (DDR), which mediates the repair mechanism, begins with the recognition of DNA breaks by poly(ADP-ribose) polymerase 1 (PARP1), whose auto-PARylation activity by adding poly-ADP-ribose (PAR) chains attracts multiple DNA repair factors (Ray Chaudhuri and Nussenzweig 2017). Among these factors are members of the MRN complex (MRE11/RAD50/NBS1), MRE11 and NBS1 which aids in the DNA end resection and activation of further DDR molecules (Qiu and Huang 2021). One of the most important DDR factors is Ataxia telangiectasia mutated (ATM) kinase which belongs to phosphoinositide 3-kinase related kinases (PIKKs) which act as signal transducers by phosphorylating target proteins for DNA damage repair and elicits its function through double stranded DNA breaks (Patil, Pabla, and Dong 2013). ATM phosphorylation activity recruits downstream factors such as histone H2A.X, checkpoint protein Chk1, Chk2 and BRCA1 (Roy, Chun, and Powell 2011). The histone variant H2A.X is phosphorylated at serine 139 (γ H2A.X) within seconds and is regarded as a reliable marker of double stranded DNA breaks (Rogakou et al. 2000; Rogakou et al. 1998). Importantly the checkpoint kinases of the PIKKs family including ATM phosphorylate and stabilize tumor suppressor p53 which connects DNA damage response to the cell cycle regulation (Shibata and Jeggo 2021).

The exact mechanism by which POP4 participates in double stranded DNA repair by homology-directed repair still needs to be elucidated in further detail. However, the initial link of Pop4 involvement in DDR came from the phosphoproteomic analysis of the DDR after initiation of double stranded DNA breaks which revealed POP4 phosphorylation on S/TQ motif serine 10 by PIKKs along with POP1 and RPP38 (Beli et al. 2012). Depletion of *Pop4/Rpp29* in a human osteosarcoma cell line showed compelling evidence of sustained accumulation of broken DNA after induction of

double stranded DNA breaks in a neutral comet assay which revealed the importance of *Pop4* for DDR (Abu-Zhayia et al. 2017). Furthermore, this *Pop4/Rpp29* depletion induced the phosphorylation of several DDR components including H2A.X. In line with this result, the pancreatic islets of *Pop4* β KO mice have presented higher amounts of γ H2A.X positive stained cells within the insulin positive stained areas at the prediabetic age similar to diabetic db/db pancreatic islets which in both cases impacts only a minority of cells. Though, *Pop4/Rpp29* has shown to be phosphorylated, it appeared not to be executed by ATM (Abu-Zhayia et al. 2017). Moreover, the recruitment of *Pop4/Rpp29* to DNA damaged sites was dependent on PARP1 activity however not by PARylation but by binding to PAR moieties which suggest an interaction partner in-between PARP1 and POP4/RPP29 (Abu-Zhayia et al. 2017). Furthermore, another subunit of RNase P *Rpp21* was shown to participate in DDR and independent of *Pop4/Rpp29* however both were dependent on the H1 RNA subunit. Therefore, a proposed non-canonical variant of RNase P consisting of Pop4/Rpp29, Rpp21 and H1 RNA subunit might be implicated in the HDR (Abu-Zhayia et al. 2017). Among those different genes in double stranded DNA damage response in particular *Parp1*, *Atm* and *Trp53* (p53) were differentially expressed in the islet transcriptome of *Pop4* β KO. Surprisingly, both expression of *Parp1* and *Atm* was markedly lower expressed in the islet transcriptome of *Pop4* β KO mice compared to the control. PARP1, the first member of the PARP family, is important for the early recruitment of DDR proteins and deficiency delays DDR response (Ray Chaudhuri and Nussenzweig 2017). Interestingly, PARP1 activity seems to be important for beta cell insulin secretion however overactivation stimulates beta cell death while knockout revealed resistance to diabetes progression (Kanev et al. 2023; Dadheech et al. 2022). Noticeably, PARP1 and ATM physically interact forming a complex and their activity is determined by each other (Aguilar-Quesada et al. 2007). As ATM contains a PAR binding domain, *in vitro* study have determined ATM activity by binding to PAR moieties (Ray Chaudhuri and Nussenzweig 2017). The ATM gene was identified as the causal for Ataxia telangiectasia, a human DNA damage response disorder characterized by radiosensitivity (Shibata and Jeggo 2021). Interestingly, ATM has been described to regulate DNA damage induced apoptosis by STZ treatment in a rat beta cell line and p53 activity appears independent of ATM induction (Uhlemeyer et al. 2020) which offers an explanation for the opposing regulation of *Atm* and *Trp53* gene expression in the islets transcriptome. Moreover, silencing or inhibition of *Atm/ATM* increased cell

death upon induction of the p53 signaling pathway by Nutlin-3 treatment (Uhlemeyer et al. 2020) indicating that the downregulation of *Atm* in the islet transcriptome of *Pop4* β KO mice might contribute to the observed beta cell death. Intriguingly, mouse models with impaired DNA repair mechanism such as the Ligase 4 or DNA excision repair protein *Ercc1* display similar beta cell death induced diabetes to *Pop4* β KO mice. Ligase 4 is required for non-homologous end joining and deficiency renders the cell hypersensitive to DNA damage and can result in premature senescence. Mice whole body deficient in Ligase 4 causes embryonic lethality, which was shown to be rescued by a *p53* deficiency however mice still succumb to a lymphomas prematurely (Tavana et al. 2010). A hypomorphic *p53* mutation that defects apoptosis signaling combined with Ligase 4 depletion shows increased senescence and a diabetic phenotype at 3-5 months of age due to DNA damage in the beta cells (Tavana et al. 2010). Deficiency in *Ercc1*, a key DNA repair gene is reported to develop increased insulin sensitivity due to suppression of the somatotrophic axis however these mice show reduced plasma insulin and beta cell area with increased DNA damage markers (Huerta Guevara et al. 2021). *Ercc1* is a key DNA repair gene for the nucleotide excision repair mechanism and together with XPF nuclease forms heterodimer to catalyse the 5' incision to excise the DNA lesion (Huerta Guevara et al. 2021). A beta cell specific deletion validates the importance of *Ercc1* for the beta cell survival and mice develop adult-onset diabetes. The *Ercc1* knock out mice develops decreased beta cell function due to increased DNA damage in the beta cells and this was validated in the beta cell specific *Ercc1* knock out mice. The β -*Ercc1*KO mice develop an adult-onset diabetes, impaired glucose tolerance and reduced insulin secretion (Yousefzadeh et al. 2023). The diabetes onset of both models at an adult stage is comparable to our model. However, differences in the phenotype of these mouse models compared to *Pop4* β KO mice may occur due to the different DNA damage repair mechanism each mouse model addresses. Whether DNA damage is the driver for the loss of insulin expression and beta cell mass remain to be further explored. However, since homology directed repair can be only utilized in the S/G2 phase of the cell cycle (Smirnikhina et al. 2022). Most pancreatic beta cells remain in a quiescent state while only a minority of beta cells which are able to proliferate may utilize homology directed DNA repair. Besides that if homology directed DNA repair does not work, the non-homologous DNA repair processes can compensate for the missing function and was shown to be faster and more efficiently used in replicative cells (Mao et al. 2008). Therefore, this suggests *Pop4* function in

homology directed repair of double stranded DNA repair to be unlikely indirectly impairing DNA repair mechanism in pancreatic beta cells. However, the downregulation of important DNA repair response markers may indicate an impairment in proper DNA damage response, nonetheless.

5.3.3 *Pop4*'s role in histone 3.3 chromatin assembly

Another role of POP4 as aforementioned is the regulation of histone 3.3 incorporation for chromatin assembly (Newhart et al. 2016; Shastrula et al. 2018). Chromatin describes the complex of DNA wrapped around hetero octamer of histones H2A, H2B, H3, H4 to form the nucleosome structure and thereby this packages the DNA into a highly compact arrangement. Proper histone deposition therefore is important for maintaining chromatin structure and provides epigenetic information for gene regulation. The histone 3.3 (H3.3) is a conserved histone replacement variant of H3, synthesized throughout the cell cycle and the assembly in chromatin occurs replication independent (Ray-Gallet and Almouzni 2021; Szenker, Ray-Gallet, and Almouzni 2011). Normally, the classical chromatin assembly in DNA replication occurs following the replication fork during S phase and are also assembled during DNA gap repair in response to DNA damage (Robinson and Schultz 2003). The alternative replication independent chromatin assembly is present to replace histones that may have irreversibly modified posttranslational modifications. H3.3 marks transcriptional activity at euchromatin but also has been shown to accumulate at silent loci in heterochromatin and telomeres where it is required for transcriptional repression of telomeric repeats and pericentric heterochromatin (Szenker, Ray-Gallet, and Almouzni 2011). Deposition of H3.3 in transcriptional active loci of the chromatin was proposed to help in active transcription possibly by more accessible chromatin structure (Tagami et al. 2004). Further, H3.3 is predominantly present in non-replicative cells that exhibit a quiescent post mitotic state (Ray Chaudhuri and Nussenzweig 2017). The assembly of histones into chromatin relies on chromatin assembly factors that can modify, bind and remodel the nucleosome and histone chaperones which are important for the incorporation. For deposition of H3.3 both HIRA and DAXX-ATRAX chaperones complexes are important for the enrichment of H3.3 at different genomic sites. The Histone Regulator A (HIRA) complex together with Asf1 have been shown to incorporate H3.3 at euchromatic transcriptionally active region while histone chaperones Death Domain associated protein (DAXX) and Alpha-Thalassemia/mental retardation X-linked syndrome protein

(ATRX) regulate H3.3 deposition at repressed loci, telomeres and pericentric heterochromatin (Ray-Gallet and Almouzni 2021). Newhart and colleagues, for the first time have shown a role of POP4 as an upstream regulator of H3.3 nucleosome deposition facilitating incorporation via ATRX-DAXX together with RPP21 and POP1 as a RNase P variant (Newhart et al. 2016). Silencing of *Rpp29* increased H3.3 chromatin deposition indicating that RPP29 normally represses H3.3 chromatin incorporation (Newhart et al. 2016). Another non-canonical role of RNase P is the requirement in the transcription of tRNA genes and rRNA genes which implicate RNase P role in both transcription and processing of tRNAs (Jarrous and Reiner 2007). Subsequent studies of *Rpp29* regulation of H3.3 incorporation has shown that the deposition of H3.3 occurs at actively transcribed tRNA and rRNA genes, mRNA and sense/anti-sense RNA (Shastrula et al. 2018) which intriguingly links the H3.3 deposition to regulation of tRNA and rRNA genes. Further, depletion of *Rpp29* increased H3.3 incorporation at promoter sites and gene bodies promoting the transcription of these genes in mRNA and proteins levels (Shastrula et al. 2018). The facilitated incorporation of H3.3 was shown to be accompanied by euchromatic deposition of Histone 3 trimethylation at lysine position 4 and 36 (H3K4me3 and H3K36me3) and heterochromatic deposition of Histone 3 acetylation at lysine position 14 and Histone 3 trimethylation at lysine position 9 (H3K14ac and H3K9me3) (Shastrula et al. 2018). Interestingly, H3K4 methylation has been shown to be important for maintaining gene expression of genes in insulin biosynthesis and overall beta cell function (Vanderkruk et al. 2023). Further, overexpression of *Rpp29* accelerated transgene chromatin compaction (Newhart et al. 2016). Moreover, besides interaction of RPP29 with H3.3, another interaction was uncovered to C-terminal of histone 2B (Shastrula et al. 2018). The N-terminus of human *Rpp29/Pop4* only present in eukaryotes has been shown to interact with H3.3 through a specific region (Shastrula et al. 2018). Interestingly, the overexpression of H3.3 together with ASF1B histone chaperone promotes proliferation of human pancreatic beta cells (Paul et al. 2016). Anti-silencing function 1 (ASF1) a conserved histone chaperone, regulates transcription by de-repressing silent loci (Paul et al. 2016). Overexpression of *Asf1b* induced genes for replication while suppressing genes for apoptosis (Paul et al. 2016). Therefore, H3.3 chromatin assembly has been shown to regulate beta cell proliferation. The cellular proliferation marker Ki-67 (MKI67) plays a role in rRNA synthesis and is expressed during all active phases of the cell cycle including G1, S, G2 and mitosis.

The results of the proliferation marker Ki67 showed a decline in proliferative beta cells with increasing age in both *Pop4* β KO and control. This is in line with describing the decline in proliferation capacity of pancreatic beta cells with aging (Kulkarni et al. 2012). Interestingly though, *Pop4* β KO mice at the early timepoint of 3 weeks of age depicted a higher percentage of proliferative cells within the seen beta cell areas. This appears surprising as blood glucose levels and plasma insulin were unaltered between control and *Pop4* β KO mice. Additionally, the number of beta cells calculated through beta cell identity marker *Nkx6.1* and beta cell area at 3 weeks of age show a minor tendency of more beta cells affirming this result. A study has shown that reduced insulin production was able to induce beta cell proliferation (Szabat et al. 2016). Taken together, the direct influence of *Pop4/Rpp29* on chromatin assembly of a non-canonical histone variant which is associated to epigenetic gene regulation, aging and proliferation appear to be intriguingly in the context of pancreatic beta cell failure of the *Pop4* β KO mice.

5.4 Conclusion and outlook

In conclusion, this thesis has demonstrated for the first time in an *in vivo* mouse model the beta cell autonomous role of the endoribonuclease subunit *Pop4*. The beta cell specific deletion of exon 4 and 5 showed initial effects on beta cell function and with increasing age to impaired beta cell survival in the mouse model. In particular, the gradual loss of beta cell mass appears to start in early adulthood and mediates the hyperglycemia and the manifestation of diabetes in the mouse model. The prediabetic phase of the mice is characterized by dysfunction of insulin secretion, decreased insulin gene expression and further indicates an insulin maturation defect. The islet transcriptome confirmed the defect in insulin secretion and processing as genes known to mediate insulin secretion and beta cell identity were downregulated, while upregulation of the genes encoding for p53/p21 axis suggested apoptosis and senescence as processes mediating the beta cell failure and demise. Initial study investigating the DNA repair maker could suggest that DNA damage plays a role in the observed beta cell demise. The process leading to the observed beta cell demise is likely degenerative and the phenotype may result from a combination of processes in which *Pop4* is involved. However, in this study, the focus on the prediabetic phase could not reveal the processes mediating beta cell dysfunction and demise, as this time point already suggests secondary effects as observed from the islet

transcriptome. Therefore, further studies at a time point prior to the prediabetic phase may reveal the mechanism mediating beta cell dysfunction and process in which *Pop4* is involved in. In addition, insulin production and proliferation at an early time point needs to be more closely monitored. Since the effect of the deletion of exons 4 and 5 on the protein structure of POP4 has not been experimentally validated, investigation of the identity of the POP4 protein or the RNase P/MRP complex using protein mass spectroscopy may help in the interpretation of the functional impact of POP4. To clarify whether both apoptotic and senescent beta cells are apparent within the pancreatic islets, immunostaining of apoptotic markers such as cleaved caspase 3, p53 or TUNEL staining and senescence markers such as p21, p16 and beta-galactosidase staining or protein abundance can be analyzed by Western blot of pancreatic beta cells/islets in a diabetic phase. In addition, since *Pop4* functions in chromatin assembly through interaction with H3.3, chromatin immunoprecipitation sequencing (CHIP-seq) of pancreatic beta cells to identify H3.3 incorporation could help to determine if this process is impaired. To study tRNA abundance, tRNA sequencing or non-coding RNA study may be useful to elucidate the contribution to the phenotype. Further studies should investigate the importance of *Pop4* in human beta cell biology and its role in the development of diabetes.

6 Abbreviations

°C	Degree Celsius
µm	Micro meter
ADP	Adenosine diphosphat
ANOVA	Analysis of variance
A. U.	Arbitrary units
AUC	Area under the curve
ATP	Adenosine triphosphat
B6	C57BL/6J
BAC	Bacterial artificial chromosome
Bidest.	bidestillata
bp	Base pairs
C3H	C3H/HeJ mouse strain
CGM	Continuous glucose monitoring
cDNA	Complementary DNA
Chr.	chromosome
cM	centimorgan
CPDB	Consensus Pathway Database
db	Genetically Diabetic obese mice
DPP-4	Dipeptidyl peptidase 4
DDZ	'Deutsches Diabetes Zentrum'
dL	Dezi Liter
DNA	Desoxyribo nucleic acid
DIO	Diet induced obesity
ds	Double stranded
E	embryonic
e. g.	Latin: <i>exempli gratia</i> – for example
e. i.	Latin: <i>id est</i> – that is
ER	Endoplasmatic reticulum
ETOH	ethanol
FACS	Fluorescence activated cell sorting
Fwd	forward
G	gravity

GIP	Gastric insulinotrope polypeptide
GLP-1	Glucagon-like peptide 1
GO	Gene ontology
GSIS	Glucose stimulated insulin secretion
GWAS	Genome-wide association study
h	hours
H ₂ O ₂	Hydroxide peroxide
HbA1c	Glycosylated hemoglobin
HFD	High-fat diet
HRP	Horseradish peroxidase
Hz	Hertz
Ins	Insulin
IMPC	International Mouse Phenotyping Consortium
ipGTT	Intraperitoneal glucose tolerance test
kcal	Kilo calorie
KEGG	Kyoto Encyclopedia of Genes and Genomes
KOMP	Knockout Mouse Project
LADA	Latent autoimmune diabetes in adults
LOD	Logarithm of the odd
mb	Mega base
mg	Milli-gram
min	minute
MODY	Maturity onset diabetes of the young
mRNA	Messenger RNA
MRP	Mitochondrial RNA processing
n	Number
NMR	Nuclear magnetic resonance
NOD	Non obese diabetic mice
nt	nucleotid
NZO	New Zealand obese
PBS	Phosphate buffered saline
Pop4	Processing of precursor 4
PP	Pancreatic polypeptid
Prox	Proximal

qPCR	Quantitative polymerase chain reaction
QTL	Quantitative trait loci
rcf	Relative centrifuge force
RCS	Recombinant congenic strain
RNA	Ribnucleic acid
ROS	Reactive oxygen species
rpm	Revolutions per minute
Rpp29	Ribonucleases P protein
rRNA	Ribosomal RNA
RT	Room temperature
<i>RT</i>	Real time
SD	Standard deviation
sec	Second
SEM	Standard error of the mean
SGLT-2	Sodium glucose transporter 2
SNP	Single-nucleotid polymorphism
Tab.	Table
TCA	Tricarboxylic Acid Cycle
T1D	Type 1 diabetes mellitus
T2D	Type 2 diabetes mellitus
tRNA	Transfer RNA
UPR	Unfolded protein response
UTR	Untranslated region
WHO	World Health Organization
WT	Wildtype

7 References

- Abdulle, L. E., J. L. Hao, O. P. Pant, X. F. Liu, D. D. Zhou, Y. Gao, A. Suwal, and C. W. Lu. 2019. 'MALAT1 as a Diagnostic and Therapeutic Target in Diabetes-Related Complications: A Promising Long-Noncoding RNA', *Int J Med Sci*, 16: 548-55.
- Abdulreda, M. H., and P. O. Berggren. 2021. 'The pancreatic islet: a micro-organ in control', *CellR4 Repair Replace Regen Reprogram*, 9.
- Abu-Zhayia, E. R., H. Khoury-Haddad, N. Guttmann-Raviv, R. Serruya, N. Jarrous, and N. Ayoub. 2017. 'A role of human RNase P subunits, Rpp29 and Rpp21, in homology directed-repair of double-strand breaks', *Sci Rep*, 7: 1002.
- Adams, M. T., and B. Blum. 2022. 'Determinants and dynamics of pancreatic islet architecture', *Islets*, 14: 82-100.
- Adrain, C., E. M. Creagh, and S. J. Martin. 2001. 'Apoptosis-associated release of Smac/DIABLO from mitochondria requires active caspases and is blocked by Bcl-2', *EMBO J*, 20: 6627-36.
- Aga, H., N. Hallahan, P. Gottmann, M. Jaehnert, S. Osburg, G. Schulze, A. Kamitz, D. Arends, G. Brockmann, T. Schallschmidt, S. Lebek, A. Chadt, H. Al-Hasani, H. G. Joost, A. Schurmann, and H. Vogel. 2020. 'Identification of Novel Potential Type 2 Diabetes Genes Mediating beta-Cell Loss and Hyperglycemia Using Positional Cloning', *Front Genet*, 11: 567191.
- Aguayo-Mazzucato, C. 2020. 'Functional changes in beta cells during ageing and senescence', *Diabetologia*, 63: 2022-29.
- Aguilar-Quesada, R., J. A. Munoz-Gamez, D. Martin-Oliva, A. Peralta, M. T. Valenzuela, R. Matinez-Romero, R. Quiles-Perez, J. Menissier-de Murcia, G. de Murcia, M. Ruiz de Almodovar, and F. J. Oliver. 2007. 'Interaction between ATM and PARP-1 in response to DNA damage and sensitization of ATM deficient cells through PARP inhibition', *BMC Mol Biol*, 8: 29.
- Ahlqvist, E., P. Storm, A. Karajamaki, M. Martinell, M. Dorkhan, A. Carlsson, P. Vikman, R. B. Prasad, D. M. Aly, P. Almgren, Y. Wessman, N. Shaat, P. Spiegel, H. Mulder, E. Lindholm, O. Melander, O. Hansson, U. Malmqvist, A. Lernmark, K. Lahti, T. Forsen, T. Tuomi, A. H. Rosengren, and L. Groop. 2018. 'Novel subgroups of adult-onset diabetes and their association with outcomes: a data-driven cluster analysis of six variables', *Lancet Diabetes Endocrinol*, 6: 361-69.
- Ahren, J., B. Ahren, and N. Wierup. 2010. 'Increased beta-cell volume in mice fed a high-fat diet: a dynamic study over 12 months', *Islets*, 2: 353-6.
- Akhaury, K., and S. Chaware. 2022. 'Relation Between Diabetes and Psychiatric Disorders', *Cureus*, 14: e30733.
- Al Bitar, S., and H. Gali-Muhtasib. 2019. 'The Role of the Cyclin Dependent Kinase Inhibitor p21(cip1/waf1) in Targeting Cancer: Molecular Mechanisms and Novel Therapeutics', *Cancers (Basel)*, 11.
- Altenhofen, D., J. M. Khuong, T. Kuhn, S. Lebek, S. Gorigk, K. Kaiser, C. Binsch, K. Griess, B. Knebel, B. F. Belgardt, S. Cames, S. Eickelschulte, T. Stermann, A. Rasche, R. Herwig, J. Weiss, H. Vogel, A. Schurmann, A. Chadt, and H. Al-Hasani. 2023. 'E96V Mutation in the Kdelr3 Gene Is Associated with Type 2 Diabetes Susceptibility in Obese NZO Mice', *Int J Mol Sci*, 24.
- Amero, C. D., W. P. Boomersshine, Y. Xu, and M. Foster. 2008. 'Solution structure of Pyrococcus furiosus RPP21, a component of the archaeal RNase P holoenzyme, and interactions with its RPP29 protein partner', *Biochemistry*, 47: 11704-10.
- Anderson, M. S., and J. A. Bluestone. 2005. 'The NOD mouse: a model of immune dysregulation', *Annu Rev Immunol*, 23: 447-85.

- Arroyo, Maria Nicol, Jonathan Alex Green, Miriam Cnop, and Mariana Igoillo-Esteve. 2021. 'tRNA Biology in the Pathogenesis of Diabetes: Role of Genetic and Environmental Factors', *International Journal of Molecular Sciences*, 22: 496.
- Asahara, S., T. Matsuda, Y. Kido, and M. Kasuga. 2009. 'Increased ribosomal biogenesis induces pancreatic beta cell failure in mice model of type 2 diabetes', *Biochem Biophys Res Commun*, 381: 367-71.
- Asplund, O., P. Storm, V. Chandra, G. Hatem, E. Ottosson-Laakso, D. Mansour-Aly, U. Krus, H. Ibrahim, E. Ahlqvist, T. Tuomi, E. Renstrom, O. Korsgren, N. Wierup, M. Ibberson, M. Solimena, P. Marchetti, C. Wollheim, I. Artner, H. Mulder, O. Hansson, T. Otonkoski, L. Groop, and R. B. Prasad. 2022. 'Islet Gene View-a tool to facilitate islet research', *Life Sci Alliance*, 5.
- Aubrey, B. J., G. L. Kelly, A. Janic, M. J. Herold, and A. Strasser. 2018. 'How does p53 induce apoptosis and how does this relate to p53-mediated tumour suppression?', *Cell Death Differ*, 25: 104-13.
- Baba, Y., M. Nakano, Y. Yamada, I. Saito, and Y. Kanegae. 2005. 'Practical range of effective dose for Cre recombinase-expressing recombinant adenovirus without cell toxicity in mammalian cells', *Microbiol Immunol*, 49: 559-70.
- Babaya, N., M. Nakayama, H. Moriyama, R. Gianani, T. Still, D. Miao, L. Yu, J. C. Hutton, and G. S. Eisenbarth. 2006. 'A new model of insulin-deficient diabetes: male NOD mice with a single copy of Ins1 and no Ins2', *Diabetologia*, 49: 1222-8.
- Banday, M. Z., A. S. Sameer, and S. Nissar. 2020. 'Pathophysiology of diabetes: An overview', *Avicenna J Med*, 10: 174-88.
- Bankhead, P., M. B. Loughrey, J. A. Fernandez, Y. Dombrowski, D. G. McArt, P. D. Dunne, S. McQuaid, R. T. Gray, L. J. Murray, H. G. Coleman, J. A. James, M. Salto-Tellez, and P. W. Hamilton. 2017. 'QuPath: Open source software for digital pathology image analysis', *Sci Rep*, 7: 16878.
- Banting, F. G., and C. H. Best. 1922. 'Nutrition classics. The Journal of Laboratory and Clinical Medicine, Vol. VII, 1922: The internal secretion of the pancreas. By F. G. Banting, and C. H. Best', *Nutr Rev*, 45: 55-7.
- Barrabi, C., K. Zhang, M. Liu, and X. Chen. 2023. 'Pancreatic beta cell ER export in health and diabetes', *Front Endocrinol (Lausanne)*, 14: 1155779.
- Barsby, Tom, and Timo Otonkoski. 2022. 'Maturation of beta cells: lessons from in vivo and in vitro models', *Diabetologia*, 65: 917-30.
- Basile, G., R. N. Kulkarni, and N. G. Morgan. 2019. 'How, When, and Where Do Human beta-Cells Regenerate?', *Curr Diab Rep*, 19: 48.
- Beli, P., N. Lukashchuk, S. A. Wagner, B. T. Weinert, J. V. Olsen, L. Baskcomb, M. Mann, S. P. Jackson, and C. Choudhary. 2012. 'Proteomic investigations reveal a role for RNA processing factor THRAP3 in the DNA damage response', *Mol Cell*, 46: 212-25.
- Bich, L., M. Mossio, and A. M. Soto. 2020. 'Glycemia Regulation: From Feedback Loops to Organizational Closure', *Front Physiol*, 11: 69.
- Birkenfeld, A. L., and V. Mohan. 2024. 'Prediabetes remission for type 2 diabetes mellitus prevention', *Nat Rev Endocrinol*.
- Bonner-Weir, S. 2021. 'New evidence for adult beta cell neogenesis', *Cell Stem Cell*, 28: 1889-90.
- Borges, H. L., R. Linden, and J. Y. Wang. 2008. 'DNA damage-induced cell death: lessons from the central nervous system', *Cell Res*, 18: 17-26.
- Brawerman, G., J. Pipella, and P. J. Thompson. 2022. 'DNA damage to beta cells in culture recapitulates features of senescent beta cells that accumulate in type 1 diabetes', *Mol Metab*, 62: 101524.
- Bray, N. L., H. Pimentel, P. Melsted, and L. Pachter. 2016. 'Near-optimal probabilistic RNA-seq quantification', *Nat Biotechnol*, 34: 525-7.

- Brownrigg, G. P., Y. H. Xia, C. M. J. Chu, S. Wang, C. Chao, J. A. Zhang, S. Skovso, E. Panzhinskiy, X. Hu, J. D. Johnson, and E. J. Rideout. 2023. 'Sex differences in islet stress responses support female beta cell resilience', *Mol Metab*, 69: 101678.
- Cantley, J., and D. Eizirik. 2021. '100 YEARS OF INSULIN: 100 years of insulin: progress, current perspectives and future challenges', *J Endocrinol*, 252: E1-E3.
- Cerf, M. E. 2013. 'Beta cell dysfunction and insulin resistance', *Front Endocrinol (Lausanne)*, 4: 37.
- Cha, J., C. Aguayo-Mazzucato, and P. J. Thompson. 2023. 'Pancreatic beta-cell senescence in diabetes: mechanisms, markers and therapies', *Front Endocrinol (Lausanne)*, 14: 1212716.
- Chadt, A., and H. Al-Hasani. 2020. 'Glucose transporters in adipose tissue, liver, and skeletal muscle in metabolic health and disease', *Pflugers Arch*, 472: 1273-98.
- Chadt, A., K. Leicht, A. Deshmukh, L. Q. Jiang, S. Scherneck, U. Bernhardt, T. Dreja, H. Vogel, K. Schmolz, R. Kluge, J. R. Zierath, C. Hultschig, R. C. Hoeben, A. Schurmann, H. G. Joost, and H. Al-Hasani. 2008. 'Tbc1d1 mutation in lean mouse strain confers leanness and protects from diet-induced obesity', *Nat Genet*, 40: 1354-9.
- Champy, M. F., M. Selloum, V. Zeitler, C. Caradec, B. Jung, S. Rousseau, L. Pouilly, T. Sorg, and J. Auwerx. 2008. 'Genetic background determines metabolic phenotypes in the mouse', *Mamm Genome*, 19: 318-31.
- Chen, C., C. M. Cohrs, J. Stertmann, R. Bozsak, and S. Speier. 2017. 'Human beta cell mass and function in diabetes: Recent advances in knowledge and technologies to understand disease pathogenesis', *Mol Metab*, 6: 943-57.
- Chen, D., T. C. Thayer, L. Wen, and F. S. Wong. 2020. 'Mouse Models of Autoimmune Diabetes: The Nonobese Diabetic (NOD) Mouse', *Methods Mol Biol*, 2128: 87-92.
- Cheng, M., L. Ren, X. Jia, J. Wang, and B. Cong. 2024. 'Understanding the action mechanisms of metformin in the gastrointestinal tract', *Front Pharmacol*, 15: 1347047.
- Chentoufi, A. A., and C. Polychronakos. 2002. 'Insulin expression levels in the thymus modulate insulin-specific autoreactive T-cell tolerance: the mechanism by which the IDDM2 locus may predispose to diabetes', *Diabetes*, 51: 1383-90.
- Chu, S., J. M. Zengel, and L. Lindahl. 1997. 'A novel protein shared by RNase MRP and RNase P', *RNA*, 3: 382-91.
- Cnop, M., N. Welsh, J. C. Jonas, A. Jorns, S. Lenzen, and D. L. Eizirik. 2005. 'Mechanisms of pancreatic beta-cell death in type 1 and type 2 diabetes: many differences, few similarities', *Diabetes*, 54 Suppl 2: S97-107.
- Cohen, A., R. Reiner, and N. Jarrous. 2003. 'Alterations in the intracellular level of a protein subunit of human RNase P affect processing of tRNA precursors', *Nucleic Acids Res*, 31: 4836-46.
- Cosentino, C., M. Cnop, and M. Igoillo-Esteve. 2019. 'The tRNA Epitranscriptome and Diabetes: Emergence of tRNA Hypomodifications as a Cause of Pancreatic beta-Cell Failure', *Endocrinology*, 160: 1262-74.
- Cosentino, C., S. Toivonen, E. Diaz Villamil, M. Atta, J. L. Ravanat, S. Demine, A. A. Schiavo, N. Pachera, J. P. Deglasse, J. C. Jonas, D. Balboa, T. Otonkoski, E. R. Pearson, P. Marchetti, D. L. Eizirik, M. Cnop, and M. Igoillo-Esteve. 2018. 'Pancreatic beta-cell tRNA hypomethylation and fragmentation link TRMT10A deficiency with diabetes', *Nucleic Acids Res*, 46: 10302-18.
- Dadheech, N., A. Srivastava, R. G. Shah, G. M. Shah, and S. Gupta. 2022. 'Role of poly(ADP-ribose) polymerase-1 in regulating human islet cell differentiation', *Sci Rep*, 12: 21496.

- Daniels Gatward, L. F., M. R. Kennard, L. I. F. Smith, and A. J. F. King. 2021. 'The use of mice in diabetes research: The impact of physiological characteristics, choice of model and husbandry practices', *Diabet Med*, 38: e14711.
- de Koning, E. J. P., and F. Carlotti. 2021. 'Stem cell-based islet replacement therapy in diabetes: A road trip that reached the clinic', *Cell Stem Cell*, 28: 2044-46.
- De Paoli, M., A. Zakharia, and G. H. Werstuck. 2021. 'The Role of Estrogen in Insulin Resistance: A Review of Clinical and Preclinical Data', *Am J Pathol*, 191: 1490-98.
- Del Prato, S. 2003. 'Loss of early insulin secretion leads to postprandial hyperglycaemia', *Diabetologia*, 46 Suppl 1: M2-8.
- Dewanjee, S., S. Das, A. K. Das, N. Bhattacharjee, A. Dihingia, T. K. Dua, J. Kalita, and P. Manna. 2018. 'Molecular mechanism of diabetic neuropathy and its pharmacotherapeutic targets', *Eur J Pharmacol*, 833: 472-523.
- Dinic, S., J. Arambasic Jovanovic, A. Uskokovic, M. Mihailovic, N. Grdovic, A. Tolic, J. Rajic, M. Dordevic, and M. Vidakovic. 2022. 'Oxidative stress-mediated beta cell death and dysfunction as a target for diabetes management', *Front Endocrinol (Lausanne)*, 13: 1006376.
- Dittrich, H. M. 1989. '[History of the discovery of pancreatic diabetes by von Mering and Minkowski 1889. A historical overview on the occasion of the 100th anniversary]', *Z Gesamte Inn Med*, 44: 335-40.
- Dominguez-Oliva, A., I. Hernandez-Avalos, J. Martinez-Burnes, A. Olmos-Hernandez, A. Verduzco-Mendoza, and D. Mota-Rojas. 2023. 'The Importance of Animal Models in Biomedical Research: Current Insights and Applications', *Animals (Basel)*, 13.
- Dooley, J., L. Tian, S. Schonefeldt, V. Delghingaro-Augusto, J. E. Garcia-Perez, E. Pasciuto, D. Di Marino, E. J. Carr, N. Oskolkov, V. Lyssenko, D. Franckaert, V. Lagou, L. Overbergh, J. Vandebussche, J. Allemeersch, G. Chabot-Roy, J. E. Dahlstrom, D. R. Laybutt, N. Petrovsky, L. Socha, K. Gevaert, A. M. Jetten, D. Lambrechts, M. A. Linterman, C. C. Goodnow, C. J. Nolan, S. Lesage, S. M. Schlenner, and A. Liston. 2016. 'Genetic predisposition for beta cell fragility underlies type 1 and type 2 diabetes', *Nat Genet*, 48: 519-27.
- Dor, Y., J. Brown, O. I. Martinez, and D. A. Melton. 2004. 'Adult pancreatic beta-cells are formed by self-duplication rather than stem-cell differentiation', *Nature*, 429: 41-6.
- Drews, G., P. Krippeit-Drews, and M. Dufer. 2010. 'Oxidative stress and beta-cell dysfunction', *Pflugers Arch*, 460: 703-18.
- Dutta, S., and P. Sengupta. 2016. 'Men and mice: Relating their ages', *Life Sci*, 152: 244-8.
- Eledrisi, M. S., and A. N. Elzouki. 2020. 'Management of Diabetic Ketoacidosis in Adults: A Narrative Review', *Saudi J Med Med Sci*, 8: 165-73.
- Elmore, S. 2007. 'Apoptosis: a review of programmed cell death', *Toxicol Pathol*, 35: 495-516.
- ElSayed, N. A., G. Aleppo, V. R. Aroda, R. R. Bannuru, F. M. Brown, D. Bruemmer, B. S. Collins, M. E. Hilliard, D. Isaacs, E. L. Johnson, S. Kahan, K. Khunti, J. Leon, S. K. Lyons, M. L. Perry, P. Prahalad, R. E. Pratley, J. J. Seley, R. C. Stanton, R. A. Gabbay, and Association on behalf of the American Diabetes. 2023. '2. Classification and Diagnosis of Diabetes: Standards of Care in Diabetes-2023', *Diabetes Care*, 46: S19-S40.
- Esakova, O., and A. S. Krasilnikov. 2010. 'Of proteins and RNA: the RNase P/MRP family', *RNA*, 16: 1725-47.
- Ewels, P., M. Magnusson, S. Lundin, and M. Kaller. 2016. 'MultiQC: summarize analysis results for multiple tools and samples in a single report', *Bioinformatics*, 32: 3047-8.
- Fagerlund, R. D., A. Perederina, I. Berezin, and A. S. Krasilnikov. 2015. 'Footprinting analysis of interactions between the largest eukaryotic RNase P/MRP protein Pop1 and RNase P/MRP RNA components', *RNA*, 21: 1591-605.

- Fang, M., D. Wang, J. Coresh, and E. Selvin. 2021. 'Trends in Diabetes Treatment and Control in U.S. Adults, 1999-2018', *N Engl J Med*, 384: 2219-28.
- Farmaki, P., C. Damaskos, N. Garmpis, A. Garmpi, S. Savvanis, and E. Diamantis. 2020. 'Complications of the Type 2 Diabetes Mellitus', *Curr Cardiol Rev*, 16: 249-51.
- Fontaine, D. A., and D. B. Davis. 2016. 'Attention to Background Strain Is Essential for Metabolic Research: C57BL/6 and the International Knockout Mouse Consortium', *Diabetes*, 65: 25-33.
- Force, I. D. F. Clinical Guidelines Task. 2006. 'Global Guideline for Type 2 Diabetes: recommendations for standard, comprehensive, and minimal care', *Diabet Med*, 23: 579-93.
- Freeman, H. C., A. Hugill, N. T. Dear, F. M. Ashcroft, and R. D. Cox. 2006. 'Deletion of nicotinamide nucleotide transhydrogenase: a new quantitative trait locus accounting for glucose intolerance in C57BL/6J mice', *Diabetes*, 55: 2153-6.
- Freeman, H., K. Shimomura, E. Horner, R. D. Cox, and F. M. Ashcroft. 2006. 'Nicotinamide nucleotide transhydrogenase: a key role in insulin secretion', *Cell Metab*, 3: 35-45.
- Gao, T., B. McKenna, C. Li, M. Reichert, J. Nguyen, T. Singh, C. Yang, A. Pannikar, N. Doliba, T. Zhang, D. A. Stoffers, H. Edlund, F. Matschinsky, R. Stein, and B. Z. Stanger. 2014. 'Pdx1 maintains beta cell identity and function by repressing an alpha cell program', *Cell Metab*, 19: 259-71.
- Georgia, S., C. Hinault, D. Kawamori, J. Hu, J. Meyer, M. Kanji, A. Bhushan, and R. N. Kulkarni. 2010. 'Cyclin D2 is essential for the compensatory beta-cell hyperplastic response to insulin resistance in rodents', *Diabetes*, 59: 987-96.
- Ghosh, C., N. Das, S. Saha, T. Kundu, D. Sircar, and P. Roy. 2022. 'Involvement of Cdkal1 in the etiology of type 2 diabetes mellitus and microvascular diabetic complications: a review', *J Diabetes Metab Disord*, 21: 991-1001.
- Goke, B. 2008. 'Islet cell function: alpha and beta cells--partners towards normoglycaemia', *Int J Clin Pract Suppl*: 2-7.
- Goyal, S., J. Rani, M. A. Bhat, and V. Vanita. 2023. 'Genetics of diabetes', *World J Diabetes*, 14: 656-79.
- Gradwohl, G., A. Dierich, M. LeMeur, and F. Guillemot. 2000. 'neurogenin3 is required for the development of the four endocrine cell lineages of the pancreas', *Proc Natl Acad Sci U S A*, 97: 1607-11.
- Gribben, C., C. Lambert, H. A. Messal, E. L. Hubber, C. Rackham, I. Evans, H. Heimberg, P. Jones, R. Sancho, and A. Behrens. 2021. 'Ductal Ngn3-expressing progenitors contribute to adult beta cell neogenesis in the pancreas', *Cell Stem Cell*, 28: 2000-08 e4.
- Guerrier-Takada, C., K. Gardiner, T. Marsh, N. Pace, and S. Altman. 1983. 'The RNA moiety of ribonuclease P is the catalytic subunit of the enzyme', *Cell*, 35: 849-57.
- Guo, S., C. Dai, M. Guo, B. Taylor, J. S. Harmon, M. Sander, R. P. Robertson, A. C. Powers, and R. Stein. 2013. 'Inactivation of specific beta cell transcription factors in type 2 diabetes', *J Clin Invest*, 123: 3305-16.
- Guo, W., N. A. Tzioutziou, G. Stephen, I. Milne, C. P. Calixto, R. Waugh, J. W. S. Brown, and R. Zhang. 2021. '3D RNA-seq: a powerful and flexible tool for rapid and accurate differential expression and alternative splicing analysis of RNA-seq data for biologists', *RNA Biol*, 18: 1574-87.
- Gupta, S., S. Acharya, and S. Shukla. 2022. 'A Look Into the Next Century After 100 Years of Insulin', *Cureus*, 14: e30133.
- Gutgesell, R. M., R. Nogueiras, M. H. Tschop, and T. D. Muller. 2024. 'Dual and Triple Incretin-Based Co-agonists: Novel Therapeutics for Obesity and Diabetes', *Diabetes Ther*.

- Gutierrez, G. D., A. S. Bender, V. Cirulli, T. L. Mastracci, S. M. Kelly, A. Tsirigos, K. H. Kaestner, and L. Sussel. 2017. 'Pancreatic beta cell identity requires continual repression of non-beta cell programs', *J Clin Invest*, 127: 244-59.
- Hamilton, D. L., and K. Abremski. 1984. 'Site-specific recombination by the bacteriophage P1 lox-Cre system. Cre-mediated synapsis of two lox sites', *J Mol Biol*, 178: 481-6.
- Hanafusa, T., and A. Imagawa. 2007. 'Fulminant type 1 diabetes: a novel clinical entity requiring special attention by all medical practitioners', *Nat Clin Pract Endocrinol Metab*, 3: 36-45; quiz 2p following 69.
- Harreiter, J., and M. Roden. 2023. '[Diabetes mellitus: definition, classification, diagnosis, screening and prevention (Update 2023)]', *Wien Klin Wochenschr*, 135: 7-17.
- Herwig, R., C. Hardt, M. Lienhard, and A. Kamburov. 2016. 'Analyzing and interpreting genome data at the network level with ConsensusPathDB', *Nat Protoc*, 11: 1889-907.
- Hesselton, D., R. M. Anderson, M. Beinart, and D. Y. Stainier. 2009. 'Distinct populations of quiescent and proliferative pancreatic beta-cells identified by HOTcre mediated labeling', *Proc Natl Acad Sci U S A*, 106: 14896-901.
- Horwitz, E., L. Krogvold, S. Zhitomirsky, A. Swisa, M. Fischman, T. Lax, T. Dahan, N. Hurvitz, N. Weinberg-Corem, A. Klochender, A. C. Powers, M. Brissova, A. Jorns, S. Lenzen, B. Glaser, K. Dahl-Jorgensen, and Y. Dor. 2018. 'beta-Cell DNA Damage Response Promotes Islet Inflammation in Type 1 Diabetes', *Diabetes*, 67: 2305-18.
- Hou, J. C., L. Min, and J. E. Pessin. 2009. 'Insulin granule biogenesis, trafficking and exocytosis', *Vitam Horm*, 80: 473-506.
- Huang, W., L. J. Hickson, A. Eirin, J. L. Kirkland, and L. O. Lerman. 2022. 'Cellular senescence: the good, the bad and the unknown', *Nat Rev Nephrol*, 18: 611-27.
- Huerta Guevara, A. P., S. J. McGowan, M. Kazantzis, T. R. Stallons, T. Sano, N. L. Mulder, A. Jurdzinski, T. H. van Dijk, B. J. L. Eggen, J. W. Jonker, L. J. Niedernhofer, and J. K. Kruit. 2021. 'Increased insulin sensitivity and diminished pancreatic beta-cell function in DNA repair deficient Ercc1(d/-) mice', *Metabolism*, 117: 154711.
- Hull, R. L., K. Kodama, K. M. Utzschneider, D. B. Carr, R. L. Prigeon, and S. E. Kahn. 2005. 'Dietary-fat-induced obesity in mice results in beta cell hyperplasia but not increased insulin release: evidence for specificity of impaired beta cell adaptation', *Diabetologia*, 48: 1350-8.
- Hull, R. L., J. R. Willard, M. D. Struck, B. M. Barrow, G. S. Brar, S. Andrikopoulos, and S. Zraika. 2017. 'High fat feeding unmasks variable insulin responses in male C57BL/6 mouse substrains', *J Endocrinol*, 233: 53-64.
- Hummel, K. P., M. M. Dickie, and D. L. Coleman. 1966. 'Diabetes, a new mutation in the mouse', *Science*, 153: 1127-8.
- Ikegami, H., N. Babaya, and S. Noso. 2021. 'beta-Cell failure in diabetes: Common susceptibility and mechanisms shared between type 1 and type 2 diabetes', *J Diabetes Investig*, 12: 1526-39.
- Jackson, S. J., N. Andrews, D. Ball, I. Bellantuono, J. Gray, L. Hachoumi, A. Holmes, J. Latcham, A. Petrie, P. Potter, A. Rice, A. Ritchie, M. Stewart, C. Strepka, M. Yeoman, and K. Chapman. 2017. 'Does age matter? The impact of rodent age on study outcomes', *Lab Anim*, 51: 160-69.
- Jarrous, N. 2002. 'Human ribonuclease P: subunits, function, and intranuclear localization', *RNA*, 8: 1-7.
- Jarrous, N., P. S. Eder, D. Wesolowski, and S. Altman. 1999. 'Rpp14 and Rpp29, two protein subunits of human ribonuclease P', *RNA*, 5: 153-7.
- Jarrous, N., and F. Liu. 2023. 'Human RNase P: overview of a ribonuclease of interrelated molecular networks and gene-targeting systems', *RNA*, 29: 300-07.
- Jarrous, N., and R. Reiner. 2007. 'Human RNase P: a tRNA-processing enzyme and transcription factor', *Nucleic Acids Res*, 35: 3519-24.

- Jarrous, N., J. S. Wolenski, D. Wesolowski, C. Lee, and S. Altman. 1999. 'Localization in the nucleolus and coiled bodies of protein subunits of the ribonucleoprotein ribonuclease P', *J Cell Biol*, 146: 559-72.
- Jiang, T., and S. Altman. 2001. 'Protein-protein interactions with subunits of human nuclear RNase P', *Proc Natl Acad Sci U S A*, 98: 920-5.
- Jiang, T., C. Guerrier-Takada, and S. Altman. 2001. 'Protein-RNA interactions in the subunits of human nuclear RNase P', *RNA*, 7: 937-41.
- Jo, S., M. Beetch, E. Gustafson, A. Wong, E. Oribamise, G. Chung, S. Vadrevu, L. S. Satin, E. Bernal-Mizrachi, and E. U. Alejandro. 2023. 'Sex Differences in Pancreatic beta-Cell Physiology and Glucose Homeostasis in C57BL/6J Mice', *J Endocr Soc*, 7: bvad099.
- Jonas, W., O. Kluth, A. Helms, S. Voss, M. Jahnert, P. Gottmann, T. Speckmann, B. Knebel, A. Chadt, H. Al-Hasani, A. Schurmann, and H. Vogel. 2022. 'Identification of Novel Genes Involved in Hyperglycemia in Mice', *Int J Mol Sci*, 23.
- K. Flurkey, J. M. Curren, D.E. Harrison. 2007. 'Mouse Models in Aging Research', In *American College of Laboratory Animal Medicine, The Mouse in Biomedical Research (Second Edition)*, Academic Press., Chapter 20.
- Kamburov, A., C. Wierling, H. Lehrach, and R. Herwig. 2009. 'ConsensusPathDB--a database for integrating human functional interaction networks', *Nucleic Acids Res*, 37: D623-8.
- Kan, Y., X. Lu, L. Feng, X. Yang, H. Ma, J. Gong, and J. Yang. 2022. 'RPP30 is a novel diagnostic and prognostic biomarker for gastric cancer', *Front Genet*, 13: 888051.
- Kanehisa, M., and Y. Sato. 2020. 'KEGG Mapper for inferring cellular functions from protein sequences', *Protein Sci*, 29: 28-35.
- Kanehisa, M., Y. Sato, and M. Kawashima. 2022. 'KEGG mapping tools for uncovering hidden features in biological data', *Protein Sci*, 31: 47-53.
- Kaneto, H., G. Xu, N. Fujii, S. Kim, S. Bonner-Weir, and G. C. Weir. 2002. 'Involvement of c-Jun N-terminal kinase in oxidative stress-mediated suppression of insulin gene expression', *J Biol Chem*, 277: 30010-8.
- Kanev, P. B., A. Ategin, S. Stoyanov, and R. Aleksandrov. 2023. 'PARP1 roles in DNA repair and DNA replication: The basi(c)s of PARP inhibitor efficacy and resistance', *Semin Oncol*.
- Kayo, T., and A. Koizumi. 1998. 'Mapping of murine diabetogenic gene *mody* on chromosome 7 at D7Mit258 and its involvement in pancreatic islet and beta cell development during the perinatal period', *J Clin Invest*, 101: 2112-8.
- Kim, A., K. Miller, J. Jo, G. Kilimnik, P. Wojcik, and M. Hara. 2009. 'Islet architecture: A comparative study', *Islets*, 1: 129-36.
- Kim, H., M. Kim, S. K. Im, and S. Fang. 2018. 'Mouse Cre-LoxP system: general principles to determine tissue-specific roles of target genes', *Lab Anim Res*, 34: 147-59.
- Klein, S., A. Gastaldelli, H. Yki-Jarvinen, and P. E. Scherer. 2022. 'Why does obesity cause diabetes?', *Cell Metab*, 34: 11-20.
- Koeck, T., A. H. Olsson, M. D. Nitert, V. V. Sharoyko, C. Ladenvall, O. Kotova, E. Reiling, T. Ronn, H. Parikh, J. Taneera, J. G. Eriksson, M. D. Metodiev, N. G. Larsson, A. Balhuizen, H. Luthman, A. Stancakova, J. Kuusisto, M. Laakso, P. Poulsen, A. Vaag, L. Groop, V. Lyssenko, H. Mulder, and C. Ling. 2011. 'A common variant in TFB1M is associated with reduced insulin secretion and increased future risk of type 2 diabetes', *Cell Metab*, 13: 80-91.
- Kouzuma, Y., M. Mizoguchi, H. Takagi, H. Fukuhara, M. Tsukamoto, T. Numata, and M. Kimura. 2003. 'Reconstitution of archaeal ribonuclease P from RNA and four protein components', *Biochem Biophys Res Commun*, 306: 666-73.

- Kulkarni, A., C. Muralidharan, S. C. May, S. A. Tersey, and R. G. Mirmira. 2022. 'Inside the beta Cell: Molecular Stress Response Pathways in Diabetes Pathogenesis', *Endocrinology*, 164.
- Kulkarni, R. N., E. B. Mizrachi, A. G. Ocana, and A. F. Stewart. 2012. 'Human beta-cell proliferation and intracellular signaling: driving in the dark without a road map', *Diabetes*, 61: 2205-13.
- Kumari, R., and P. Jat. 2021. 'Mechanisms of Cellular Senescence: Cell Cycle Arrest and Senescence Associated Secretory Phenotype', *Front Cell Dev Biol*, 9: 645593.
- Laakso, M., and L. Fernandes Silva. 2022. 'Genetics of Type 2 Diabetes: Past, Present, and Future', *Nutrients*, 14.
- Lan, P., B. Zhou, M. Tan, S. Li, M. Cao, J. Wu, and M. Lei. 2020. 'Structural insight into precursor ribosomal RNA processing by ribonuclease MRP', *Science*, 369: 656-63.
- Lebovitz, H. E. 2019. 'Thiazolidinediones: the Forgotten Diabetes Medications', *Curr Diab Rep*, 19: 151.
- Leenders, F., N. Groen, N. de Graaf, M. A. Engelse, T. J. Rabelink, E. J. P. de Koning, and F. Carlotti. 2021. 'Oxidative Stress Leads to beta-Cell Dysfunction Through Loss of beta-Cell Identity', *Front Immunol*, 12: 690379.
- Lei, X. G., and M. Z. Vatamaniuk. 2011. 'Two tales of antioxidant enzymes on beta cells and diabetes', *Antioxid Redox Signal*, 14: 489-503.
- Leiter, E. H., P. C. Reifsnnyder, K. Flurkey, H. J. Partke, E. Junger, and L. Herberg. 1998. 'NIDDM genes in mice: deleterious synergism by both parental genomes contributes to diabetogenic thresholds', *Diabetes*, 47: 1287-95.
- Lenzen, S. 2008. 'The mechanisms of alloxan- and streptozotocin-induced diabetes', *Diabetologia*, 51: 216-26.
- Leroux, L., P. Desbois, L. Lamotte, B. Duvillie, N. Cordonnier, M. Jackerott, J. Jami, D. Bucchini, and R. L. Joshi. 2001. 'Compensatory responses in mice carrying a null mutation for Ins1 or Ins2', *Diabetes*, 50 Suppl 1: S150-3.
- Li, M., X. Chi, Y. Wang, S. Setrerrahmane, W. Xie, and H. Xu. 2022. 'Trends in insulin resistance: insights into mechanisms and therapeutic strategy', *Signal Transduct Target Ther*, 7: 216.
- Ling, C., and T. Ronn. 2019. 'Epigenetics in Human Obesity and Type 2 Diabetes', *Cell Metab*, 29: 1028-44.
- Liu, M., J. Sun, J. Cui, W. Chen, H. Guo, F. Barbetti, and P. Arvan. 2015. 'INS-gene mutations: from genetics and beta cell biology to clinical disease', *Mol Aspects Med*, 42: 3-18.
- Loonstra, A., M. Vooijs, H. B. Beverloo, B. A. Allak, E. van Drunen, R. Kanaar, A. Berns, and J. Jonkers. 2001. 'Growth inhibition and DNA damage induced by Cre recombinase in mammalian cells', *Proc Natl Acad Sci U S A*, 98: 9209-14.
- Lv, W., X. Wang, Q. Xu, and W. Lu. 2020. 'Mechanisms and Characteristics of Sulfonylureas and Glinides', *Curr Top Med Chem*, 20: 37-56.
- Lygerou, Z., P. Mitchell, E. Petfalski, B. Seraphin, and D. Tollervy. 1994. 'The POP1 gene encodes a protein component common to the RNase MRP and RNase P ribonucleoproteins', *Genes Dev*, 8: 1423-33.
- Maassen, J. A., T Hart LM, E. Van Essen, R. J. Heine, G. Nijpels, R. S. Jahangir Tafrechi, A. K. Raap, G. M. Janssen, and H. H. Lemkes. 2004. 'Mitochondrial diabetes: molecular mechanisms and clinical presentation', *Diabetes*, 53 Suppl 1: S103-9.
- Madisen, L., T. A. Zwingman, S. M. Sunkin, S. W. Oh, H. A. Zariwala, H. Gu, L. L. Ng, R. D. Palmiter, M. J. Hawrylycz, A. R. Jones, E. S. Lein, and H. Zeng. 2010. 'A robust and high-throughput Cre reporting and characterization system for the whole mouse brain', *Nat Neurosci*, 13: 133-40.

- Magee, R., and I. Rigoutsos. 2020. 'On the expanding roles of tRNA fragments in modulating cell behavior', *Nucleic Acids Res*, 48: 9433-48.
- Makino, S., K. Kunimoto, Y. Muraoka, Y. Mizushima, K. Katagiri, and Y. Tochino. 1980. 'Breeding of a non-obese, diabetic strain of mice', *Jikken Dobutsu*, 29: 1-13.
- Mann, H., Y. Ben-Asouli, A. Schein, S. Moussa, and N. Jarrous. 2003. 'Eukaryotic RNase P: role of RNA and protein subunits of a primordial catalytic ribonucleoprotein in RNA-based catalysis', *Mol Cell*, 12: 925-35.
- Mao, Z., M. Bozzella, A. Seluanov, and V. Gorbunova. 2008. 'Comparison of nonhomologous end joining and homologous recombination in human cells', *DNA Repair (Amst)*, 7: 1765-71.
- Markan, K. R., M. J. Jurczak, and M. J. Brady. 2010. 'Stranger in a strange land: roles of glycogen turnover in adipose tissue metabolism', *Mol Cell Endocrinol*, 318: 54-60.
- Martens, P. J., C. Gysemans, and C. Mathieu. 2021. '100 YEARS OF INSULIN: Arresting or curing type 1 diabetes: an elusive goal, but closing the gap', *J Endocrinol*, 249: T1-T11.
- Martin, A. N., and Y. Li. 2007. 'RNase MRP RNA and human genetic diseases', *Cell Res*, 17: 219-26.
- Mauvais-Jarvis, F. 2015. 'Sex differences in metabolic homeostasis, diabetes, and obesity', *Biol Sex Differ*, 6: 14.
- Meigs, J. B., L. A. Cupples, and P. W. Wilson. 2000. 'Parental transmission of type 2 diabetes: the Framingham Offspring Study', *Diabetes*, 49: 2201-7.
- Mekada, K., and A. Yoshiki. 2021. 'Substrains matter in phenotyping of C57BL/6 mice', *Exp Anim*, 70: 145-60.
- Merino, B., and M. Garcia-Arevalo. 2021. 'Sexual hormones and diabetes: The impact of estradiol in pancreatic beta cell', *Int Rev Cell Mol Biol*, 359: 81-138.
- Mi, H., A. Muruganujan, and P. D. Thomas. 2013. 'PANTHER in 2013: modeling the evolution of gene function, and other gene attributes, in the context of phylogenetic trees', *Nucleic Acids Res*, 41: D377-86.
- Moin, A. S. M., and A. E. Butler. 2019. 'Alterations in Beta Cell Identity in Type 1 and Type 2 Diabetes', *Curr Diab Rep*, 19: 83.
- Molla-Herman, A., A. M. Valles, C. Ganem-Elbaz, C. Antoniewski, and J. R. Huynh. 2015. 'tRNA processing defects induce replication stress and Chk2-dependent disruption of piRNA transcription', *EMBO J*, 34: 3009-27.
- Moriyama, H., N. Abiru, J. Paronen, K. Sikora, E. Liu, D. Miao, D. Devendra, J. Beilke, R. Gianani, R. G. Gill, and G. S. Eisenbarth. 2003. 'Evidence for a primary islet autoantigen (preproinsulin 1) for insulinitis and diabetes in the nonobese diabetic mouse', *Proc Natl Acad Sci U S A*, 100: 10376-81.
- Mukherjee, N., L. Lin, C. J. Contreras, and A. T. Templin. 2021. 'beta-Cell Death in Diabetes: Past Discoveries, Present Understanding, and Potential Future Advances', *Metabolites*, 11.
- Mundlos, Stefan, Mariana Igoillo-Esteve, Anne Genin, Nelle Lambert, Julie Désir, Isabelle Pirson, Baroj Abdulkarim, Nicolas Simonis, Anais Drielsma, Lorella Marselli, Piero Marchetti, Pierre Vanderhaeghen, Décio L. Eizirik, Wim Wuyts, Cécile Julier, Ali J. Chakera, Sian Ellard, Andrew T. Hattersley, Marc Abramowicz, and Miriam Cnop. 2013. 'tRNA Methyltransferase Homolog Gene TRMT10A Mutation in Young Onset Diabetes and Primary Microcephaly in Humans', *PLoS Genetics*, 9.
- Muzzin, P., R. C. Eisensmith, K. C. Copeland, and S. L. Woo. 1996. 'Correction of obesity and diabetes in genetically obese mice by leptin gene therapy', *Proc Natl Acad Sci U S A*, 93: 14804-8.
- Nagy, A. 2000. 'Cre recombinase: the universal reagent for genome tailoring', *Genesis*, 26: 99-109.

- Natrajan, R., A. Mackay, P. M. Wilkerson, M. B. Lambros, D. Wetterskog, M. Arnedos, K. K. Shiu, F. C. Geyer, A. Langerod, B. Kreike, F. Reyat, H. M. Horlings, M. J. van de Vijver, J. Palacios, B. Weigelt, and J. S. Reis-Filho. 2012. 'Functional characterization of the 19q12 amplicon in grade III breast cancers', *Breast Cancer Res*, 14: R53.
- Newhart, A., S. L. Powers, P. K. Shastrula, I. Sierra, L. M. Joo, J. E. Hayden, A. R. Cohen, and S. M. Janicki. 2016. 'RNase P protein subunit Rpp29 represses histone H3.3 nucleosome deposition', *Mol Biol Cell*, 27: 1154-69.
- Nishimura, W., T. Kondo, T. Salameh, I. El Khattabi, R. Dodge, S. Bonner-Weir, and A. Sharma. 2006. 'A switch from MafB to MafA expression accompanies differentiation to pancreatic beta-cells', *Dev Biol*, 293: 526-39.
- Ohn, J. H., S. H. Kwak, Y. M. Cho, S. Lim, H. C. Jang, K. S. Park, and N. H. Cho. 2016. '10-year trajectory of beta-cell function and insulin sensitivity in the development of type 2 diabetes: a community-based prospective cohort study', *Lancet Diabetes Endocrinol*, 4: 27-34.
- Omar-Hmeadi, M., and O. Idevall-Hagren. 2021. 'Insulin granule biogenesis and exocytosis', *Cell Mol Life Sci*, 78: 1957-70.
- Oyadomari, S., A. Koizumi, K. Takeda, T. Gotoh, S. Akira, E. Araki, and M. Mori. 2002. 'Targeted disruption of the Chop gene delays endoplasmic reticulum stress-mediated diabetes', *J Clin Invest*, 109: 525-32.
- Paredes-Flores, M. A., N. Rahimi, and S. S. Mohiuddin. 2025. 'Biochemistry, Glycogenolysis.' in, *StatPearls* (Treasure Island (FL)).
- Patil, M., N. Pabla, and Z. Dong. 2013. 'Checkpoint kinase 1 in DNA damage response and cell cycle regulation', *Cell Mol Life Sci*, 70: 4009-21.
- Paul, P. K., M. E. Rabaglia, C. Y. Wang, D. S. Stapleton, N. Leng, C. Kendzioriski, P. W. Lewis, M. P. Keller, and A. D. Attie. 2016. 'Histone chaperone ASF1B promotes human beta-cell proliferation via recruitment of histone H3.3', *Cell Cycle*, 15: 3191-202.
- Pavlo, Petakh, I. Kamyshna, and A. Kamyshnyi. 2023. 'Effects of metformin on the gut microbiota: A systematic review', *Mol Metab*, 77: 101805.
- Phillips, D. I., P. M. Clark, C. N. Hales, and C. Osmond. 1994. 'Understanding oral glucose tolerance: comparison of glucose or insulin measurements during the oral glucose tolerance test with specific measurements of insulin resistance and insulin secretion', *Diabet Med*, 11: 286-92.
- Popoviciu, M. S., N. Kaka, Y. Sethi, N. Patel, H. Chopra, and S. Cavalu. 2023. 'Type 1 Diabetes Mellitus and Autoimmune Diseases: A Critical Review of the Association and the Application of Personalized Medicine', *J Pers Med*, 13.
- Prasad, R. B., and L. Groop. 2015. 'Genetics of type 2 diabetes-pitfalls and possibilities', *Genes (Basel)*, 6: 87-123.
- Prystupa, K., G. E. Delgado, A. P. Moissl, M. E. Kleber, A. L. Birkenfeld, M. Heni, A. Fritsche, W. Marz, and R. Wagner. 2023. 'Clusters of prediabetes and type 2 diabetes stratify all-cause mortality in a cohort of participants undergoing invasive coronary diagnostics', *Cardiovasc Diabetol*, 22: 211.
- Pugach, E. K., P. A. Richmond, J. G. Azofeifa, R. D. Dowell, and L. A. Leinwand. 2015. 'Prolonged Cre expression driven by the alpha-myosin heavy chain promoter can be cardiotoxic', *J Mol Cell Cardiol*, 86: 54-61.
- Qiu, S., and J. Huang. 2021. 'MRN complex is an essential effector of DNA damage repair', *J Zhejiang Univ Sci B*, 22: 31-37.
- Ramzy, A., D. M. Thompson, K. A. Ward-Hartstonge, S. Ivison, L. Cook, R. V. Garcia, J. Loyal, P. T. W. Kim, G. L. Warnock, M. K. Levings, and T. J. Kieffer. 2021. 'Implanted pluripotent stem-cell-derived pancreatic endoderm cells secrete glucose-responsive C-peptide in patients with type 1 diabetes', *Cell Stem Cell*, 28: 2047-61 e5.

- Rashbrook, V. S., J. T. Brash, and C. Ruhrberg. 2022. 'Cre toxicity in mouse models of cardiovascular physiology and disease', *Nat Cardiovasc Res*, 1: 806-16.
- Ray Chaudhuri, A., and A. Nussenzweig. 2017. 'The multifaceted roles of PARP1 in DNA repair and chromatin remodelling', *Nat Rev Mol Cell Biol*, 18: 610-21.
- Ray-Gallet, D., and G. Almouzni. 2021. 'The Histone H3 Family and Its Deposition Pathways', *Adv Exp Med Biol*, 1283: 17-42.
- Redondo, M. J., and N. G. Morgan. 2023. 'Heterogeneity and endotypes in type 1 diabetes mellitus', *Nat Rev Endocrinol*, 19: 542-54.
- Reiner, R., N. Alfiya-Mor, M. Berrebi-Demma, D. Wesolowski, S. Altman, and N. Jarrous. 2011. 'RNA binding properties of conserved protein subunits of human RNase P', *Nucleic Acids Res*, 39: 5704-14.
- Rena, G., D. G. Hardie, and E. R. Pearson. 2017. 'The mechanisms of action of metformin', *Diabetologia*, 60: 1577-85.
- Riant, E., A. Waget, H. Cogo, J. F. Arnal, R. Burcelin, and P. Gourdy. 2009. 'Estrogens protect against high-fat diet-induced insulin resistance and glucose intolerance in mice', *Endocrinology*, 150: 2109-17.
- Rieck, S., and K. H. Kaestner. 2010. 'Expansion of beta-cell mass in response to pregnancy', *Trends Endocrinol Metab*, 21: 151-8.
- Ritchie, M. E., B. Phipson, D. Wu, Y. Hu, C. W. Law, W. Shi, and G. K. Smyth. 2015. 'limma powers differential expression analyses for RNA-sequencing and microarray studies', *Nucleic Acids Res*, 43: e47.
- Robinson, K. M., and M. C. Schultz. 2003. 'Replication-independent assembly of nucleosome arrays in a novel yeast chromatin reconstitution system involves antisilencing factor Asf1p and chromodomain protein Chd1p', *Mol Cell Biol*, 23: 7937-46.
- Roden, Michael, and Gerald I. Shulman. 2019. 'The integrative biology of type 2 diabetes', *Nature*, 576: 51-60.
- Roder, P. V., B. Wu, Y. Liu, and W. Han. 2016. 'Pancreatic regulation of glucose homeostasis', *Exp Mol Med*, 48: e219.
- Rodger, W. 1991a. 'Insulin-dependent (type I) diabetes mellitus', *CMAJ*, 145: 1227-37.
- . 1991b. 'Non-insulin-dependent (type II) diabetes mellitus', *CMAJ*, 145: 1571-81.
- Rogakou, E. P., W. Nieves-Neira, C. Boon, Y. Pommier, and W. M. Bonner. 2000. 'Initiation of DNA fragmentation during apoptosis induces phosphorylation of H2AX histone at serine 139', *J Biol Chem*, 275: 9390-5.
- Rogakou, E. P., D. R. Pilch, A. H. Orr, V. S. Ivanova, and W. M. Bonner. 1998. 'DNA double-stranded breaks induce histone H2AX phosphorylation on serine 139', *J Biol Chem*, 273: 5858-68.
- Rorsman, P., and F. M. Ashcroft. 2018. 'Pancreatic beta-Cell Electrical Activity and Insulin Secretion: Of Mice and Men', *Physiol Rev*, 98: 117-214.
- Rosen, B., J. Schick, and W. Wurst. 2015. 'Beyond knockouts: the International Knockout Mouse Consortium delivers modular and evolving tools for investigating mammalian genes', *Mamm Genome*, 26: 456-66.
- Rossmannith, W., P. Giege, and R. K. Hartmann. 2024. 'Discovery, structure, mechanisms, and evolution of protein-only RNase P enzymes', *J Biol Chem*, 300: 105731.
- Roy, R., J. Chun, and S. N. Powell. 2011. 'BRCA1 and BRCA2: different roles in a common pathway of genome protection', *Nat Rev Cancer*, 12: 68-78.
- Saisho, Y. 2020. 'SGLT2 Inhibitors: the Star in the Treatment of Type 2 Diabetes?', *Diseases*, 8.
- Salinno, Cota, Ponce Bastidas, Medina Tarquis, Lickert, and Bakhti. 2019. 'β-Cell Maturation and Identity in Health and Disease', *International Journal of Molecular Sciences*, 20: 5417.

- Sanger, F., and E. O. Thompson. 1953. 'The amino-acid sequence in the glycol chain of insulin. I. The identification of lower peptides from partial hydrolysates', *Biochem J*, 53: 353-66.
- Santoro, A., T. E. McGraw, and B. B. Kahn. 2021. 'Insulin action in adipocytes, adipose remodeling, and systemic effects', *Cell Metab*, 33: 748-57.
- Schallschmidt, T., S. Lebek, D. Altenhofen, M. Damen, Y. Schulte, B. Knebel, R. Herwig, A. Rasche, T. Stermann, A. Kamitz, N. Hallahan, M. Jahnert, H. Vogel, A. Schurmann, A. Chadt, and H. Al-Hasani. 2018. 'Two Novel Candidate Genes for Insulin Secretion Identified by Comparative Genomics of Multiple Backcross Mouse Populations', *Genetics*, 210: 1527-42.
- Scherneck, S., H. Vogel, M. Nestler, R. Kluge, A. Schurmann, and H. G. Joost. 2010. 'Role of zinc finger transcription factor *zfp69* in body fat storage and diabetes susceptibility of mice', *Results Probl Cell Differ*, 52: 57-68.
- Schindelin, J., I. Arganda-Carreras, E. Frise, V. Kaynig, M. Longair, T. Pietzsch, S. Preibisch, C. Rueden, S. Saalfeld, B. Schmid, J. Y. Tinevez, D. J. White, V. Hartenstein, K. Eliceiri, P. Tomancak, and A. Cardona. 2012. 'Fiji: an open-source platform for biological-image analysis', *Nat Methods*, 9: 676-82.
- Scott, L. J., K. L. Mohlke, L. L. Bonnycastle, C. J. Willer, Y. Li, W. L. Duren, M. R. Erdos, H. M. Stringham, P. S. Chines, A. U. Jackson, L. Prokunina-Olsson, C. J. Ding, A. J. Swift, N. Narisu, T. Hu, R. Pruim, R. Xiao, X. Y. Li, K. N. Conneely, N. L. Riebow, A. G. Sprau, M. Tong, P. P. White, K. N. Hetrick, M. W. Barnhart, C. W. Bark, J. L. Goldstein, L. Watkins, F. Xiang, J. Saramies, T. A. Buchanan, R. M. Watanabe, T. T. Valle, L. Kinnunen, G. R. Abecasis, E. W. Pugh, K. F. Doheny, R. N. Bergman, J. Tuomilehto, F. S. Collins, and M. Boehnke. 2007. 'A genome-wide association study of type 2 diabetes in Finns detects multiple susceptibility variants', *Science*, 316: 1341-5.
- Sharin, E., A. Schein, H. Mann, Y. Ben-Asouli, and N. Jarrous. 2005. 'RNase P: role of distinct protein cofactors in tRNA substrate recognition and RNA-based catalysis', *Nucleic Acids Res*, 33: 5120-32.
- Sharoyko, V. V., M. Abels, J. Sun, L. M. Nicholas, I. G. Mollet, J. A. Stamenkovic, I. Gohring, S. Malmgren, P. Storm, J. Fadista, P. Spegel, M. D. Metodiev, N. G. Larsson, L. Eliasson, N. Wierup, and H. Mulder. 2014. 'Loss of TFB1M results in mitochondrial dysfunction that leads to impaired insulin secretion and diabetes', *Hum Mol Genet*, 23: 5733-49.
- Shastrula, P. K., P. J. Lund, B. A. Garcia, and S. M. Janicki. 2018. 'Rpp29 regulates histone H3.3 chromatin assembly through transcriptional mechanisms', *J Biol Chem*, 293: 12360-77.
- Shaukat, A. N., E. G. Kaliatsi, I. Skeparnias, and C. Stathopoulos. 2021. 'The Dynamic Network of RNP RNase P Subunits', *Int J Mol Sci*, 22.
- Shibata, A., and P. A. Jeggo. 2021. 'ATM's Role in the Repair of DNA Double-Strand Breaks', *Genes (Basel)*, 12.
- Siersbaek, M. S., N. Ditzel, E. K. Hejbol, S. M. Praestholm, L. K. Markussen, F. Avolio, L. Li, L. Lehtonen, A. K. Hansen, H. D. Schroder, L. Krych, S. Mandrup, L. Langhorn, P. Bollen, and L. Grontved. 2020. 'C57BL/6J substrain differences in response to high-fat diet intervention', *Sci Rep*, 10: 14052.
- Silva, I. B. B., C. H. Kimura, V. P. Colantoni, and M. C. Sogayar. 2022. 'Stem cells differentiation into insulin-producing cells (IPCs): recent advances and current challenges', *Stem Cell Res Ther*, 13: 309.
- Singh, G., M. Krauthamer, and M. Bjälme-Evans. 2022. 'Wegovy (semaglutide): a new weight loss drug for chronic weight management', *J Investig Med*, 70: 5-13.

- Singh, R., M. Gholipourmalekabadi, and S. H. Shafikhani. 2024. 'Animal models for type 1 and type 2 diabetes: advantages and limitations', *Front Endocrinol (Lausanne)*, 15: 1359685.
- Skarnes. 2011. 'A conditional knockout resource for the genome-wide study of mouse gene function'.
- Skovso, S., P. Overby, J. Memar-Zadeh, J. T. C. Lee, J. C. C. Yang, I. Shanina, V. Sidarala, E. Levi-D'Ancona, J. Zhu, S. A. Soleimanpour, M. S. Horwitz, and J. D. Johnson. 2022. 'beta-Cell Cre Expression and Reduced Ins1 Gene Dosage Protect Mice From Type 1 Diabetes', *Endocrinology*, 163.
- Smirnikhina, S. A., M. I. Zaynitdinova, V. A. Sergeeva, and A. V. Lavrov. 2022. 'Improving Homology-Directed Repair in Genome Editing Experiments by Influencing the Cell Cycle', *Int J Mol Sci*, 23.
- Son, J., and D. Accili. 2023. 'Reversing pancreatic beta-cell dedifferentiation in the treatment of type 2 diabetes', *Exp Mol Med*, 55: 1652-58.
- Soneson, C., M. I. Love, and M. D. Robinson. 2015. 'Differential analyses for RNA-seq: transcript-level estimates improve gene-level inferences', *F1000Res*, 4: 1521.
- Song, A. J., and R. D. Palmiter. 2018. 'Detecting and Avoiding Problems When Using the Cre-lox System', *Trends Genet*, 34: 333-40.
- Song, J., Y. Xu, X. Hu, B. Choi, and Q. Tong. 2010. 'Brain expression of Cre recombinase driven by pancreas-specific promoters', *Genesis*, 48: 628-34.
- Southekal, S., S. K. Shakyawar, P. Bajpai, A. Elkholy, U. Manne, N. K. Mishra, and C. Guda. 2023. 'Molecular Subtyping and Survival Analysis of Osteosarcoma Reveals Prognostic Biomarkers and Key Canonical Pathways', *Cancers (Basel)*, 15.
- Spears, E., I. Serafimidis, A. C. Powers, and A. Gavalas. 2021. 'Debates in Pancreatic Beta Cell Biology: Proliferation Versus Progenitor Differentiation and Transdifferentiation in Restoring beta Cell Mass', *Front Endocrinol (Lausanne)*, 12: 722250.
- Sridhara, S. 2024. 'Multiple structural flavors of RNase P in precursor tRNA processing', *Wiley Interdiscip Rev RNA*, 15: e1835.
- Steiner, D. J., A. Kim, K. Miller, and M. Hara. 2010. 'Pancreatic islet plasticity: interspecies comparison of islet architecture and composition', *Islets*, 2: 135-45.
- Steinthorsdottir, V., G. Thorleifsson, I. Reynisdottir, R. Benediktsson, T. Jonsdottir, G. B. Walters, U. Styrkarsdottir, S. Gretarsdottir, V. Emilsson, S. Ghosh, A. Baker, S. Snorraddottir, H. Bjarnason, M. C. Ng, T. Hansen, Y. Bagger, R. L. Wilensky, M. P. Reilly, A. Adeyemo, Y. Chen, J. Zhou, V. Gudnason, G. Chen, H. Huang, K. Lashley, A. Doumatey, W. Y. So, R. C. Ma, G. Andersen, K. Borch-Johnsen, T. Jorgensen, J. V. van Vliet-Ostaptchouk, M. H. Hofker, C. Wijmenga, C. Christiansen, D. J. Rader, C. Rotimi, M. Gurney, J. C. Chan, O. Pedersen, G. Sigurdsson, J. R. Gulcher, U. Thorsteinsdottir, A. Kong, and K. Stefansson. 2007. 'A variant in CDKAL1 influences insulin response and risk of type 2 diabetes', *Nat Genet*, 39: 770-5.
- Sternberg, N., and D. Hamilton. 1981. 'Bacteriophage P1 site-specific recombination. I. Recombination between loxP sites', *J Mol Biol*, 150: 467-86.
- Sticht, J., M. Alvaro-Benito, and S. Konigorski. 2021. 'Type 1 Diabetes and the HLA Region: Genetic Association Besides Classical HLA Class II Genes', *Front Genet*, 12: 683946.
- Sun, H., P. Saedi, S. Karuranga, M. Pinkepank, K. Ogurtsova, B. B. Duncan, C. Stein, A. Basit, J. C. N. Chan, J. C. Mbanya, M. E. Pavkov, A. Ramachandaran, S. H. Wild, S. James, W. H. Herman, P. Zhang, C. Bommer, S. Kuo, E. J. Boyko, and D. J. Magliano. 2022. 'IDF Diabetes Atlas: Global, regional and country-level diabetes prevalence estimates for 2021 and projections for 2045', *Diabetes Res Clin Pract*, 183: 109119.
- Suriano, F., S. Vieira-Silva, G. Falony, M. Roumain, A. Paquot, R. Pelicaen, M. Regnier, N. M. Delzenne, J. Raes, G. G. Muccioli, M. Van Hul, and P. D. Cani. 2021. 'Novel

- insights into the genetically obese (ob/ob) and diabetic (db/db) mice: two sides of the same coin', *Microbiome*, 9: 147.
- Surwit, R. S., C. M. Kuhn, C. Cochrane, J. A. McCubbin, and M. N. Feinglos. 1988. 'Diet-induced type II diabetes in C57BL/6J mice', *Diabetes*, 37: 1163-7.
- Suzuki, K., K. Hatzikotoulas, L. Southam, H. J. Taylor, X. Yin, K. M. Lorenz, R. Mandla, A. Huerta-Chagoya, G. E. M. Melloni, S. Kanoni, N. W. Rayner, O. Bocher, A. L. Arruda, K. Sonehara, S. Namba, S. S. K. Lee, M. H. Preuss, L. E. Petty, P. Schroeder, B. Vanderwerff, M. Kals, F. Bragg, K. Lin, X. Guo, W. Zhang, J. Yao, Y. J. Kim, M. Graff, F. Takeuchi, J. Nano, A. Lamri, M. Nakatochi, S. Moon, R. A. Scott, J. P. Cook, J. J. Lee, I. Pan, D. Taliun, E. J. Parra, J. F. Chai, L. F. Bielak, Y. Tabara, Y. Hai, G. Thorleifsson, N. Grarup, T. Sofer, M. Wuttke, C. Sarnowski, C. Gieger, D. Noursome, S. Trompet, S. H. Kwak, J. Long, M. Sun, L. Tong, W. M. Chen, S. S. Nongmaithem, R. Noordam, V. J. Y. Lim, C. H. T. Tam, Y. Y. Joo, C. H. Chen, L. M. Raffield, B. P. Prins, A. Nicolas, L. R. Yanek, G. Chen, J. A. Brody, E. Kabagambe, P. An, A. H. Xiang, H. S. Choi, B. E. Cade, J. Tan, K. A. Broadaway, A. Williamson, Z. Kamali, J. Cui, M. Thangam, L. S. Adair, A. Adeyemo, C. A. Aguilar-Salinas, T. S. Ahluwalia, S. S. Anand, A. Bertoni, J. Bork-Jensen, I. Brandslund, T. A. Buchanan, C. F. Burant, A. S. Butterworth, M. Canouil, J. C. N. Chan, L. C. Chang, M. L. Chee, J. Chen, S. H. Chen, Y. T. Chen, Z. Chen, L. M. Chuang, M. Cushman, J. Danesh, S. K. Das, H. J. de Silva, G. Dedoussis, L. Dimitrov, A. P. Dumaty, S. Du, Q. Duan, K. U. Eckardt, L. S. Emery, D. S. Evans, M. K. Evans, K. Fischer, J. S. Floyd, I. Ford, O. H. Franco, T. M. Frayling, B. I. Freedman, P. Genter, H. C. Gerstein, V. Giedraitis, C. Gonzalez-Villalpando, M. E. Gonzalez-Villalpando, P. Gordon-Larsen, M. Gross, L. A. Guare, S. Hackinger, L. Hakaste, S. Han, A. T. Hattersley, C. Herder, M. Horikoshi, A. G. Howard, W. Hsueh, M. Huang, W. Huang, Y. J. Hung, M. Y. Hwang, C. M. Hwu, S. Ichihara, M. A. Ikram, M. Ingelsson, M. T. Islam, M. Isono, H. M. Jang, F. Jasmine, G. Jiang, J. B. Jonas, T. Jorgensen, F. K. Kamanu, F. R. Kandeel, A. Kasturiratne, T. Katsuya, V. Kaur, T. Kawaguchi, J. M. Keaton, A. N. Kho, C. C. Khor, M. G. Kibriya, D. H. Kim, F. Kronenberg, J. Kuusisto, K. Lall, L. A. Lange, K. M. Lee, M. S. Lee, N. R. Lee, A. Leong, L. Li, Y. Li, R. Li-Gao, S. Ligthart, C. M. Lindgren, A. Linneberg, C. T. Liu, J. Liu, A. E. Locke, T. Louie, J. Luan, A. O. Luk, X. Luo, J. Lv, J. A. Lynch, V. Lyssenko, S. Maeda, V. Mamakou, S. R. Mansuri, K. Matsuda, T. Meitinger, O. Melander, A. Metspalu, H. Mo, A. D. Morris, F. A. Moura, J. L. Nadler, M. A. Nalls, U. Nayak, I. Ntalla, Y. Okada, L. Orozco, S. R. Patel, S. Patil, P. Pei, M. A. Pereira, A. Peters, F. J. Pirie, H. G. Polikowsky, B. Porneala, G. Prasad, L. J. Rasmussen-Torvik, A. P. Reiner, M. Roden, R. Rohde, K. Roll, C. Sabanayagam, K. Sandow, A. Sankareswaran, N. Sattar, S. Schonherr, M. Shahriar, B. Shen, J. Shi, D. M. Shin, N. Shojima, J. A. Smith, W. Y. So, A. Stancakova, V. Steinthorsdottir, A. M. Stilp, K. Strauch, K. D. Taylor, B. Thorand, U. Thorsteinsdottir, B. Tomlinson, T. C. Tran, F. J. Tsai, J. Tuomilehto, T. Tusie-Luna, M. S. Udler, A. Valladares-Salgado, R. M. van Dam, J. B. van Klinken, R. Varma, N. Wacher-Rodarte, E. Wheeler, A. R. Wickremasinghe, K. W. van Dijk, D. R. Witte, C. S. Yajnik, K. Yamamoto, K. Yamamoto, K. Yoon, C. Yu, J. M. Yuan, S. Yusuf, M. Zawistowski, L. Zhang, W. Zheng, V. A. Million Veteran Program, L. J. Raffel, M. Igase, E. Ipp, S. Redline, Y. S. Cho, L. Lind, M. A. Province, M. Fornage, C. L. Hanis, E. Ingelsson, A. B. Zonderman, B. M. Psaty, Y. X. Wang, C. N. Rotimi, D. M. Becker, F. Matsuda, Y. Liu, M. Yokota, S. L. R. Kardia, P. A. Peyser, J. S. Pankow, J. C. Engert, A. Bonnefond, P. Froguel, J. G. Wilson, W. H. H. Sheu, J. Y. Wu, M. G. Hayes, R. C. W. Ma, T. Y. Wong, D. O. Mook-Kanamori, T. Tuomi, G. R. Chandak, F. S. Collins, D. Bharadwaj, G. Pare, M. M. Sale, H. Ahsan, A. A. Motala, X. O. Shu, K. S. Park, J. W. Jukema, M. Cruz, Y. I. Chen, S. S. Rich, R. McKean-Cowdin, H.

- Grallert, C. Y. Cheng, M. Ghanbari, E. S. Tai, J. Dupuis, N. Kato, M. Laakso, A. Kottgen, W. P. Koh, D. W. Bowden, C. N. A. Palmer, J. S. Kooner, C. Kooperberg, S. Liu, K. E. North, D. Saleheen, T. Hansen, O. Pedersen, N. J. Wareham, J. Lee, B. J. Kim, I. Y. Millwood, R. G. Walters, K. Stefansson, E. Ahlqvist, M. O. Goodarzi, K. L. Mohlke, C. Langenberg, C. A. Haiman, R. J. F. Loos, J. C. Florez, D. J. Rader, M. D. Ritchie, S. Zollner, R. Magi, N. A. Marston, C. T. Ruff, D. A. van Heel, S. Finer, J. C. Denny, T. Yamauchi, T. Kadowaki, J. C. Chambers, M. C. Y. Ng, X. Sim, J. E. Below, P. S. Tsao, K. M. Chang, M. I. McCarthy, J. B. Meigs, A. Mahajan, C. N. Spracklen, J. M. Mercader, M. Boehnke, J. I. Rotter, M. Vujkovic, B. F. Voight, A. P. Morris, and E. Zeggini. 2024. 'Genetic drivers of heterogeneity in type 2 diabetes pathophysiology', *Nature*, 627: 347-57.
- Szabat, M., M. M. Page, E. Panzhinskiy, S. Skovso, M. Mojibian, J. Fernandez-Tajes, J. E. Bruin, M. J. Broun, J. T. Lee, E. E. Xu, F. Taghizadeh, S. O'Dwyer, M. van de Bunt, K. M. Moon, S. Sinha, J. Han, Y. Fan, F. C. Lynn, M. Trucco, C. H. Borchers, L. J. Foster, C. Nislow, T. J. Kieffer, and J. D. Johnson. 2016. 'Reduced Insulin Production Relieves Endoplasmic Reticulum Stress and Induces beta Cell Proliferation', *Cell Metab*, 23: 179-93.
- Szenker, E., D. Ray-Gallet, and G. Almouzni. 2011. 'The double face of the histone variant H3.3', *Cell Res*, 21: 421-34.
- Tabak, A. G., M. Jokela, T. N. Akbaraly, E. J. Brunner, M. Kivimaki, and D. R. Witte. 2009. 'Trajectories of glycaemia, insulin sensitivity, and insulin secretion before diagnosis of type 2 diabetes: an analysis from the Whitehall II study', *Lancet*, 373: 2215-21.
- Tagami, H., D. Ray-Gallet, G. Almouzni, and Y. Nakatani. 2004. 'Histone H3.1 and H3.3 complexes mediate nucleosome assembly pathways dependent or independent of DNA synthesis', *Cell*, 116: 51-61.
- Takano, C., E. Ogawa, and S. Hayakawa. 2023. 'Insulin Resistance in Mitochondrial Diabetes', *Biomolecules*, 13.
- Tavana, O., N. Puebla-Osorio, M. Sang, and C. Zhu. 2010. 'Absence of p53-dependent apoptosis combined with nonhomologous end-joining deficiency leads to a severe diabetic phenotype in mice', *Diabetes*, 59: 135-42.
- Tay, V. S. Y., S. Devaraj, T. Koh, G. Ke, K. C. Crasta, and Y. Ali. 2019. 'Increased double strand breaks in diabetic beta-cells with a p21 response that limits apoptosis', *Sci Rep*, 9: 19341.
- Taylor, C. A., W. Shawlot, J. X. Ren, and S. Mukhopadhyay. 2019. 'Generation and Validation of Tissue-Specific Knockout Strains for Toxicology Research', *Curr Protoc Toxicol*, 81: e86.
- Thomas, H. E., M. D. McKenzie, E. Angstetra, P. D. Campbell, and T. W. Kay. 2009. 'Beta cell apoptosis in diabetes', *Apoptosis*, 14: 1389-404.
- Thomas, P. D., D. Ebert, A. Muruganujan, T. Mushayahama, L. P. Albou, and H. Mi. 2022. 'PANTHER: Making genome-scale phylogenetics accessible to all', *Protein Sci*, 31: 8-22.
- Thompson, P. J., A. Shah, V. Ntranos, F. Van Gool, M. Atkinson, and A. Bhushan. 2019. 'Targeted Elimination of Senescent Beta Cells Prevents Type 1 Diabetes', *Cell Metab*, 29: 1045-60 e10.
- Thomsen, S. K., and A. L. Gloyn. 2014. 'The pancreatic beta cell: recent insights from human genetics', *Trends Endocrinol Metab*, 25: 425-34.
- Thorens, B., D. Tarussio, M. A. Maestro, M. Rovira, E. Heikkila, and J. Ferrer. 2015. 'Ins1(Cre) knock-in mice for beta cell-specific gene recombination', *Diabetologia*, 58: 558-65.
- Thyagarajan, B., M. J. Guimaraes, A. C. Groth, and M. P. Calos. 2000. 'Mammalian genomes contain active recombinase recognition sites', *Gene*, 244: 47-54.

- Tomita, T. 2016. 'Apoptosis in pancreatic beta-islet cells in Type 2 diabetes', *Bosn J Basic Med Sci*, 16: 162-79.
- Tonnies, T., S. Rockl, A. Hoyer, C. Heidemann, J. Baumert, Y. Du, C. Scheidt-Nave, and R. Brinks. 2019. 'Projected number of people with diagnosed Type 2 diabetes in Germany in 2040', *Diabet Med*, 36: 1217-25.
- Tornovsky-Babeay, S., D. Dadon, O. Ziv, E. Tzipilevich, T. Kadosh, R. Schyr-Ben Haroush, A. Hija, M. Stolovich-Rain, J. Furth-Lavi, Z. Granot, S. Porat, L. H. Philipson, K. C. Herold, T. R. Bhatti, C. Stanley, F. M. Ashcroft, P. In't Veld, A. Saada, M. A. Magnuson, B. Glaser, and Y. Dor. 2014. 'Type 2 diabetes and congenital hyperinsulinism cause DNA double-strand breaks and p53 activity in beta cells', *Cell Metab*, 19: 109-21.
- Tosur, M., and L. H. Philipson. 2022. 'Precision diabetes: Lessons learned from maturity-onset diabetes of the young (MODY)', *J Diabetes Investig*, 13: 1465-71.
- Toye, A. A., J. D. Lippiat, P. Proks, K. Shimomura, L. Bentley, A. Hugill, V. Mijat, M. Goldsworthy, L. Moir, A. Haynes, J. Quarterman, H. C. Freeman, F. M. Ashcroft, and R. D. Cox. 2005. 'A genetic and physiological study of impaired glucose homeostasis control in C57BL/6J mice', *Diabetologia*, 48: 675-86.
- Uhlemeyer, C., N. Muller, K. Griess, C. Wessel, C. Schlegel, J. Kuboth, and B. F. Belgardt. 2020. 'ATM and P53 differentially regulate pancreatic beta cell survival in Ins1E cells', *PLoS One*, 15: e0237669.
- Uhlemeyer, C., N. Muller, M. Rieck, J. Kuboth, C. Schlegel, K. Griess, T. F. Dorweiler, S. Heiduschka, J. Eckel, M. Roden, E. Lammert, M. Stoffel, and B. F. Belgardt. 2023. 'Selective ablation of P53 in pancreatic beta cells fails to ameliorate glucose metabolism in genetic, dietary and pharmacological models of diabetes mellitus', *Mol Metab*, 67: 101650.
- Van Belle, T. L., P. Taylor, and M. G. von Herrath. 2009. 'Mouse Models for Type 1 Diabetes', *Drug Discov Today Dis Models*, 6: 41-45.
- van Eenennaam, H., G. J. Pruijn, and W. J. van Venrooij. 1999. 'hPop4: a new protein subunit of the human RNase MRP and RNase P ribonucleoprotein complexes', *Nucleic Acids Res*, 27: 2465-72.
- Vanderkruk, B., N. Maeshima, D. J. Pasula, M. An, C. L. McDonald, P. Suresh, D. S. Luciani, F. C. Lynn, and B. G. Hoffman. 2023. 'Methylation of histone H3 lysine 4 is required for maintenance of beta cell function in adult mice', *Diabetologia*, 66: 1097-115.
- Varghese, S. S., and S. Dhawan. 2023. 'Senescence: a double-edged sword in beta-cell health and failure?', *Front Endocrinol (Lausanne)*, 14: 1196460.
- Verma, G., A. Bowen, S. Gheibi, A. Hamilton, S. Muthukumar, L. R. Cataldo, O. Asplund, J. Esguerra, A. Karagiannopoulos, C. Lyons, E. Cowan, C. Bellodi, R. Prasad, M. Fex, and H. Mulder. 2022. 'Ribosomal biogenesis regulator DIMT1 controls beta-cell protein synthesis, mitochondrial function, and insulin secretion', *J Biol Chem*, 298: 101692.
- Vogel, H., A. Kamitz, N. Hallahan, S. Lebek, T. Schallschmidt, W. Jonas, M. Jahnert, P. Gottmann, L. Zellner, T. Kanzleiter, M. Damen, D. Altenhofen, R. Burkhardt, S. Renner, M. Dahlhoff, E. Wolf, T. D. Muller, M. Bluher, H. G. Joost, A. Chadt, H. Al-Hasani, and A. Schurmann. 2018. 'A collective diabetes cross in combination with a computational framework to dissect the genetics of human obesity and Type 2 diabetes', *Hum Mol Genet*, 27: 3099-112.
- Vogel, H., F. Mirhashemi, B. Liehl, F. Taugner, O. Kluth, R. Kluge, H. G. Joost, and A. Schurmann. 2013. 'Estrogen deficiency aggravates insulin resistance and induces beta-cell loss and diabetes in female New Zealand obese mice', *Horm Metab Res*, 45: 430-5.

- Vogel, H., S. Scherneck, T. Kanzleiter, V. Benz, R. Kluge, M. Stadion, S. Kryvykh, M. Blucher, N. Kloting, H. G. Joost, and A. Schurmann. 2012. 'Loss of function of Ifi202b by a microdeletion on chromosome 1 of C57BL/6J mice suppresses 11beta-hydroxysteroid dehydrogenase type 1 expression and development of obesity', *Hum Mol Genet*, 21: 3845-57.
- Walker, S. C., and D. R. Engelke. 2006. 'Ribonuclease P: the evolution of an ancient RNA enzyme', *Crit Rev Biochem Mol Biol*, 41: 77-102.
- Wang, Z., and D. C. Thurmond. 2009. 'Mechanisms of biphasic insulin-granule exocytosis - roles of the cytoskeleton, small GTPases and SNARE proteins', *J Cell Sci*, 122: 893-903.
- Wanner, E., H. Thoppil, and K. Riabowol. 2020. 'Senescence and Apoptosis: Architects of Mammalian Development', *Front Cell Dev Biol*, 8: 620089.
- Wei, F. Y., T. Suzuki, S. Watanabe, S. Kimura, T. Kaitsuka, A. Fujimura, H. Matsui, M. Atta, H. Michiue, M. Fontecave, K. Yamagata, T. Suzuki, and K. Tomizawa. 2011a. 'Deficit of tRNA(Lys) modification by Cdkal1 causes the development of type 2 diabetes in mice', *J Clin Invest*, 121: 3598-608.
- Wei, Fan-Yan, Takeo Suzuki, Sayaka Watanabe, Satoshi Kimura, Taku Kaitsuka, Atsushi Fujimura, Hideki Matsui, Mohamed Atta, Hiroyuki Michiue, Marc Fontecave, Kazuya Yamagata, Tsutomu Suzuki, and Kazuhito Tomizawa. 2011b. 'Deficit of tRNALys modification by Cdkal1 causes the development of type 2 diabetes in mice', *Journal of Clinical Investigation*, 121: 3598-608.
- Weir, G. C., and S. Bonner-Weir. 1990. 'Islets of Langerhans: the puzzle of intraislet interactions and their relevance to diabetes', *J Clin Invest*, 85: 983-7.
- . 2013. 'Islet beta cell mass in diabetes and how it relates to function, birth, and death', *Ann N Y Acad Sci*, 1281: 92-105.
- . 2021. 'Reduced glucose-induced first-phase insulin release is a danger signal that predicts diabetes', *J Clin Invest*, 131.
- Welting, T. J., B. J. Kikkert, W. J. van Venrooij, and G. J. Pruijn. 2006. 'Differential association of protein subunits with the human RNase MRP and RNase P complexes', *RNA*, 12: 1373-82.
- Westphal, D., R. M. Kluck, and G. Dewson. 2014. 'Building blocks of the apoptotic pore: how Bax and Bak are activated and oligomerize during apoptosis', *Cell Death Differ*, 21: 196-205.
- Wicksteed, B., M. Brissova, W. Yan, D. M. Opland, J. L. Plank, R. B. Reinert, L. M. Dickson, N. A. Tamarina, L. H. Philipson, A. Shostak, E. Bernal-Mizrachi, L. Elghazi, M. W. Roe, P. A. Labosky, M. G. Myers, Jr., M. Gannon, A. C. Powers, and P. J. Dempsey. 2010. 'Conditional gene targeting in mouse pancreatic ss-Cells: analysis of ectopic Cre transgene expression in the brain', *Diabetes*, 59: 3090-8.
- Woodhams, M. D., P. F. Stadler, D. Penny, and L. J. Collins. 2007. 'RNase MRP and the RNA processing cascade in the eukaryotic ancestor', *BMC Evol Biol*, 7 Suppl 1: S13.
- Wrzeszczynski, K. O., V. Varadan, J. Byrnes, E. Lum, S. Kamalakaran, D. A. Levine, N. Dimitrova, M. Q. Zhang, and R. Lucito. 2011. 'Identification of tumor suppressors and oncogenes from genomic and epigenetic features in ovarian cancer', *PLoS One*, 6: e28503.
- Wu, Jian, Shuangshuang Niu, Ming Tan, Chenhui Huang, Mingyue Li, Yang Song, Qianmin Wang, Juan Chen, Shaohua Shi, Pengfei Lan, and Ming Lei. 2018. 'Cryo-EM Structure of the Human Ribonuclease P Holoenzyme', *Cell*, 175: 1393-404.e11.
- Xiao, S., J. J. Day-Storms, C. Srisawat, C. A. Fierke, and D. R. Engelke. 2005. 'Characterization of conserved sequence elements in eukaryotic RNase P RNA reveals roles in holoenzyme assembly and tRNA processing', *RNA*, 11: 885-96.

-
- Yoshioka, M., T. Kayo, T. Ikeda, and A. Koizumi. 1997. 'A novel locus, Mody4, distal to D7Mit189 on chromosome 7 determines early-onset NIDDM in nonobese C57BL/6 (Akita) mutant mice', *Diabetes*, 46: 887-94.
- You, W., J. Yang, Y. Liu, W. Wang, L. Zhu, W. Wang, J. Yang, and F. Chen. 2019. 'Fulminant type 1 diabetes mellitus: Two case reports', *Medicine (Baltimore)*, 98: e14319.
- Yousefzadeh, M. J., A. P. Huerta Guevara, A. C. Postmus, R. R. Flores, T. Sano, A. Jurdzinski, L. Angelini, S. J. McGowan, R. D. O'Kelly, E. A. Wade, L. V. Gonzalez-Espada, D. Henessy-Wack, S. Howard, T. A. Rozgaja, C. E. Trussoni, N. F. LaRusso, B. J. L. Eggen, J. W. Jonker, P. D. Robbins, L. J. Niedernhofer, and J. K. Kruit. 2023. 'Failure to repair endogenous DNA damage in beta-cells causes adult-onset diabetes in mice', *Aging Biol*, 1.
- Zaharia, O. P., K. Strassburger, A. Strom, G. J. Bonhof, Y. Karusheva, S. Antoniou, K. Bodis, D. F. Markgraf, V. Burkart, K. Mussig, J. H. Hwang, O. Asplund, L. Groop, E. Ahlqvist, J. Seissler, P. Nawroth, S. Kopf, S. M. Schmid, M. Stumvoll, A. F. H. Pfeiffer, S. Kabisch, S. Tselmin, H. U. Haring, D. Ziegler, O. Kuss, J. Szendroedi, M. Roden, and Group German Diabetes Study. 2019. 'Risk of diabetes-associated diseases in subgroups of patients with recent-onset diabetes: a 5-year follow-up study', *Lancet Diabetes Endocrinol*, 7: 684-94.
- Zeggini, E., M. N. Weedon, C. M. Lindgren, T. M. Frayling, K. S. Elliott, H. Lango, N. J. Timpson, J. R. Perry, N. W. Rayner, R. M. Freathy, J. C. Barrett, B. Shields, A. P. Morris, S. Ellard, C. J. Groves, L. W. Harries, J. L. Marchini, K. R. Owen, B. Knight, L. R. Cardon, M. Walker, G. A. Hitman, A. D. Morris, A. S. Doney, Consortium Wellcome Trust Case Control, M. I. McCarthy, and A. T. Hattersley. 2007. 'Replication of genome-wide association signals in UK samples reveals risk loci for type 2 diabetes', *Science*, 316: 1336-41.
- Zhang, H., K. Colclough, A. L. Gloyn, and T. I. Pollin. 2021. 'Monogenic diabetes: a gateway to precision medicine in diabetes', *J Clin Invest*, 131.
- Zhao, X., M. Wang, Z. Wen, Z. Lu, L. Cui, C. Fu, H. Xue, Y. Liu, and Y. Zhang. 2021. 'GLP-1 Receptor Agonists: Beyond Their Pancreatic Effects', *Front Endocrinol (Lausanne)*, 12: 721135.
- Zhou, B., F. Wan, K. X. Lei, P. Lan, J. Wu, and M. Lei. 2024. 'Coevolution of RNA and protein subunits in RNase P and RNase MRP, two RNA processing enzymes', *J Biol Chem*, 300: 105729.
- Zhou, Z., V. Ribas, P. Rajbhandari, B. G. Drew, T. M. Moore, A. H. Fluitt, B. R. Reddish, K. A. Whitney, S. Georgia, L. Vergnes, K. Reue, M. Liesa, O. Shirihai, A. M. van der Blik, N. W. Chi, S. K. Mahata, J. P. Tiano, S. C. Hewitt, P. Tontonoz, K. S. Korach, F. Mauvais-Jarvis, and A. L. Hevener. 2018. 'Estrogen receptor alpha protects pancreatic beta-cells from apoptosis by preserving mitochondrial function and suppressing endoplasmic reticulum stress', *J Biol Chem*, 293: 4735-51.
- Zhu, M., C. Wu, X. Wu, G. Song, M. Li, and Q. Wang. 2023. 'POP1 promotes the progression of breast cancer through maintaining telomere integrity', *Carcinogenesis*, 44: 252-62.

8 List of Tables

Table 1: Mouse strains	19
Table 2: Mouse diets and dietary composition	19
Table 3: List of expendable materials and supplier	20
Table 4: Chemicals and solutions with supplier information	21
Table 5: Buffer or solution composition and application	23
Table 6: DNA ladder and supplier	24
Table 7: Polymerases for PCR and supplier	24
Table 8: Genotyping Primer sequences and the position in the genome	24
Table 9: Primer sequences to validate ablation of Exon 4 and 5	25
Table 10: Primer sequences for RT-qPCR	25
Table 11: Antibodies with supplier information	25
Table 12: Kits, their application and supplier	26
Table 13: Devices and supplier	27
Table 14: Computer software or online tools, manufacturer and application	29
Table 15: Reaction setup for the Pop4 PCR reaction	38
Table 16: PCR reaction program to amplify Pop4 sequence	38
Table 17: Reaction setup for the Ins1^{Cre} PCR reaction	39
Table 18: PCR reaction program to amplify Ins1^{Cre} sequence	39
Table 19: Reaction setup for the tdTomato PCR reaction	39
Table 20: PCR reaction program to amplify tdTomato sequence	40
Table 21: Reaction setup for the validation of the deletion of Exons 4+5	40
Table 22: PCR reaction program to amplify Exon4+5 of Pop4 sequence	40
Table 23: Reaction setup for cDNA synthesis	43
Table 24: cDNA synthesis programm	44
Table 25: Composition for one well of qPCR sample	44
Table 26: qPCR settings in QuantStudio 7 Flex	45
Table 27: Embedding protocol of the Shandon Excelsior Tissue processor	46
Table 28: HE Staining protocol	47
Table 29: Immunostaining protocol	48

9 List of Figures

Figure 1: Previous data on Pop4 relation to insulin secretion function.	16
Figure 2. Schematic representation of the genomic sequence for the mouse crosses to generate the beta cell specific ablation in the Pop4 gene.	31
Figure 3. Breeding scheme to obtain littermate control and Pop4 β KO mice.....	31
Figure 4. Phenotyping timeline for Pop4 β KO animals and controls.....	32
Figure 5. Genotyping of the mice by PCR and gel electrophoresis.....	53
Figure 6. Validation of Cre activity by tdTomato fluorescence in pancreatic islet and single endocrine cells.	54
Figure 7. Validation of ablation of exons 4 and 5 of Pop4 gene in beta-cells on gDNA and mRNA level.	55
Figure 8. Quantitative gene expression of exon 4 to exon junction 5-6 of <i>Pop4</i> in different tissues.	56
Figure 9: Amino acid sequence alignment of the wildtype (WT) POP4 and the putative POP4 with deletion of exon 4 and 5 (Pop4KO).	57
Figure 10: Predicted mouse protein structure of POP4 and the putative POP4 with deletion of exons 4 and 5.	58
Figure 11. Blood glucose development and diabetes prevalence of male and female mice on standard chow diet.	59
Figure 12: Body weight development of male and female mice on chow diet. ...	60
Figure 13. Body composition of lean and fat mass of males and females mice.	61
Figure 14: Fasted blood glucose and plasma insulin levels of males and females on a chow diet.	62
Figure 15. Comparison of metabolic traits on 60% high fat diet vs chow diet in female mice.....	63
Figure 16. Body composition of lean and fat mass of females mice on chow and high fat diet (HFD).	64
Figure 17. Diabetes prevalence and HOMA-IR at 3, 8 and 11 weeks of age for the female mice on chow compared to HFD.....	65
Figure 18: Intraperitoneal glucose tolerance test at 8 weeks of age in male mice.	66
Figure 19. Insulin secretion assay and protein content in isolated pancreatic islets.	67
Figure 20. Representative images of HE stained pancreatic islet.....	69
Figure 21. Morphometrics of pancreatic sections and respective pancreatic islet areas.....	70
Figure 22. Representative images of immunostainings detection of Insulin and Glucagon in pancreatic tissue sections to visualize beta cell and alpha cell area.....	72
Figure 23. Quantification of immunostained insulin positive and glucagon positive area.	73
Figure 24. Representative images of immunostainings detection in pancreatic tissue sections to visualize beta cell identity and proliferation.	74
Figure 25. Quantification of immunostained beta cell identity marker NKX6.1 and proliferation marker KI67.	75
Figure 26. Representative immunostaining images to investigate DNA damage marker γ H2A.X in beta cell area.....	76
Figure 27. Quantification of γ H2A.X positive stained nuclei.	77

Figure 28. Beta Cell ultrastructure obtained by transmission electron microscopy of isolated islets at 8 weeks of age.	78
Figure 29: Morphometric of nucleus and mitochondrial Area.....	79
Figure 30: Morphometrics of beta cells and insulin vesicles.	79
Figure 31: Comparison of beta cells under basal and glucose stimulated condition.	80
Figure 32. Assessment inter- and intra-variability of samples.	81
Figure 33. Differential gene expression analysis.....	82
Figure 34. Gene ontology analysis of differentially regulated genes using Panther tool.	83
Figure 35. Consensus Pathway DB over-representation analysis of differentially down- and upregulated genes.	85
Figure 36. Gene expression of pancreatic islet hormones and cell markers.	86
Figure 37. Gene expression differences in the insulin secretion pathway.	87
Figure 38. Genes involved in canonical function of POP4.....	89
Figure 39. Genes of double stranded (DSB) DNA repair response.	90
Figure 40. Gene expression differences in the apoptosis pathway. A schematic representation of protein interaction and involvement in the apoptosis pathway.	92
Figure 41. Gene expression differences in the senescence pathway. A schematic representation of protein interaction and involvement in the senescence pathway.	93

10 Acknowledgement

First of all, I would like to express my deepest gratitude to my professor and mentor, Prof. Hadi Al-Hasani, for the trust he placed in me to work on this project and for accepting me as a Ph.D. student. Discussions with you have helped me immensely to pursue and reflect on this project more deeply, and you have guided me in prioritizing the various steps with your knowledge of the field. Next, I would like to thank my supervisor Dr. Alexandra Chadt. Through her support and excellent coordination skills, she gave me the tools to work in a more structured way and helped me in many ways with the project, from mouse work to all the input during meetings and correcting this work. I would also like to emphasize my gratitude to Dr. Bengt-Frederik Belgardt, whose deep knowledge in the beta cell field provided many methods and protocols that contributed to this work, and whose support in histology was of great help.

I would like to especially thank Dr. Delsi Altenhofen for her encouragement and guidance in starting this very special project. Her ambition and diligence have always been a great inspiration to me. Thank you for your help with the mouse work, especially islet isolation, KO validation, and assistance with many analyses. Also, thank you for always being so positive and supportive and for all the wise advice you have given me. I would also like to thank the QTL team, especially Tanja Kuhn, whose preparatory work made this project possible and who also contributed to my familiarization with the topic, and Dr. Sarah Görigk for the cooperation and the great time we spent together. Next, the dear Pop4 team, with Katharina Kaiser and Marina Tautz, whose cooperation, exchange, support and friendship were immensely helpful in this project. I have really enjoyed our time together during our joint Ph.D. and I hope we will stay in touch.

I would like to thank Dr. Stefan Majda and Dr. Christian Binsch for their support in the analysis of the transcriptome data. I am very thankful for Christian Binsch kindness and his cookies kept me sane during long hours in the lab. Also I would like to thank Dr. Nadine Teichweyde from the IUF and Celina Uhlemeyer from the Institute for vascular and islet cell biology at the DDZ for their help with the FACS analysis and especially Celina for her support in the immunohistology. I would like to thank Dr. Jürgen Weiß, Kay Jeruschke and Carmen Weidlich for the processing of the histology samples and the preparation of the electron microscopy images. Thank you Carmen for your supportive, encouraging and wise words. Next, I would like to thank everyone who helped with the genotyping of the mice, especially Annette Kurowski, Heidrun

Podini and all the assistants with the Project namely Birgit Knobloch, Delia Bahn, Carina Heitmann, Angelika Horigghs, Dagmar Grittner and Antonia Osmer. I would like to thank the student assistants Alexander Bauer, Iannis Charnay and Timo Rhiem, who contributed to the project with their help. I would also like to thank all the animal caretakers which tough work is really admirable. Also to my student's Melanie Kollberg and Aleyna Erbas I thank you both for your enthusiasm in your own respective project's, for helping me in developing teaching skills and for your understanding in any of my lacking skills. An additional thank you to Christian Binsch, Katharina Kaiser, Sebastian Sill and Angela Pelligra for reading and correction of my thesis.

I would like to thank everyone in the amazing team of the Institute of Clinical and Pathobiochemistry for their support and the wonderful time together during lunchbreaks, brunches together or just the time in the lab. Thank you to Dr. Christian Springer, Dr. Samaneh Eickelschulte, Dr. Aleksandra Nikolic, Didi Humpert, Anna Scheel, Dr. Pia Förster, Sebastian Sill and Leon Peifer-Weiß and many more. Also thank you to Dr. Birgit Knebel, Dr. Jörg Kotzka and Dr. Magriet Ouwens for the discussions in meetings and support with any question.

Huge thank you to the Vivid Graduate School, for taking me in as an associate PhD and providing me with a network of excellent researchers and fellow PhDs.

Last but not least I want to thank my family and friends for their endless support, especially my boyfriend Jonas Schön. Without his ever-going encouragement, help and love, I would not have been able to conquer these challenging times. I want to thank my mum, my dad and my brother for their support and for being understanding during this whole time that I was lacking in supporting them. Thank you to all my friends which now and again kept me sane and their huge support including Celine Rodrigues, Sophie Takahashi, Anna-Lene Kiffe-Delf, Dennis Rosche, Mai Thao Nguyen, Martin Grunwald and many more. And I want to acknowledge myself for putting in the hours, sweat and tears into this work and staying resilient through those exciting and challenging times which helped me with learning and developing invaluable skills. I am immensely grateful for the big support and encouragement from everybody especially in times I struggled and needed support to keep going. I have never felt so much love as I have during this time and I will be forever grateful to everyone's kindness and support!

11 Eidesstaatliche Erklärung

Hiermit versichere ich, dass ich diese Dissertation von mir selbständig und ohne unzulässige fremde Hilfe unter Beachtung der „Grundsätze zur Sicherung guter wissenschaftlicher Praxis“ and der Heinrich-Heine Universität Düsseldorf verfasst habe. Alle Zitate und Abbildungen wurden als solche kenntlich gemacht.

Ich erkläre weiterhin, dass ich bisher noch keinen Promotionsversuch unternommen habe. Die vorliegende Arbeit wurde in dieser oder ähnlicher Form oder auch im Rahmen einer anderen Prüfung noch nicht eingereicht.

Düsseldorf, den 14.08.24

Jenny Khuong